The Evolution of Vortical Patterns and Vortices in Mesoscale Convective Complexes

by Michael A. Fortune

Colorado State University

DEPARTMENT OF ATMOSPHERIC SCIENCE

PAPER NO.
449

THE EVOLUTION OF VORTICAL PATTERNS AND VORTICES IN MESOSCALE CONVECTIVE -COMPLEXES

by

Michael A. Fortune

Department of Atmospheric Science

Colorado State University

Fort Collins, CO 80523

Research Supported by

The National Science Foundation

under grants ATM-8512480 and ATM-8814913

and by

The National Oceanic and Atmospheric Administration

under contract NA85RAH05045

Atmospheric Science Paper No. 449

ABSTRACT OF DISSERTATION

THE EVOLUTION OF VORTICAL PATTERNS AND VORTICES IN MESOSCALE CONVECTIVE COMPLEXES

The evolution and flow structure of four mesoscale convective complexes (MCCs) that manifested some form of vortical pattern of convective rainfall were investigated with datasets from the PRE–STORM field program. Intersecting convective bands that resembled an extratropical, frontal–wave cyclone evolved in the growth stage of three cases. A spiral pattern also emerged in one case, while the fourth developed a comma–shaped occlusion. A strong divergent wind response to the mesoscale heat source was observed in all systems, but only a weak rotational wind developed in the frontal wave systems. A meso–α–scale vortex was probably not responsible for the frontal wave pattern; rather the pattern resulted from the intersection of a mesoscale cold front advancing into the most unstable air with an existing stationary front. The convectively active core of the MCCs propagated with the intersection.

When upper level directional shear spread a stratiform cloud in more than one direction around the core, and when intense convection developed well south of the core and the front, the eventual spin–up of a vortex was fostered. In other cases, advection of the stratiform cloud north of the core may have hindered spin–up because a dry mid–level inflow beneath the cloud developed counter to the direction of rotation.

A conceptual model of the mesoscale frontal–wave cyclone employs the conveyor belt model of the extratropical cyclone. The warm conveyor belt is accelerated from the core upward and rearward in a jet within the former stationary frontal zone; the dry airstream converges from all possible directions beneath the more heavily precipitating part of the

stratiform cloud; the cool conveyor belt on the north side descends from the 4 to 7 km layer into the core region. Conditional symmetric instability may have initiated mesoscale overturning in a 1 km deep layer in the low levels of the stationary frontal zone. The conceptual models presented here for a **weakly rotating** (frontal wave) MCC and a **strongly rotating** MCC are compared with conceptual models of larger–scale extratropical cyclones and smaller–scale supercell thunderstorms.

ACKNOWLEDGEMENTS

I am indebted to Professor William R. Cotton for encouraging me to explore the more productive lines of research in this effort, and for sound advice and good judgement. Thanks are due to all members of my committee for comments that have improved the manuscript, especially to Margaret A. LeMone for a particularly thoroughgoing review. I am grateful to the managers of the PRE-STORM field program, particularly John B. Cunning, for the opportunity to fly through five mesoscale convective systems on board the NOAA P-3 aircraft and to assist in collecting data on the flights.

This manuscript could not have been produced without the dedicated support of Laneigh Brumit and Brenda Thompson over a period of several months. They struggled with new text–formatting software that has often tried our patience but has produced a lovely manuscript. The care that Lucy McCall puts into her drafting is evident in the quality of the 70 figures in the thesis. Thanks are also due to Judy Sorbie for preparing the 3-D perspective drawing of an MCC in chapter 9.

Most of the data as well as guidance and/or software for its analysis, were cheerfully provided by David P. Jorgensen, Jose G. Meitín, and John A. Augustine of the National Severe Storms Laboratory branch in Boulder, CO (formerly the Weather Research Program), and by James Toth and Sue Chen when they were at Colorado State University. Thanks are due to Edward A. Brandes for an early draft of his manuscript on the mesoscale convective vortex in the May 7, 1985 storm, which has been referenced throughout this work.

My colleague Ray L. McAnelly deserves special recognition as a collaborator on many facets of the analysis of the episode of June 3, 4, 1985. Ray was also responsible for the digitized radar mapping and analysis software and many of the Doppler radar syntheses,

and he contributed with many discussions and reviews of early manuscripts. I am also grateful to Sandra Henry and Tom Peterson for assistance in analyzing and mapping radar and rawinsonde data, and to Doug Burks for graphics software.

Finally, the support and encouragement of my friends Clinton T. Rhodes, Donald K. Park, and John Pollack, who together helped me to set goals and priorities and adopt a realistic timetable, will never be forgotten.

This research was supported by the National Science Foundation under grants ATM-8512480 and ATM-8814913, and by the National Oceanic and Atmospheric Administration under contract NA85RAH05045.

TABLE OF CONTENTS

LIST OF FIGURES

LIST OF TABLES

Chapter 1

INTRODUCTION

Ever since the *mesoscale convective complex* (MCC), described by Maddox (1980), and the more general mesoscale convective *system* (MCS) have been recognized as distinct manifestations of moist convection in the atmosphere, it has been noted that their convectively active elements develop in a variety of spatial patterns within the system. One form of MCS has been recognized for a long time: the squall line, described in the *Glossary of Meteorology* (Huschke, 1959) as a mature instability line, a narrow band of active thunderstorms, not necessarily continuous, from 50 to 300 km long and 15 to 80 km wide, which is associated with a dome of rain–cooled air that creates a pseudo–front where the squall winds meet the warm ambient air. However, it came to be observed that organized *non-linear* convective activity, or even apparently *un*organized convective activity, does evolve into mesoscale convective systems. Their characteristic circular or oval cloud shields, which are plainly not linear, are a clue that the mesoscale organizing processes need not be two dimensional.

Some work has been done on categorizing the spatial patterns of convective activity, and their geometry relative to the stratiform rain cloud, in mesoscale rain systems. As an example, Blanchard and Watson (1986) classified the 21 storm systems in one field experiment into three major types: convective–line systems, "random" outbreaks, and rotational systems. Papers on the classification of mesoscale rain systems are reviewed in the next chapter.

Since Johnston (1982) reported comma–shaped clouds and apparent cyclonic motion in dissipating mesoscale cloud systems, the search has intensified to seek and describe vortices in these cloud systems. Because they release large amounts of latent heat on the

mesoscale, a scale larger than the component convective cells, it was expected that the atmosphere would respond to the heat source by some form of mesoscale overturning. Since the heat was sometimes released over distances approaching the Rossby radius of deformation, it was expected that the initial convergent response would adjust to geostrophic balance (Cotton et al., 1989) and lead to an inertially stable warm core vortex (Zhang and Fritsch, 1988b). In the last ten years a number of mesoscale, convectively–generated vortices have been observed and described; they have also been simulated numerically. A few have been proven to be warm core and inertially stable, and to persist for 2 days or more. These investigations are also surveyed in Chapter 2.

It might be expected that such an evolving cyclone would manifest circular symmetry and patterns of rotation in its cloud components. Indeed, spiral and comma–shaped cloud bands have been reported in the *dissipating* stages of many MCS since Johnston's (1982) report. Spiral bands of enhanced radar reflectivity were detected in an MCS by Leary and Rappaport (1987). Less often, it was reported that the convective components of mature mesoscale convective systems developed in patterns reminiscent of the larger scale extratropical cyclone. Specifically, some of the convective activity developed along bands that curved into a central core just like warm fronts and cold fronts curve into a larger scale vortex of a wave cyclone. Some MCCs have been characterized as *occluding* systems in analogy to the later stages of the extratropical cyclone when the cold front occludes with the warm front and a dry air stream intrudes as far as the core of the cyclone. Various conceptual models have been put forth to explain the evolution of atmospheric cyclones on a variety of scales from the thunderstorm to the synoptic scale. In Chapter 2, we review those models that emphasize the interaction between the component air masses or air streams, especially in cyclones evolving toward an occlusion.

This thesis examines the characteristics and the evolution of a select group of mesoscale convective complexes that manifested some form of vortical pattern during most of their life cycle. The MCCs were observed during the Oklahoma–Kansas Preliminary Regional Experiment for STORM–Central (OK PRE–STORM) in May and June, 1985 (Cunning, 1986), a field program that was designed to investigate mesoscale convective systems

with new or supplemental observing networks having time and space resolution appropriate to the target storms. The cases studied here (four intensively and two superficially studied) exhibited a variety of convective organizations including spiral, occluding, and S–shaped wave patterns. Some also had structures like fronts which appeared to demarcate airstreams of different origins and properties.

The six cases included frontal wave bands, occluding, spiral, and even chaotic spatial patterns. The patterns can and did change during the life of the MCC, from early to mature to dissipating changes. Most of these cases exhibited chaotic development of convective activity in part of their life cycles. In at least one case the chaotic mode reigned throughout the life cycle; in another, an occluding squall line and meso–vortex developed from chaotic convection soon after the MCC initiated. What were the similarities and the differences among the patterns in the various cases? We attribute some of the differences from case to case, and from one stage to another, to observable meteorological conditions.

An important goal is to determine whether these MCCs did develop a mesoscale vortex, and whether they did so before or after the vortical convective patterns were established. Did the mesoscale cyclogenesis go hand–in–hand with a particular distribution of convective activity? Was the vortical wind circulation causing the convective bands and clusters to line up along frontal boundaries or spiral arms, or on the other hand did a certain arrangement of the convective cells enable a vortex to spin up, while another arrangement would impede it? Was the spatial pattern of convection likely to maintain a latent heat source in one location, during the time it takes an inertially stable cyclone to become established?

We will explore the analogy between the apparently vortical MCC and the evolving extratropical cyclone. The component air streams of the larger cyclone have been depicted as "conveyor belts" which slide over, under, and around each other as they pass through the disturbance, and which interact along sharply defined "fronts" or boundaries on which much of the interesting weather occurs. How useful is such an analogy to understanding vortical mesoscale convective systems? We present evidence for analogs of the three "belts" whose paths are charted in the larger scale cyclone: the warm conveyor belt, the cold conveyor belt, and the dry airstream.

Extending the analogy further, it has been suggested that convective overturning need not occur entirely in *vertical* updrafts and downdrafts after some stage in the evolution of MCCs. Rather, the motions might be organized in slantwise fashion in sloping frontal zones. The sloping upglide and downglide motions may be forced by externally applied pressure gradients, or they may be a response to symmetric instability, or conditional symmetric instability. Such instability can develop under certain special conditions in sloping zones of temperature gradient, and would lead to spontaneous overturning on slanted mesoscale surfaces. The possible role of symmetric instability in organizing the convection in two MCCs will be explored in the thesis.

On a smaller scale, Lemon and Doswell (1979) described the evolution of the supercell thunderstorm in direct analogy to the occluding extratropical cyclone. Rotunno and Klemp (1985) extended the analogy to describe the interaction of ambient wind shear with the updrafts and downdrafts of the supercell. We explore the relevance of the supercell, with its component mesocyclone, to the structure and evolution of the meso–α–scale occluding convective system.

A conceptual model of the two–dimensional mesoscale convective system organized around a squall line has emerged in the last 12 years, and has been tested against numerical simulations and field observations. From the evidence of four of the cases studied here, we present a three–dimensional conceptual model of the mesoscale convective wave–cyclone evolving towards an occlusion. Some systems do attain the stage of occlusion while others do not; the reasons for this will be discussed. Finally, we discuss the probability of occurrence of excessive rainfall that may cause flooding, strong sustained winds, hail and other severe weather in certain regions of vortical mesoscale rain systems.

Chapter 2

SURVEY OF RELEVANT RESEARCH

Previous and ongoing research in three areas is summarized in this chapter: patterns of organization of convective storms within mesoscale rain systems; the process of occlusion on different scales; and the mesoscale convective vortex. Previous studies of those convective systems to be examined in later chapters are also introduced here.

2.1 Modes of convective organization in mesoscale rain systems

Before the concept of the mesoscale convective complex was introduced by Maddox (1980), Clark et al. (1980) classified convective systems that produce heavy rain according to the size and shape of the cloud shields on enhanced infrared satellite images. Two of their sub–types appear to describe those mesoscale convective complexes that are not squall lines and that are in a dynamically weak environment: their "mesoscale quasi–tropical circulation pattern", and their type III pattern of wedge–shaped systems.

The strongest convective activity was most often noted in the right rear quadrant. The strongest activity in the composited MCC of Maddox (1981) was also located in its right rear quadrant, and occasionally was oriented on lines parallel to the movement of the system. This may result from the tendency of an MCC to propagate along an existing front.

Upon examining the radar patterns and rawinsonde data of 21 MCS observed in the PRE-STORM experiment, Blanchard and Watson (1986) grouped them into three categories of organization. The convective line category included 48% of the systems, nearly all of which had a stratiform cloud. "Random" outbreaks of convective cells, and cells embedded in stratiform echo, constituted 24% of the cases. In the third category they put MCS with some evidence of rotation, either an occluding pattern of convective

echo, or a vortical pattern in the stratiform echo or the remnant clouds. This category also had 24% of the cases. Thus, the two prototypes of interest to us were observed to occur as often (48%) as the prototype of the convective line with stratiform echo.

Bluestein and Jain (1985, 1987) classified both severe and nonsevere squall lines in the three spring months in Oklahoma according to four modes of convective development. In the broken line mode, a line of discrete cells merges into a solid line; in the back building mode, new cells periodically develop upstream of older cells. Their two modes of interest here are the "broken areal" mode, in which an amorphous area of cells is transformed into a solid line, and the "embedded areal" mode in which a convective line forms within stratiform precipitation. Both of these latter modes of MCS formation were observed in our cases. These authors focused on systems with convective lines at some point in their lifetime, so that some MCCs, particularly those with chaotic patterns of convective clusters, would have been excluded.

They found fewer differences among the synoptic environments than one would expect. The broken areal systems were the type most frequently observed at night. The convective inhibition (CIN) parameter, a measure of the negative buoyancy of a parcel beneath the level of free convection, was significantly lower for broken areal systems than for broken lines. Not surprisingly, severe squall lines grew in environments of higher convective available potential energy (CAPE) and lower CIN than the nonsevere lines. Both severe and nonsevere lines tended to be aligned along the low–level shear, which was large in magnitude, and 30° to 50° to the left of the shear above 7 km. This tendency was also observed in the case studies in this thesis.

McAnelly and Cotton (1986) studied the internal organizing process of large MCCs that developed in the High Plains during an eight day episode, the chronology of which was described by Wetzel et al. (1983). Their thunderstorms were localized in meso–β–scale clusters or bands, which originated on larger meso–α–scale axes such as mountain ranges or hills, fronts, pressure troughs, dry lines, or outflow boundaries produced by earlier rain systems. Confluent flow at 700 mb tended to aid the merging or interacting of clusters, and when they did merge, the α–scale system developed apace. The best

development occurred where two of these large scale axes intersected. Decay of the MCCs was associated with divergent movement of the β–scale clusters. Western MCCs had meso-β clusters configured in a more chaotic fashion than the eastern MCCs located in the upper Mississippi valley, except that steady–state convective bands tended to form parallel to active cold fronts, and squall lines formed when the vertical wind shear was strong. Finally, the largest MCCs propagated discretely, about twice as fast as their meso–β–scale components.

In extending a masters thesis by P. Dodge at the University of Washington, Houze et al. (1989) classified radar echo organization, environments and the severe weather of six years of spring rainstorms in Oklahoma. The storms were classified by their degree of fit to a prototype of a leading convective line with trailing stratiform echo, from "strongly" to "weakly" classifiable to "unclassifiable". They were also ranked by their degree of symmetry. Only 14 of the 63 cases strongly resembled the leading line prototype, while fully *one–third* were deemed unclassifiable because of a lack of resemblance. All systems, whether classifiable or not, were equally likely to have produced severe weather, but damaging hail was much more frequent with the unclassifiable systems. The MCC, as originally defined by Maddox (1980), was a subset completely contained within the set of major rain events, but only one–fourth of the major rain events met the stringent criteria for an MCC. There was a slight tendency for the MCCs to exhibit unclassifiable structures. Elsewhere these authors employ the term "chaotic" to describe the organization of the unclassifiable rainstorms, analogous to the "random" category of Blanchard and Watson (1986), and to the description of most cases in this thesis as evincing "random" or "chaotic" patterns of convective echo.

In their survey, unclassifiable storms had larger shear magnitudes, and more unidirectional shear, than the classifiable line-type systems. This contrasts with the finding of McAnelly and Cotton (1986) that chaotic systems exhibited lower Richardson numbers, and cooler temperatures at the surface. The latter authors found that such systems tended to develop more often in the western High Plains, where a drier subcloud environment favored more intense downdrafts and associated outflow boundaries. The western systems

also contained more of the meso–β–scale convective cores, therefore, more outflow boundaries on which new convective cells could develop in the manner suggested by Purdom and Sinclair (1988).

The hypothesis that a stable boundary layer may be the important factor in allowing the convective echo to develop chaotic patterns, was advanced earlier by Fortune and McAnelly (1986) although they did not evoke downdrafts as a reason. They contrasted the organization of convective echo in a slow–moving MCC on a frontal wave with that in a rapidly moving MCC that propagated discretely. In the latter system, which is also studied as "system C" in this thesis, new cells and clusters formed in chaotic patterns, then merged into larger clusters which generated stratiform cloud. The region of new developing cells propagated faster than any of the echo did, and faster than the wind at any level beneath 200 mb. The rapid and chaotic appearance of new cells was thought to be due to a rapid recovery of convective instability in a layer decoupled from a surface layer stabilized by previous MCCs. Reasons for this will be discussed in Chapter 9.

Zipser (1977) described and depicted the source and nature of downdrafts in mesoscale rain systems that stabilize the environment in their wake. The shallow stable layer of cool air was shown to flow out from convective downdrafts in rainfall sufficiently intense to keep the downdraft air saturated. The warm, dry, well–mixed layer above the stable layer, and separated from it by a pronounced inversion, was shown to originate in downdrafts sinking gently beneath the widespread, high–based stratiform cloud, in light rain; the rainfall rate was not sufficient to saturate the air. This profile of a dry, mesoscale unsaturated downdraft atop a nearly saturated, cool layer at the surface, is depicted in Fig. 2.1 and was termed an "onion" sounding from the general shape on the figure. The unsaturated gently sinking air is in the widest part of the onion shape, the "bulb"; the saturated surface air is in the "root" portion, and the stratiform cloud is in the "stem".

2.2 Research on MCCs similar to those investigated in this work

Some features of the MCCs chosen for study in this thesis have been analysed previously or simultaneously by others. The studies are reviewed briefly in this section, and discussed further in later chapters together with results of this author.

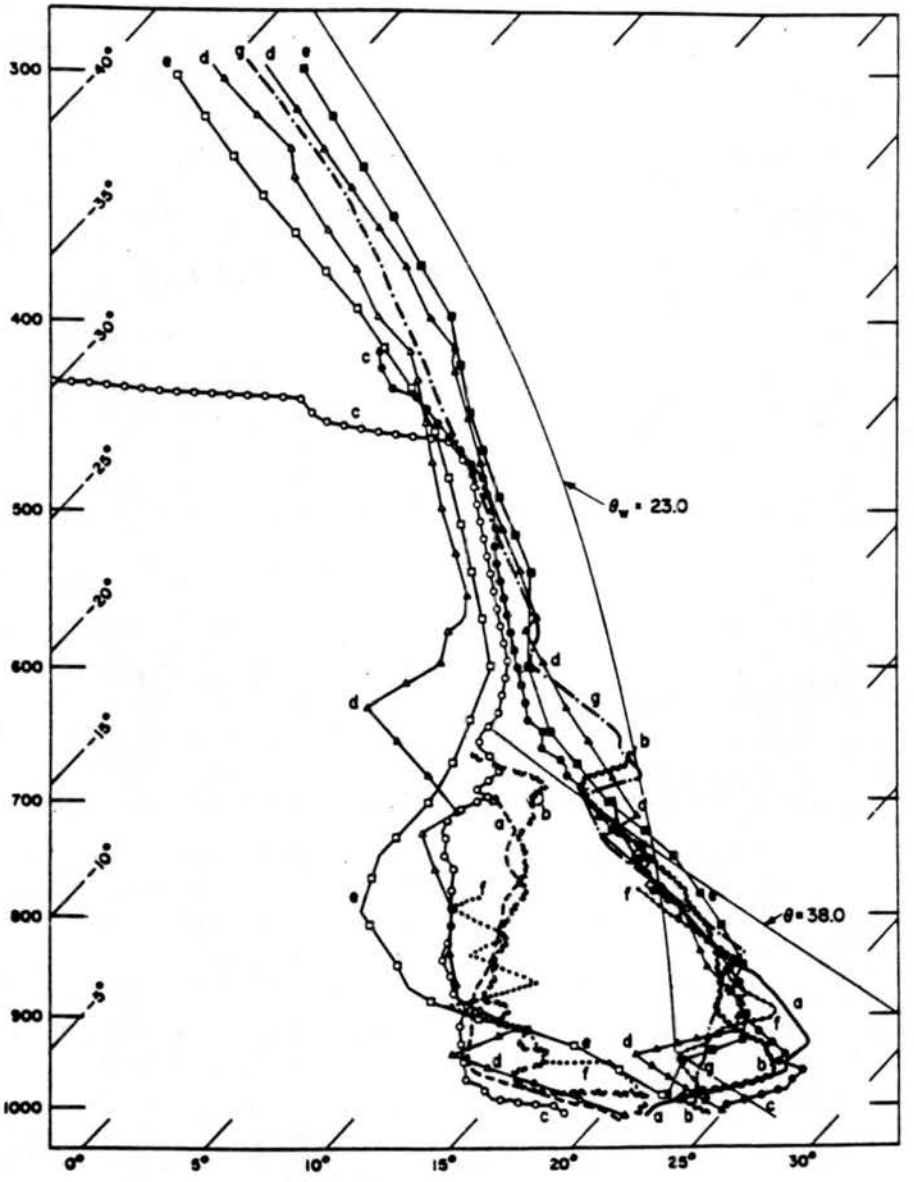

Figure 2.1: Characteristic soundings of temperature and dew point in regions behind squall lines. From Zipser (1977).

A two–part study of an MCC that occurred in the episode on 3, 4 June 1985 ("system B" in this thesis) was presented by Smull and Augustine (1989), who noted that the pattern of convection evolved from "extremely irregular" in the formative stages to a pair of convective bands that intersected in an "open–wave" pattern at maturity. Analysis of soundings showed convergence coinciding with the bands in low levels, but centered in the stratiform region northwest of the apex of the open wave, in mid levels. No evidence of rear–to–front inflow was seen behind the strongly convective north–south line, although such inflow existed in the stratiform region. Their dual–Doppler analysis illustrated dissimilar structure in the two convective bands. The north–south line had a multicellular structure and some properties of a squall line. The broader, east–west band lacked a gust front and cellular structure, but was organized on the meso–β–scale. The formation of the rear inflow was attributed to stratiform processes because it occurred just beneath the stratiform cloud base and far removed from the convection. The same structure was reported for this MCC by Leary and Bals (1989), who also reported a secondary band of convection parallel to the east–west band but located within the northern stratiform region.

Precipitation that fell in this same MCC was reported to be 63% convective and 37% stratiform by Meitín and Watson (1989). The rate of convective rainfall peaked twice (also reported by McAnelly and Cotton, 1989), with the first peak occurring $7\frac{1}{2}$ *hours before* the stratiform rainfall peaked. When the latter did peak, during the decay phase of the MCC, maximum ascent was found at 300 mb and within the stratiform cloud, above the zone of maximum descent at 700 mb.

The surface pressure features of this much–studied MCC were analysed by Stumpf (1988). Unlike the northern half which was largely stratiform, the southern half of the system did not develop surface meso–highs or wake meso–lows. Their location in the northern half suggested that the circulations within and beneath the stratiform cloud produced the wake low. Pressure gradients between high and low attained values up to 2 mb per 10 km, capable of causing sustained strong winds on the surface.

Rockwood et al. (1984) reported a dual MCC which was not studied in this thesis but which shared remarkable similarities to our prototype. Two MCCs propagated along a well

defined stationary front through eastern Kansas and Missouri. An intense, meso–β–scale *surface* cyclone developed on the outflow boundary of the first system (which replaced the front), and just *ahead* of the gust front and meso–high of the second MCC. Hail, wind damage and heavy downpours of rain were associated with this feature. The cyclone grew to meso–α–scale proportions over the next 6 h as it tracked into Missouri, and large hourly rainfall accumulations accompanied the progression. Their Fig. 33 showed a bow–shaped, or comma–shaped convective echo in the meso-low. Flash flooding in Missouri was caused by torrential rains from the second MCC falling on saturated soil 6 h after heavy rainfall fell from the first system.

Brandes (1989), Verlinde and Cotton (1988) and Houze et al. (1989a) examined the development of mesoscale cyclonic vortices in three MCCs that occurred on 7 May, 17 June, and 28 May, respectively, in the PRE–STORM program. Their work is discussed below in Section 2.4 and evaluated in later chapters.

2.3 The occlusion process on different scales

The process of occlusion has been observed on scales both larger and smaller than the mesoscale rain system. The development of the larger scale extratropical cyclones towards a stage of occlusion is still an active topic of observation and modelling. The leading conceptual models are here summarized with an emphasis on the conveyor belt approach. One mesoscale phenomenon that may or may not involve an occlusion process is the "polar low", lately receiving more attention. Finally, something like an occlusion has been observed in the supercell thunderstorm, near the lower bound of the meso–β–scale.

Conceptual models of the passage of airstreams having different origins and properties through midlatitude cyclones has been summarized by Carlson (1980). The distinct airstreams were identified by following trajectories on surfaces of constant θ in dry air, but on surfaces of constant wet bulb potential temperature θ_w in cloud. Three major airstreams were described. Air in the *warm conveyor belt* originates in low level easterly flow in subtropical latitudes, flows poleward into the cyclone, attains saturation near the warm front where it ascends rapidly in precipitating cloud, and exits with the upper level

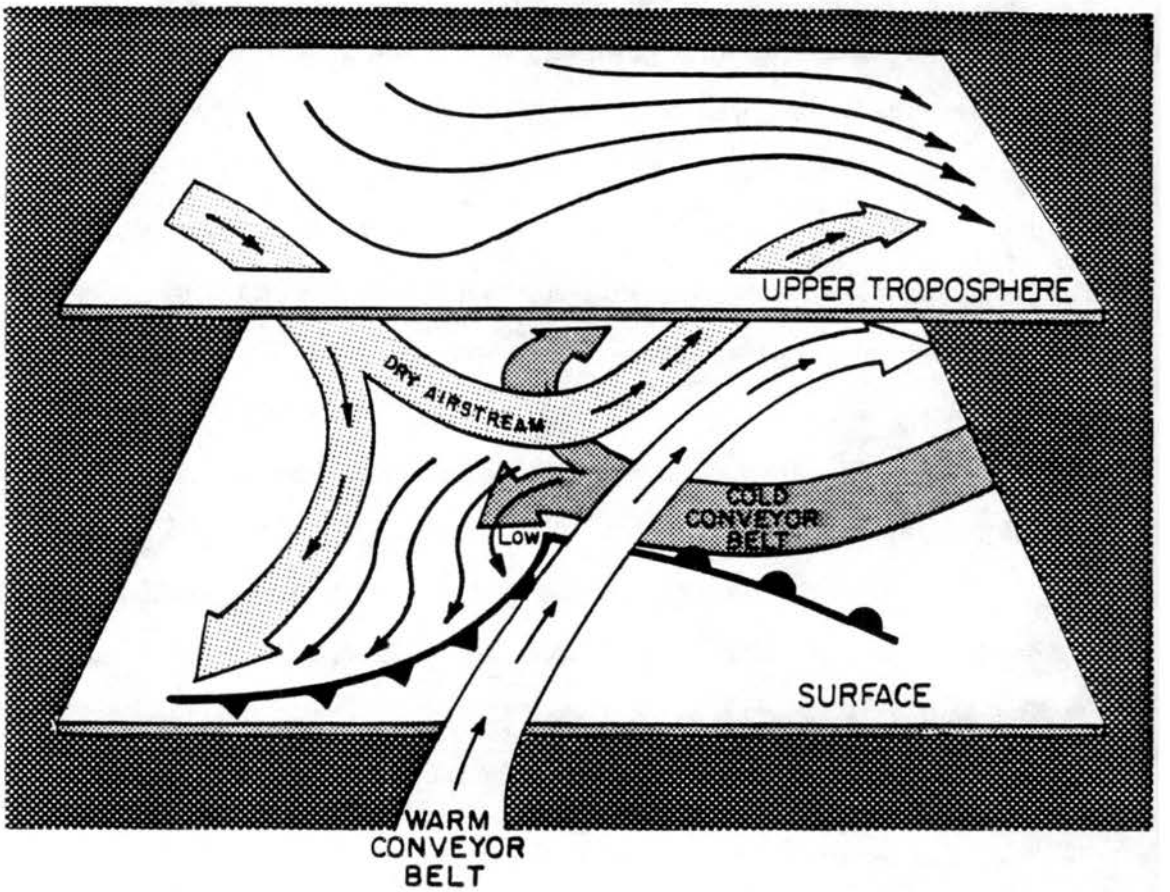

Figure 2.2: The arrangement of three conveyor belts of airstreams within an extratropical cyclone. From Cotton (1989).

anticyclonic flow near the ridge. The properties of the warm conveyor belt were much discussed earlier by Browning (1971), Browning and Harrold (1970), and Harrold (1973).

A diagram reproduced from Cotton (1989) may help to visualize the 3 conveyor belts (Fig. 2.2). Air in the *cold conveyor belt* originates in low level polar air in the anticyclone east of the disturbance, and flows into the cyclone from the east, underneath the warm belt, where it is saturated by rain falling from above. Then it begins to ascend rapidly and cyclonically in deep precipitating cloud under the jet streak, then turns sharply to exit as mid–level flow under the jet stream. The low and middle level clouds that form the "head" of the comma pattern north and west of the cyclone are in the cold conveyor belt. Finally, a dry airstream (to be called here a *dry conveyor belt*) originates in the upper troposphere in the ridge *upstream* of the disturbance. It descends from upper levels to approximately 700 mb as it flows from the ridge to the trough. The western portion flows

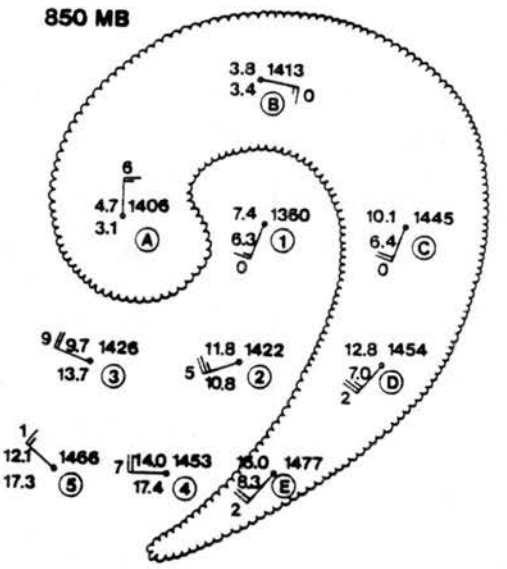

Figure 2.3: Representation of a comma cloud with the ten zones used to composite data with respect to the system. From Carr and Millard (1985).

equatorward anticyclonically. The eastern stream begins to ascend after it passes through the trough. The confluence of this dry air with the western edge of the warm (and moist) conveyor belt produces a sharp edge on the cirrus cloud shield that is so prominent on satellite images of developing cyclones. A similar confluence is seen at mid levels, north of the disturbance, between the dry stream and the cold conveyor belt. Ludlam (1980) has analyzed the diffluent, descending trajectories in the upper level frontal zone and the dry airstream.

Carr and Millard (1985) composited data for wave cyclones just before and after the occlusion process, with respect to the comma cloud on satellite images. The ten regions of compositing are shown on Fig. 2.3. The circulation center was located on the eastern side of the comma head at low levels, but on the southern edge at mid levels, and it tilted to the southwest with height. The circulation was closed up to 400 mb. The upper cold front, which separated the dry airstream from the warm conveyor belt, sloped *downstream* with height. The advection of low–valued θ_e air over the moist boundary layer increased the convective instability there, in the zone between the cold front at the surface and the front aloft. Indeed, the region most likely to experience severe weather was zone D (Fig. 2.3); zones 1 and C destabilize during the day and also experience severe weather.

Businger and Walter (1988) flew the P–3 aircraft in mesoscale comma clouds in the Gulf of Alaska. Several comma clouds which developed in a cold core trough consisted of bands of cumulonimbus oriented 60 to 75 km apart, along the wind shear in the cloud layer. They investigated whether conditional symmetric instability (CSI) or wave–CISK could have organized the convection this way. In favor of CSI, the atmosphere was nearly neutral to slantwise displacement, and the bands did not propagate faster than the mean wind. But the bands were cellular, not continuous lines of uniform ascent. Symmetric instability still could have drawn potentially unstable air into symmetric rolls, where the instability would have been released convectively. Wave–CISK was ruled out because the bands did not propagate with respect to the mean wind.

The conveyor belt model was invoked by Whitaker et al. (1988) to describe some of the processes of rapid deepening of a cyclone in the Presidents' Day snowstorm. In their simulation, the three belts converged in the rapidly developing, low level cyclone as they passed through a region of maximum potential vorticity. The absolute vorticity increased primarily through stretching associated with the convergence below 700 mb. Vertical advection of vorticity then extended the vortex to the middle layers. Large divergence of mass in all airstreams near 500 mb, northeast of the developing cyclone, acted to deepen and propagate the surface low. The simulated phase of rapid development occurred when stratospheric air with high potential vorticity propagated in the dry conveyor belt downward and eastward, and arrived over the region of low level vorticity. The superposition of both regions of high potential vorticity permitted explosive increases in absolute vorticity. Referring to Hoskins et al. (1985), they added that each region would reinforce the vorticity in the other region as long as the lower level vortex remains a bit downstream of the upper vortex. The reasoning is equivalent to that of Peterssen (1971) for "Type B" cyclogenesis.

Satellite images of a rapidly deepening cyclone over England gave evidence for these conceptual models (Young et al., 1987) The development of "baroclinic leaf" cloud masses and dry slots was interpreted as an intrusion of a dry airstream with high potential vorticity into a warm conveyor belt. Inasmuch as the baroclinic leaf precedes the formation of

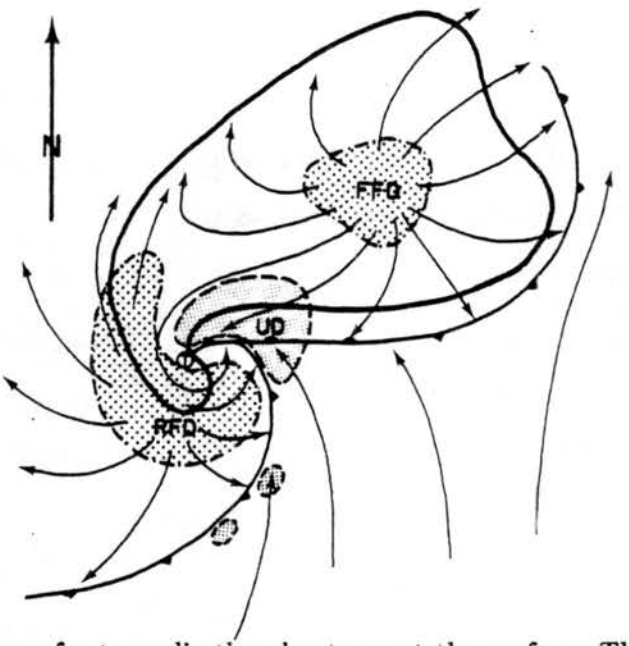

Figure 2.4: Plan view of a tornadic thunderstorm at the surface. The gust front and occluded wave are depicted with frontal symbols; the updraft (UD), forward flank downdraft (FFD), and rear flank downdraft (RFD) are stippled. The circled T locates the tornadic mesocyclone. From Lemon and Doswell (1979).

the dry slot by some 10 hours, these observations were shown to have forecasting value for explosively deepening ("bomb") cyclones. The zone of very low relative humidity associated with probable stratospheric air within a jet streak was also visible on water vapor imagery long before the zone began intruding into the future comma–shaped cloud mass.

Others have described the evolution of mesoscale precipitation areas within larger cyclonic disturbances. Three types of such rain areas were found by Atkinson and Smithson (1978) in a frontal wave on a warm front in England: one was linear and parallel to the front; a second was linear and normal to the front; and a third was amorphous and propagated through the front. The linear rain areas were comprised of 3 to 4 smaller rain areas whose velocities and lifetimes determined the behavior of the large areas. The small area convection originated in potential instability between 500 and 600 mb released by large scale lifting.

A model of the tornadic supercell which resembles an occluding cyclone but on the meso–γ–scale has been advanced by Lemon and Doswell (1979) and depicted in Fig. 2.4. In addition to the main downdraft on the forward flank of the main cell, they propose

that another downdraft develops on the rear flank where mid–level flow is blocked by the main updraft. Convergence is enhanced at the junction of the outflows of the two downdrafts, and vorticity is generated on the boundary between the updraft and the rear flank downdraft. The boundary forms like an occlusion, with a mesocyclone at its apex, where a tornado may or may not form. Lemon and Doswell modified the notion of a mesocyclone as a rotating updraft ; in their depiction the cyclone becomes divided, with strongly cyclonic updrafts in one half, and cyclonic downdrafts in the other half. The source region of these rear downdrafts is dry air from upstream from 7 to 10 km in height. When it reaches the surface, this air is drier, colder, and less filled with rain than the air of the forward downdraft. It thus interacts more vigorously with the warm inflow air than the forward downdrafts.

The contrast between the properties of the rear downdraft and the updraft was a key element of Rotunno and Klemp's (1985) modification of the conceptual model of a supercell. The contrast leads to baroclinic generation of vorticity, strongest in the lowest levels, along the gust–front boundary between them. The updraft then tilts this horizontal vorticity into the vertical. Eventually, the low level rotation around the apex of the occlusion exceeds the middle level rotation in the divided parent mesocyclone. A cyclostrophic low pressure zone is found in the center of a rotating updraft. Thus when the rotation becomes faster in the low levels, a pressure gradient directed downward into the low level occluding vortex becomes established. According to Klemp and Rotunno (1983), this downward force retards the updraft in the vortex, and *drives* the rear–flank downdraft.

This view is fundamentally different from Lemon and Doswell's (1979) conception and ascribes only a passive role to the mid–level mesocyclone. That role is to transport potentially cold air to the forward left flank where it descends in the saturated, forward flank downdraft. There, the cold pool interacts with the updraft to tilt the horizontal, baroclinically generated vorticity into cyclonic vertical vorticity near the occlusion. Then the cyclostrophic reduction of pressure in that vortex induces rear flank downdrafts, as described in the previous paragraph.

2.4 Mesoscale convective vortices

Evidence for mesoscale vortices in some of the longer lasting convective systems has accumulated over the last ten years. It was earlier observed that tropical squall lines (which would now be called mesoscale convective systems) develop centers of cyclonic vorticity, if not necessarily closed cyclones. Such a center was seen at 650 mb in composited relative winds in the rear of an oceanic squall line by Gamache and Houze (1982) and in the mid–level winds computed from cloud motions around a continental African squall line by Fortune (1980). Both systems were observed during the GATE experiment in 1974.

Johnston (1982) reported 26 cases of comma shaped patterns and apparent mesoscale vortices in the satellite images of dissipating MCCs in the United States. Analysis of cloud motion wind vectors in some of them confirmed the presence of cyclonic vorticity centers. All cases were located in anticyclonic wind shear in high levels and near the moisture axis in low levels.

Ogura and Liou (1980) reported that a squall line in 1976 displayed a maximum of vorticity in middle levels. Radar depictions of a chain of comma–shaped echoes in the same system by Smull and Houze (1985) suggested that the vortex decayed into smaller vortices with time.

Soundings were composited for the long lasting convective complex which caused the disastrous flash floods in Johnstown, PA in 1977. There was a mesoscale cyclonic circulation in the relative wind field which was stronger and more extensive with height, up to 500 mb (Bosart and Sanders, 1981). It was in thermal wind balance with cold anomalies below that level. The pattern of strong cyclonic vorticity in middle levels within 150 km of the center, beneath intense anticyclonic vorticity at the tropopause, was likened to the structure of tropical cyclones.

A banded structure was observed in the stratiform echo of another MCC at the mature stage by Leary and Rappaport (1987). The rainbands were weak convective features at least 50 km long and up to 50 km wide. The center of curvature of the rainbands was correlated with an apparent vorticity center at 600 and 500 mb in the relative winds

obtained from conventional soundings. This suggested that the mesoscale circulation of the MCC interacted with the fine scale pattern of precipitation.

In a study of still another MCC observed in PRE–STORM, Johnson et al. (1988) correlated the intensification of a mid–level vortex with the collapse of a cold pool and the rapid transformation of a surface meso–high into a meso–low, when stratiform rain ended. The authors attributed the transformation to a total collapse of the cold pool, evaporation of all precipitation, and subsequent adiabatic warming and hydrostatic lowering of surface pressure. They reason that sustained inflow in mid–levels spun up cyclonic vorticity which already had been present along a shear line. Then the cyclone intensified even more when the cold pool collapsed beneath it.

Dual Doppler analysis of a meso-β multicellular complex that was a building block of another MCC in PRE-STORM (17 June) revealed a couplet of deep vortices smaller than those discussed above (Verlinde and Cotton, 1988). The cyclonic vortex was only 40 km across, at best, strongest at the height of 6 km, but it extended from 3 to 11 km and perhaps more; thus it extended through the depth of the cloud. The tilting of horizontal vorticity into the vertical contributed most to its growth; during its decay it appeared to be breaking into smaller vortices.

With single Doppler radar Stirling and Wakimoto (1989) also observed trains of these smaller (50 km) vortices in the stratiform cloud. They were associated with "hook" echoes with weak centers of reflectivity, apparently caused by inflow of dry air from above 5 km.

Other observations of mesoscale cyclogenesis in convective systems include: a mid level vortex on the rear edge of a stratiform region of another MCC in PRE-STORM (28 May), observed in dual Doppler wind fields by Rutledge and Houze (1989), and in single Doppler data with color depictions by Houze et al. (1989a). The circulation was seen in system-relative winds from 2 to 8 km in height. Brandes (1989) documented the evolution of a mesoscale convective vortex very well with supplemental rawinsoundings and dual Doppler scanning. This vortex grew to be quite deep (through the entire troposphere) extensive, and persistent, and it was associated with a remarkable comma shaped cloud. This MCC (7 May 1985, in PRE-STORM) is analyzed more extensively in chapter 7.

In addition to the above studies of individual cases, some compositing studies have supported the generality of mid level cyclonic circulation in MCCs. Composited results of 134 MCCs from eight years are discussed by Cotton et al. (1989). Weak positive vorticity existed only in the 700 to 900 mb layer of the composite, although the vorticity definitely increased from early to final stages in all levels from 700 to 350 mb. The systems developed in large scale anticyclonic flow which masked the evolving mesoscale positive vorticity in the composited average.

The typical MCC developed downstream of a trough of a weak short wave at 500 mb, according to Maddox (1983) who composited synoptic soundings for 10 cases. As the MCC matured and decayed, the trough intensified and became co–located with the system. The MCC grew in a precursor region of upward motion, a response *primarily to warm advection* rather than differential vorticity advection, despite the presence of the short wave. The MCC was found in a warm ridge at this level, and the temperature was never in good balance with the winds. Maddox also commented on the frequent appearance of comma clouds after the MCCs decayed.

Mesoscale numerical models have reproduced the warm core mesoscale convective vortex. In a three dimensional nested grid simulation of the MCC that led to the Johnstown flood, Zhang and Fritsch (1987) obtained a vortex 100 to 200 km in diameter, strongest between 850 and 700 mb, that extended to the surface and endured some 18 hours. It was initiated by ascent in a meso–α–scale short wave, in a nearly saturated environment with weak vertical shear and horizontal deformation. It was then maintained by latent heating in stratiform (resolvable) condensation in the low and middle levels; inertial stability acted to maintain the circulation in decaying stages of the precipitation system. The authors concluded that both deep convection with moist downdrafts and the mesoscale flow structure were necessary for the mesovortex to develop.

Another simulation of another MCC by the same model (Zhang and Fritsch, 1988a) highlighted the role of the vortex. Without explicit condensation resolved on the scale of the numerical grid, the model reproduced only a squall line but not the vortex. And without including the effect of moisture on virtual temperature and density in the ideal gas law, the model again failed to generate a warm core vortex and the MCC.

A mesoscale vortex clearly seen in satellite and radar imagery developed in Oklahoma in a benign dynamic environment, but with frontal forcing in low levels (Menard and Fritsch, 1989). The vortex became inertially stable in middle levels and persisted for 2 days in a regime of little wind, weak shear, and low CAPE. It was accompanied by local showers and depressed afternoon temperatures. Surface frictional convergence into the center and morning heating may have combined to initiate a new cycle of deep convection, which would have maintained the vortex against dissipation. Zhang and Fritsch (1988) report a simulation that reproduced much of the observed behavior of this MCS, including amplification of a meso–α–scale trough, the vertical profile of winds and vorticity, the near lack of movement of the vortex, and the distribution of rainfall. The vortex was nearly stationary because it seemed to be rooted in the low level deformation field that was also nearly stationary. A long–lived surface mesolow did not form in either the observations or the model. This was believed to be due to a pronounced tilt of the vortex downstream with height. In the simulation, the upward motion and vorticity fields in the MCS were out of phase with those in the front. The propagation of the MCS was attributed to this phase difference.

Tripoli and Cotton (1989a) simulated the origin of convective storms over the Rocky Mountains and their subsequent development into an observed MCC over the High Plains. The two dimensional simulation did not reproduce a mature MCC; rather it depicted the interactions of vertical circulations on the alpha, beta, and gamma mesoscales such that a complex of cumulonimbi generated a meso–α–scale wind system that resembled a nascent MCC. Two of their stages of MCC development are of interest here. In their stage 5, repeated and successive meso-β convective cluster circulations eventually heated up a core sufficiently so that the core slowly grew geostrophically to meso–α–scale. The cluster circulations grew and collapsed on 2 h time scales. When the clusters were growing, the convection was concentrated in a band in the core region; when the clusters were breaking down, the convection tended to spread over widely spread elements. Secondly, during their stage 6, radiative cooling of the top of the stratiform cloud, after the sun set, destabilized the upper troposphere, which led to a strong meso–β pulse of convection. It also

increasingly ducted the upward moving, convectively generated gravity wave energy back into the troposphere, into the incipient MCC. This had the effect of spreading the single meso-β core over several weaker convective clusters. The uplifting in randomly scattered clusters helped to project the latent heating onto the meso–α–scale. The simulated larger vortex gradually spun down around midnight in the absence of a low level jet. It was believed that a three dimensional simulation with a low level jet would have had the vortex strengthening through the night.

In sensitivity experiments designed to isolate the important dynamics, Tripoli and Cotton (1989b) found that the meso–α–scale orographic slope flow organized the geostrophic response to the convective heating. This response seemed slow and inefficient, since it was fighting the dispersal of convective heating in meso–β–scale gravity waves. Among the factors that aided the geostrophic response and protected the young system from being dispersed by the gravity waves, two stand out. The existing mountain / plains slope flow tended to focus mesoscale upward motion in a core area at the western edge of the low level inversion over the plains. The MCC could develop more easily in this core. Secondly, the cloud–top cooling at night tended to keep more gravity wave energy inside the MCC, as explained above, and aided an organized response on the scale of the cloud shield rather than the clusters.

The effect of nocturnal cooling on the rear inflow was modelled by Chen and Cotton (1988), who found that it strengthened both the mesoscale updraft and the downdraft, and thus the mid–level inflow. The unstated implication was that radiative cooling enhances the meso–α–scale cyclonic circulation, and thus improves the longevity of the MCC.

2.5 Life cycle of an MCC

In the original definition of a mesoscale convective complex, Maddox (1980) defined the initiation, maximum extent, and termination of a complex according to the measured area of its cloud top colder than certain temperatures on infrared satellite images of the storm system. The duration, size, and shape of an MCC were also defined by these temperature criteria and these stages of its life cycle. These three key stages were redefined

Table 2.1: MCC Life Cycle Classification. From Cotton et al. (1989).

Subperiod	Temporal Center of Period
MCC-12 h	10-15 hours before initial subperiod
Pre-MCC	3 hours before initial subperiod
Initial	IR cloud shield area colder than -54° C first exceeds 50×10^3 km^2
Growth	Mid-point between initial and mature subperiods
Mature	Maximum areal extent of IR cloud shield colder than -54° C
Decay	Mid-point between mature and dissipation subperiods
Dissipation	IR cloud shield area colder than -54° C goes below 50×10^3 km^2
Post-MCC	3 hours after dissipation subperiod

slightly and intermediate stages were added by Cotton et al. (1989) when they composited the properties of 134 MCCs. Their stages as defined in Table 2.1 will be used in our case studies. Note especially that the "mature" stage occurs when the cloud shield (colder than -54° C) attains its maximum area, and the "growth" stage is reached midway between "initiation" and maturity of a system.

The changes in the intensity, volume, and area of precipitation, both convective and stratiform in nature, were investigated by McAnelly and Cotton (1989) through the life cycle of MCCs. The peak rainfall intensities were observed about one hour after initiation; the peak volume was well centered in the mature stage; and the peak area of rainfall occurred about one hour after that. The authors proposed two additional stages of the life cycle. During the *mesoconvective* stage the cloud shield exhibits a unified, nearly circular appearance; this stage was found to begin when convective rainfall rates peaked, and to end when the rainfall covered the greatest area, and it lasted about four hours. In the stage of *thermal minimum* the central region of coldest cloud tops (< -63° C) reached its largest and coldest extent—usually one hour before maturity. As the evolution of vortical convective patterns and the flow fields in specific MCCs are studied in the following chapters, these life cycle stages are referenced in order to study the evolution in a standard time frame.

Chapter 3

DATA SOURCES AND PROCEDURES

3.1 The field experiment

A major field program was undertaken in May and June of 1985 to investigate the structure and dynamics of mesoscale convective weather systems. A collaborative effort of the National Oceanic and Atmospheric Administration (NOAA), the National Center for Atmospheric Research (NCAR), and at least ten university groups, the Oklahoma–Kansas Preliminary Regional Experiment for STORM–Central (OK PRE–STORM) was conducted in Oklahoma and Kansas with two goals in mind (Cunning, 1986):

- To test new instrument systems and sensing strategies, such as radar wind profilers and airborne Doppler radars, as part of a coordinated program of observation of mesoscale weather systems; and

- To begin investigations into the development of these weather systems, in order to focus the scientific objectives of the future STORM–I program.

Fifteen MCS formed in or passed through the observational network of PRE–STORM during the two months of the experiment. There were sixteen operational missions that utilized most of the observing systems; many missions were targeted at more than one convective system. An overview of these missions and of the observing systems can be found in the *Daily Operations Summary* (Meitín and Cunning, 1985). Overviews of radar data collection are found in Meitín (1987) and of aircraft missions in Meitín (1988).

Of these fifteen mesoscale systems, a subset of six MCS were chosen as candidates for investigation of vortical organization or development. These systems occurred on 7 May, 21 May, 16–17 June, and three systems on 3–4 June 1985.

3.2 Radar data and processing

Six surveillance radars of the National Weather Service (NWS) were especially equippe with digitizing recorders for this experiment as part of the Radar Data Processor (RADAP-II) program. The digitized data were used extensively in this study. Locations and ranges of these radars are plotted in Fig. 3.2. Data were recorded at range spacing (gates) of one nautical mile (1.85 km), at increments of 2° in azimuth and 2° in elevation angle. The lowest elevation angle (the so-called *base scan*) was used almost exclusively in this study. The digitizers converted the analog signal into sixteen discrete values, that correspond to 16 ranges of reflectivity (Sladewski, 1986). One radar, at Wichita, KS was also equipped with a high-resolution digitizer from the Hurricane Research Division (HRD) of NOAA. This digitizer, hereafter referred to as the "HRD", provided greater range and resolution, and operated more reliably and frequently, than the RADAP digitizer at Wichita. An unfortunate effect of the use of two types of digitizers is the appearance in this study of two different radar depictions.

All these radars, like most of the NWS radars outside the experimental area, also recorded scans on film in the traditional way. The microfilm depictions from five sites outside the PRE-STORM area were used to follow the evolution of systems that exited the experimental network.

3.3 Doppler radar processing

NCAR operated a pair of 5 cm Doppler radars northwest of Wichita for the experiment. The CP-3 radar at Nickerson, KS and the CP-4 radar at Cheney Lake are located in Fig. 3.1. Data from two common scanning modes were used in this study. In the surveillance mode, a radar scanned all azimuths around the site, in elevation steps that incremented at 0.8° at low angles and increased to 3.6° at elevations of 50° or more. In sector scanning mode, the two radars scanned the same region of sky by scanning sectors usually 90° wide in azimuth. The radars were synchronized within one second. Data were averaged over four range gates of 260 m each.

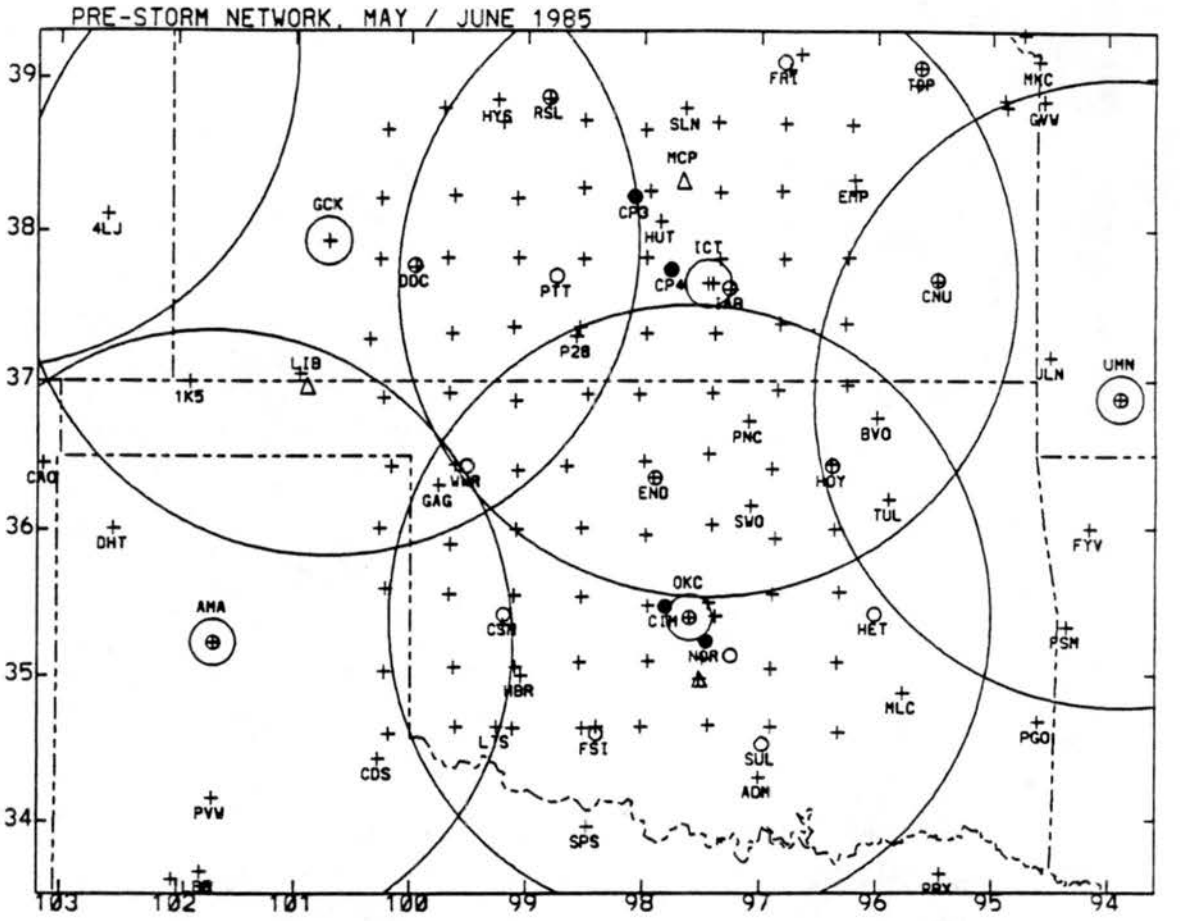

Figure 3.1: Station networks in the PRE–STORM experiment. Crosses mark the automated surface stations in the PAM and SAM networks; crosses with three letter identifiers mark observing sites at FAA airports; radars with digitizers are marked as in Fig. 3.2; Doppler radars are marked with black circles; rawinsonde stations are marked with small open circles; wind profilers are marked with triangles.

We used the NCAR Doppler data collected during the third MCC ("system C") on 4 June 1985, from 0800 UTC when the radars were powered up until 1115 UTC when the system was going out of range. All the chosen volumes were interpolated to Cartesian grids with the SPRINT / CEDRIC software described by Mohr et al. (1986) and Miller et al. (1986). Reflectivity maps at 1 km resolution were printed for every 20 min. of evolution. At two times dual Doppler synthesis of horizontal velocity fields were done; the first at 1020 UTC captured the convective core region of system C, at 1 km resolution. The second volume at 1040 UTC covered a broader region (the maximum observable) that included a large part of the stratiform echo; the horizontal resolution was 1.5 km, the vertical 0.67 km.

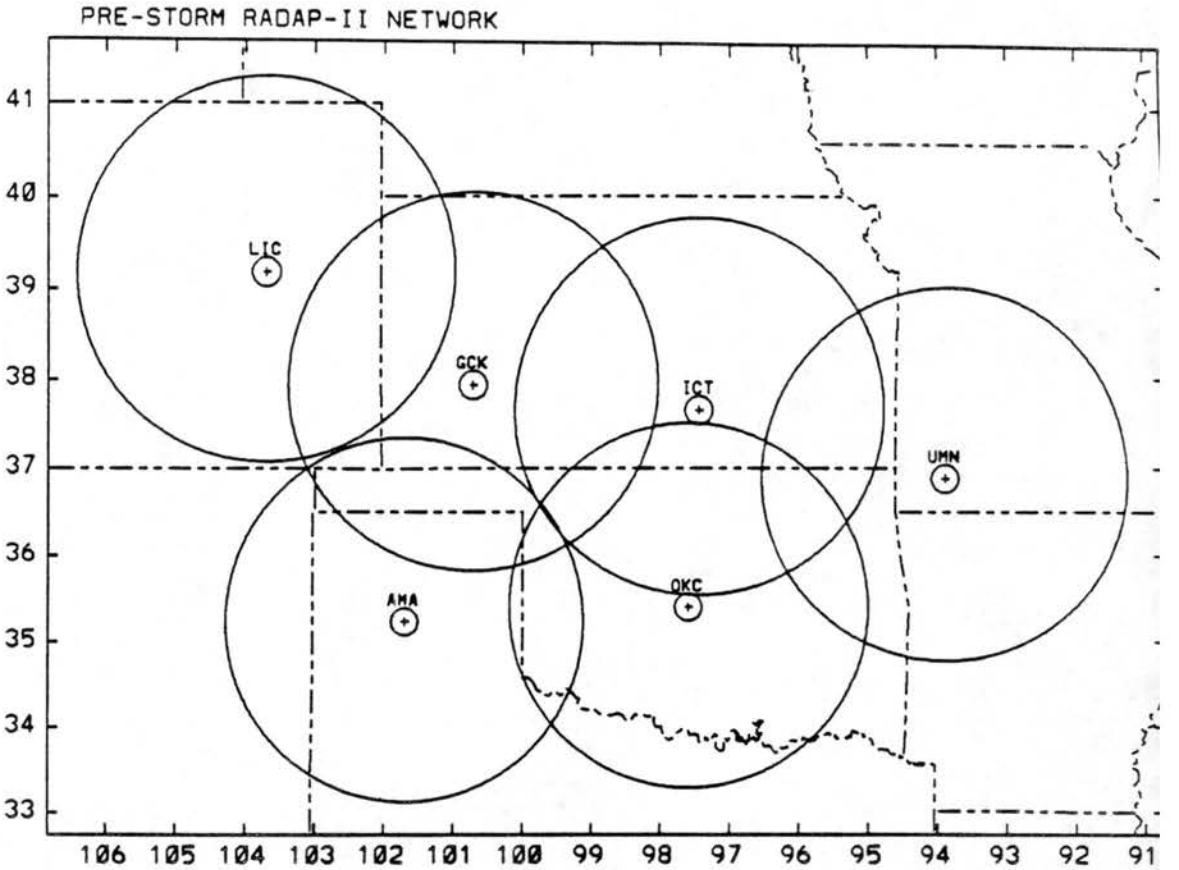

Figure 3.2: Locations and maximum range of the six National Weather Service radars equipped with RADAP digitizers for the PRE–STORM experiment.

Further analysis of the Doppler data started with the subtraction of a system motion of 20 m s^{-1} from 235° . The relative u and v components were then filtered by a least squares method within a radius of influence of 2 grid points (diameter of 3 km). The reflectivity data were smoothed horizontally, within a radius of only 1 grid point, in order to produce smoother displays than the raw data. Vertical velocity w was obtained from downward integration of horizontal divergence, from the highest level of of wind data at 11.7 km where w was assumed zero. Maps of relative wind vectors, divergence, vorticity, and vertical motion were displayed at several key height levels.

All data were then rotated into a reference frame with a new X–axis oriented along the direction of MCC motion (from 235°). Vertical cross sections of the new wind components u^*, v^*, and w^* were plotted along and perpendicular to this direction.

3.4 Satellite images

Copies of standard sectors of satellite images received at National Weather Service offices via LASERFAX facsimile were kindly supplied by the Weather Service. These images from the GOES satellite were usually available every half hour, and alternated between a visible image and an enhanced infrared image one half hour later. The cloud-top temperature criteria used by Maddox (1981) could be used with the enhancement applied to the images.

J. Augustine, of the Weather Research Program, NOAA, Boulder CO, had measured the cloud top area as a function of cloud top temperature, and the location and geometry of MCCs as part of an annual survey published regularly since 1980. He supplied the author with data beyond what appeared in Augustine and Howard (1988).

3.5 Surface analyses

Two sources of surface observations on different scales were merged in these analyses. Hourly observations at airports collected by the Federal Aviation Administration (FAA) provided synoptic–scale data at the locations marked with a cross (+) and a three letter identifier on Fig. 3.1. The special observations at these sites were also scanned for reports of significant weather in the MCCs.

A mesoscale network of automated surface stations was deployed for the experiment at the locations of the unmarked crosses in Fig. 3.1. The northern 40 stations comprised the Portable Automated Mesonetwork (PAM) of the Field Observing Facility of the National Center for Atmospheric Research (NCAR). The southern 40 stations had been in place for some time as the Surface Automated Mesonetwork (SAM) of the National Severe Storms Laboratory (NSSL). The stations, spaced an average of 50 km apart on a rectangular grid, recorded station pressure, temperature, wet bulb temperature, u and v components of the wind, and rainfall every five minutes. Data from the PAM and SAM meso-networks were combined but pressure data from FAA stations were not used because of uncertainty about their calibration (the temperature and wind data were used). The

fronts were positioned after subjective analysis of streamlines, convergence lines, pressure, temperature and moisture fields.

The dataset had undergone editing (in particular to correct a systematic error of wet bulb temperatures) before it was received for this study. The mesoscale analysis of pressure required attention to surface elevation, instrumental drift, systematic station errors, and the mixing of dissimilar data sets. The procedures of Stumpf (1988) were followed in his treatment of these errors in a thesis devoted to the "wake lows" and other pressure phenomena of system B. His station–specific pressure corrections applicable to the episode on June 3 and 4 were employed here. His method of reduction of station pressure to a common elevation of 480 m was also followed. Some of his analyses of system B served as input to the re-analyses exemplified by Fig. 5.9.

3.6 Atmospheric soundings

The operational rawinsonde network of the National Weather Service was supplemented by 12 sounding sites staffed by the military services during special missions. These launched soundings every 90 minutes or every 3 hr when called on to do so. The NWS and the supplemental sites are both located on Fig. 3.1 by open circles. Frequent supplemental soundings were taken during four of the six cases of vortical MCCs. For the principal episode studied, a ten hour series of soundings was initiated as system A exited the network; thus we did not devote much analysis to the upper air data of system A, but did so for system B which was well observed. System C traversed the Kansas portion of the network just after sounding activities were called off in that portion.

Three radar wind-profiling systems observed vertical profiles of horizontal wind from approximately 1.8 km above ground level (AGL) to, usually, some height above 11 km, at the three sites marked by triangles in Fig. 3.1. Data from Norman (NOR) was averaged over one hour intervals, while data from McPherson (MCP) and Liberal (LIB) were averaged over one half hour. Wind profiles were obtained in conditions of light rain and high wind, when balloons were often lost, but profiles in convective portions of storms were often too noisy to be useful.

Wind data from profilers and rawinsoundings were analyzed in three ways. Time–height sections of observed winds depicted evolution at a station, while hodographs depicted the vertical structure. Winds were also averaged in 0.5 km or 1 km layers for input to calculations of mean wind and mean shear in layers.

Temperature data were edited to remove spurious superadiabatic layers that were common in some of the soundings. Skew T–log p diagrams of temperature and moisture, with winds added, were extensively used. Further analysis of the thermal data included computation of the lifting condensation level (LCL) of parcels lifted from the surface or elevated levels, and the potential buoyancy of the parcels as calculated by Weismann and Klemp (1986). They suggested a bulk Richardson number, obtained by dividing the potential buoyancy by the mean shear from the surface to 6 km, which was also calculated.

3.7 Horizontal analyses

Profiler, rawinsounding, aircraft, and Doppler radar data were combined at appropriate times on surface charts and constant pressure level charts, with radar reflectivity overlaid. Some analyses were done at the 0° C level, the level of maximum wind, and the 300 m AGL level (which was chosen to be in the cool easterly air beneath a shallow front).

After the propagation of the mesoscale systems was estimated as a function of time (see below), system–relative winds were calculated and charted for certain levels and stages of the life cycle. Charts were prepared both manually and with the General Meteorological Package (GEMPAK) available at the Department of Atmospheric Science of Colorado State University. With GEMPAK some objective analysis of wind, vorticity, potential temperature θ and equivalent potential temperature θ_e was also undertaken.

3.8 Aircraft data

Two NOAA P-3 Orion aircraft were available to survey mesoscale convective systems in the near vicinity of convective regions or inside stratiform regions. Observations of wind, temperature and moisture from a variety of environments, including pseudo-vertical soundings as well as horizontal sections, were used in some of the cases. Care was taken

to use data only from straight-line, unaccelerated flight segments, and temperature data were considered reliable only if they came from a Rosemount sensor and its trend agreed with that observed by the (experimentally unproven) CO_2 radiometer. The range and accuracy of the meteorological parameters measured by sensors on board the P–3, and the computation of derived parameters, are described by Merceret and Davis (1981).

Both aircraft observed the storm structure with horizontally–scanning radars in the lower fuselage, and vertically scanning radars in the tail. The tail radars provided Range–Height Indicator (RHI) scans, but data from a sequence of such scans were combined into horizontal Plan Position Indicator (PPI) maps which had better spatial resolution than the PPI maps from the lower fuselage radar. One of the P–3 aircraft recorded Doppler radial velocity data from its tail radar. The data were mapped at the branch of the National Severe Storm Laboratory (formerly the Weather Research Program) of NOAA in Boulder, Colorado.

3.9 System propagation

The displacement of various features identifiable in the surface analyses, the radar echo maps composited from several radars, and the satellite images of the MCCs was measured. On the meso–β–scale, clusters of convective cores with at least some echo > 45 dBZ and surviving at least 90 minutes were tracked on radar maps. On the meso–α–scale, centers of high and low surface pressure were tracked, as well as intersections of thermal fronts and wind convergence lines that together defined an evolving wave pattern. The four features were followed long enough to provide alternative measurements of MCC motion.

3.10 Other

The occurrence of hail, damaging winds, flooding, and tornadoes was documented from reports in the Storm Data publication of NOAA.

Chapter 4

SETTING AND COMMON PROPERTIES OF AN EPISODE OF THREE VORTICAL CONVECTIVE SYSTEMS

4.1 Introduction

It has been noted that mesoscale convective systems often recur in episodes lasting several days during which excessive rainfall can occur (Wetzel et al., 1983). This chapter describes the setting of one such episode, when two of four such systems were targeted for intensive observation in the PRE-STORM experiment. We shall analyze three of the systems (denominated "A", "B", and "C") in subsequent chapters.

4.2 Synoptic Overview: surface

The MCCs propagated along a stationary front which anchored a zone of precipitation and convective weather lasting some 36 hours. The front lay parallel to and south of the Kansas/Oklahoma border, and curved through the southern Texas panhandle (Fig. 4.1). Thermal contrast was strong across this front, a difference exceeding 11 K. The southern air mass had dew point temperatures of 21° C; north of the front the cooler air had dewpoints around 18° C. The pattern of winds remained steady and convergent in this zone: east–northeast winds met winds from the south in the frontal zone; this wind pattern remained stationary as did a low pressure region over the Mexican plateau and New Mexico, and a subtropical high pressure over the Gulf of Mexico. This front remained just south of the zone through which the MCCs passed, but it underwent wave-like oscillations when systems B and C passed to the north (frontal wave cusps temporarily reconfigured its position). Then the front returned to a position like that before the episode, except 120 km farther north.

Another persistent feature is a separate trough of low pressure that extended from northeast Kansas through northwest Oklahoma and the Texas panhandle. Portions of this trough were analyzed on the national surface charts at 03, 06, and 09 UTC 4 June. The MCCs evolved in and co-existed with a local region of low pressure on this trough. By 1300 UTC the trough had returned to a configuration much like 9 hours earlier.

Wind shift lines focused low level convergence in this region. The front in Oklahoma was one such line, but storms did not develop along the front during this episode. Another prominent confluence line lay through northern and western Kansas during the interludes between the MCCs, parallel to and somewhat west of the pressure trough (so that the cool easterly wind blew through the trough). Unlike the surface front, these lines were preferred locations of new convective clusters.

Except for mesoscale effects, this pattern remained as described throughout the episode of the three MCCs from 1500 UTC 3 June to 1800 UTC 4 June 1985. After this period, the front crept slowly south and the precipitation spread into a wide band of overrunning cloud over most of Oklahoma.

4.3 Synoptic overview: upper air

The region in which the 3 MCCs developed and matured (hereafter called "the region"), that is, the PRE-STORM experimental network plus the Oklahoma and Texas panhandles, exhibited the highest mixing ratios observed in the continental United States during this period at 850, 700, and 600 mb. The moisture content, already elevated at 1200 UTC when the episode was about to begin, increased by one fourth in the next twelve hours at 850 mb. At these lower tropospheric levels, a stationary front with a well defined temperature gradient lay through the middle of the swath which the MCCs traversed, such that the active convective clusters were in the warmer air, but lay over a shallow layer of cool air some 300 m deep. Remember that this same front intersected the ground in northern Oklahoma, south of the affected region.

These features are seen in Fig. 4.2. The low level jet, between 920 and 800 mb, with speeds from 10 to 15 m/s, passed through the Panhandle region and terminated in this

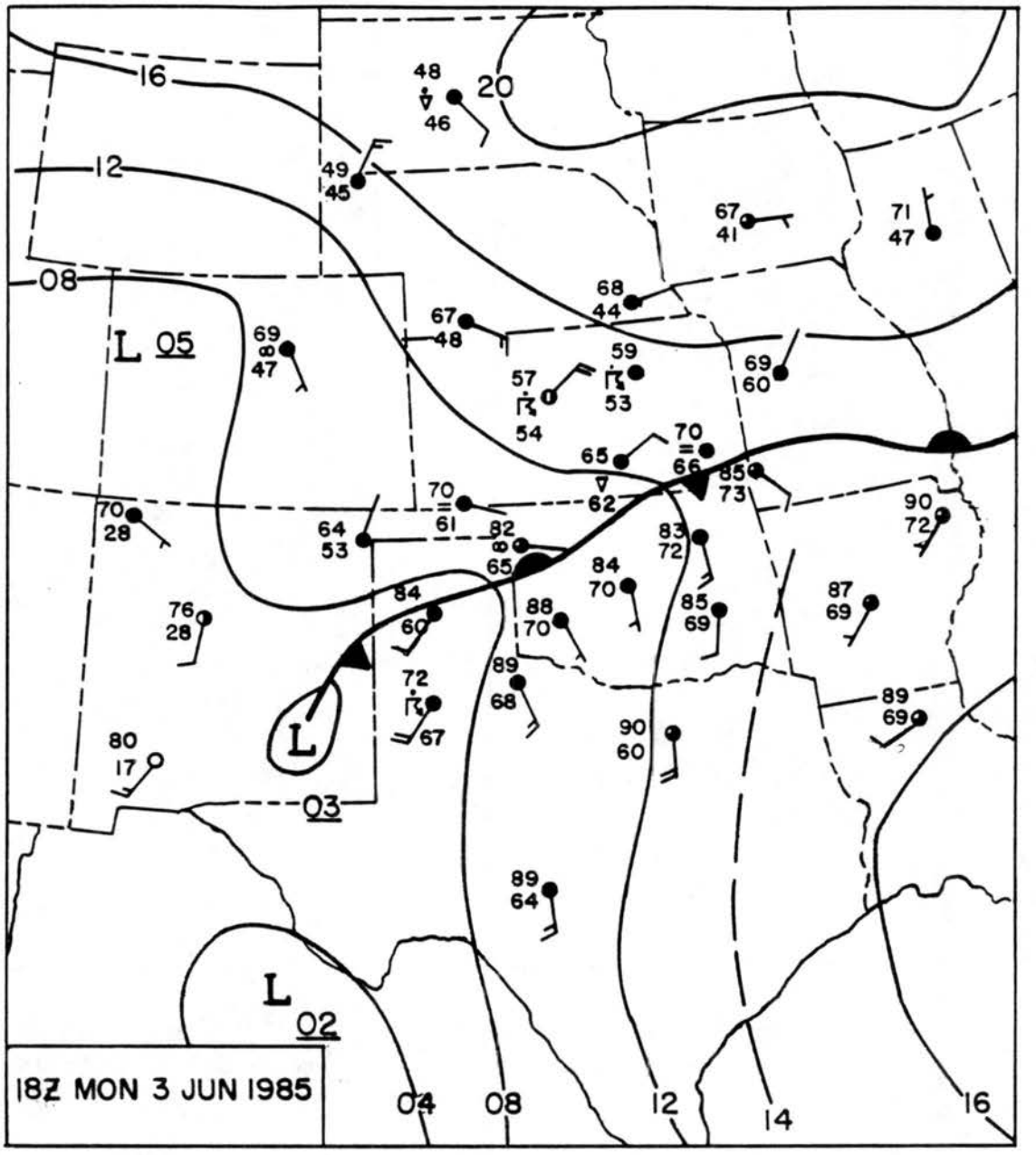

Figure 4.1: Synoptic surface conditions at 1800 UTC 3 June 1985, as the episode of three MCCs began.

frontal zone in central Kansas. The confluence and thermal gradient created warm air and moisture advection in this volume. Speeds in the low level jet increased some 50% in the 12 hour interval between panels a and b, when both systems A and B developed.

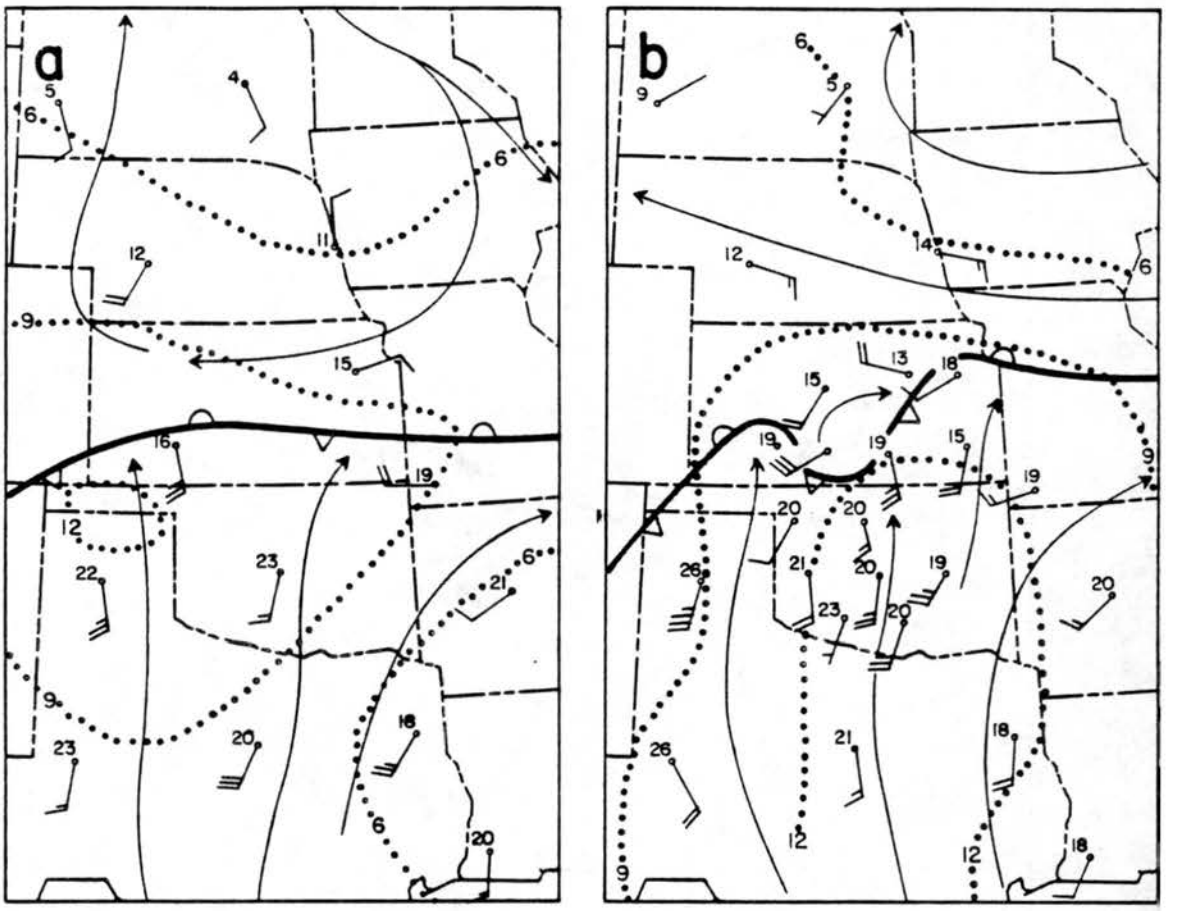

Figure 4.2: Synoptic conditions at 850 mb at (a) 1200 UTC 3 June and (b) 0000 UTC 4 June 1985. Wind and temperature (° C) are plotted conventionally; an upper level front is analyzed; streamlines (solid) and contours of mixing ratio (dotted) are added.

The entire episode occurred in anticyclonic flow at 500 mb and higher levels. The region of development remained in a geopotential ridge and an even more pronounced thermal ridge (Fig. 4.3). A cutoff cyclone was forming in western Arizona; on its eastern side a small jet with speeds up to 60 knots was found in New Mexico at 1200 UTC and just upstream of the MCCs 12 hours later. Another broad band of maximum wind stretched across the Dakotas, and Iowa. The same pattern was found at 250 mb as well (not shown). Cyclonic vorticity was concentrated in the developing cutoff trough at 1200

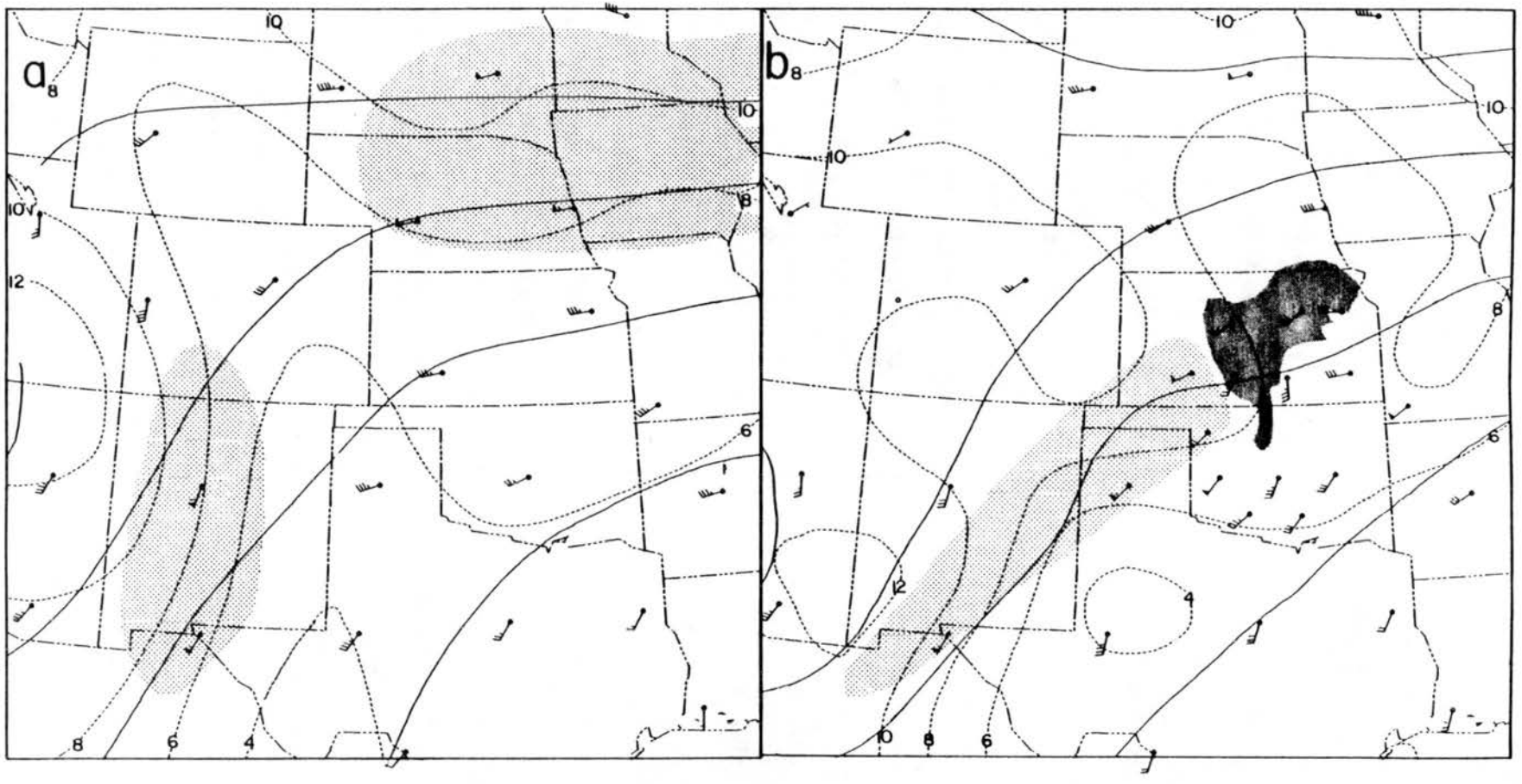

Figure 4.3: Synoptic conditions at 500 mb at (a) 1200 UTC 3 June and (b) 0000 UTC 4 June 1985. Wind is plotted conventionally and shaded areas have wind speeds greater than 50 knots. Geopotential height (solid) and absolute vorticity (dashed) are contoured, the latter in $10^{-5}s^{-1}$. The dark shading on (b) locates the precipitation echo of MCC 'B'.

UTC; advection of anticyclonic vorticity was occurring in the PRE-STORM region. By 0000 UTC a lobe of cyclonic vorticity could be seen in western Kansas, just upstream of an anticyclonic lobe in eastern Kansas. Both are believed to be effects of system B which affected some of the supplemental wind observations in the region under its influence in Fig. 4.3. By 1200 UTC 4 June as system C was departing, the region once again was under anticyclonic vorticity advection.

4.4 Environmental profiles

The MCCs traversed a region of gradients in both the east–to–west and south–to–north directions. Since a front lay through the region, we can speak of three regimes from south to north. A deep layer of conditional instability at the ground characterized the southern regime. All the severe weather reports came from the passage of a broken convective line that typically extended southward from the MCCs. The cores of the mesoscale convective systems, including the vorticity centers, traversed a second region where the frontal inversion separated a shallow layer of cool stable air on the ground from a layer of conditional instability aloft. The cool air was deeper in the third, northern regime where persistent stratiform rain characterized the weather as the systems passed.

From west to east, three regimes with different moisture content in the low levels were analyzed. Moisture content was lowest in the west where the storms initiated and began to consolidate. Moisture content was greatest in the broad lowlands through central Oklahoma and Kansas where the MCCs reached the mature stage. Low level moisture was not as great and the vertical shear was definitely reduced in the eastern regime where the MCCs declined in vigor.

A sounding representative of the southern regime in central Oklahoma is that of Enid (END) at 2110 UTC in Fig. 4.4a. In this midafternoon profile, a dry adiabatic layer extended from the surface to 780 mb, had on average mixing ratio of 17 g kg^{-1} in the lowest 100 mb, and was capped by a shallow inversion. Due to the deep moist boundary layer and perhaps to the elevated mixed layer from 570 to 470 mb, this sounding had the highest convective available potential energy (CAPE) in the episode. On mixing the

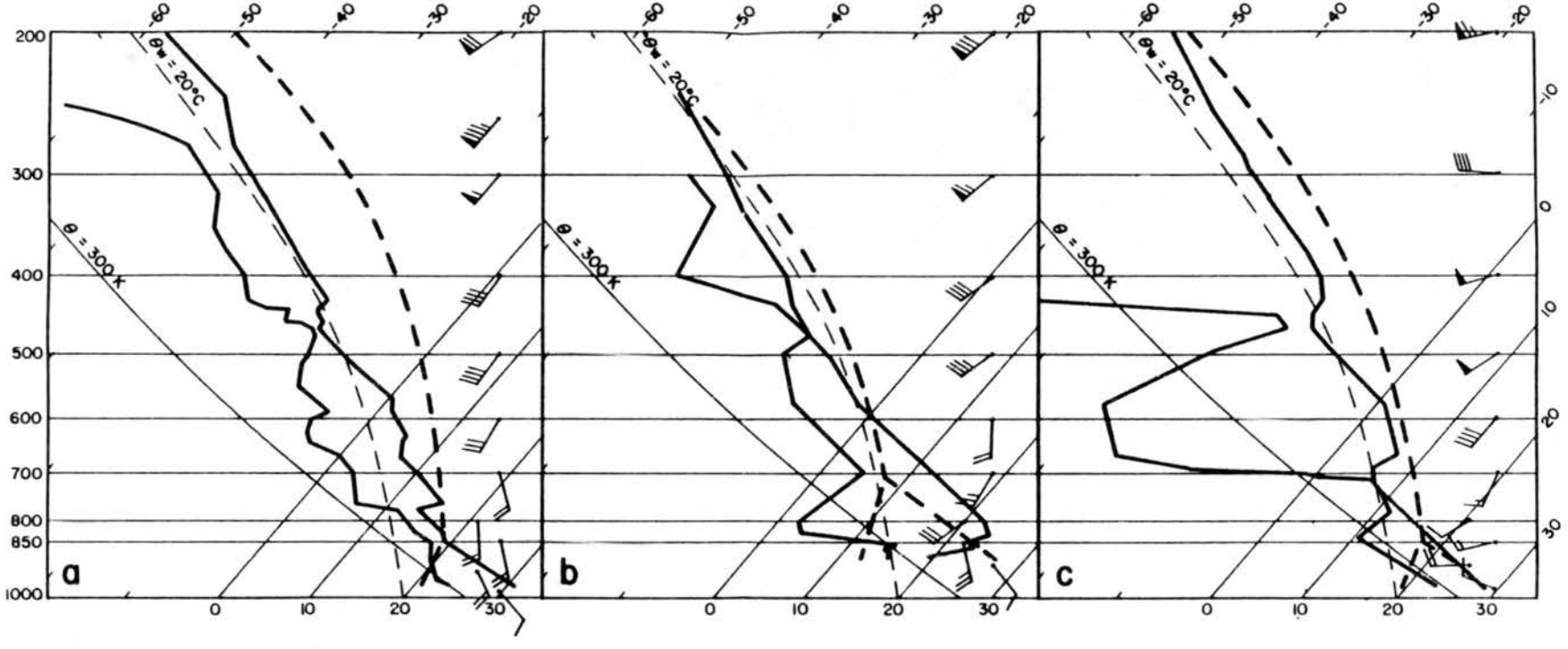

Figure 4.4: Thermodynamic and wind profiles at three contrasting locations sampling the southern regime of the MCC environment, on skew T - log p diagrams. (a) Enid (END) at 2110 UTC 3 June, (b) Amarillo (AMA) at 1200 UTC 3 June, and (c) Monett, MO (UMN) at 0000 UTC 4 June. Winds are depicted as barbes on the right; with one full barb equal to 5 ms^{-1}, and a flag equal to 25 ms^{-1}.

Table 4.1: Convective Available Potential Energy and Bulk Richardson Number in Selected Soundings

Region	Station	Time	Surface Pressure	Assumed Mixed Layer (mb)	LCL p (mb)	Buoyancy m^2/s^2	"Mean shear" $m\ s^{-1}\ km^{-1}$	Ri
Southern regime:								
Central	END	2100	968	968–868	856	3889	1.0	224
Western	AMA	1200	887	887–800	704	735	1.1	35
Eastern	UMN	0000	963	963–863	846	1914	1.3	71
In path of MCC:								
Western	DDC	1200	922	850–750	780	1246	2.2	14
Central	PTT	2100	943	910–810	857	2295	2.3	24
Central	IAB	2100	963	900–800	804	1282	2.2	15

lowest 100 mb, a parcel would have ~3900 m^2/s^2 of buoyancy as measured by CAPE, and would require no forcing to ascend from a lifting condensation level (LCL) at 856 mb and 20° C (shown in Fig. 4.4a). Wind shear was not large, as the wind veered smoothly from a direction of 140° at the surface to 240° at the tropopause where the wind speed was 52 ms^{-1}. Three hours after this sounding an F1 tornado passed through the town of Enid, and hail was also reported.

An earlier sounding at Amarillo (AMA) at 1200 represented the warm side of the front in the southern regime in the western high plains. Above a shallow but strong inversion that was probably nocturnal, there was a very deep and dry well mixed layer up to 570 mb. Surface heating to 27° C and mixing of the lowest 90 mb would have released a modest amount of convective instability as shown in Fig. 4.4b and Table 4.1, but would have to overcome negative buoyancy through a depth of 200 mb. If only the lowest 40 mb were mixed, the potential buoyancy is more than doubled, but the layer of negative buoyancy would still have been as deep.

The evening sounding at Monett (UMN; Fig. 4.4c) typified the southern regime in Missouri where the MCCs lost intensity after the mature stage. The warm air was deep, up to 700 mb, and moist. On mixing the lowest 100 mb, cloud base would still be at 850 mb, as at Enid, but CAPE values would have been half as great, and intermediate between the high value of Enid and the modest one of Amarillo. No apparent thermal cap existed here nor at Enid. The very dry layer from 670 to 570 mb had an equivalent potential temperature θ_e of ~322 K, low enough to cool considerably a potential inflow

from the southwest, via evaporation of rain. The potential for unsaturated downdrafts was large, and was largely a transient effect of the passage of MCC system A.

The common elements in the pre-MCC southern regime were: the layer from the surface up to 2 km deep was dry adiabatic in afternoon soundings; elevated moisture content permitted cloud base (or the LCL) to be near 850 mb; a dry adiabatic layer from 580 to 460 mb enhanced parcel instability; and an elevated layer of strong southerly winds, from 2 to 3 km (but higher in the west) advected warm air in. Convective instability was least in the west but very large in the central region, where severe weather occurred.

The next set of soundings lay in the path of the core regions of the mesoscale systems. Dodge City (DDC) was just west of the region where storms began to appear in chaotic fashion in systems B and C while Pratt (PTT) and Wichita (IAB) lay in the path of the evolving vortical patterns. The sounding at Dodge City (Fig. 4.5a) had a deep, mostly saturated stable layer up to 700 mb, above which dry adiabatic and dry conditions extended to 500 mb where the temperature was a cool -13° C. Surface air could not have supported convection, but lifting of the 850-750 mb layer would have released a moderate amount of buoyant energy above a cloud base at 780 mb.

Nine hours later and 110 km to the east, Pratt (PTT) exhibited more potential energy than other locations in this set. Again, surface air would not have supported convection, but the stable layer was only some 300 m deep beneath a strong frontal inversion at 880 mb. The air above the inversion had just been brought to saturation by advection of moisture in the southerly low level jet. We shall see that this was typical just before passage of the MCCs of this episode.

This region was characterized by:

- easterly flow from the surface to ~900 mb;
- southerly flow above that, to ~750 mb, which steadily increased the moisture content of that layer until near saturation just before the MCCs passed through;
- cool stable air only a few hundreds of meters deep beneath a frontal inversion of about 7 K in strength

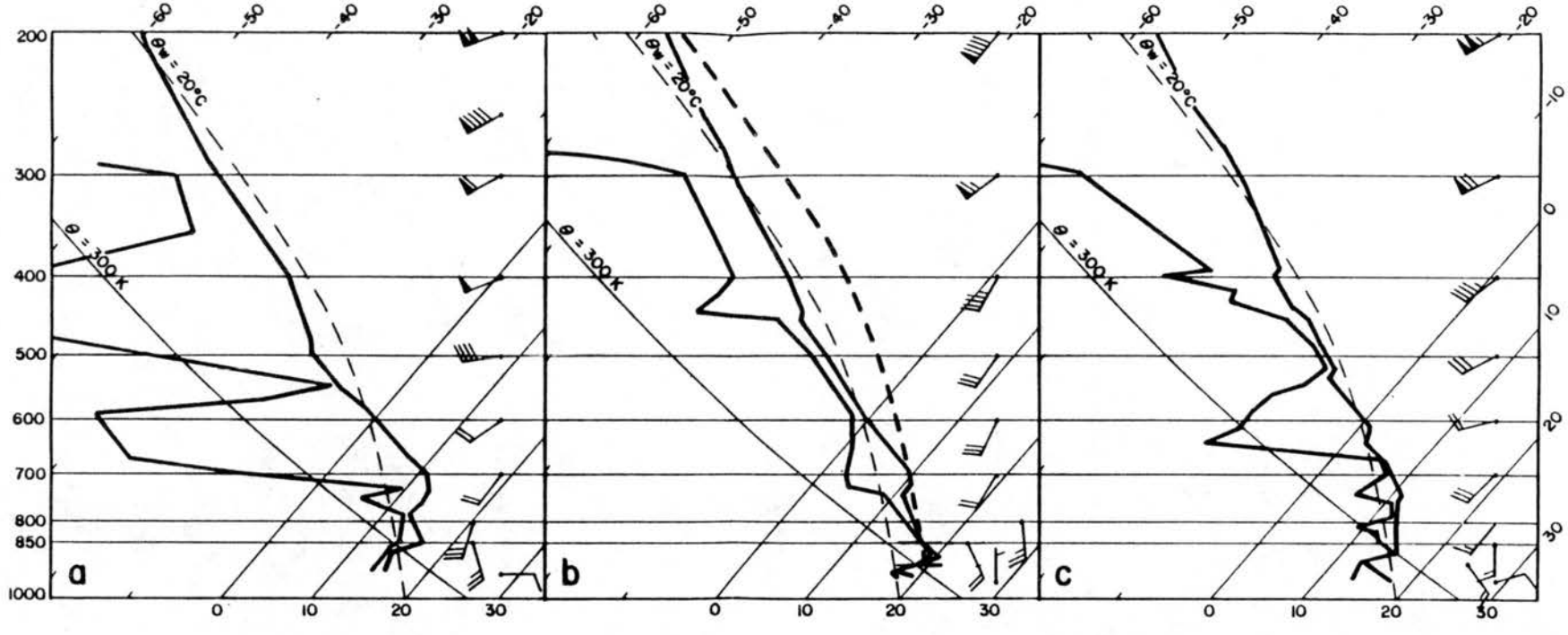

Figure 4.5: Thermodynamic and wind profiles at three locations sampling the environment through which the cores of the MCCs passed. (a) Dodge City, Kansas (DDC) at 1200 UTC 3 June, (b) Pratt, Kansas (PTT) at 2100 UTC 3 June, and (c) Russell, Kansas (RSL) at 2030 UTC 4 June.

- the middle levels were not excessively dry
- "mean shear" as defined by Weisman and Klemp was higher (more than $2 \times 10^{-3} s^{-1}$) than in the southern regime. Bulk Richardson numbers lay in the range of 15 to 25.

The third, northern region was chosen to represent the area on the cool side of the front that experienced lengthy stratiform rainfall during the passage of the MCCs. Our sample sounding is that of Russell, Kansas (RSL) at 2030 UTC in Fig. 4.5c. Unfortunately all the soundings in this region were influenced to some extent by the passage of earlier MCCs in the episode. The properties discussed here reflect conditions several hours after the first MCC departed and just before other MCCs arrived.

The profiles tended to be conditionally neutral (nearly a moist adiabatic lapse rate) although not saturated, above 700 mb to the tropopause. A dry adiabatic layer about 1 km deep was observed beneath that level in many soundings, but not in our example; the dry layer was a relic of the the unsaturated mesoscale subsidence of the earlier MCCs. From there to the surface the profile was conditionally stable, with a number of saturated and unsaturated layers. In Fig. 4.5c a strong, 5 K inversion was also present 500 m above the ground; this was observed in many soundings. The winds were easterly in this surface layer, and veered gradually from southerly to southwesterly in the deep stable layer. Wind speed increased steadily to about 60 ms^{-1} at the tropopause.

Potentially buoyant energy was observed only in the shallow saturated sub–layers within the conditionally stable layer; in Fig. 4.5C these were at 790 to 760 mb and at 700 to 650 mb. Modest values of CAPE (from 500 to 1000 $m^2 s^{-2}$) were observed there. Rather low values of mean shear led to values of Richardson number of the order of 100. The highest of these sub–layers could have supported deep (but not vigorous) convective overturning because they lay just beneath conditionally neutral or at times unstable middle layers.

Chapter 5

TWO MCCS THAT WERE ORGANIZED IN FRONTAL WAVE PATTERNS: SYSTEMS A AND B ON JUNE 3 AND 4, 1985

5.1 System A: a small but enduring MCC

The first convective complex in this episode was not targeted for special data collection by the managers of the PRE-STORM experiment, perhaps because it developed at mid-day, when MCCs were not expected to occur, or perhaps because it never became large. Nevertheless, it met the criteria for an MCC for 13 hours and propagated as a mesoscale cloud mass for some 10 more hours, as far as West Virginia where "spiral arms" of cirrus suggested that an upper level circulation remained.

The first storms were seen in the morning at 1300 UTC 3 June in the Oklahoma panhandle near 100° W. Several widely separated clusters developed under a long shield of cirrus on the anticyclonic, south side of a subtropical jet that extended from northern Mexico to Illinois. Although the synoptic–scale resolution of the wind data was not good, the panhandle region did appear to be under the entrance region of a jet streak at 250 mb, and under the ascending branch of the thermally direct transverse circulation that is expected in the entrance region (Uccellini et al., 1984). This is based on a 50 percent change of wind speed from Oklahoma City to Dodge City, transverse to the jet, and a 30 percent change going downstream from Amarillo to Dodge City. Stumpf (1988) noted that these storms began to develop in an area without any measurable surface wind convergence, although the area did lie in a mesoscale pressure trough. Stumpf and Johnson (1988) speculated that this trough reflected a deformation of a frontal surface observed from 1 to 2 km above the ground.

Within three hours the system met the criteria for initiation of an MCC, when it lay squarely in the PRE-STORM area. At this stage convective echo tended to develop along

an east-west band (between 1 and 2 on Fig. 5.1a) and also in a cluster (at 3 on the same figure) near the northwest corner of the cloud shield (see satellite images on Fig. 5.2). Over the next six hours the cloud shield expanded far to the north and east of the centers of intense precipitation, which propagated eastward (Fig. 5.2b,c,d). Our next radar snapshot at 1800 UTC, two hours after the first, continued to depict the main convective activity in the band from 1 to 2 and also in a swath roughly perpendicular to it, except that the most intense cluster at 3 was on the south margin of the system (Fig. 5.1b). Stratiform precipitation had also filled the region northeast of these features. Notice that the active convection remained on the western and southwestern edges of the cloud.

By 2025 UTC the active convection stretched along two bands M and N that formed a wave-like pattern, on Fig. 5.1c, as System A was in the growth stage before maturity. The intersection of the bands at P was nominally chosen as the **center** of this pattern, which could be tracked for $4\frac{1}{2}$ hours. The translation of the wave pattern centered on P was mapped on Fig. 5.3 from Chanute, Kansas into central Missouri. Before 2100 UTC this pattern propagated at 24.5 m s^{-1} from 265° , and so did the cloud shield. When it passed into Missouri after that time, and entered the mature phase, the convective pattern slowed to 15.5 m s^{-1} from 285° . The cloud shield viewed by satellite continued at the faster rate for two hours, but then also slowed to 15.5 m s^{-1} , a speed maintained for the next six hours.

Most of the stratiform precipitation is inferred to have been north and northeast of P, out of radar range. The coldest cloud tops were located at or just north of P for about 3 hours. System A reached maturity or maximum extent just after 2200 UTC when the cloud covered the state of Missouri (Fig. 5.2d). It propagated 7 more hours as an MCC, and apparently spun up an eventual circulation evident in its cirrus cloud bands by 1200 UTC 4 June, when it reached the Appalachians (this was 7 hours after it disqualified as an MCC).

A ten hour series of supplemental soundings was initiated as system A exited the mesoscale network. For that reason we do not devote much analysis to the upper air data in system A, but do so for system B which was well observed by the supplemental

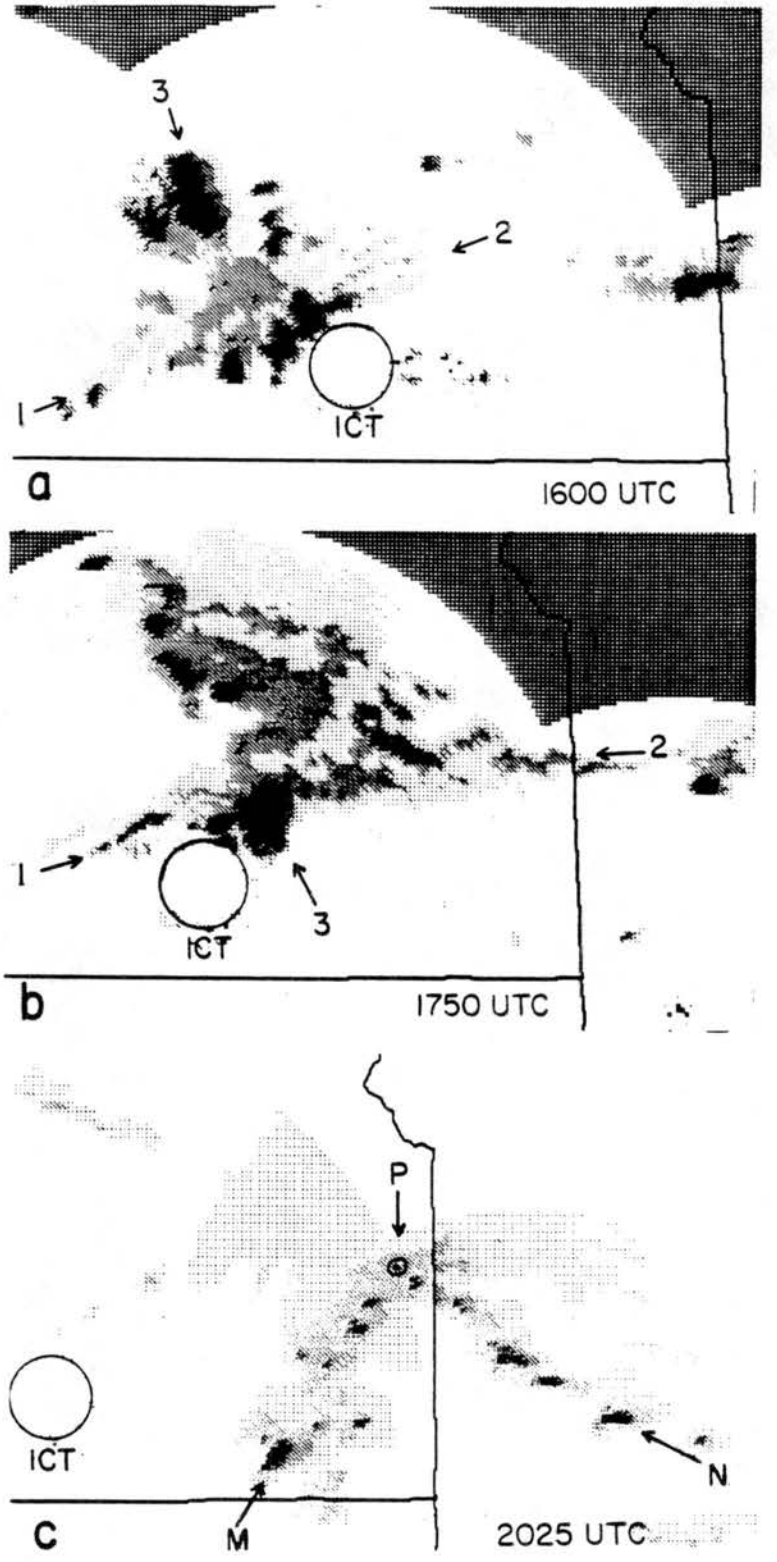

Figure 5.1: Evolution of radar reflectivity pattern in system A. (a) The initiation stage at 1600 UTC 3 June; (b) At 1750 UTC, new development continued eastward between 1 and 2, but the most intense cluster was on the south margin at 3. (c) At 2025 UTC, the convective activity aligned along bands M and N intersected at P at the center of a wave pattern.

Figure 5.2: Infrared satellite images of systems A and B (marked) over a ten hour period. (a) 1600, initiation stage of A; (b) 1800, mesoconvective stage of A, and initiation of B; (c) 2000, growth stage of A; (d) 2200 UTC 3 June, maturity of A, growth of B; (e) 0000 UTC, maturity of B; and (f) 0200 UTC 4 June, decay stage of both.

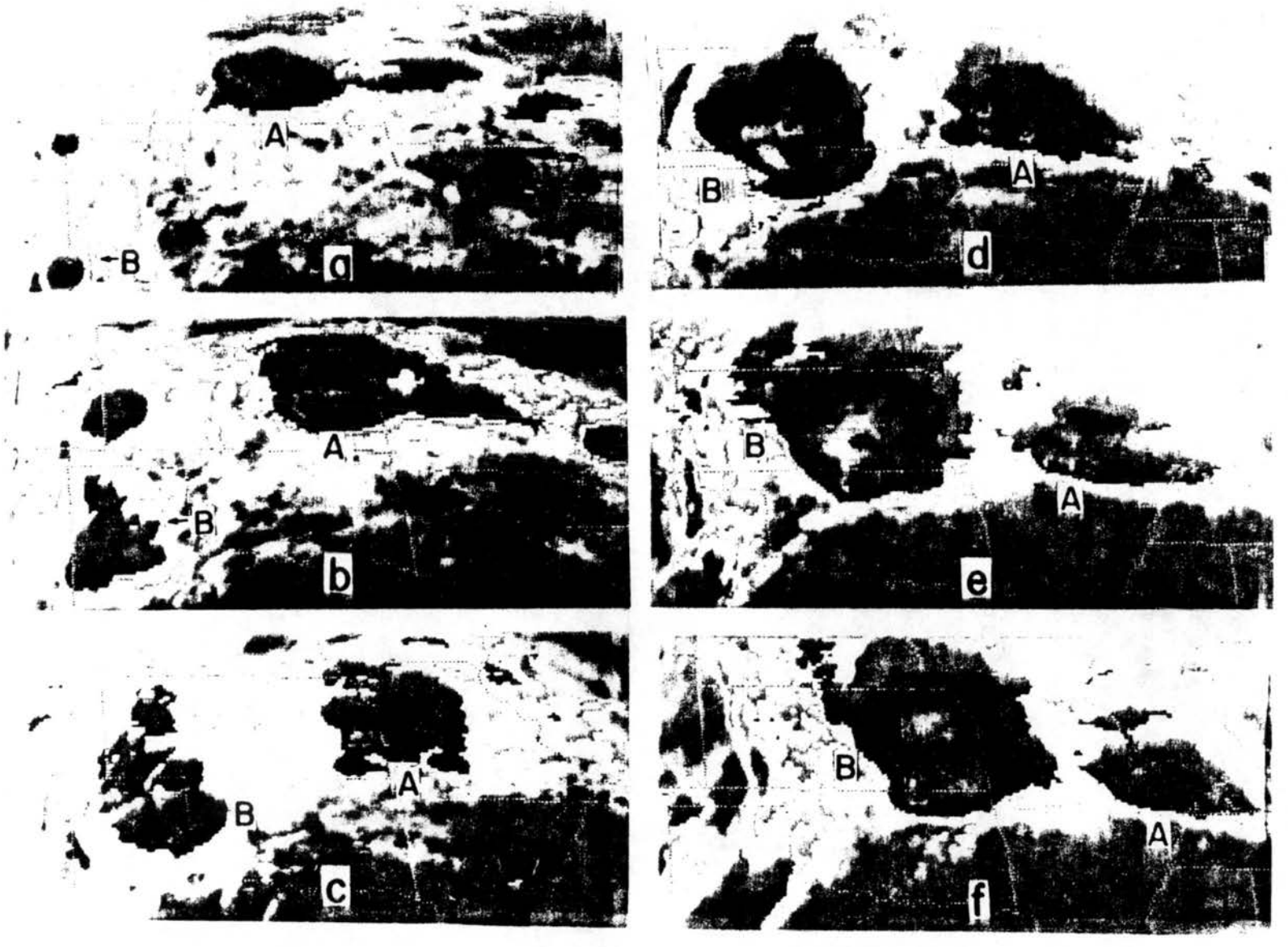
A
B
a
B
A
d
A
B
b
B
A
e
A
B
c
B
A
f

soundings. System A was observed by this data set only in its southern portion and only before maturity. One plot of system–relative winds at the growth stage appears in Fig. 5.4. At 200 m above ground level (AGL), a strong, 30 m s^{-1} outflow of cool, moist and shallow air flowed out of system A at Fort Riley (FRI), at the rear edge of stratiform rain. This outflow was, in fact, an effect of the downdrafts induced by the evaporation of rain. Only 300 m higher, these properties changed to a warm, dry outflow also observed at 850 mb (Fig. 5.4b). Later we deduce that such properties resulted from dry adiabatic subsidence of middle level inflow of ambient air, probably from the south. Vigorous inflow of moist air was observed in a deep layer south of the system, on both panels a and b, but an even stronger outflow from the rear only occurred at or beneath 200 m AGL. At the 600 mb level, chosen to represent the freezing level, the winds nearly matched the system velocity (15.5 m s^{-1} from 285°). Weak relative inflow of $\sim$ 10 m s^{-1} from the *south* was seen (panel c).

A time-height profile of winds at Chanute perhaps shows these features more clearly (Fig. 5.5). The first profile at the extreme right was at the time of Fig. 5.4, before the convective band arrived. The second profile at 2045 UTC was done in light rain just behind a strong cell in the band; the sounding was noisy and terminated at 4 km. The third profile at 2225 UTC was a clean sounding some 60 km beyond the west edge of the low-level echo. By assuming steady conditions over this 3 hour period, this figure can be interpreted like a spatial cross section of the MCC, centered on the second sounding. Relative outflow > 50 knots below 200 m AGL in the third profile caused divergence in a shallow layer. Above this from about 1 km to 4 km in height, the winds converged onto the system from the front. A fairly deep weak inflow from the southern flank developed as soon as the rain band passed, in the same middle levels. Above 5 km, the winds strongly diverged in relative outflow towards the front, so that rear–to–front flow was accelerated in advance of the MCC, and retarded behind it. The 10 hour mesoscale data set mentioned above allowed more analysis of these and other features in system B, which followed on the heels of the first.

In summary, System A began as several poorly organized meso–β–scale clusters. As stratiform cloud developed downwind to the north, the clusters tended to form on the

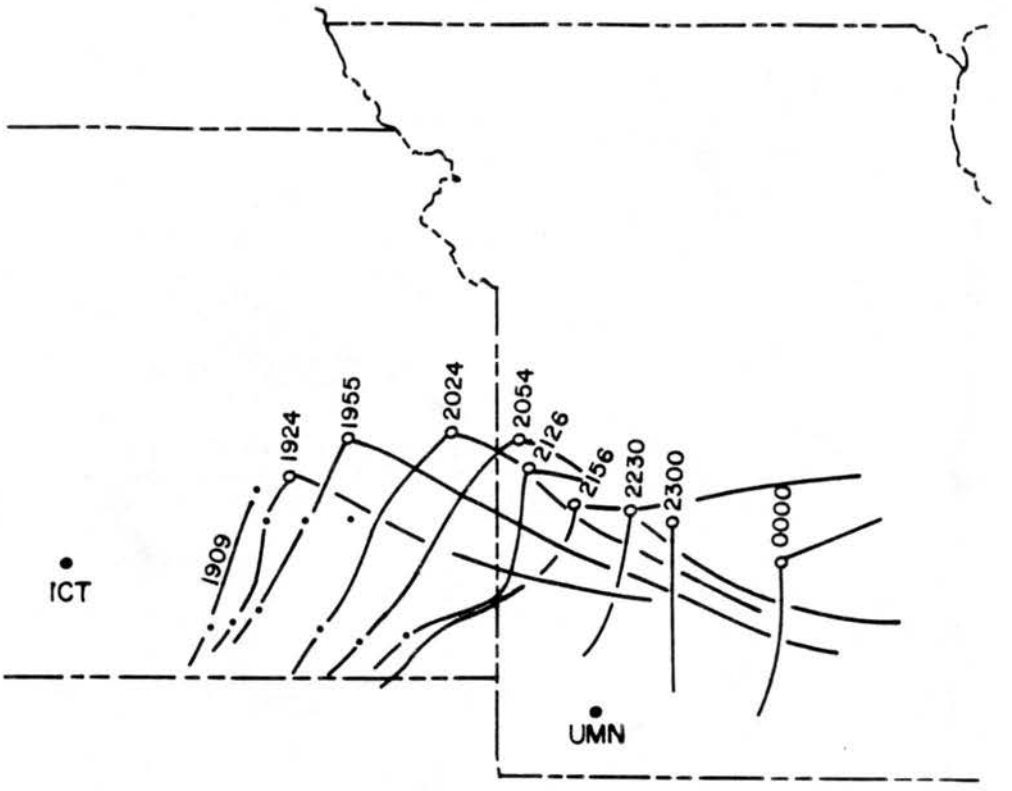

Figure 5.3: Propagation of the wave pattern on radar depictions of system A. Data were from Wichita (ICT) and Monett (UMN). The circles marking the center of the pattern are identified by UTC time.

curved southern and western margins of the cloud. After four hours convective activity was aligned along two perpendicular bands M and N that intersected in an "open wave" pattern that lasted for 5 hours. Moist inflow into the forward and southern sides was deep. Cool and moist outflow, quite strong and divergent, was confined below an inversion near 200 m above ground. In mid-levels, relative flow was weak but tended to enter from the front and the southern side. It probably descended in unsaturated downdrafts and exited the rear near 1.5 km. Large divergence above heights of 7 km tended to cause the environmental winds to be diverted around the system.

5.2 System B: an apparent mesoscale frontal wave cyclone

The second mesoscale system of the episode did not live as long as the first, but it grew much larger and did so in the Kansas network, and thus was targeted for intensive observation. The supplemental sounding network, the profilers, and all the radars were able to collect extensive data on system B; the two NOAA aircraft observed it after its

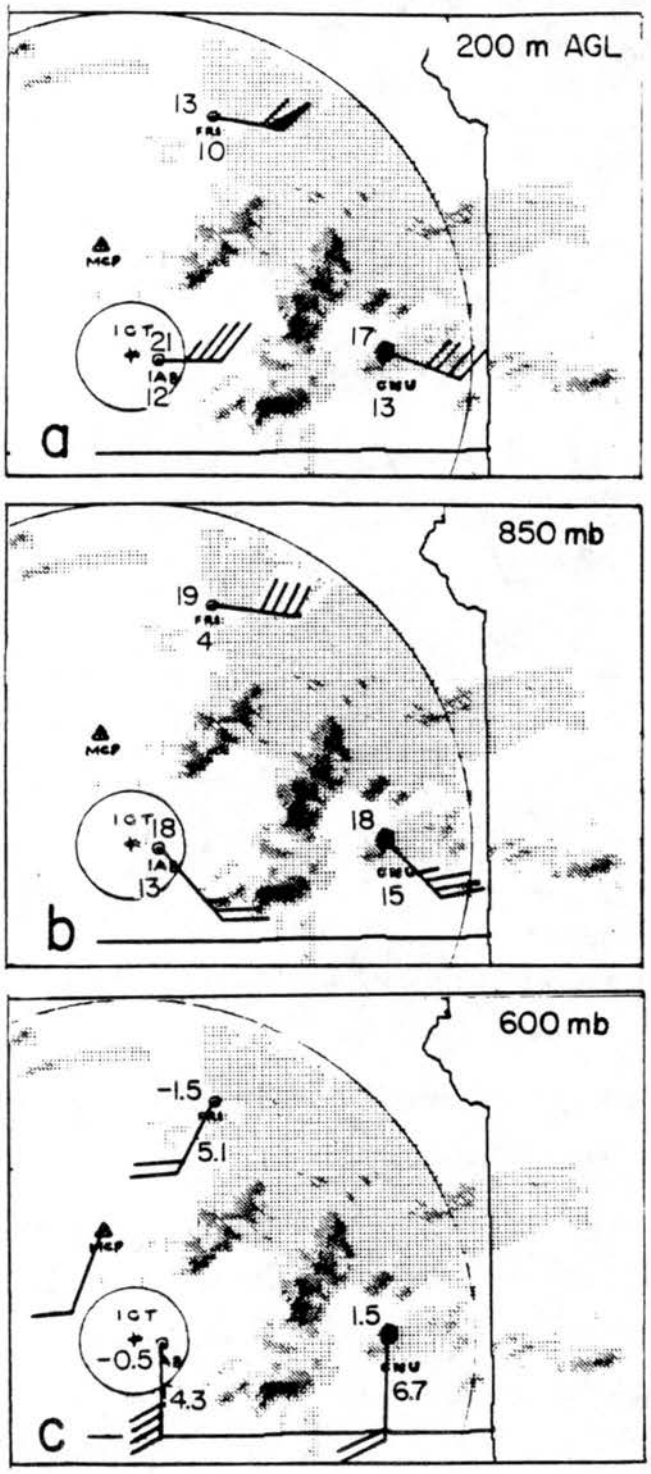

Figure 5.4: System relative winds at 1930 UTC are plotted on the radar echo of System A measured at Wichita (ICT) and Monett (not shown). The 3 levels are (a) 200 m above the ground, (b) 850 mb, and (c) 600 mb. Temperature in degrees Celsius is at upper left and mixing ratio in g kg^{-1} beneath, each station.

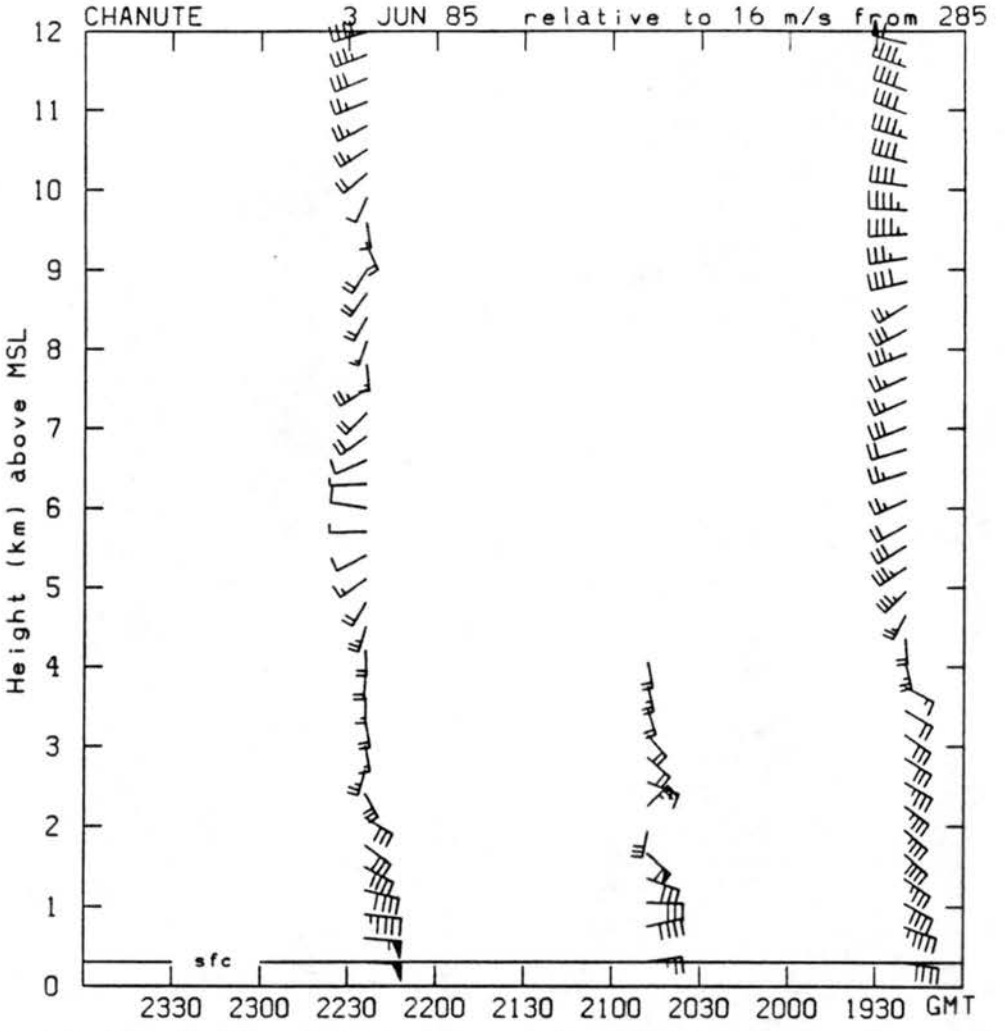

Figure 5.5: Time-height profile of system-relative wind in rawinsoundings at Chanute (CNU), Kansas, 3 June 1985. One full barb represents 5 m s^{-1} ; time increases from right to left.

mature stage. This system exhibited the best example of the open–wave frontal pattern examined in this thesis. In addition to our analysis, we discuss and evaluate the work of Stumpf (1988), Smull and Augustine (1989), Meitín and Watson (1987, 1989), Augustine and Howard (1988), and the Weather Research Program (1987) on this same mesoscale system, in order to determine the evolution and airflow structure of this MCC as an example of the frontal wave prototype.

5.2.1 Evolution of the storm components and precipitation

A number of cumulonimbus clusters exploded in separate locations on the border of New Mexico and Texas between 1530 and 1800 UTC (late morning) on 3 June. Like

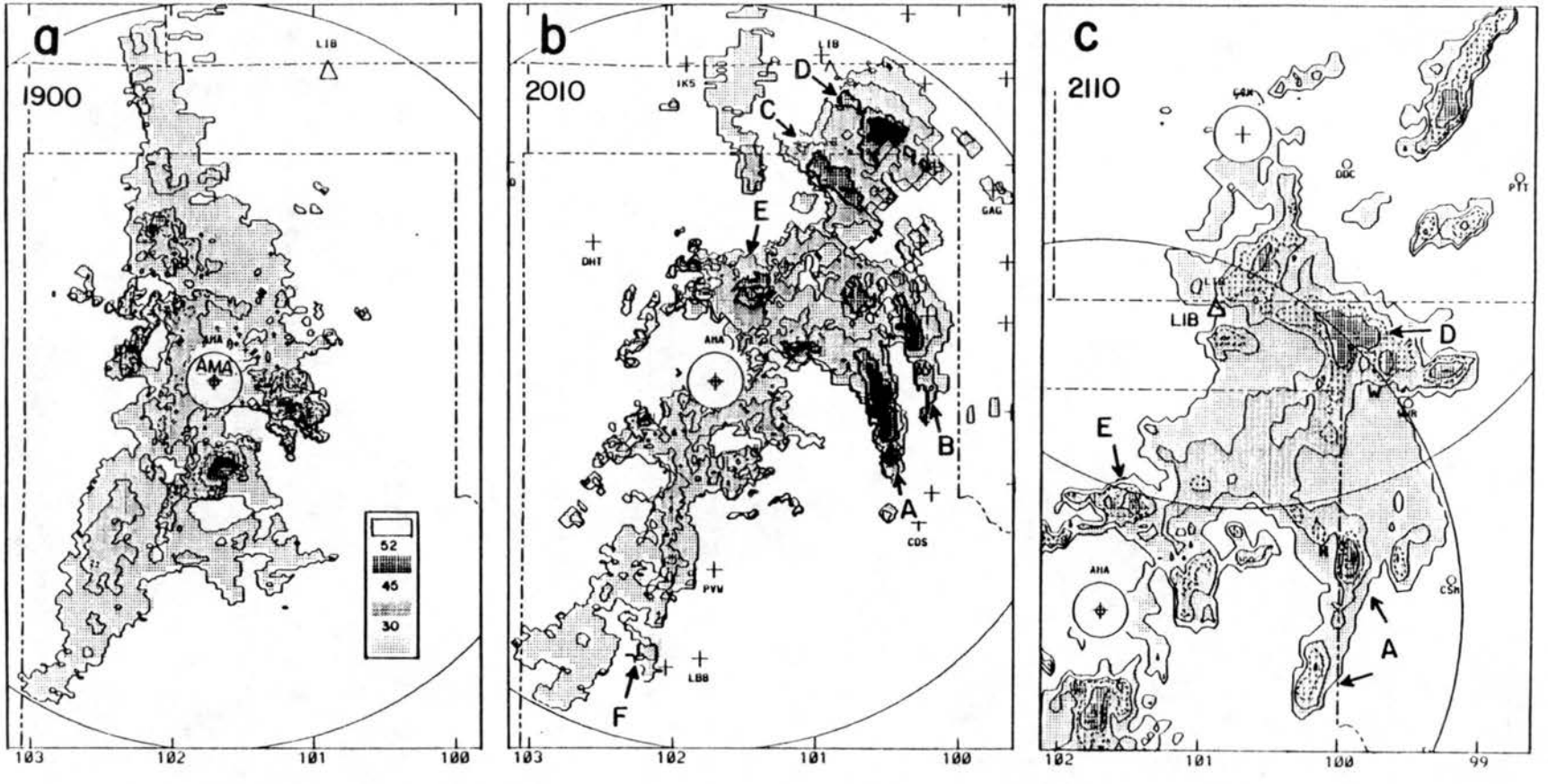

Figure 5.6: Reflectivity of system B one to three hours after initiation as an MCC on 3 June 1985, from Amarillo radar (AMA), at (a)1900 UTC , (b) 2010 UTC, (c) 2110 UTC. Reflectivity in dBZ is keyed to the grey tone shadings in the legend on each panel.

the early storms in system A, they developed under the long arc of cirrus equatorward of the jet stream, there aligned north–south. The cirrus indicated upward motion in the upper troposphere, favorable for destabilizing and moistening the middle levels. The first storms developed preferentially in a north–south swath parallel to the general slope of the terrain in the Texas panhandle, and some of the early, intense cells may have been favored by particular features such as the escarpments on the Canadian river. The preferential north–south alignment, at first unorganized, became more pronounced with time, until convection was focused on one solid multicellular line that extended south from the MCC and that propagated east in step with it. The bow shaped band of convective and stratiform echo, 400 km long, had covered much of the Texas panhandle by 1900 UTC (Fig. 5.6a), when it qualified as an MCC.

The system propagated by merging with convective line segments and isolated clusters that had developed ahead of the bow echo. Many segments developed along parallel lines, as did segments *A* and *B*, and also *C* and *D*, over 100 km ahead of the bow shaped echo between *E* and *F* at 2010 UTC (Fig. 5.6b). Some of the component storms (such as *D*) included echoes stronger than 50 dBZ more than 20 km across, and produced hail. This was the time of the first peak of convective rainfall rate (Meitín and Watson, 1987); the rate fell by 50 percent over the next 90 minutes.

During that time the merged group at *C* and *D* exhibited the greatest reflectivities and the coldest cloud tops. At the same time separate convective storms developed all over western Kansas at 2100 UTC, in the growth stage of the MCC, while the original band in the Texas panhandle lingered on (Fig. 5.6c). Although this band harbored a few strong cores, it lay outside the enhanced cloud shield where cloud top temperatures were colder than -54° C. The system, therefore, extended itself downwind to the north and northeast because new convective clusters developed some hundreds of kilometers "in front of" the existing region of convection, while the older clusters "rearward" of the region spread out and diminished in intensity. A "cluster" as used in this study is a meso–β–scale set (20–100 km across) of smaller convective storms which are identified by their high radar reflectivity; generally one observes precipitation of lower reflectivity at higher heights (and

less often at lower heights too) between the convective cores. Alternatively, a "cluster" is a meso–β–scale set of cumulonimbi jointly generating a precipitating anvil cloud. Because the new clusters formed so far ahead of the existing ones, and did so simultaneously over such a wide area, cold outflows from the existing storm are probably *not* responsible for initiating the new storms. An alternative hypothesis will be advanced in Chapter 9.

From 2200 to 2330 UTC new clusters formed in Kansas from the Nebraska border into Oklahoma. Contiguous stratiform echo began to fill most of the intervening area, unlike earlier (Fig. 5.7a). There was no further activity in western Kansas, but the original band in the Texas panhandle lingered as a broken line. Three major centers of cold cloud top (colder than -70° C) were found in the rear portion of the cloud shield. With some exceptions, these centers tended to lie above the most intense echo or above regions where intense echo had been observed in the previous hour. This was also the stage of "thermal minimum" of the cloud shield as defined by McAnelly and Cotton (1989).

A mesoscale "open wave" pattern formed between 2300 UTC 3 June and 0030 UTC 4 June on images composited from several radars (Fig. 5.7). Some of the mesoscale kinematics and the precipitation structure of this occlusion have been described by Meitín and Watson (1987). At 2200 there were two broken convective lines that had an east - west orientation (at *A* and *B* on Fig. 5.7a). Line *A* extended eastward, into the echo free region underneath the forward part of the cloud shield, and started to link southwestward, with cluster *C*. Just south of *C*, two other clusters *E* and *F* associated with cold cloud top (T < -70°) merged in the next 40 min. The region of *C*, *E* and *F* evolved later into the apex "P" of the wave pattern. The other major cluster at *D* associated with a large area of cold cloud top, in Oklahoma, evolved into the central and most active segment of the north - south convective line. This line emerged as a few intense β–scale clusters assumed predominance and as the small convective cores ceased to develop further. The stronger clusters gradually aligned along a north - south direction in the middle of the stratiform echo. More stratiform echo developed in the north while it dissipated in the south, so that the stratiform rain area was located more and more to the north and northeast of the center of the radar wave pattern. The southern part of the pattern was beginning to

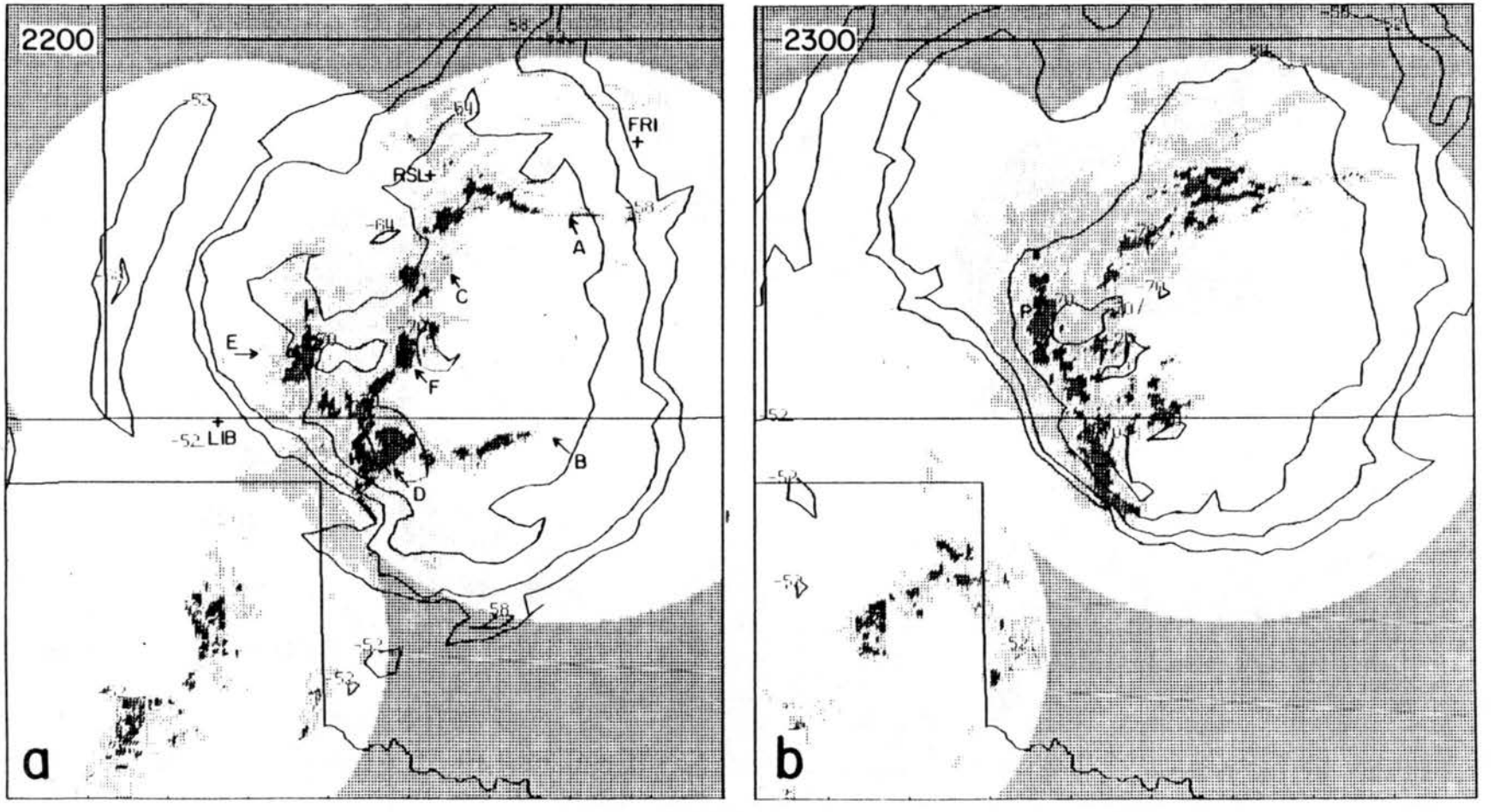

Figure 5.7: Images of reflectivity echo in the mature system B from composited base scans of several radars, at the times (a) 2200, (b) 2300, UTC 3 June, and (c) 0010 , and (d) 0109 UTC 4 June 1985. Temperature contours (dashed lines) of the cloud shield are overlaid.

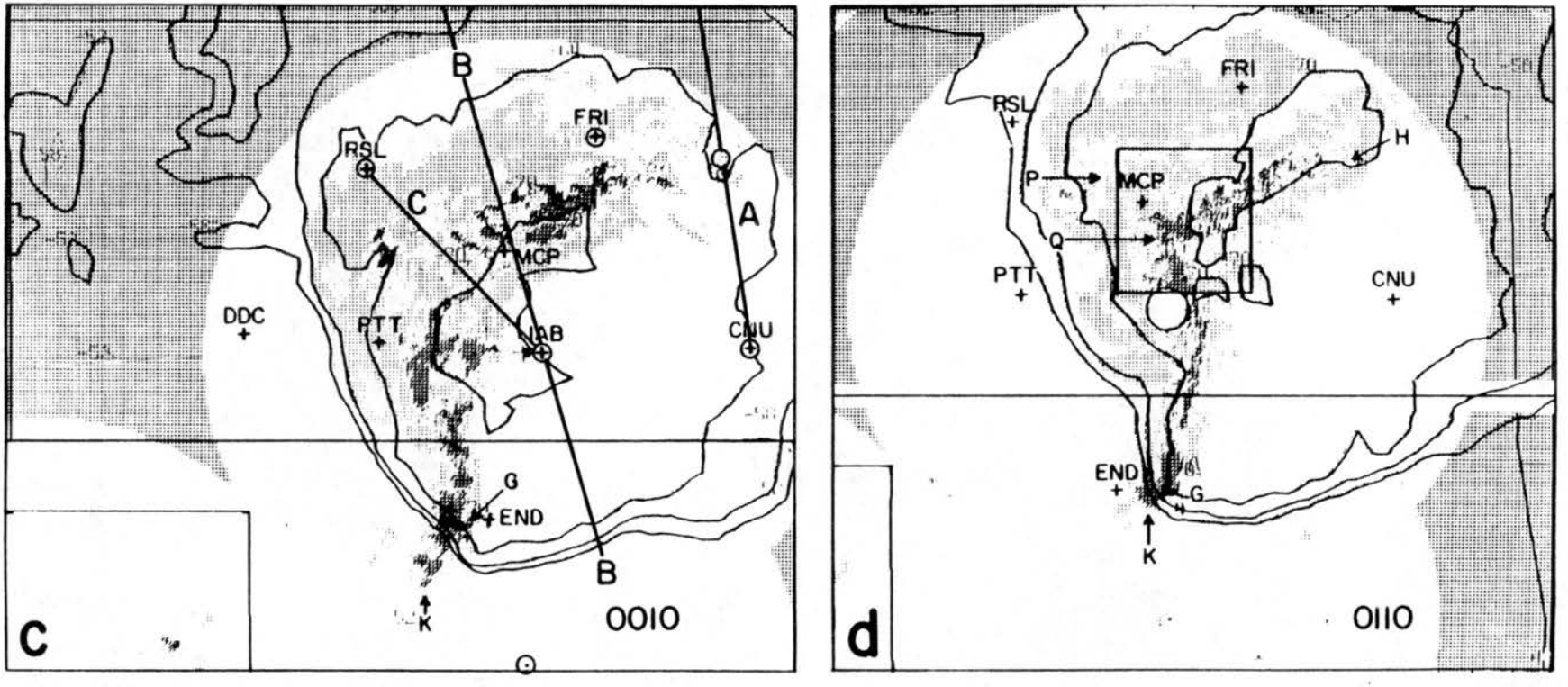

Figure 5.7: continued.

be evident by 2300 UTC on Fig. 5.7b as a broken linear band of convective echo oriented north–south, parallel to the rear edge of the cloud shield. The intense cores in Oklahoma had consolidated into a region *G* some 60 km long by 25 km wide, where at least four cores exceeded 53 dBZ (and were producing hail). An axis of cold cloud top, colder than -70° , lay parallel to *G* 15 km to the east. Relative southwesterly flow (20 to 35 ms^{-1} in the layer from 250 to 150 mb) would have accounted for the displacement. Cluster *G* is believed to be a supercell; it produced an F1 tornado which destroyed property in Enid, OK, 10 minutes after the time of panel C.

System B attained maturity at 0000 UTC 4 June when the area of cold cloud tops was greatest. The second peak of rainfall rate was observed at 0030, and it was largely convective in nature. Among the notable features on the radar and satellite images on Fig. 5.7 were (a) the coldest tops began to be located over the east - west convective band H rather than the north - south band K, for at least two hours, even though band H had fewer and less intense convective regions; and (b) the portion of the line K south of *G* remained not only far removed from stratiform echo, but even outside the enhanced area of cold cloud top (within which $T < -54°$ C) defining the MCC. The line containing *G* increasingly became bow shaped, and band *H* filled in with continuous echo, so that by 0030 UTC the echo pattern most resembled a synoptic scale frontal wave about to undergo occlusion.

The distinct regions of coldest cloud tended to merge into one large region above band *H*, which was wider (some 30 km) than band *K*. In that sense *H* resembled a warm frontal band while *K* resembled the prototype narrow cold-frontal band (Hobbs et al., 1982). There also developed a band of lower reflectivity on the north side of *H*, not unlike a transition zone; further north another band of enhanced reflectivity was observable for about an hour. At this time, (Fig. 5.7d), the apex of the pattern, where *H* and *K* joined, passed through the opportune region for dual-Doppler scanning by the CP-3 and CP-4 radars. Results of a Doppler wind field analysis of the apex region (in the box) by Smull and Augustine (1988) are discussed below.

The frontal wave was well defined during the mature stage, and resembled the larger–scale "line echo wave pattern" (U.S. Dept. of Commerce, 1987). The north–south arc *K*

intersected band H at the circle marked Q. This is considered to be the primary center of the pattern. Arc K also intersected the enhanced band of reflectivity, parallel to the primary band H but farther north in the stratiform cloud, at P, a secondary center. The primary and secondary centers were also located at earlier and later stages than shown. The pattern could reasonably be identified for a period of 4 to 5 hours in systems A and B. For B, the propagation was mapped on Fig. 5.8 along with the movement of several meso–β–scale convective clusters. As the pattern developed more of a cusp, it traversed about 450 km. Displacement velocities were measured at 19 m s^{-1} from 240 ° in the initiation stage before 2130 UTC, and 19 to 21 m s^{-1} from 260° to 270° in the mature and late stages.

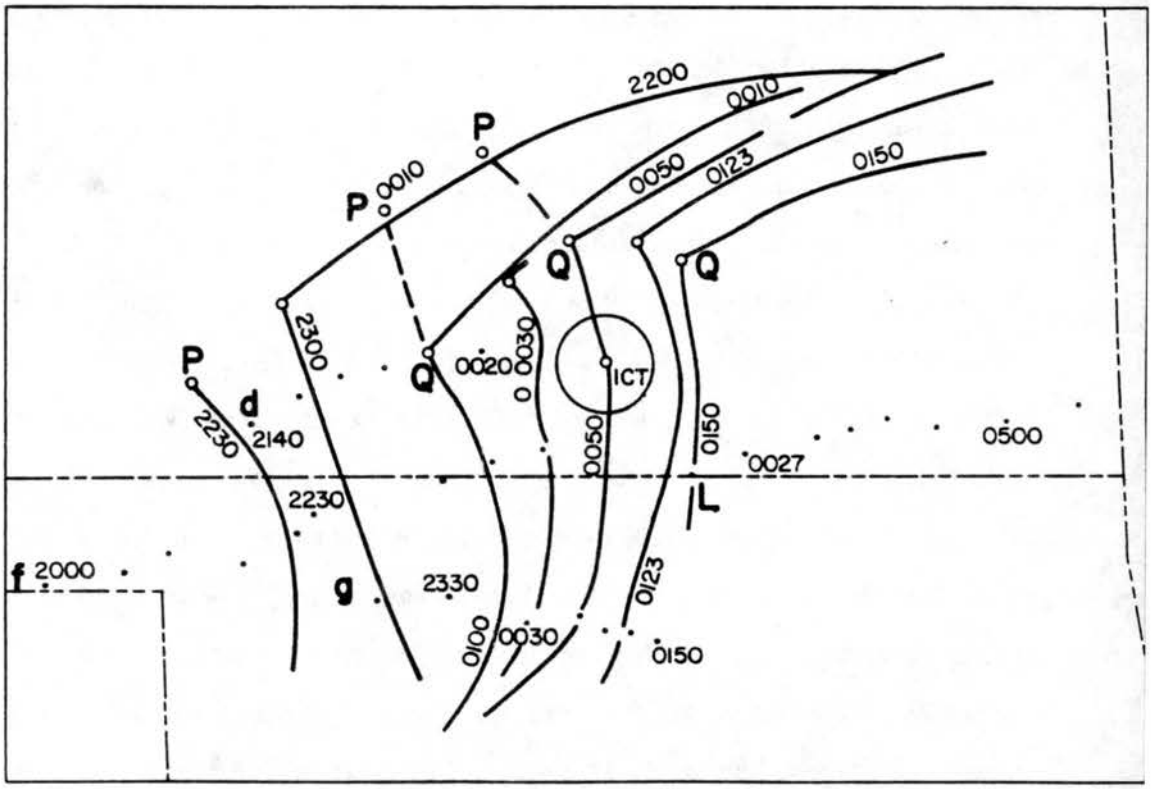

Figure 5.8: Translation of the meso-α wave pattern and some meso-β clusters in system B. P marks the center of the meso–α–pattern at first; at about 0010 another center Q was tracked. The dots labelled d,f,g, and L mark successive locations of meso–β–scale clusters.

The system rapidly lost MCC characteristics as the "mesoconvective stage", which had lasted a relatively long 7 hours, ended. The area of coldest cloud tops shifted northeast towards Kansas City at 21 ms^{-1}, now near the center of the enhanced cloud shield. The

southern end of line *K* continued to advance as a convective line segment with maximum reflectivities greater than 45 dBZ, until the decay stage at 0200 UTC when it became separated from the convective centers in Kansas. During these last 3 hours the portion in Oklahoma was not embedded in stratiform echo, like the segment in Kansas was. It remained on the southwest corner of the cloud shield, which had a sharp southern margin.

After 0200 UTC many detached convective clusters developed over much of eastern Oklahoma, well south of the cloud shield to the north. There was some tendency of these to align in broken parallel lines oriented from northeast to southwest. Cluster *G* was completely detached from the radar echo of the MCC. Meanwhile the main stratiform cloud covered an area larger than Missouri and Iowa combined and the total rainfall rate reached a maximum, even though the rain intensities were light and characteristic of stratiform rain. The upper regions of the cloud seemed to evaporate, however, as the system failed to meet the cloud-top temperature criteria by 0430 UTC. System B did meet the criteria for 10 hours and certainly underwent one of the most interesting evolutions seen on radar during the PRE-STORM experiment.

5.2.2 Evolution of surface features

Some elements of the frontal wave pattern in system B can be seen in a surface analysis done for one time (0000 UTC) by Augustine and Howard (1988). The low–level flow was convergent on a "frontal–type feature" from both front and rear. A tongue of air with high values of θ_e >345 K converged on the feature from south and southeast of the MCC. A pool of "unsaturated downdraft air" with values of θ_e some 20 K lower dominated the western margin of the MCC, and spread southward toward the mesoscale cold front that extended southwest from the cloud shield.

The mesoscale analysis of pressure required close attention to surface elevation, instrumental drift, systematic errors, and the mixture of dissimilar datasets. Stumpf (1988) took these in consideration in a thesis on the wake pressure lows and other surface features of system B. His analyses were consulted during our re–analysis of surface fields, an example of which appears in Fig. 5.9. The fronts were positioned after the streamlines, convergence lines, and temperature and moisture data were analyzed.

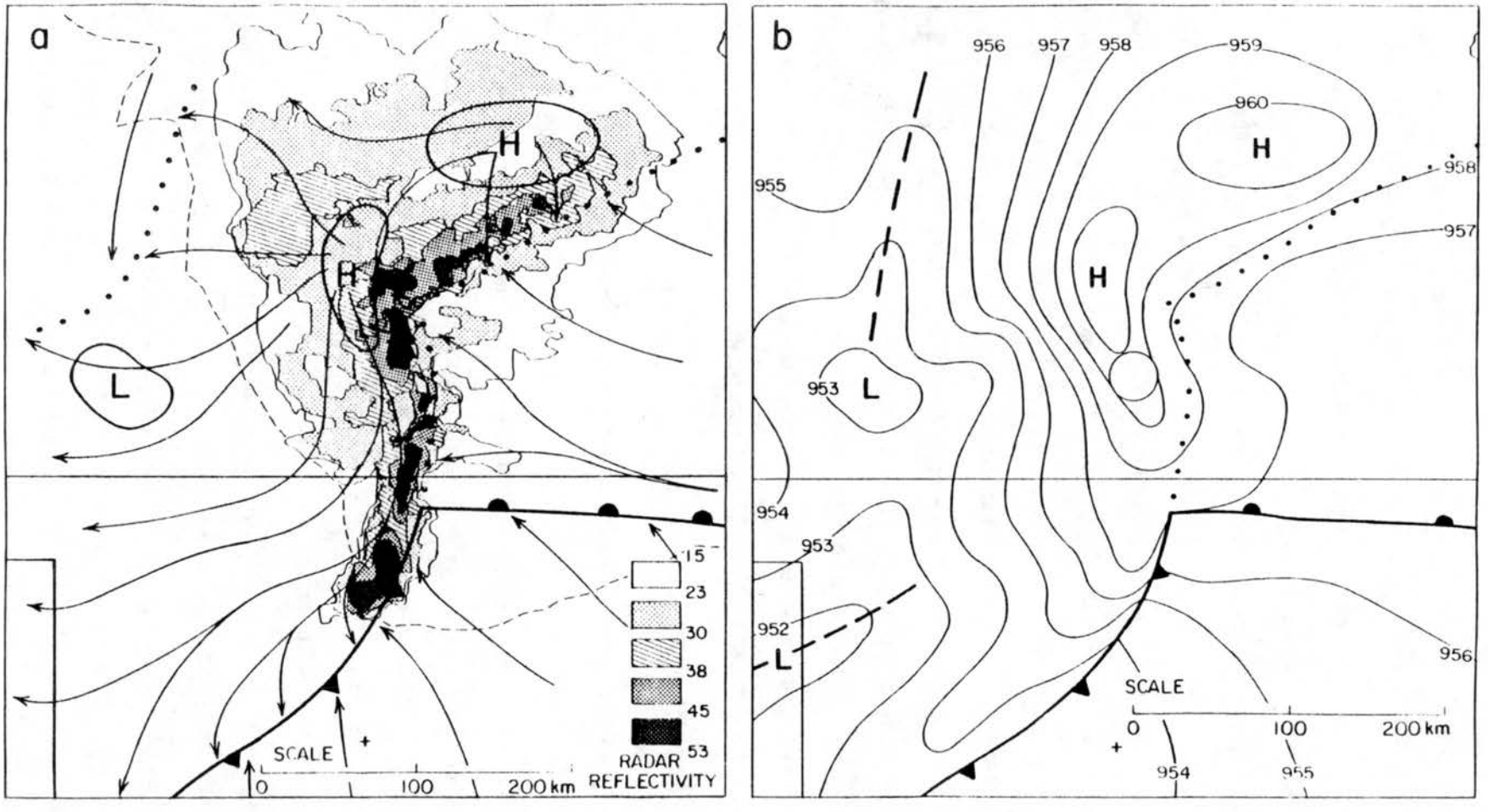

Figure 5.9: Mesoscale surface analysis of the mature system B at 0100 UTC. (a) Pressure centers, streamlines, convergence lines (dotted), and fronts superimposed on reflectivity pattern (shaded) from Wichita radar, and the -54° C contour of the margin of the cloud shield (thin dashed). (b) Isobars of pressure reduced to a standard elevation of 480 m, at 1 mb intervals; pressure troughs (thick dashed lines), other features as in (a).

There were two meso–high centers. The stronger, though smaller center was located in, and just west of the propagating apex region, where the clustering of intense convection in the previous 20 minutes would have generated the strongest downdrafts from precipitation. A weaker meso–high north of band H covered a larger area under the stratiform cloud there. The strongest pressure gradients developed between the western meso–high and the emerging wake low or trough. The development of the wake low and its influence on strong surface winds has been documented by Stumpf (1988) for this system and Johnson and Hamilton (1988) for a squall line. They felt that the wake low and strong pressure gradients were favored by areas of enhanced stratiform rainfall (observable as enhanced radar reflectivity) near the rear of the system, and abrupt descent of mid–level inflow from the rear into the rain. The rapid descent was believed to induce large pressure falls from subsidence warming not offset by precipitation cooling. These processes were evident in the northern rear quadrant of system B.

As the convective activity increasingly became focused on, among other things, the narrow multicellular line that propagated east like a pseudo–cold front or squall line, we observed that a pressure ridge of cool air was building strength along its length. The strong outflow from it toward the east, south, and southwest, induced a frontal–wave "cusp" to form on the east–west convergence line (dotted) which was the surface reflection of the stationary front aloft. The cool outflow, advancing some 400 km well south into Oklahoma, also induced a frontal wave on the "real" surface front which was just south of the state line. A second region of strong pressure gradient was located on the cold front near this southern "cusp", where the supercell thunderstorm which spawned the tornado at Enid fed on a deeper layer of unstable air in which θ_e ranged from 350 to 360 K. In turn, the intense convection there reinforced the southward push of rain–cooled outflow.

Recall that three regimes of surface air properties were analyzed before this episode began. Afternoon temperatures hovered near 30° C and the mixing ratio was $\sim$ 15 g kg^{-1} in the unstable air south of the stationary front, before system B arrived. North of the front typical values were 20° to 25° C and 13 g kg^{-1} in the shallow stable air. In northern and western Kansas where the cool air was considerably deeper, and scattered rainshowers had been present for a few hours, values were typically 16° C and 10 g kg^{-1}.

The meso–α–scale high and low pressure centers, and the intersections of fronts and confluence lines that defined the wave pattern discussed above, were tracked for 3 to 6 hours, just as in the other cases in this study. As a whole, these surface features propagated from 18 to 22 ms^{-1} in rough agreement with the movement of the open–wave pattern in the radar echo, from a direction of 240° initially and from 270° after maturity, *for this MCC only.*

5.2.3 Flow fields derived from Doppler radar

Smull and Augustine (1989) probed the reflectivity and meso–β–scale velocity fields near the center of the occluding pattern in system B at one representative time (0105 UTC) with data from the NCAR Doppler radars CP-3 and CP-4. The region of analysis is depicted by a box on Fig. 5.7d. It was about one–half hour after the frontal–wave pattern was best manifested, two hours after it began to appear, and one hour after the cold cloud tops were most extensive. The two main convective bands met near the middle of Fig. 5.10a, a junction labeled "Q" in Fig. 5.7d. The north–sound band *K* was a multicellular line south of Q. The east–west band *H* was the broader region without strong cellular echo that proceeded northeast from Q to the corner of the figure. At the 1.5 km (AGL) level in Fig. 5.10a, pronounced speed convergence of southeasterly wind was evident at the leading edge of band *K* where the gradient of reflectivity was tight. The winds are displayed relative to a reference frame moving at 15 $m\,s^{-1}$ from 265°. In the east–west band, low-level flow was confluent between the southeasterly regime on the south side, and the northeasterly regime north of the band. This agrees with the surface analyses of both systems B and C done in this study. Those analyses showed little air–mass contrast at the surface between the two regimes, even though the wind was markedly confluent. Rather, the thermal contrasts were seen at levels above 500 m AGL, above the shallow stable air.

Flow behind the apex region Q appeared anticyclonic and moving slowly relative to the system in this depiction. Smull's choice of reference frame differs from that in a previous analysis (Weather Research Program, 1987) of 18 $m\,s^{-1}$ from 240°, a choice more in accord with my best judgment of system propagation in Table 5.1 below (that choice

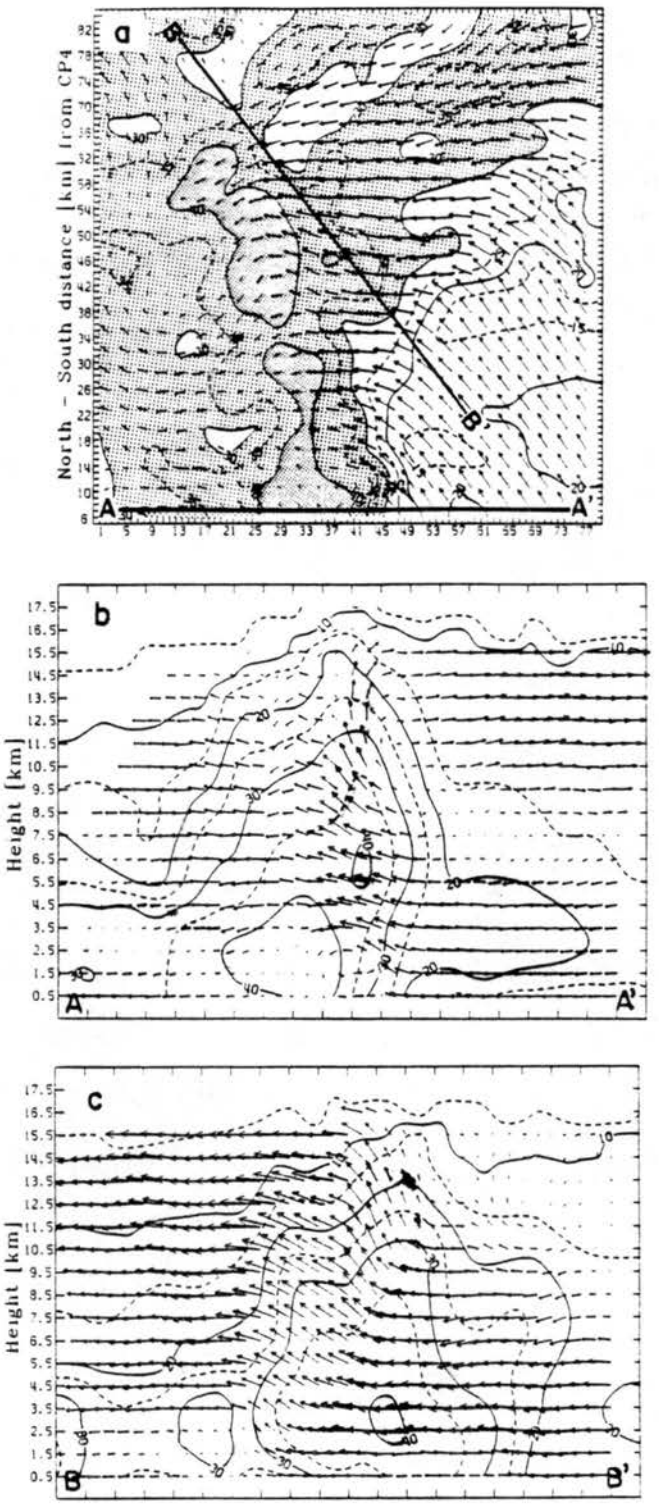

Figure 5.10: Reflectivity (dBZ) and relative velocity vectors (scale at top) from a dual–Doppler analysis of the boxed region in Fig. 5.7d. (a) Horizontal relative flow at 1.5 km AGL around the apex region Q. (b) Vertical cross section along A–A' through the north–south line *K*. (c) Cross section through the east–west band *H*. From Smull and Augustine (1989).

was 19.3 m s^{-1} from 270°). Smull's choice of the slower system velocity in Fig. 5.10a de-emphasized the low level outflow behind the convective region, made the inflow south-easterly instead of easterly, and reduced the inflow from the northeast in the northern region, in comparison with the previous choice of system velocity.

Table 5.1: Representative values of "system motion" as a function of life cycle stage

SYSTEM A

i. Developing: 24.5 ms^{-1} from 265°

ii. Mature: 15.5 ms^{-1} from 285°

SYSTEM B

i. Early (1900 to 2130): 19 ms^{-1} from 240°

ii. Developing (2130 to 2300): 22.7 ms^{-1} from 250°

iii. Mature and late (2300 to 0600): 19.3 ms^{-1} from 270°

At higher levels, there was acceleration (and divergence) of air from the front into the unusually strong echo near Q (reflectivities > 35 dBZ) at a height of 7.5 km. This flow continued to accelerate rearward toward the north and northwest, the direction that the cloud shield expanded the fastest. Such acceleration suggests that an elevated meso-low pressure perturbation like that analyzed by Lemone et al. (1984) was developing in the apex region. At the 13.5 km level the relative flow was strongly divergent from the apex region, especially toward the north.

Smull and Augustine highlighted the differences in their kinematic profiles along two cross sections through the two bands. A strong but very narrow updraft, about 10 km wide, and narrow downdrafts suggested to them that the north–south line in Fig. 5.10b was multicellular. Outflow toward the front was restricted to levels above 9 km. Outflow toward the rear was seen both above and below a flow minimum near 2.5 km above the ground. This profile of strong relative outflow in a shallow layer near the surface and

in a deep layer near 8 km agrees with our time-height wind profiles of systems B and C presented later.

The cross section along B–B' through the east–west stationary band showed a broad zone of updraft, at least 25 km wide, without cellular patterns. This may reflect in part Smull's choice of location of the cross section, as some cellular structure can be seen in the reflectivity field, though it was less than in line *K*. The ascent was both broader and more vigorous at high levels, and the front–to–rear flow was strong and deep along the direction of this section. An analysis of the possible role of conditional symmetric instability in organizing the broad sloping updraft of this band is reported in chapter 8.

The depictions of Smull and Augustine emphasized the role of the two convective bands and their intersection as key organizers of the mesoscale flow. Future analysis of Doppler wind fields in systems not as neatly organized as system B (such as our system C), would show whether the mesoscale forcing usually occurs along the prominent convective bands or, alternatively, in the whole stratiform cloud.

5.3 Evolution of mesoscale airstreams

In this section we investigate the distinct properties of various airstreams in system B with the meso–α–scale dataset from supplemental soundings and profilers, which sampled vertical profiles at 90 minute and 30 minute intervals, respectively.

5.3.1 The cold conveyor belt

The northern regions of this MCC and its near environment, and other MCCs like it, contained two distinguishable "cool" airstreams. One of them was a shallow layer, only some 500 m thick, of easterly wind from the ground up to a strong (6 K) frontal inversion. At the surface the temperature was typically 16° C, the air was saturated or nearly so and had θ_e values near 326 K. The contrast between the three regimes discussed in chapter 4 can be seen at the 900 mb level when system B was becoming an organized MCC. The northern row of stations (RSL, FRI) had temperatures near 15° C and θ_e values of 324 and 335 K; at the surface θ_e values were similar. These exemplified the properties of the

northern side of the front. The middle tier of stations seemed to lie in a transition zone. At the surface the θ_e values were 340 to 343 K; at 900 mb IAB was apparently in the warm air with a θ_e value of 353 K but PTT and CNU has similar values as at the surface. Oklahoma definitely lay south of the front, with θ_e values near 360 K at the surface and near 350 K at 900 mb.

The surface layer properties changed *very little* as the MCC passed through, except that the layer became even more shallow as the rear inflow depressed the inversion just after precipitation ceased. In system B, the surface layer persisted as a remnant of the moist downdrafts from a previous MCC, system A; the strong inversion prevented mixing out of the layer and persistent low cloud cover prevented heating of it. The surface layer was not dynamically active in these MCCs.

This is not true of the second cool airstream which we liken to a cool conveyor belt (Carlson, 1980). Both layers are depicted on the soundings at Russell (RSL) in Fig. 5.11a; at 2200, rain was beginning to fall in distinct showers around the station prior to their merger in the mesoscale rain system. See Fig. 5.7 for the locations of stations relative to the precipitation. Above the inversion at 870 mb, the air was saturated and neutral in stability at a constant value of θ_w=21° C up to 700 mb. A small amount of buoyant energy would have been released upon further lifting, as the profile at 2200 was close to the θ_w=20° C moist adiabat. But by 0000 UTC, when RSL was well within the stratiform precipitation, an inflow of cooler and drier air had destabilized the layer from 500 to 750 mb (dotted profile), so that the instability present in the 700-850 mb layer would have been magnified. System-relative northerly or northeasterly inflow (relative to the ground it was westerly, less than 10 ms^{-1}) reduced the temperature by 3 K and the θ_e by 6 K, at the 700 mb level. Before system B formed, values of θ_e throughout Kansas were near 33 K at this level; by 0000 UTC values had dropped to 326 K at those stations experiencing inflow from the north within the MCC (see Fig. 5.12a which depicts the convergence into the core region). This inflow first materialized in the 500-700 mb layer and may have been a response to the MCC–induced mesolow pressure.

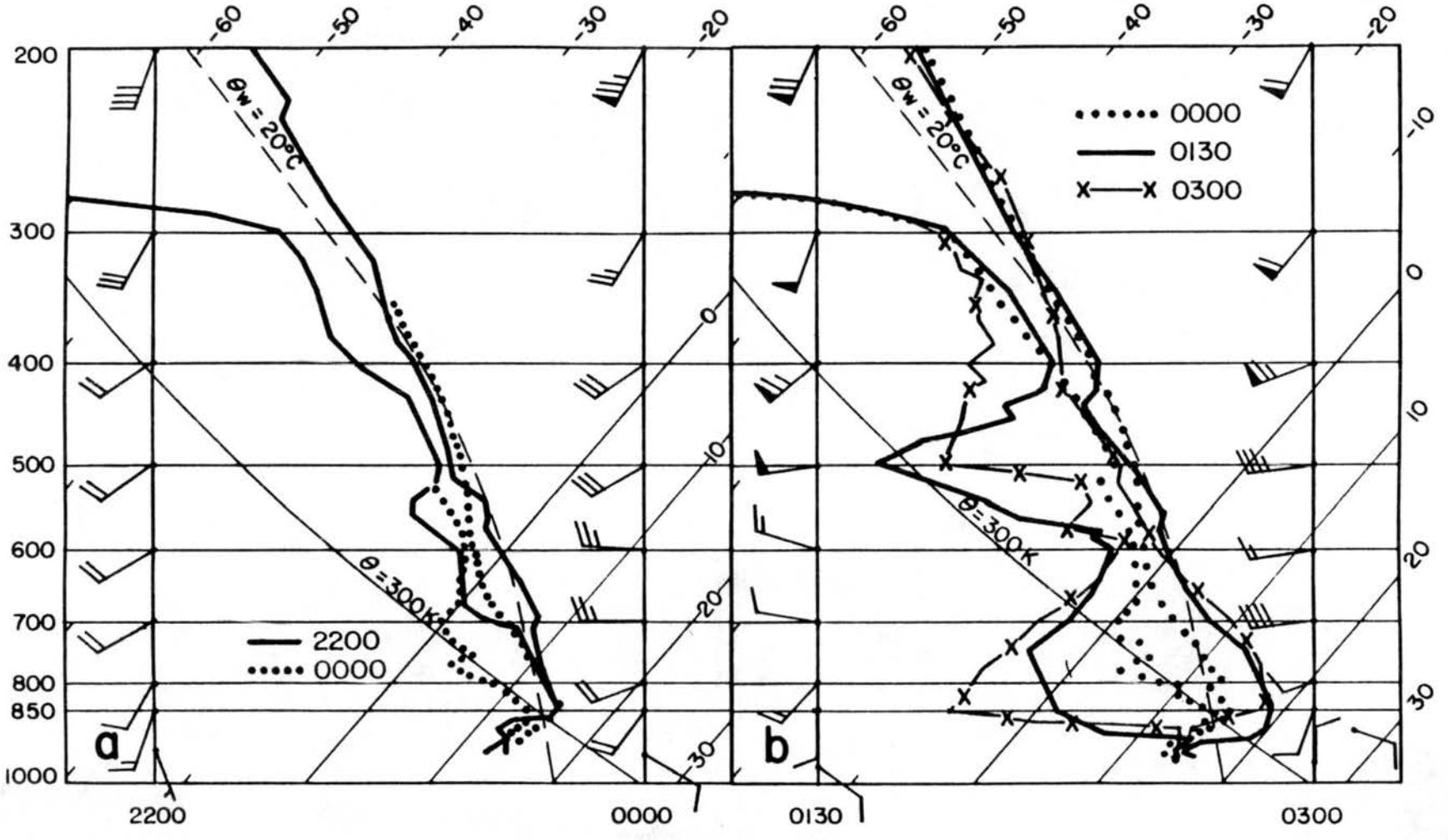

Figure 5.11: Soundings at Russell (RSL), at (a) 2200 UTC 3 June (solid) and 0000 UTC 4 June (dotted); (b) 0000 UTC, repeated (dotted), 0130 UTC (solid), and 0300 UTC (×) on 4 June. The winds are depicted as in Fig. 4.4 for the times indicated.

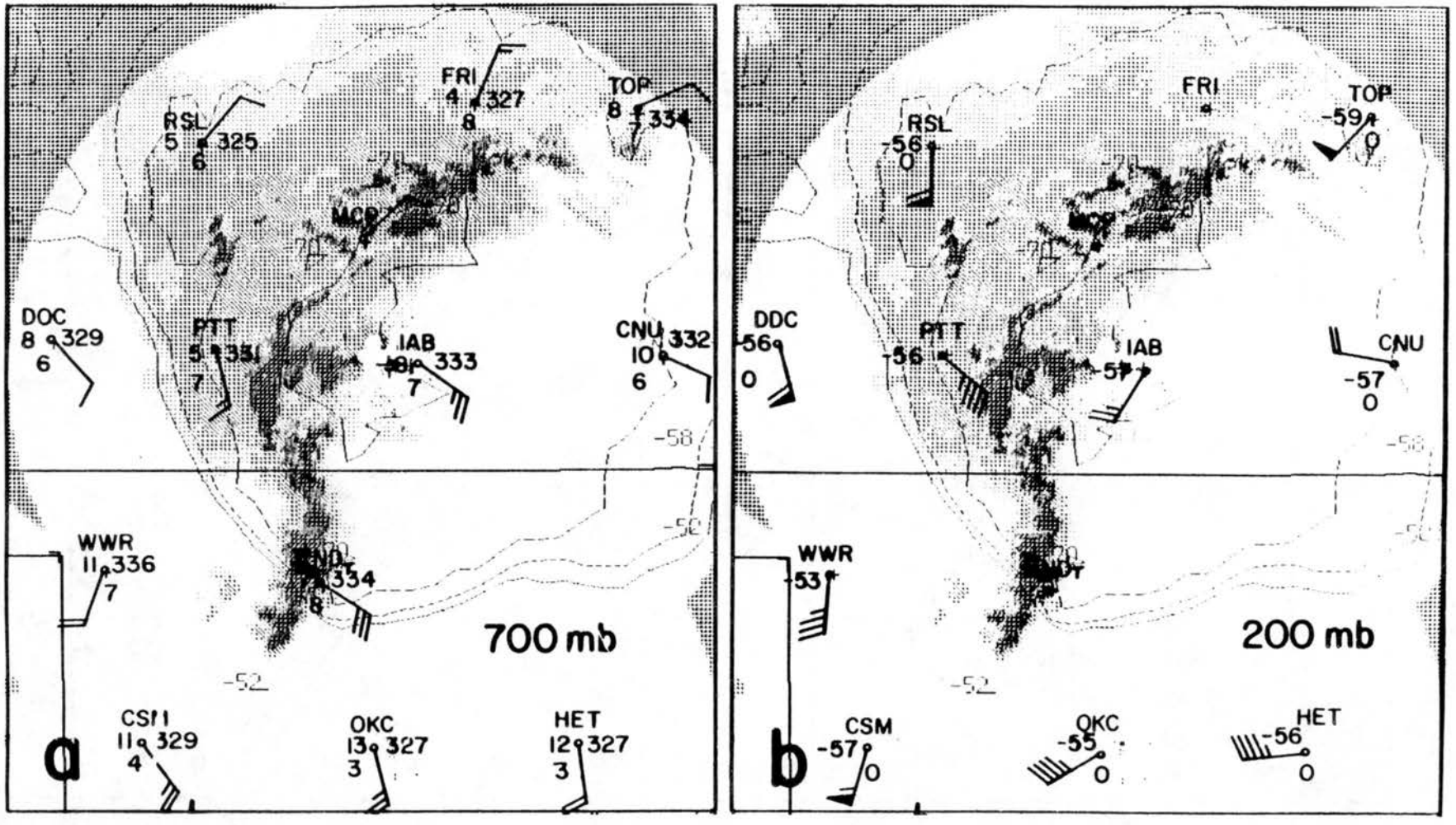

Figure 5.12: System relative rawinsonde data at (a) 700 mb and (b) 200 mb, and reflectivity at 0000 UTC, the mature stage. The system was moving at 15 ms^{-1} from 260° . Station identifier at top; temperature at upper left; θ_e at upper right in deg K; mixing ratio at bottom, of each station.

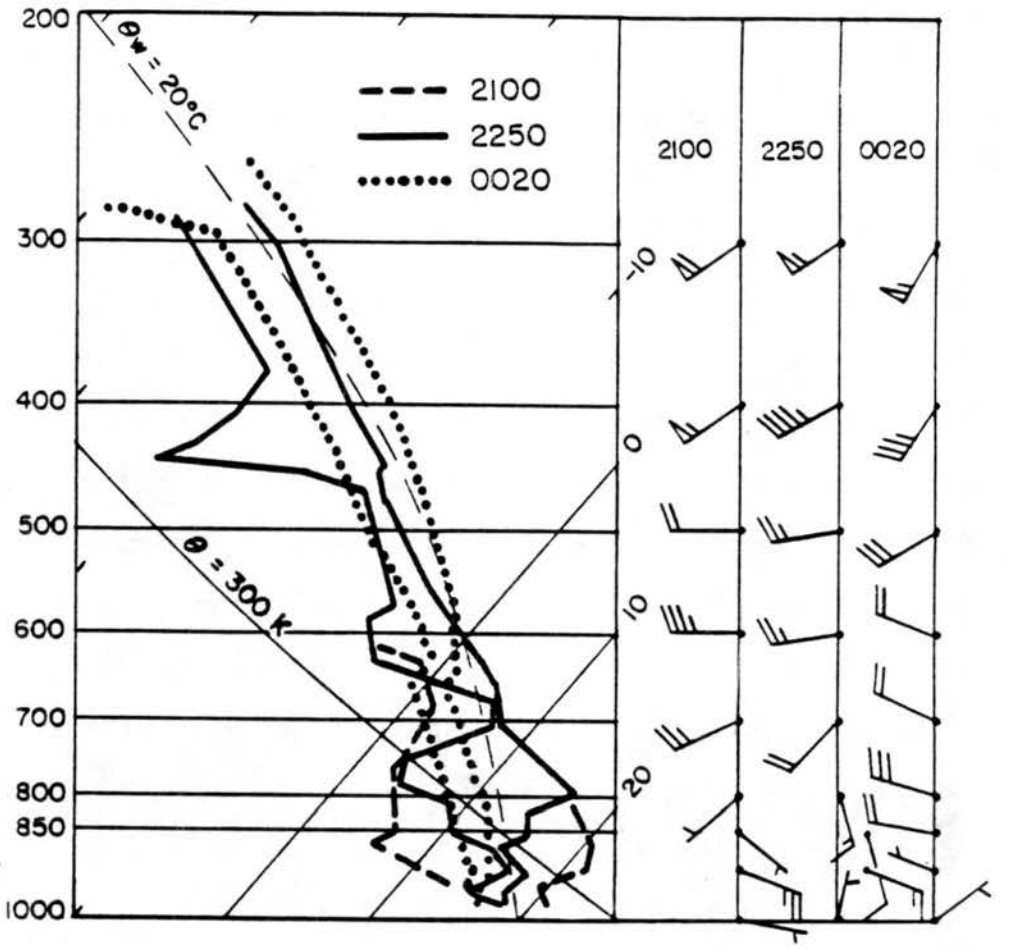

Figure 5.13: Thermodynamic and wind sounding at Fort Riley (FRI), at 2100 UTC (dashed), 2250 UTC (solid), and 0020 UTC (dotted), on 3 and 4 June. A dry adiabat (θ=300 K, thin solid line) and moist adiabat (θ_w=20° C, thin dashed line) are drawn.

The same scenario was seen later and at lower levels at Fort Riley (FRI), whose soundings appear in Fig. 5.13. At 2100 this station was still influenced by the mesoscale subsidence behind system A, and warm dry air prevailed above 920 mb (dashed profile). At 2250 system B had not yet arrived, but the layer from the surface to 800 mb had cooled and moistened in the easterly flow. The profile (solid line) had stabilized through this depth, and only a shallow layer near 700 mb had any potential instability. The cooling in this region was evidence of frontogenesis that strengthened the stationary front just south of here after recovery from the previous MCC. By 0020 Fort Riley was deep in the stratiform rain, only 30 km north of the east-west convective band H. Further cool advection and evaporation of rain led to the dotted profile in Fig. 5.13. The upper

troposphere had warmed above 600 mb, and exhibited a nearly constant θ_w of 20° to 21° C in stratiform cloud. Because the lower troposphere had a nearly constant θ_w value of 18° C, evaporation alone could not have effected the cooling; inflow of lower-valued θ_w air from the north and east must also have been responsible.

Thus the contrast between the unusually stable surface layer less than 1 km deep, and the marginally unstable air above it, was eliminated by the MCC, at least during and for several hours after its passage. A previous MCC had deposited the stable layer and strengthened the pre-existing frontal inversion. The subsequent MCC released the potential instability in the layer above it, but then drew potentially cooler air from the front and north side into the mid-levels (remember that a temperature gradient had been present). Evaporation of rain into the unsaturated inflow cooled it further. The neutral stratification and negative buoyancy of the 600-800 mb layer would argue for subsidence of this air. Its equivalent potential temperature came to have the same value as that observed at the surface, so it is concluded that the cool conveyor belt descended to the surface in saturated downdrafts within the frontal zone.

As the MCC marched eastward, the supplemental sounding stations were located increasingly to the rear of the system. Before the rain ceased to fall, subsidence set in, in two deep layers beneath the precipitating stratiform cloud. The lower of the two layers harbored system-relative northeasterly flow coming from the interior of the echo. In an absolute sense this flow consisted of weak westerlies slower than the propagating precipitation echo. Both subsidence layers are depicted on the soundings at Russell in Fig. 5.11b, on which the 0000 UTC profile (dotted) has been repeated for comparison. At that time, the base of the stratiform cloud was at 660 mb, mixing ratios were decreasing beneath cloud base, and the top of the strong inversion was at 860 mb. By 0130, when the rainfall was ending at the station, pronounced warming and drying were seen from 600 down to 750 mb. The nearly constant potential temperature ($\theta \sim 311$K) and mixing ratio (4 g kg^{-1}) suggest dry adiabatic subsidence from 600 mb. The zone beneath 750 mb also warmed and dried, and depressed the inversion down to 910 mb. The winds did not

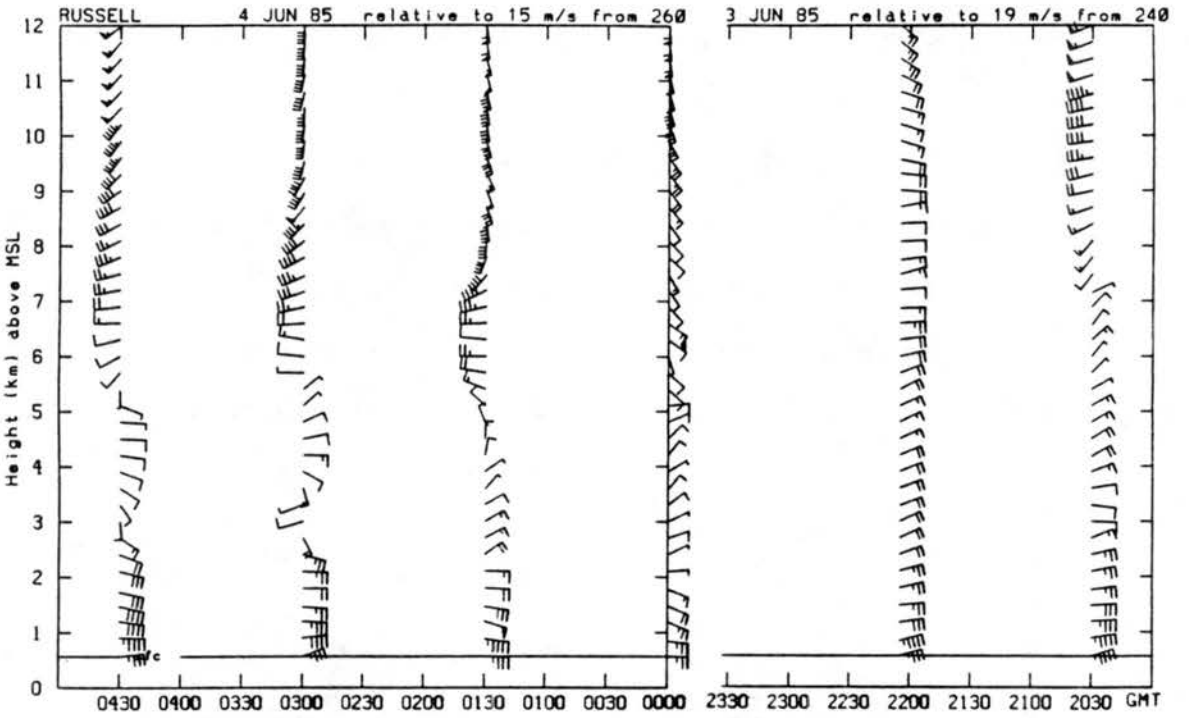

Figure 5.14: Time/height relative wind profiles at Russell. Time goes from right to left, from 2030 UTC 3 June to 0430 UTC 4 June. The system motion that was subtracted is displayed at the top.

change much in the lower subsidence zone; if anything the relative easterlies strengthened near the 2 km level (profiler time series in Fig. 5.14). The subsidence continued at 0300 UTC (profile of × in Fig. 5.11b) from 590 down to 850 mb.

In contrast, the winds increased to ~20 ms^{-1} *inflow* from the *west* in the upper subsidence zone, which extended from 420 to 520 mb at 0130 (thermal profile in Fig. 5.11b, wind profile in Fig. 5.14). Both the dry adiabatic layer and the rear inflow jet were observed to be higher farther and farther behind the MCC. A different airstream is thus believed to be subsiding in the upper onion sounding; this is the dry conveyor belt discussed elsewhere.

5.3.2 The warm conveyor belt

Using dual Doppler observations Smull and Augustine (1989) mapped the ascending branch of the warm conveyor belt near the apex region of system B (see Section 5.2.3 of this chapter). They depicted a broad zone (35 km wide) of ascent along the east–west reflectivity band, which we have called band "H". Outflow from the band filled a deep

layer from 5 to 15 km with stratiform cloud. A smaller part of the low-level inflow was lifted in a narrow (10 km wide) squall line "K" advancing into the warm air at 15 ms^{-1}, and acting like a mesoscale cold front.

Their analysis of the soundings led to the conclusion that the intense convection in line *K* was rooted in the surface layer, while the ascent in the broad band *H* was based in the layer above the shallow stable layer, but below 800 mb. From 700 to 500 mb, the strongest convergence shifted increasingly west of the apex region. Outflow from this region was directed to the northeast, north, and especially northwest, at levels from 7 to 15 km.

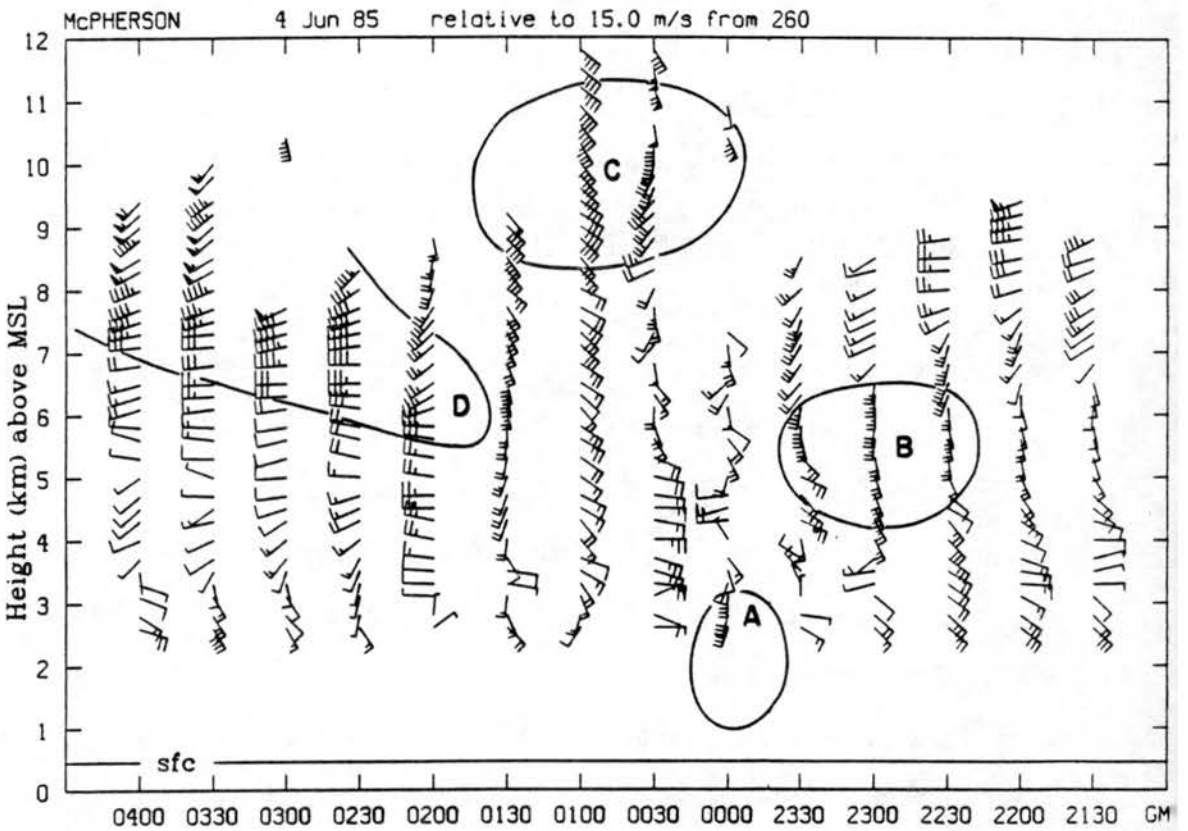

Figure 5.15: Time/height relative wind profile at the McPherson profiler, as in Fig. 5.14. The letters A,B,C,D mark phenomena discussed in the text.

Sometimes it is observed that the low level jet accelerates just before the arrival of the convective core region of an MCC. The evidence for such an acceleration is not strong in system B. But changes in the lower portion could be seen at Chanute (CNU),

where the wind increased modestly by 2 to 5 ms^{-1}, the temperature rose 1 to 2 K due to warm advection, and the mixing ratio increased 15 percent, in the layer from 500 m to 2500 m, during a 90 minute interval before the forward overhang of the stratiform cloud arrived. The subsequent events at Chanute deserve comment. The warm, moist advection had raised the convective instability substantially below 2.5 km, but it was capped by relative southerly inflow of drier, *lower*-valued θ_e air from that level up to cloud base. (This probably was part of the frontogenetic process). Precipitation from the deep stratiform cloud then led to an isothermal layer 700 m deep at the base of the cloud, beneath which the unsaturated dry adiabatic layer had been cooled by 6 K, because of melting and evaporation of the precipitation. This essentially eliminated the cap, and enabled convection to develop on this southern margin of the stratiform cloud.

A more sustained acceleration of the southerly jet was observed over a several hour period before System C (next chapter).

A pronounced acceleration of the *middle level* southerly flow *was observed* before the MCC. This was seen at elevations from 3 to 8 km at Wichita and at *B* in Fig. 5.15 at McPherson. It was also observed at Pratt and at Chanute. The transient acceleration of 1 hour or less is probably a response to the developing low pressure of the approaching mid–level meso–cyclone, and perhaps an effect of the blocking of environmental southwesterly flow by the approaching mesoscale complex. The latter point is bolstered by the fact that the mid-level wind often, though not always, veered before the MCC arrived.

Downstream blocking of flow is definitely observed in the upper troposphere. Deceleration and veering were seen above the 9 km level from 2230 to 0000 UTC at Wichita and above 8 km from 2030 to 2200 at Russell (Fig. 5.14), where stagnation and even reversal of the relative flow occurred; and at Pratt and Enid (not shown). Sometimes the reduction of speed at high levels and its increase at middle and lower middle levels led to a *homogenization* of the wind profile in the convectively active region of the MCC. An example is in Fig. 5.14 at 2200 UTC, at least above the 2 km level. It suggests that the core region of an MCC is shielded to some extent from disruption by environmental shear.

Comparing the horizontal Doppler wind field at 13.5 km by Smull in Fig. 5.10c with our larger scale relative winds at 200 mb in Fig. 5.12b, we see that outflow diverged strongly from the apex region, largely toward the north, but with a component toward the front in advance of the source region, and a component toward the rear behind the same. This was true even beyond the edge of the cloud shield.

The transitions in the high outflow layer are abrupt. The left–most and right–most wind profiles in Fig. 5.14 sampled the undisturbed flow above, say, 10 km. Then at 2200 the 30 ms^{-1} flow stagnated and reversed; at 0000 when the interior of the stratiform cloud was sampled, outflow was directed due north (on the left flank of the MCC) at 30 ms^{-1} for over three hours. With its 30 minute sampling, the McPherson profiler caught the rapid transition of the upper winds just when the apex region passed the site at 0045 UTC (region *C* in Fig. 5.15).

Augustine (personal communication) reported a 3 K warm core at 350 mb and a 3 to 6 K cold core at 150 mb, both centered on the middle rear margin of the cloud shield of system B. Most of the upward flux of air with high CAPE therefore sloped west and behind the apex region.

We infer that the path of the warm conveyor belt in system B is as follows (it may be helpful to refer to the plan view in Fig. 9.4 and the conceptual model in Fig. 9.5 in chapter 9). A portion having very high θ_e values near 360 K flowed north at ground level and was engulfed by the supercell–like storms on the southern end of the pseudo–cold front in Oklahoma. This air ascended in vertical updrafts and exited both forward and rearward at 150 mb. The major portion of the conveyor belt rode over the shallow cool air north of the surface cold front, without release of convective instability, in the 900–800 mb layer. It then encountered the developing meso–β–scale core region where convective clusters propagated along the elevated stationary frontal zone from 900 to 700 mb. The instability which had been capped was released, at first in widely separated clusters, later in a continuous east–west reflectivity band that developed from the merger of those clusters. Here the conveyor belt rose in steeply sloped meso–β–scale convective

ascent which was largely non-cellular. Outflow occurred in a deep zone from 5 to 15 km filled with stratiform cloud.

Above 8 km, the outflow was directed northeast from the forward region of stratiform echo, north from the apex region, and northwest from the rear region. The cold anomaly at the tropopause resulted from overshooting beyond the equilibrium level; its location on the rear margin of the precipitation, due west of the apex, implied that the core of the warm conveyor belt sloped front-to-rear with height. There was a sharp rear edge to both the precipitation echo and the cloud, where the upper winds were diverted north and accelerated around the left side of the MCC. The sharp cloud boundary resembled an upper level front where the moist, ice–laden outflow from the MCC encountered the diverted ambient winds.

Note that this path does not depend on any cyclonic rotation of the warm ascending airstream. It is possible that most of the cyclogenesis in middle levels occurred in the descending airstreams. The ascending stream acquired anticyclonic curvature after it rose past the height of the warm anomaly.

5.3.3 The dry mid–level inflow

Rear inflow was observed quite early in system B. The Liberal (LIB) profiler was well positioned to observe it at 2100 UTC when the MCC was midway in its growth stage (see map in Fig. 5.6c). The convective band just east of LIB was less than one hour old and precipitating stratiform echo had not yet appeared, though a sizable cloud shield had developed. The inflow was observable for at least five hours after 2100 UTC in a narrow unchanging layer from 5.5 to 6.5 km in height (Fig. 5.16). Note that the inflow formed at a height which was a "steering level": before the MCC approached at 2030, the winds were light and changed direction at the 6 km level in this relative frame of reference.

Stumpf (1988) analyzed a convergence line at the mature stage (0000 UTC) along the rear margin of system B where front–to–rear flow encountered dry rear–to–front flow. This line extended from south to north along or just behind the strongly convective line in Oklahoma, then along the rear margin of stratiform echo. He found "strong rear inflow"

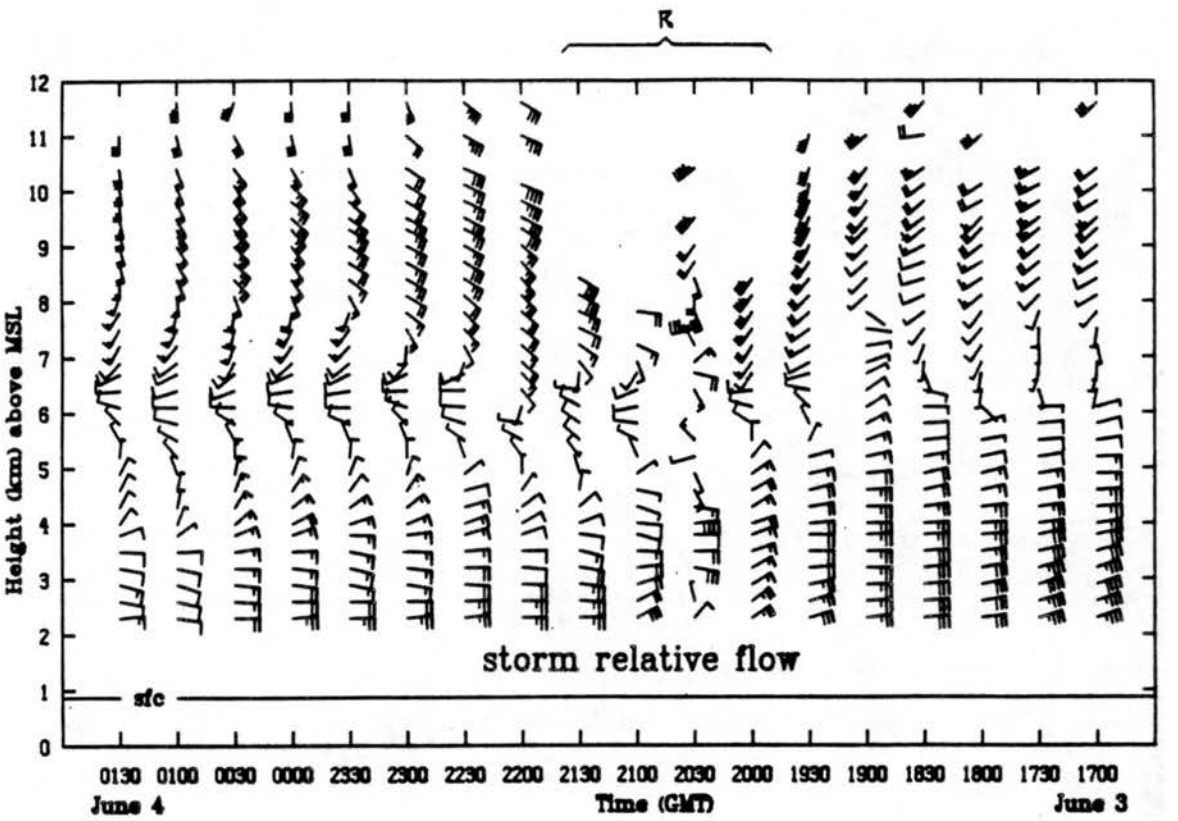

Figure 5.16: Time/height cross section of winds from the Liberal (LIB) profiler, as in Fig. 5.14. From Augustine and Howard (1988).

above the freezing level and descending slightly from 400 to 500 mb at the northern sounding stations. Weak, dry rear inflow was found at the central tier of stations (IAB and PTT); it did not penetrate the system very far. A well defined rear inflow was not present at the southern stations END or WWR.

Stumpf (1988) also reported an analysis of a dual Doppler velocity field on the southwest rear margin of system B; the analysis was done by B.F. Smull (of the National Severe Storm Laboratory branch in Boulder, Colorado), but not reported elsewhere. He reported rear inflow of $\sim$ 12 ms^{-1} from 4.5 to 6.5 km along the base of the anvil. The inflow proceeded as far as a convergence zone which coincided with the 15 dBZ reflectivity contour on the rear margin, and which sloped rearward with height. Rather than descending gradually, the inflow encountered opposing flow and abruptly descended not far into the precipitation zone, in the zone of virga. The intense localized subsidence and associated

warming were hypothesized by Stumpf to cause extreme pressure falls on the east side of the surface wake low.

Our rawinsonde and profiler analysis confirms that the character of the dry inflow changed from north to south. In the north, where stations were in stratiform precipitation for the longest time, the profiles had a double vertical structure as discussed in section 5.3.1. There it was stated that inflow from the north dried out the lower "onion" part of the profile in Fig 5.11. The upper zone appeared to be part of the high (5 to 7 km), non-descending rear inflow that has an abrupt onset and that seems typical of this type of MCC. The onset coincided with the departure of the stratiform echo. At that time (0130 UTC), the inflow resembled a westerly jet, up to 20 ms^{-1} in the relative sense, with strong shear at its base near 5.5 km, and strong backing of the wind at its top at cloud base.

5.4 Kinematic profiles of the mesoscale airflow

In order to determine whether the vorticity was increasing in this MCC at any level and in any quadrant, one can apply the kinematic analysis technique of Bellamy (1949) to the mesoscale dataset of supplemental soundings at the growth and mature stages. A set of triangles can be drawn to analyze appropriate regions of the storm system as in Fig. 5.17. At 0000 UTC, the mature stage, a polygon formed of 9 triangles enclosed nearly all of the MCC. Different triangles were chosen for the analyses at 2230 UTC (the growth stage) and 0130 UTC (the post–mature stage) but at these times the polygons enclosed much less of the radar echo of the system.

The technique involves computing line integrals of the wind components around the perimeter of triangles formed by the points of observation. Ceselski and Sapp (1975) and others assert that this method is less prone to error and produces less noisy second–order derivatives than objective analysis. Bosart (1986) and Bosart and Sanders (1981) employed Bellamy's approach in their budget analysis of the Johnstown flood. There are, nevertheless, the following sources of error. It is assumed that the wind varies linearly from one observation point to the next, and thus that the areal average vorticity and

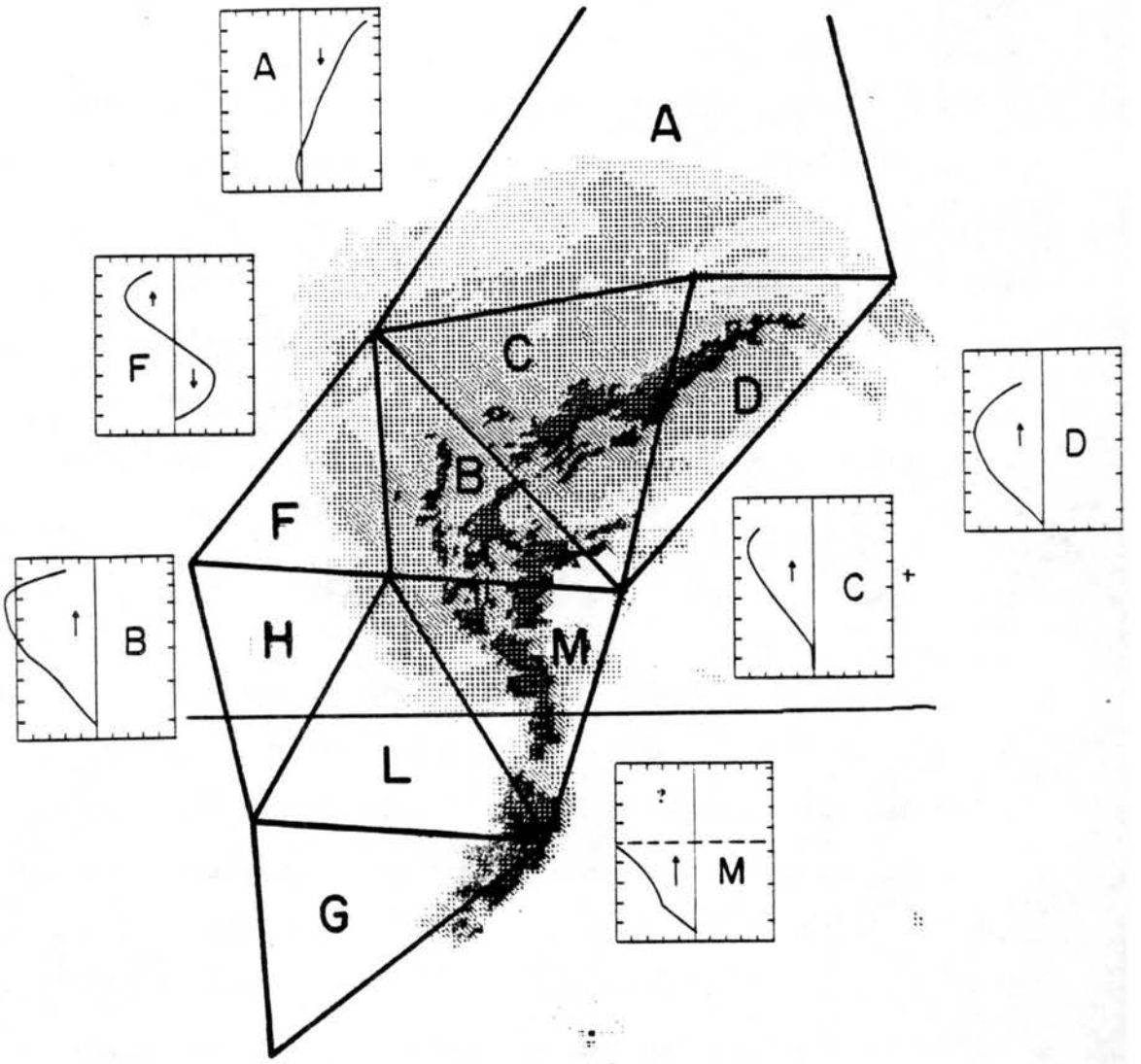

Figure 5.17: Locations of the Bellamy triangles as marked by capital letters on the rada echo of system B at 0000 UTC. Vertical profiles of vertical motion ω in 6 triangles ar displayed around the periphery.

divergence in any triangle is the same as the point values at the centroid of the triangle. A glance at Fig. 5.17 leads one to suspect that the assumption of a linear wind field is violated near the convective lines. Secondly, failure to account for the drift of the balloon with height can lead to errors of the order of a few percent; this error can be serious near the tropopause. Finally, the measurement errors of the balloon–tracking system are magnified when one computes the difference of two large but nearly identical values of, say, wind speed at the two observation points.

It was mentioned that the sounding network did not completely enclose the MCC at 2230 and 0130 UTC. Loss of portions of the vertical profiles made analyses at these hours even less representative. Data from the Liberal profiler was used at 2230 UTC, but the absence of data below 800 mb from Liberal meant that 2 of the 6 triangles (or about one–half of the area of echo) did not contribute to the area averages in the low levels. Similarly, the termination of one sounding (FRI) at 850 mb eliminated the contribution of 2 triangles that enclosed nearly all the stratiform rain area, the stationary frontal band and the apex region at the later time. Early termination of soundings caused less serious data dropouts at 0000 UTC.

Profiles of divergence (dashed) and relative vorticity (solid) are plotted in Fig. 5.18 at the three times. The profiles are area–weighted averages of those triangles with data at the three vertices, at any given level. Since triangle A was more than three times larger than the others and was located mostly outside the MCC, its inclusion considerably weakened the signal in the areal averages. The profiles in Fig. 5.18 have been computed without the contribution of triangle A. A uniform profile of moderate convergence was analyzed from the surface up to 400 mb at the growth stage (2230 UTC, panel a). The vorticity signal was very weak in these layers. High–level divergence was just getting underway.

At the mature stage (Fig. 5.18b), convergence intensified and exceeded 0.5×10^{-4} s^{-1} in the mid layers from 825 to 450 mb, and anticyclonic, divergent outflow had become established in the high levels, from 150 to 350 mb. This agrees with results previously reported for a mesoscale convective system. However, the vorticity profile was *essentially*

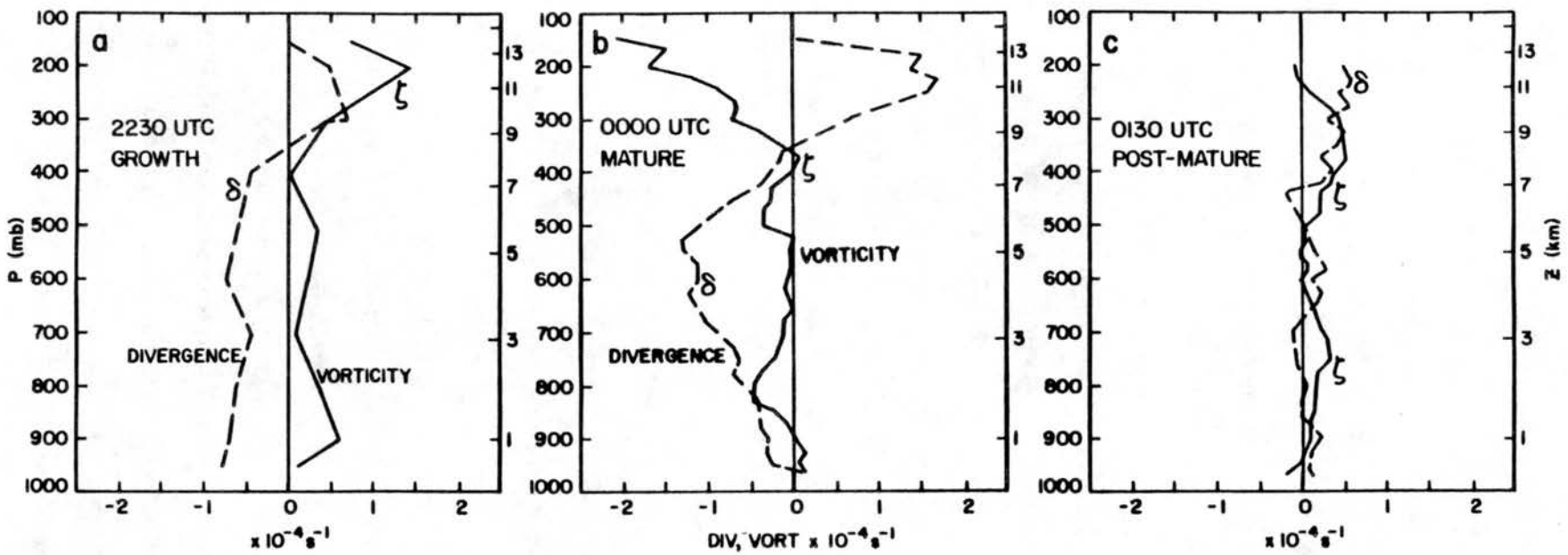

Figure 5.18: Vertical profiles of horizontal divergence δ and relative vorticity ζ in the polygons containing the MCC, at (a) 2230 UTC 3 June, (b) 0000 UTC 4 June, and (c) 0130 UTC 4 June. The profiles in (b) omit the contribution from triangle A.

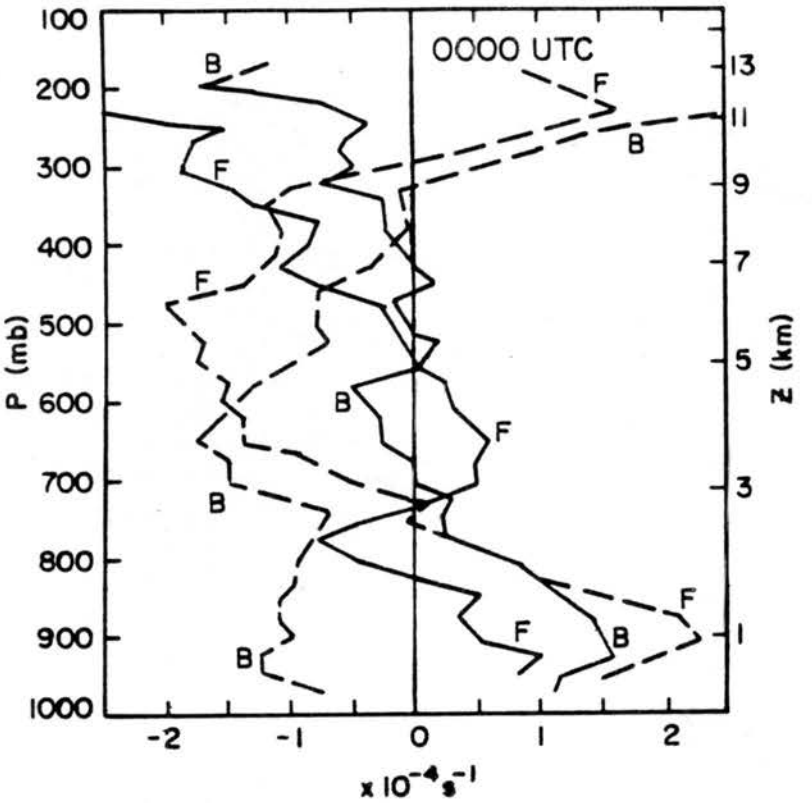

Figure 5.19: Vertical profiles of divergence (dashed) and relative vorticity (solid) in two triangles B and F located on Fig. 5.17.

zero from the surface to 400 mb, and the divergence expected near the surface was also not observed. Results from two individual triangles are depicted in Fig. 5.19. The strongest cyclonic vorticity was located in triangle B, which included the apex region, and F, where the rear inflow was strongest. Relative vorticity exceeded 10^{-4} s^{-1} (equivalent to the Coriolis parameter) beneath 825 mb in B, and was weaker but positive in F at those levels. Vorticity was also cyclonic in F in a portion of the middle troposphere, but not in B. In both triangles the outflow was highly divergent and anticyclonic above 300 mb.

Convergence was strong in deep layer from the surface to 450 mb in the apex region B. It was also strong from 700 mb up to 300 mb in the rear inflow region F; beneath that divergence was pronounced.

After maturity, the profiles of both divergence and vorticity were weaker (Fig. 5.18c), but it must be remembered that no portion of the stratiform region nor the core of the MCC could be sampled at the later time.

The divergence was vertically integrated to yield vertical motion ω in pressure coordinates at time 0000 UTC. Customarily, a second integration is computed with a correction to the divergence at each level in order to force ω to zero at the surface and at 100 mb. This was not done here because data from 8 of the 9 possible triangles were missing at 100 mb. So many soundings terminated below 100 mb that it was decided to report the uncorrected results. Vertical motion was not computed at 2230 UTC because of the above–mentioned absence of a significant portion of the data below 800 mb, nor at 0130 UTC because of the significant data losses above that level.

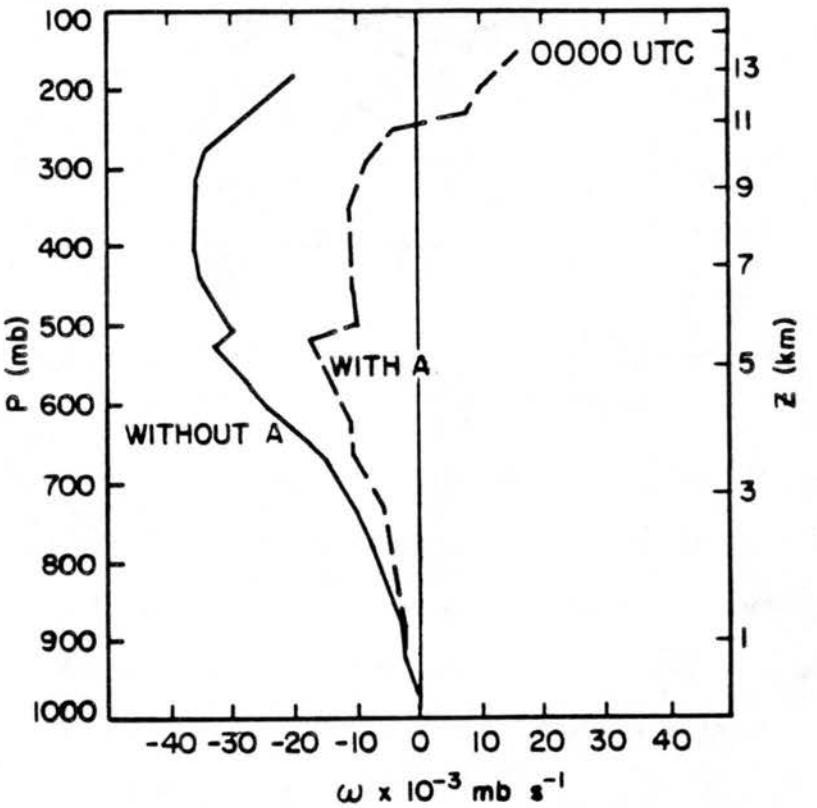

Figure 5.20: Vertical profile of vertical motion ω in p–coordinates, for the polygon of 9 triangles, at 0000 UTC. The contribution of triangle A is excluded in the solid profile included in the dashed profile. Units of ω are 10^{-3} mb s^{-1} or roughly cm s^{-1}.

The area–averaged vertical motion is plotted in Fig. 5.20 with and without the inclusion of the large triangle A; this one triangle is seen to have a large effect at upper levels not only because of its large area but also because sinking was prevalent in that region. With A excluded, rising motion is seen to be prevalent from 500 to at least 200 mb, a

speeds of roughly 30 cm s^{-1} in the area average. Significantly, descent is not observed at any level in the area average.

The vertical motion profiles in sub–regions of system B are plotted around the periphery of the radar echo in Fig. 5.17. Strongest ascent is analyzed in the apex region (B) and regions containing the east–west convective band (C and D), but note that the level of strongest ascent descends from west to east. The strong ascent in the lower troposphere in triangle M is representative of a more convectively active region. Finally, the rear inflow region (F) exhibits an S–shaped profile of ascent above 5 km and equally strong descent below 5 km.

This analysis failed to reveal system–wide, meso–α–scale vorticity of either sign beneath about 400 mb, although the apex region and the rear inflow region did exhibit moderate cyclonic vorticity that increased with time, in the low and middle levels respectively. There *was* a strong convergent response in mid–levels and a divergent one in high levels. When comparison is made with MCCs that exhibited a stronger vortical convective pattern and stronger vorticity in later chapters, it is concluded that system B represents a prototype of MCC that never achieves a geostrophically balanced state although it tends to evolve in that direction.

5.5 Discussion of system B

System B grew to be the largest and best developed example of a mesoscale frontal wave in the cases studied. The wave pattern was manifested for 3 to 4 hours in the distribution of convective storm echo and in the gradients of wind and temperature at the surface and in the lower troposphere.

The first storms developed in a north–south swath parallel to the general slope of the terrain in the Texas panhandle. Convection later became focused on one solid multicellular line that extended south from the MCC and that propagated east in step with it. This line acted like a cold front in the overall frontal wave pattern, even to the point of demarcating air masses.

The cool air behind this front was associated with a ridge of meso–high pressure; peak pressures were found just west of the apex region where the two convective bands intersected and where rising motion was especially concentrated. The other meso–high pressure center, a broader and weaker one, was situated under stratiform cloud north of the east–west pseudo–warm front. The convection on the latter boundary lacked cellular structure; Doppler radar data suggest that air entered it from the southeast beneath 3 km, and ascended in sloping fashion to the upper half of the troposphere in a zone 30 km wide.

A pronounced signal of low pressure and convergent inflow developed in the middle troposphere just west of the apex region. The convergence was displaced increasingly west with height, and so was the upper tropospheric rising motion. This may have been a consequence of the rapid propagation of the apex region while the updrafts took time to reach cloud top.

Although the divergent wind response was evident, system B may not have fostered its convection long enough for the rotational wind to respond to the pressure anomalies. Kinematic analyses did not exhibit a consistent cyclonic signal from time to time or from level to level. It is felt that two factors hindered the cyclogenesis in this system. Strong southerly flow persisted parallel to and behind the pseudo–cold front in middle levels, in a direction counter to any cyclonic circulation behind this front. The other factor was the maintenance of the stratiform cloud or at least the precipitating portion of it, in the northern half of the MCC. This caused rear inflow of the dry airstream to develop most strongly in the northern region, less so in the apex, and not at all south of the apex. Rear inflow into the northern side would have opposed cyclonic spin–up around the convectively active apex region. The stratiform region and the convectively active region were simply misplaced for optimal spin up and consequent long life of the mesoscale convective complex.

System B apparently failed to develop further from the frontal wave stage to a true occlusion. As such, the development of the mesoscale cold front may have less to do with spin–up of the meso–α–scale cyclone, and more to do with the preferential developmen

of convection on the southern margins of the incipient MCS, where conditionally unstable air is deepest and the highest values of CAPE are to be found. Once a few intense cells merge into a meso–β–scale cluster or squall line, the positive feedback of a growing cold pool may begin. Due to density differences the chilled air would spread south and east into the warm air, rather than north into air which is increasingly chilled by mesoscale downdrafts from the apex region.

The configuration of convection in frontal–wave bands seemed to promise a long–lived cyclone, but the northward advection of the stratiform precipitation away from the two intersecting bands may have inhibited further cyclogenesis.

Chapter 6

SYSTEM C: A CHAOTIC PATTERN OF CONVECTION EVOLVED INTO A SPIRAL PATTERN

Only 10 hours after system B swept through Kansas, yet another large and rapidly evolving convective mesosystem passed through the same area. "System C" was able to tap convective available potential energy over a broad region within 7 hours after system B stabilized the troposphere. Its convective entities were widely dispersed in no obvious spatial pattern for about three hours, but then they coalesced into a spiral pattern different in important ways from Systems A and B.

6.1 Evolution of convective components

A narrow intense convective line formed along the northern slope of the Canadian river valley between Amarillo (AMA) and the Oklahoma panhandle after 0400 UTC 4 June. It was oriented 40 km wide and 300 km long by 0600 UTC (see Fig. 6.2a). During these 2 hr, the line developed a sharp bend or "cusp" at O midway along its length. It developed north of a mesoscale cloud shield that originated from thunderstorms nine hours earlier in high terrain in southeastern New Mexico. The southern system, which propagated along the stationary front into western Oklahoma for some 6 h, barely attained the duration criteria for an MCC. The two systems were separated by a narrow region of lower cloud tops. Both systems are visible on satellite images in Fig. 6.1a.

System C attained the criteria for an MCC by 0630 UTC. At "initiation", the radar echo pattern contained a broken band from "O" toward the direction 60° (toward B), and a solid line of echo extending south of O (Fig. 6.2b). These two bands formed a right angle pattern that continued to evolve into the meso–α wave pattern of the mature stage: there was continuity through the developing stages. The convective rainfall rate and volume

had already reached a sharp peak at 0530 UTC, and had "collapsed" to minimum values by the time of initiation (McAnelly and Cotton, 1989a). Both the area and volume of convective and stratiform rainfall then began to increase steadily until sometime between the growth and the mature stage.

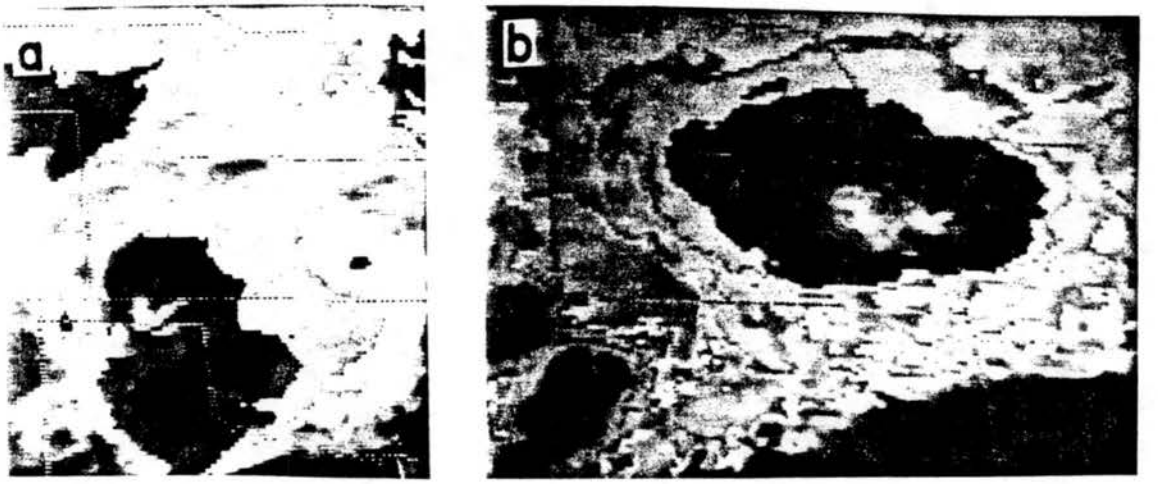

Figure 6.1: Satellite images of system C at (a) 0600, and (b) 1030 UTC 4 June 1985 with MB enhancement.

The next set of clusters formed in two well separated areas. The first is exemplified by cluster B, which formed within 100 km of the main system. Separate lines formed parallel to the two axes of the right angle, so that the convective echo tended to expand north and south, and also to extend the original line east–northeast toward the direction 65°. The development of separate clusters like C, and new lines parallel to older lines can be seen on Fig. 6.3a. The stratiform echo began to be advected north of the new clusters as well as spread out west of them, as the older clusters dissipated.

Another set of clusters developed north, east, and southeast of Wichita (ICT), some 300 km from the original cluster, but in the same direction (65°) toward which the MCC was propagating. One cluster had developed cloud tops as cold as −58°C as early as 0600 UTC, at the time of Fig. 6.2a. By 0720 UTC, three new clusters of meso–β–scale dimensions had developed north and east of Wichita (Fig. 6.3a,b). The first set of clusters developed underneath the main cloud shield. The other, more distant set did not, rather several small cloud shields grew and finally merged with the main MCC only after two hours.

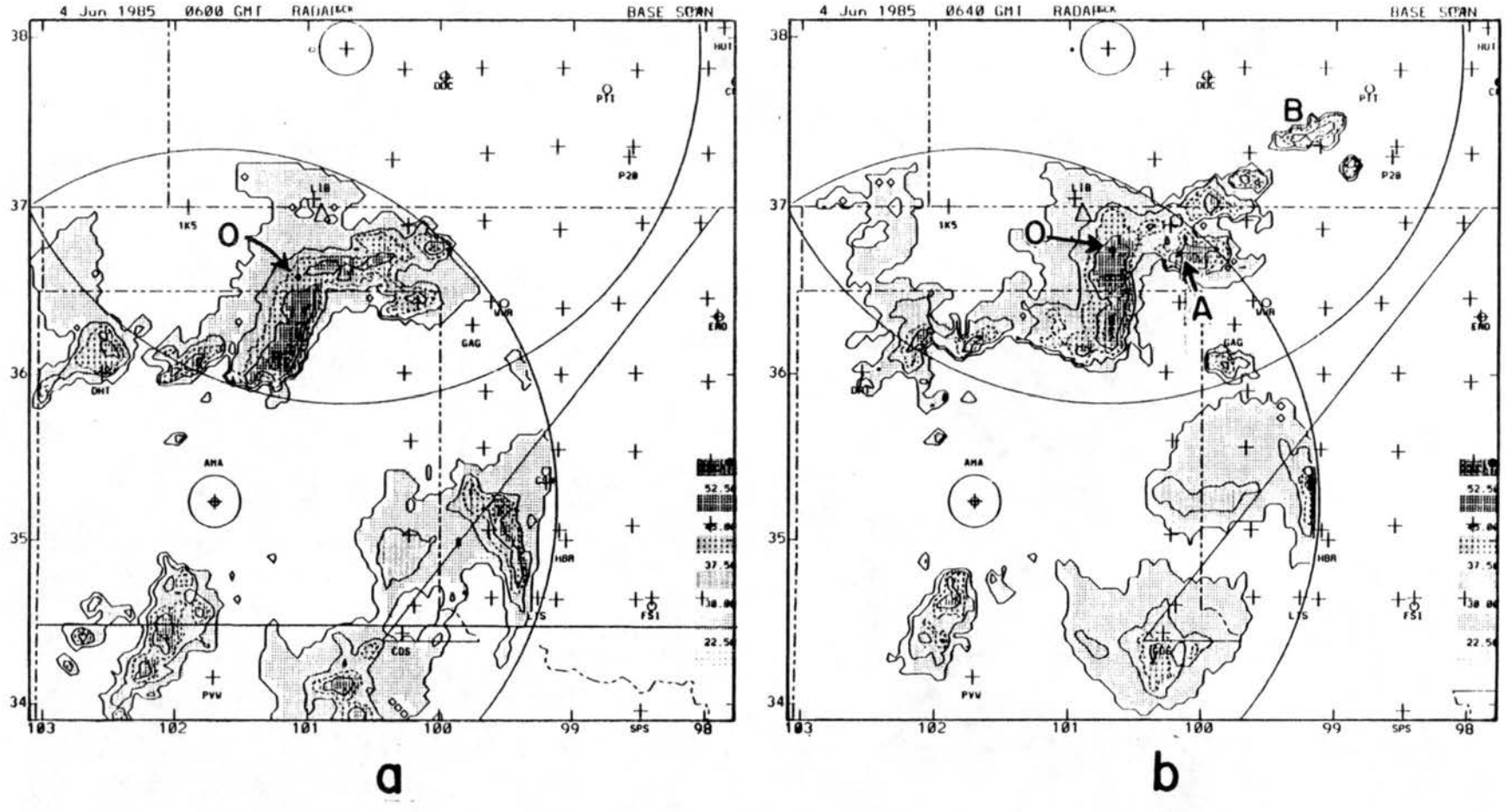

Figure 6.2: Images of reflectivity of System C in its initial stages from radars at GCK and AMA at (a) 0600 and (b) 0640 UTC 4 June. The 3 solid contours represent 15, 30, and 45 dBZ, dashed contours represent intermediate levels. The six levels of reflectivity are keyed to gray shadings in the legend. System C formed in the panhandle region; the southern system is another MCC.

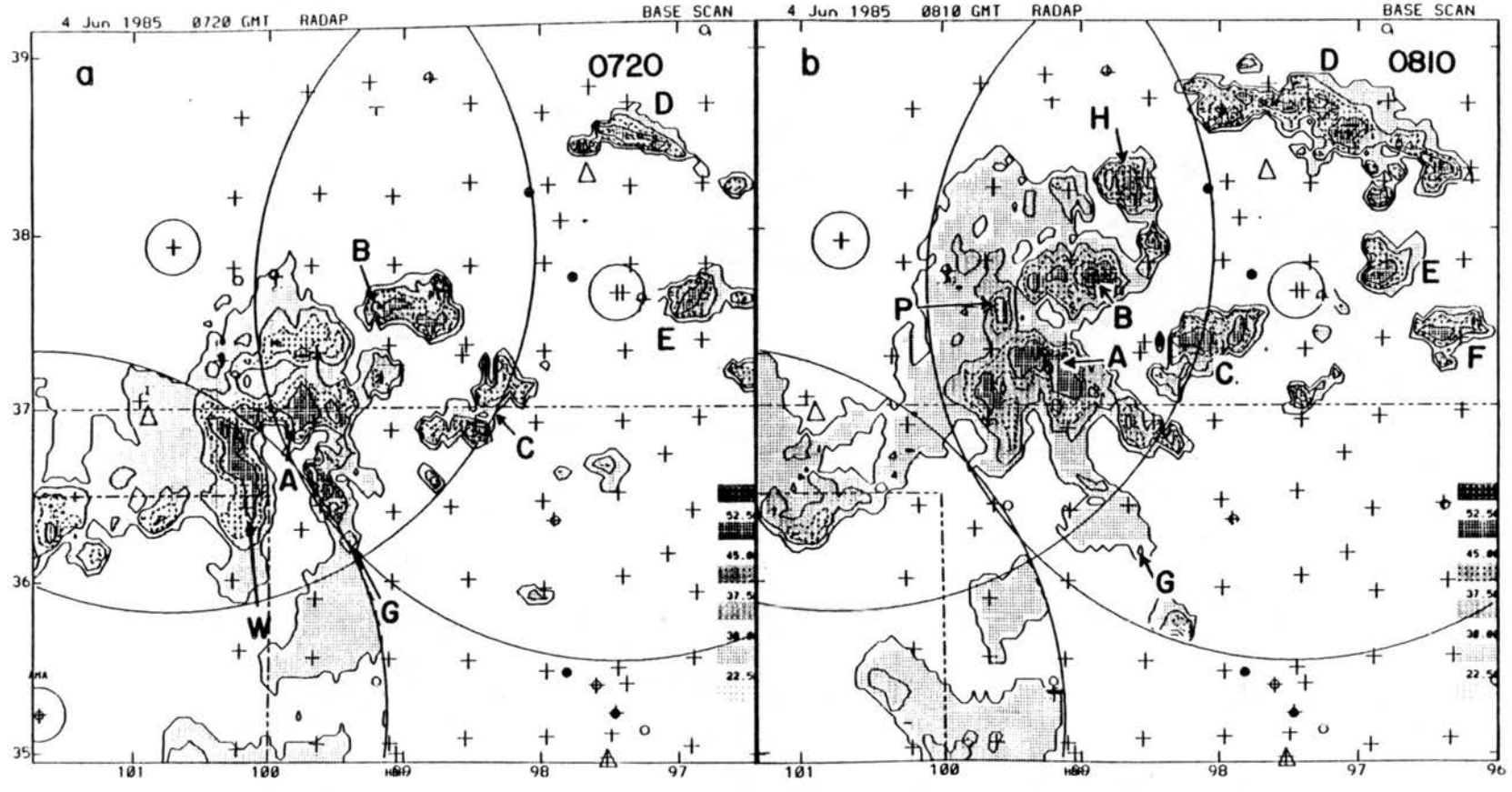

Figure 6.3: Images of the developing / organizing stages of System C, from GCK, AMA, and ICT radars at (a) 0720, (b) 0810, (c) 0830 and (d) 0900 UTC 4 June, as in the previous figure.

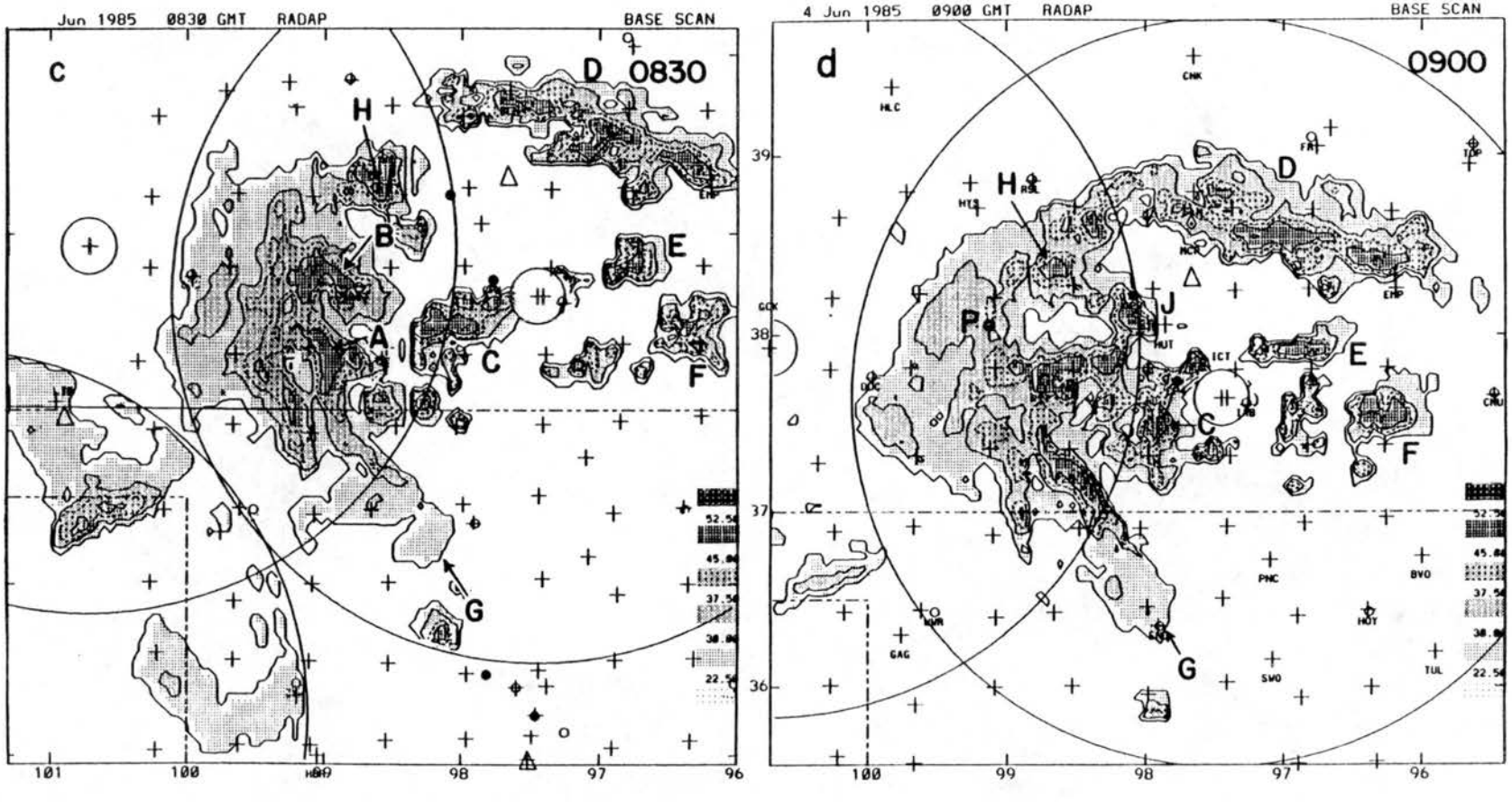

Figure 6.3: Continued.

The evolution of the discrete clusters within the range of Wichita is depicted at roughly half hour intervals. The major cluster D elongated in both directions, broadened, and harbored over a dozen centers of intense echo; nevertheless it remained essentially stationary. The NCAR Doppler radars observed large numbers of cumulonimbus cells that moved erratically within band D. It lost its separate identity only after 3 hours, when it merged with clusters in the central core of the MCC, and then became part of the stratiform cloud. We will see that band D was associated with a stationary baroclinic zone just like the east–west band in the previous chapter. During the same three hours, clusters E and F remained separate and nearly stationary.

On the larger scale (Fig. 6.3), the original band of convective storms which had covered the Oklahoma panhandle persisted for some 5 hours. A persistent shield of stratiform rain filled in the area between the meso–β clusters after 0800 UTC, east of longitude 100°W. West of this longitude, such a shield never developed, and the convective echoes dissipated.

The chaotic arrangement of clusters in the early stage gradually changed into a pattern of intersecting convective bands by the growth stage. This re-arrangement is depicted on the four panels of Fig. 6.3; it is due partly to the faster clusters like A and C catching up with the nearly stationary ones like B, E, and F. The stationary band D also lengthened in both directions until it eventually merged with band G, which was a new alignment of convective clusters transverse to the direction of system motion. Thus by 0900 when the MCC was in its "growth" stage and also began its mesoconvective period, the gaps had been filled and the system had a structure resembling intersecting fronts, with band D being the warm or stationary front, band G the cold front, and P the **apex** or center of the pattern.

It then started to transform into a "spiral arm" pattern. A heavy curve is superimposed on Fig. 6.4a just outside the spiral to emphasize some alignments of echo centers. The spiral band developed *inward* of the previous intersecting wave pattern (compare Fig. 6.3d and 6.4a). There were fewer convective regions with reflectivity more intense than 52 dBZ, but the stratiform echo was larger and deeper. Finally at 1000 UTC a spiral pattern was most apparent (Fig. 6.4a), and lasted through the mesoconvective and mature phases of the life cycle.

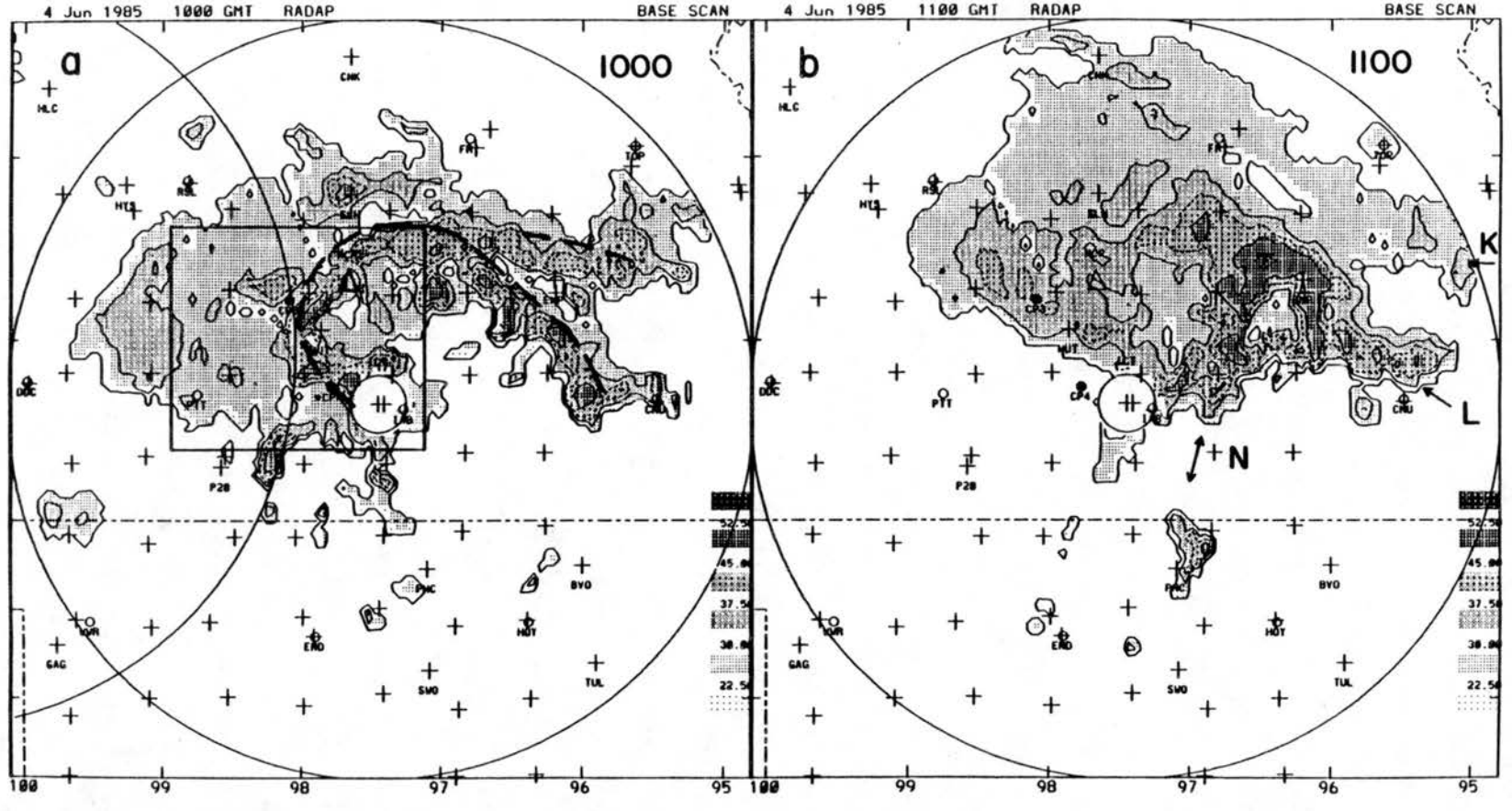

Figure 6.4: Images of the mature stages of System C, from GCK and ICT radars at (a) 1000, and (b) 1100 UTC 4 June, as in Fig. 6.3. The rectangle on (a) locates the domain of a dual Doppler analysis; the triangle locates the McPherson profiler.

The clusters differed greatly in their propagation. Those such as E and F, located east of the advancing precipitation and cloud shield of the MCC, advanced at a typical rate of 8 m s^{-1} from nearly south (200°). Those such as A within the mesoscale rain system, advanced from the southwest at typically 20 m s^{-1}, a rate comparable to the overall radar pattern. The north–south band tended to advance from the west at $\sim$ 15 m s^{-1}, more slowly than the meso–α–scale system. In fact, after the mature stage (1100 UTC), the band *G* and its equivalent in system B tended to increasingly trail back to the southwest.

On Fig. 6.3d the intersection of line G (advancing from the west) with band H–D (practically stationary) is marked with a circle at P. The pattern was mapped for some 5 hours on over nearly the same path as System B. The evolution of the pattern from an open wave into a small occlusion is suggested.

Centers of coldest cloud top appeared over the large central region of the cloud shield (Fig. 6.1): this defined the so–called "thermal minimum" stage at 1030. Spiral, occlusion or other such patterns were not detected on the cloud top imagery, however. From 1030 to 1200 UTC, the mature stage, the central cold cloud region coalesced before it again divided into eastern and western centers.

To the north and west of the emerging spiral patterns of convective clusters, the stratiform echo continued to expand and lose its "noisy" structure (Fig. 6.4b). At the time of maximum extent of cloud top at 1100 UTC, two parallel bands were evident on both radar and satellite data. At this stage a few broken convective lines curved south, outside the MCC, into Oklahoma just as occurred in system B. The coldest cloud tops were located over the junction of bands L and N at 1200 UTC as the MCC propagated into Missouri, when we lost good data coverage of it.

6.2 Surface features

Just as with system B, the surface data from the mesoscale and the FAA airport networks were analyzed at least every hour. The surface fronts and wind shift lines changed shape in response to system C. On Fig. 6.5, the stationary front bulged north some 150 km directly south of the active portion of the MCC. The wave "cusp" co–existed with a

weak low pressure center of mesoscale dimensions and without any precipitation. To the north, wind converged on a shear line (dashed) oriented east–west, on which many new clusters developed, as in system B. Unlike that system, many also developed chaotically south of the line. There was no low pressure in this region until later. Another shear line extended south from this one to the weak meso–low on the front in Oklahoma. A short–lived narrow convective line co–existed with the second shear line.

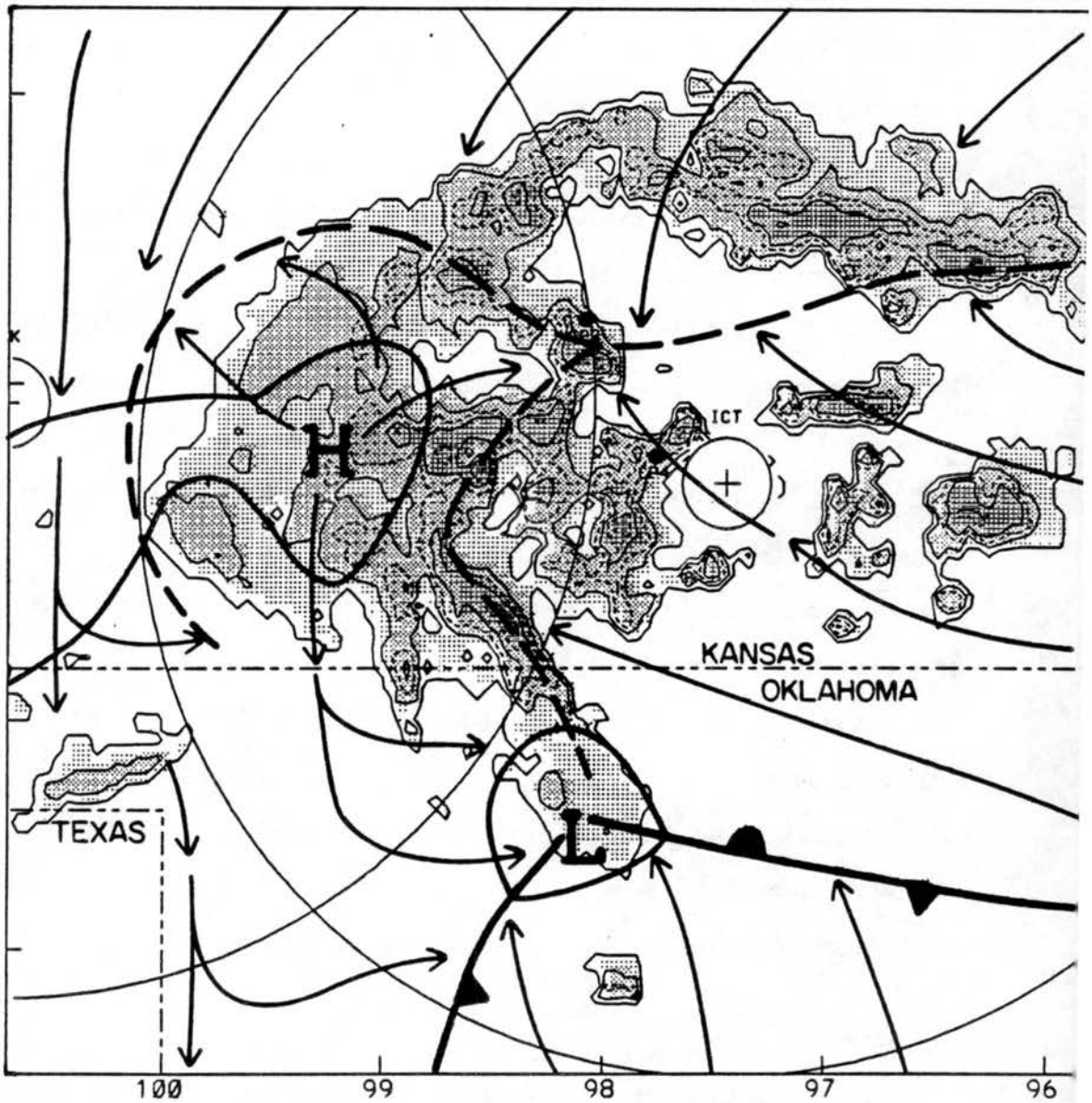

Figure 6.5: Radar reflectivity and surface analysis when the occluding pattern was developing at 0900 UTC. Pressure centers are enclosed by one isobar; streamlines are added; dashed lines are axes of wind convergence.

During the following two hours the shear lines propagated east with the MCC and were associated with numerous developing clusters of intense radar echo. The surface fields resembled a weaker version of the frontal wave fields of system B. The most intense clusters were found near the triple point intersection, which later coincided with the western–most part of the spiral convective band. When the precipitating system had moved into Missouri, a wind shift line formed again near its original position.

Diffluent meso–high pressure centers and confluent low centers accompanied the MCC. A meso–high center of about +3 mb lay well within the region of stratiform echo (Figs. 6.5 and 6.6). A meso–low developed by 1000 UTC along the curved rear edge of the stratiform rain echo. This location and shape were consistent with those pressure fields described by Johnson and Hamilton (1988) for a squall line.

A surface analysis in Fig. 6.6 one hour before maturity identified the four features that were tracked in surface data. The meso–high center of pressure and the meso–low center could be tracked for 3 to 4 hours. The triple point on the frontal wave in Oklahoma, at ③ south of the MCC, and the triple point at ④which was at the intersection of convergence lines in the surface wind field, were also followed. The propagation of these four features, as well as the fronts that defined the evolving wave pattern, were mapped for system C. The same mapping was done for system B; system A was not so analyzed because it reached maturity east of the surface meso–network.

Overall agreement of the propagation velocities was lacking in system C. A "fast" velocity of 29 m s^{-1} from 245° characterized the movement of the meso–high, the surface wind field pattern, and the satellite observed cloud shield. This differed from the propagation of the meso–β–scale convective clusters and the meso–α–scale echo wave pattern, which advanced at 20 to 23 ms^{-1}. The propagation velocities are summarized in Table 6.2, which should be compared with the propagation of systems A and B in Table 5.1.

An interesting finding is that the surface wind field evolved a pattern similar to those in systems A and B. The northern triple point developed in a region with no air mass contrast at the surface, but with numerous convective clusters which did not line up neatly along the convergence axes but were located in a rough way near the lines and their

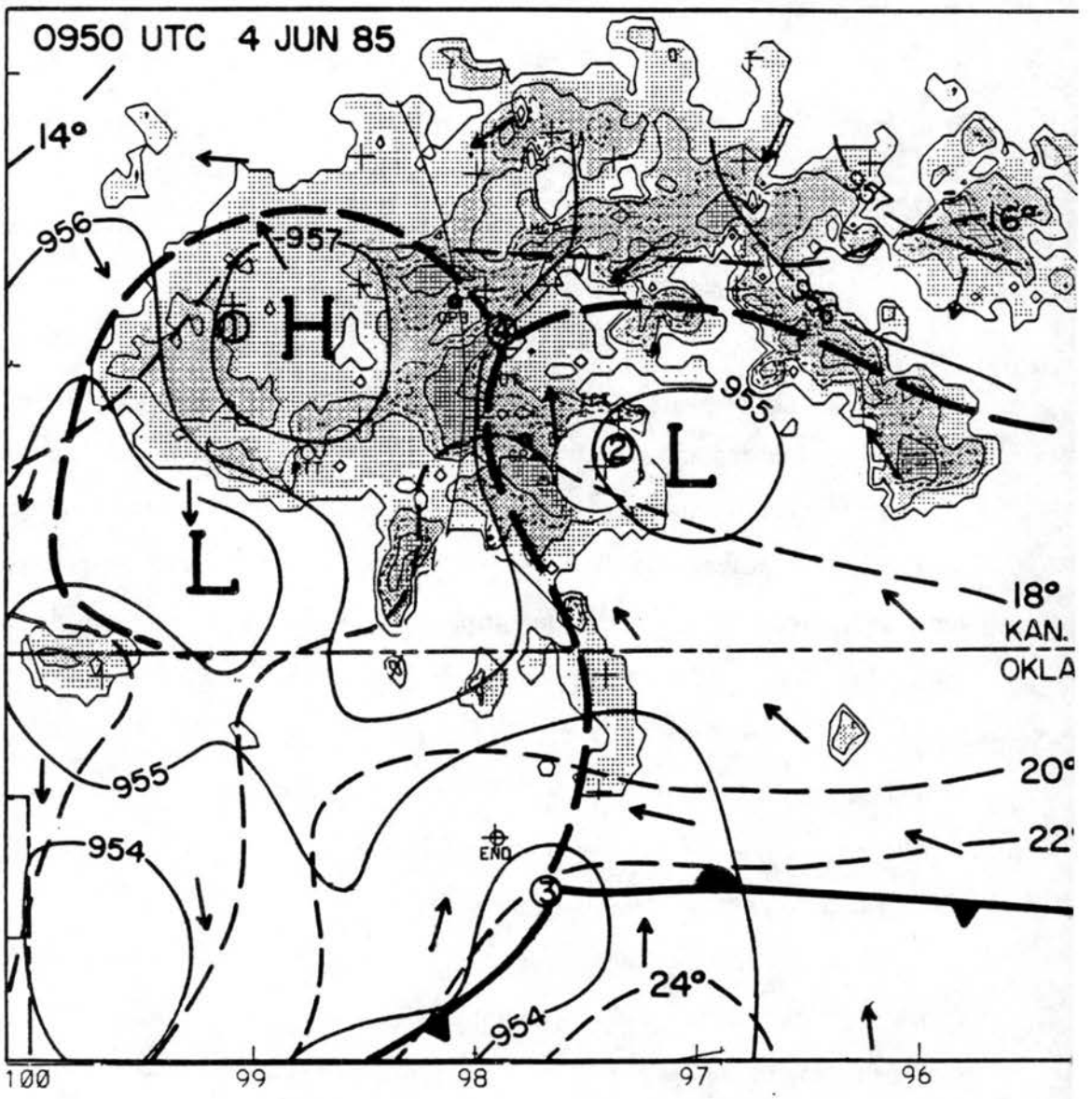

Figure 6.6: Surface meso–analysis of system C at 0950 UTC 4 June, overlaid on the radar reflectivity. The symbols represent: ③ Apex of wave on the surface front south of the MCC ④ Apex of intersecting wave pattern in the wind field. Thin solid lines represent isobars of adjusted pressure (mb); thin dashed lines, isotherms (° C); heavy dotted lines axes of wind confluence.

Table 6.1: Movement of features observable in surface data, radar and satellite images of system C as a function of life cycle stage.

SYSTEM C

i. Early (0400 to 0730): 24.4 ms^{-1} from 227°

ii. Developing (0730 to 0930): Must use two patterns:

- RADAR elements on both meso-α and meso-β-scales, and frontal wave, share 20 ms^{-1} from 235° .
- CLOUD SHIELD, wind surface field pattern, and MESO-HIGH, share 29.1 ms^{-1} from 245°

iii. Mature and Late (0930 to 1200):

- RADAR elements, 23 ms^{-1} from 255°
- CLOUD SHIELD, wind field at surface and MESO-HIGH, 29.1 ms^{-1} from 245° .

---

intersection. The southern triple point formed on a front with air mass contrast, but no convective activity. It is apparent from the similarities to system B that the convectively unstable air, evident at the surface south of the front, "overrode" the stable air in northern Oklahoma and Kansas to subsequently enter convective updrafts in the clusters that developed in the north.

6.3 Upper level properties of the system

It had been decided to terminate the launching of supplemental soundings in Kansas at 0600 UTC, just when system C qualified as an MCC in the Oklahoma panhandle. Three to six hours later, system C passed directly through the network.[1] The profiler at McPher-

---

[1]Stations in Oklahoma continued to launch soundings through 1200 UTC which provided some information on the effects of the MCC on the southern flank.

son collected data during the passage of the inner spiral convective region and subsequent stratiform region of the MCC. The NOAA 43 (P–3 Orion) aircraft traversed the convective region while it was transforming from a chaotic distribution of cells and clusters (at 0830 UTC, Fig. 6.3c) to a structure with intersecting frontal bands (at 0900, Fig. 6.3d). It then collected microphysical data, and made one ascending and one descending sounding, on the rear margin of the stratiform cloud.

At 0900 the southern terminus of the weakening convective line *G* passed Enid when a sounding was taken. The winds above 7 km (from the west–southwest) were reduced from previous values as the line appeared to block the flow. One hour later, acceleration and rear–to–front flow were observed from 5 to 7.5 km in height, even this far south. This is consistent with a developing low pressure center and perhaps cyclonic inflow into the MCC. Velocities above that level continued to be diminished, which implied diversion of upper tropospheric flow around the north side of the MCC but relative stagnation on the south side (which is consistent with anticyclonic outflow). The effects were absent by 1200 UTC.

Between systems B and C, the wind profile at McPherson exhibited constant shear from a constant direction of 250° from 3 to 9 km in height (data were not collected below 2.5 km). No change occurred even as convective clusters formed in chaotic patterns around the site, except that the wind flow above 7 km appeared to be blocked after 0830. At 0930 the profiler found itself within the inner curl of the newly formed spiral band; at 1000 it was on the band (triangle on the map in Fig. 6.4a). At these times, transient relative inflow toward the apex region was observed from the *southeast* at 3 to 4 km in height, and from the *northeast* at 5 to 7 km. The site was in stratiform rain during the next two profiles which showed uniform front–to–rear flow. At 1130 the rear margin of the rainfall echo passed the site; the profile showed rear inflow (maximum inflow of 8 $\mathrm{m\,s^{-1}}$) from 4.5 to 7 km. These results are all consistent with the Doppler radar results described in the next section; the profiler lay north of a cyclonic shear line (to be described) where front–to–rear flow prevailed after passage of the apex region, and before the rear edge of the stratiform cloud passed.

The P–3 aircraft traversed the MCC from east to west between 0830 and 0900 at the 530 mb level, and from west to east between 1000 and 1030 at 465 mb. While in the stratiform cloud, front–to–rear flow with a slight component from the north was measured throughout. While outside the cloud to the west, rear–to–front flow was seen. The data are combined with Doppler data and mapped in Section 6.6 below. The edge of the deep A stratiform cloud appeared to be a sharp boundary between cloudy ascending outflow and dry descending inflow to the MCC. The aircraft observed the cloud base at 650 mb at a temperature of +2° C.

6.4 Earlier internal circulation

A velocity field was synthesized from dual Doppler data at 1000 UTC by Ray McAnelly of Colorado State University. The domain of this analysis is shown as a rectangle on the large scale map in Fig. 6.4a; the analysis is 40 minutes earlier than our more detailed analysis presented in the next section. A large portion of the spiral convective band was inside the domain at 1000 UTC, and changes in the airflow can be seen from the earlier to the later time.

Shear axes or frontal–like boundaries (dashed lines) were evident on Fig. 6.7a at the 3 km level. One axis went from the western edge eastward to the spiral convective band (dotted), specifically to its west–facing portion at P. Like the later analysis, this boundary separated southerly or southwesterly inflow from strong easterly or northeasterly front–to–rear flow. The boundary was evident from T to P at 5 km as well (Fig. 6.7b).
(A remnant of front–to–rear flow which is like the flow at higher levels lay south of P.)
The shear zone R, discussed at greater length in the following section, can be seen here to correspond with the convective band which was the inner terminus of the spiral at 1000 UTC. On comparing the locations of these boundaries at the two times, it is seen that the whole pattern was advected with the system in the interim.

The rear inflow (in the southwest corner of Fig. 6.7a) was not as strong nor as intrusive, especially at the 5 km level, as it was later. Thus the dry inflow not only moved with the MCC but also intruded further into the precipitation region and evaporated the cloud from the base up.

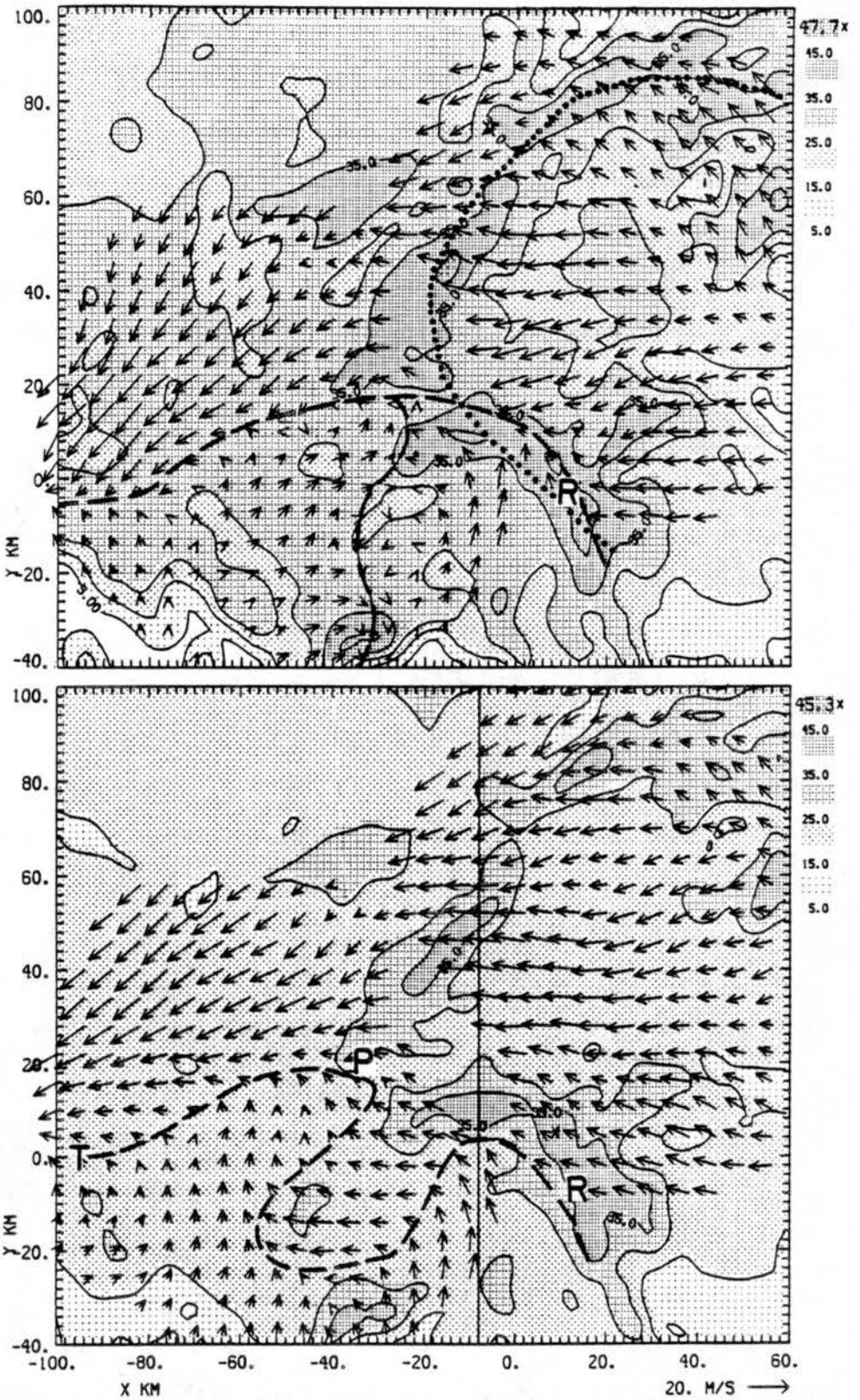

Figure 6.7: Relative wind and reflectivity at an earlier time, 10:00 UTC, (a) at the 3 km level, and (b) at the 5 km level. Symbols as in Fig. 6.10. Dotted line locates the spiral convective band which terminates at R. T marks a vorticity center.

In agreement with the profiler data discussed earlier, inflow from the east was accelerated into the spiral band (dotted) in low and middle levels. The band at R received inflow from both sides, but remarkably, the convergence was stronger in the 3 to 5 km layer than in the boundary layer.

A north–south vertical section along x = −8 km cut through the spiral band twice (Fig. 6.8). In both cuts *a* and *b*, the ascending motion was pronounced through the troposphere. The zone of rising motion sloped north with height in region *a*, at the receiving end of the narrow southerly jet at 2 to 4 km. This may be an analogue of the sloping warm conveyor belt observed in system B, although it is not known how widespread sloping zones were in system C. Finally, moderate *downward* velocities were observed at the 3, 5, and 7 km levels in a region of northeasterly flow just north of the spiral band in this section (region *c*). Although this needs to be confirmed with data from other regions, it may be a manifestation of the cool conveyor belt.

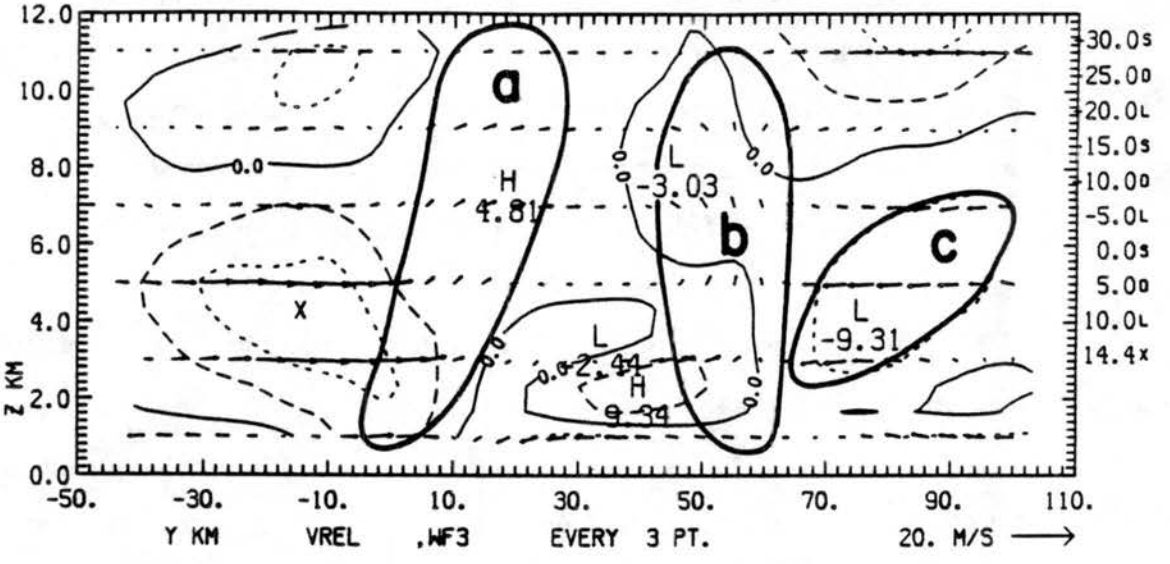

Figure 6.8: South–to–north cross section along x = −8 km, cutting twice through the spiral band. Location of section is shown in Fig. 6.7b. The *v* component wind is contoured; the vectors include the *w* component as well. Regions a, b, and c are discussed in the text.

6.5 Later internal circulation

Some 40 minutes after the time of the above analysis and about the time that the cloud shield reached maximum extent, (the **mature** stage and also the time of "thermal

minimum"), another dual Doppler wind field was analyzed by us for 1040 UTC. This time the largest possible area was analyzed; the volume is the rectangle on Fig. 6.17, overlaid on the base–scan composite of reflectivity from the National Weather Service radars at Wichita (center) and Garden City (off the map). The volume contained both a large area of stratiform echo, much of which exceeded 30 dBZ, west of the Doppler radars, and much convective echo east of the radars. The rear edge of the cloud system was located in the southwest quadrant of the rectangle and was rapidly advancing. From 1000 to 1040 the convective echo was becoming aligned along more or less continuous bands in a spiral pattern as discussed in section 6.1.

This can be seen more clearly on Fig. 6.4a when the spiral pattern, centered just north of Wichita, was emerging in place of the intersecting wave pattern that had been present for 90 minute. The "apex" of that pattern, observed at earlier times, was located along the axis from P to Q.

The system relative wind at the 1.7 km level in the large volume is plotted on Fig. 6.9. An axis of cyclonic shear (dashed line) extended south from R; east of the axis the inflow was southerly and underwent deformation as it approached another axis M from the south. West of R it was northerly and increasingly divergent toward the rear margin of the precipitation echo. This shear zone was about 30 km wide. An echo–free notch was seen at N at this and higher levels. The relative flow was easterly in a broad region north of R and M, near the center of the MCC. The deformation zone between this flow and the southerly flow is probably the old stationary front.

A more complex flow was seen at 3 km (Fig. 6.10). The southerly airstream east of R had a localized jet which curved cyclonically around R, through P, and continued as an easterly jet through U. The southerly jet was associated with some clusters of decaying convection (the eastern regions where the reflectivity was greater than 35 dBZ on Fig. 6.9 and 6.10). More clusters were located just beyond the eastern border of these figures. The shear is still evident on the R axis. This was the lowest level at which inflow from the rear was observed, south of another axis of cyclonic shear (dashed line) from D to R. The westerly inflow interacted with the northerly flow to produce an anticyclonic gyre at S some 20 km southwest of R; the air is believed to be descending in the gyre at S.

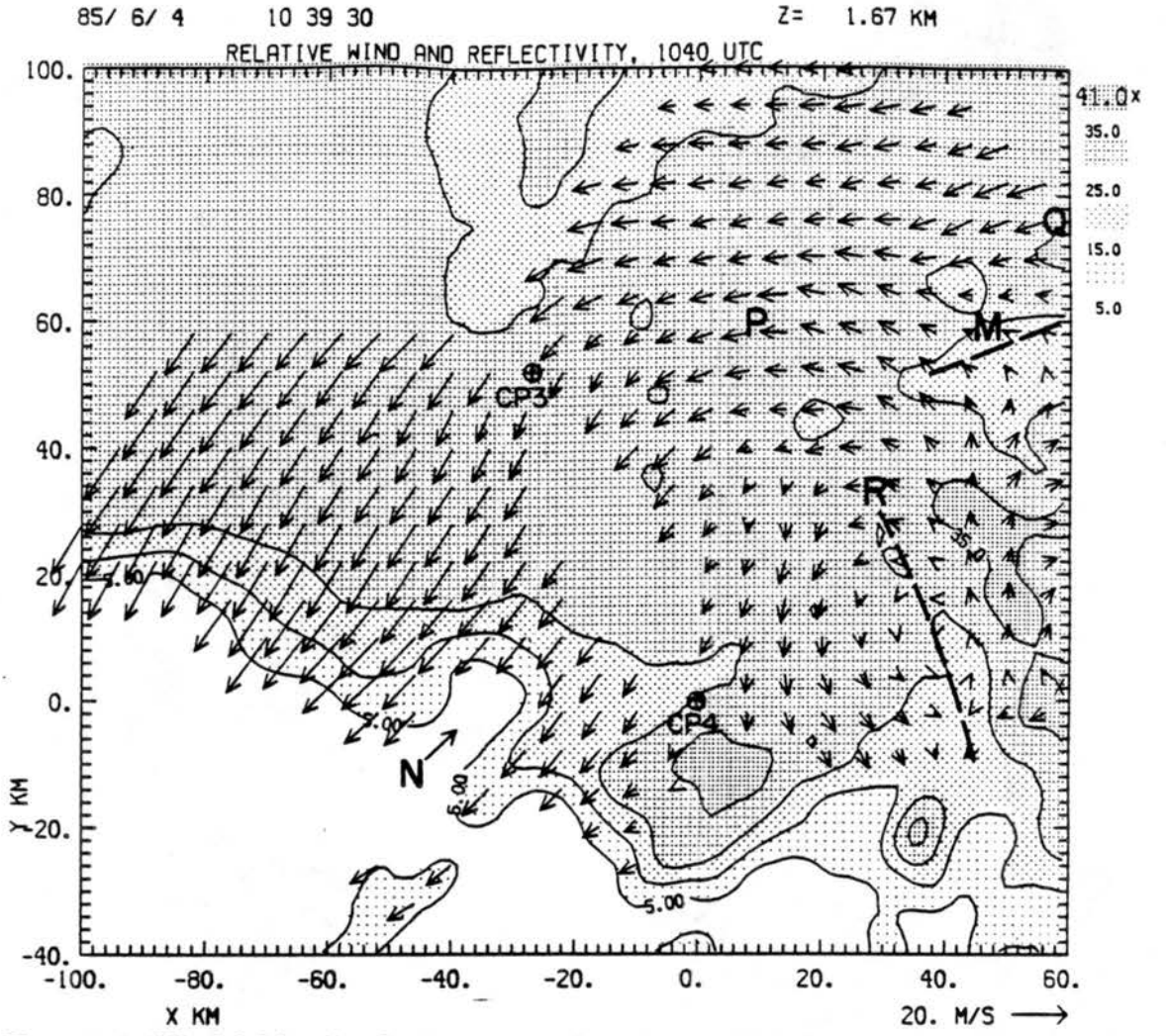

Figure 6.9: Wind field and reflectivity at 1.7 km above sea level in the domain of the box on Fig. 6.17. The vectors are proportional to a standard length shown in the lower right. The dBZ levels are keyed to the legend in the upper right. A system motion of 20 m s^{-1} from 235° has been subtracted from wind data in this and subsequent figures. Letters identify features discussed in the text.

Convergence was maximized just northwest of R and just east of D. Vorticity was weak at this level, except that it was greater along the two dashed shear axes and also in region U. The deformation field was also concentrated in these regions, and in a band extending east from P through A′. The latter may be a quasi–stationary frontal zone, or may be caused by the convective cluster which formed the inner end of the spiral.

The rear inflow was strongest and most widespread at the 5 km level (Fig. 6.11). The maximum speeds in the rear–to–front regime were observed on the southwest margin of the precipitation. As the wind backed with height in this region, the flow tended to enter

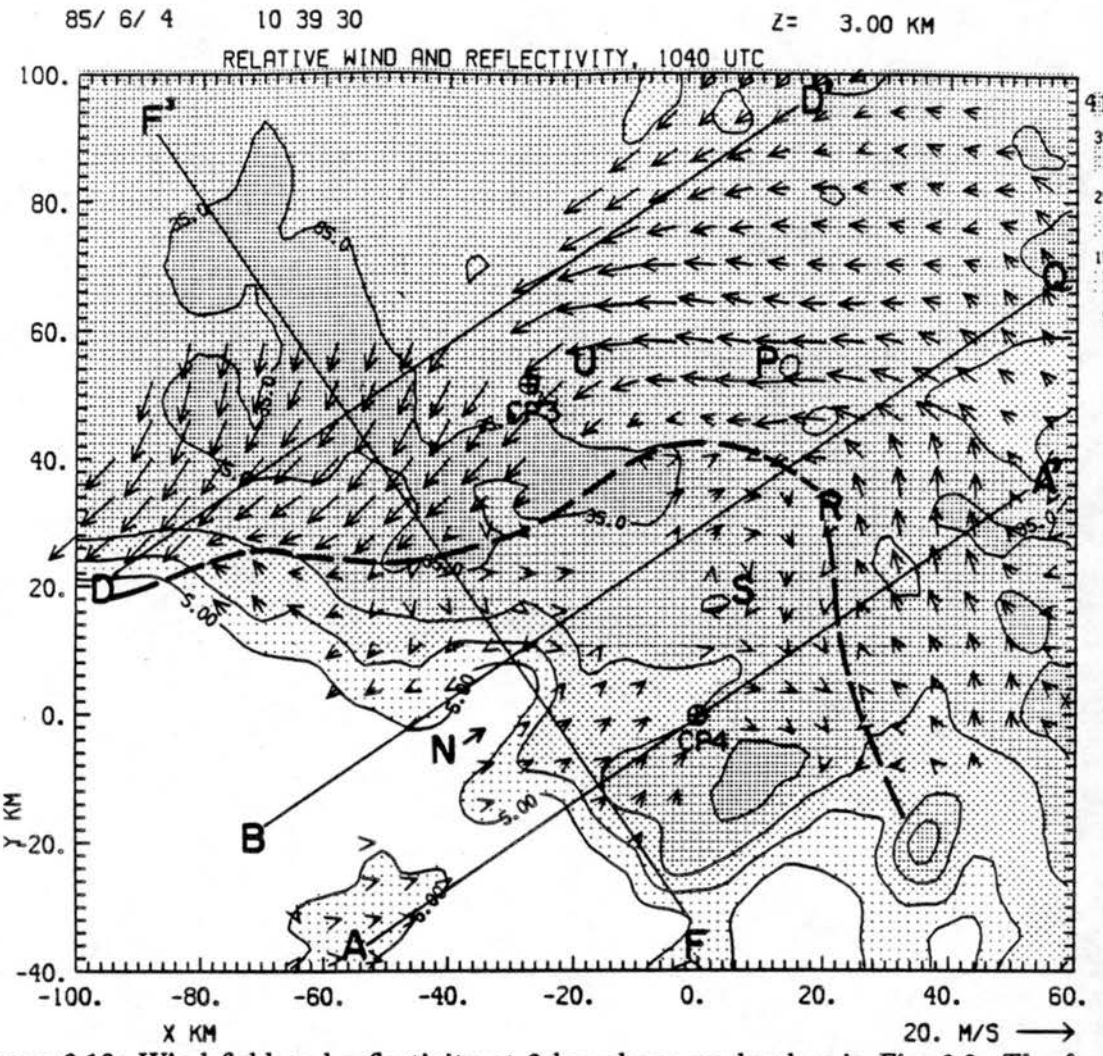

Figure 6.10: Wind field and reflectivity at 3 km above sea level as in Fig. 6.9. The four lines labelled A-A', B-Q, D-D', and F-F' locate vertical cross sections in subsequent figures. The Doppler radars CP3 and CP4 are labelled in the center. The heavy dashed lines mark axes of horizontal shear.

the system more from the south at this level, and penetrate as far as the dashed line T–R. The regions of highest vorticity, enclosed by the closed curves on Fig. 6.11, extended from T along and north of the shear axis to the vicinity of P, and from there southward to R. A closed cyclonic gyre about 25 km in diameter was located at T in this frame of reference; a weaker cyclonic center was seen at R in a slightly slower moving frame of reference (for example, one moving with the mean wind at this level, 18 $m\,s^{-1}$). The southerly jet converged with the southeasterly flow east of R, and (like the flow at lower levels) curved around R through P towards T. In the middle levels these streamlines were also confluent

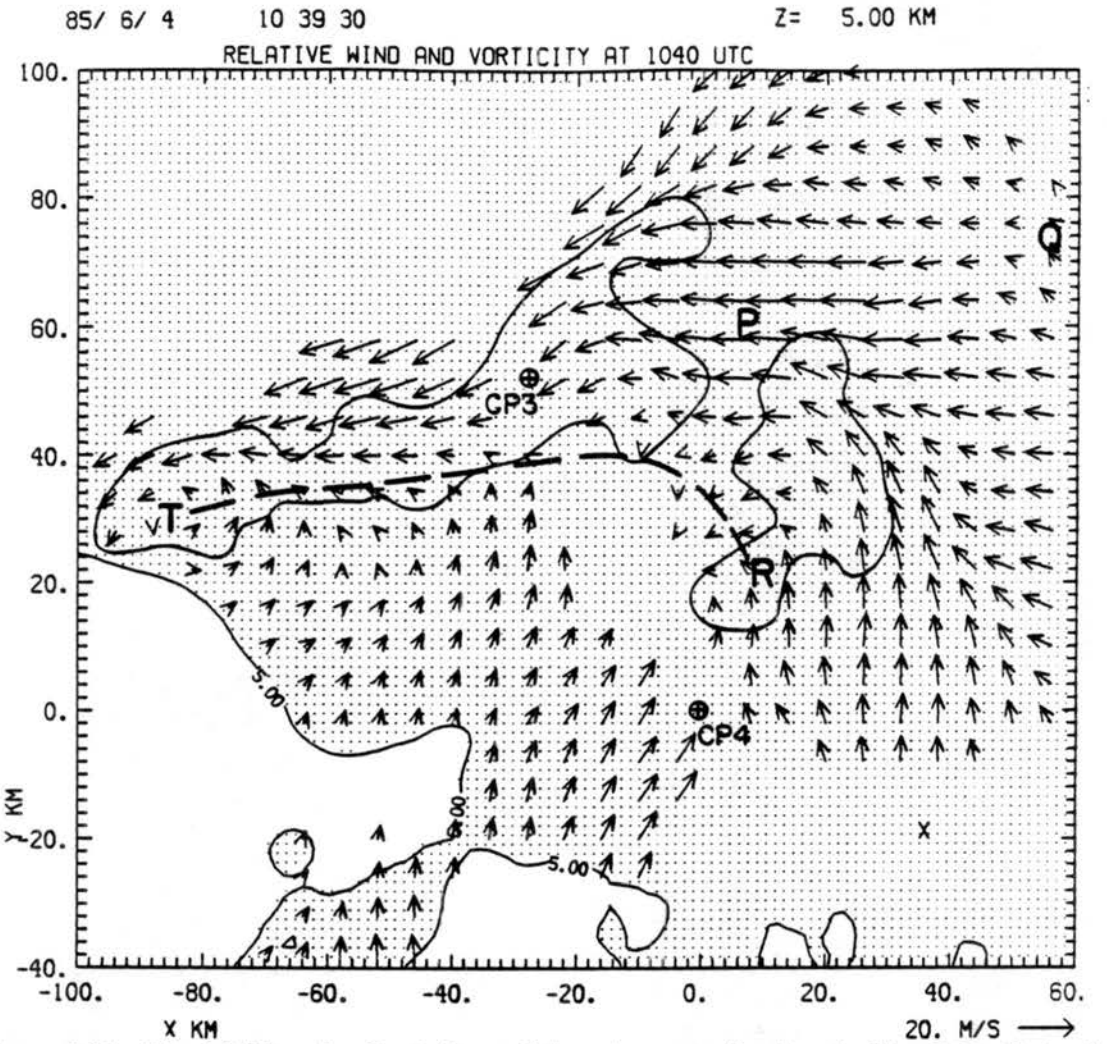

Figure 6.11: Wind field and reflectivity at 5 km above sea level as in Fig. 6.10. Only the reflectivity greater than 5 dBZ is contoured and shaded. The other contour in the center encloses the area where cyclonic vorticity exceeded $5 \times 10^{-4} s^{-1}$.

with a slightly anticyclonic jet from the northeast aligned along D–D' (for location see previous figure).

Closer examination of the deformation field pinpointed these regions of convergence as salient frontal zones. A "total deformation" field, defined as

$$\left(\frac{\partial v}{\partial x} + \frac{\partial u}{\partial y}\right)^2 + \left(\frac{\partial u}{\partial x} - \frac{\partial v}{\partial y}\right)^2,$$

was plotted at the 4.3 km level in Fig. 6.12 because deformation was maximized at this level; significantly, this is the melting level. With minor exceptions both the shearing and stretching terms contributed to the high values in the shaded zones. In addition to the

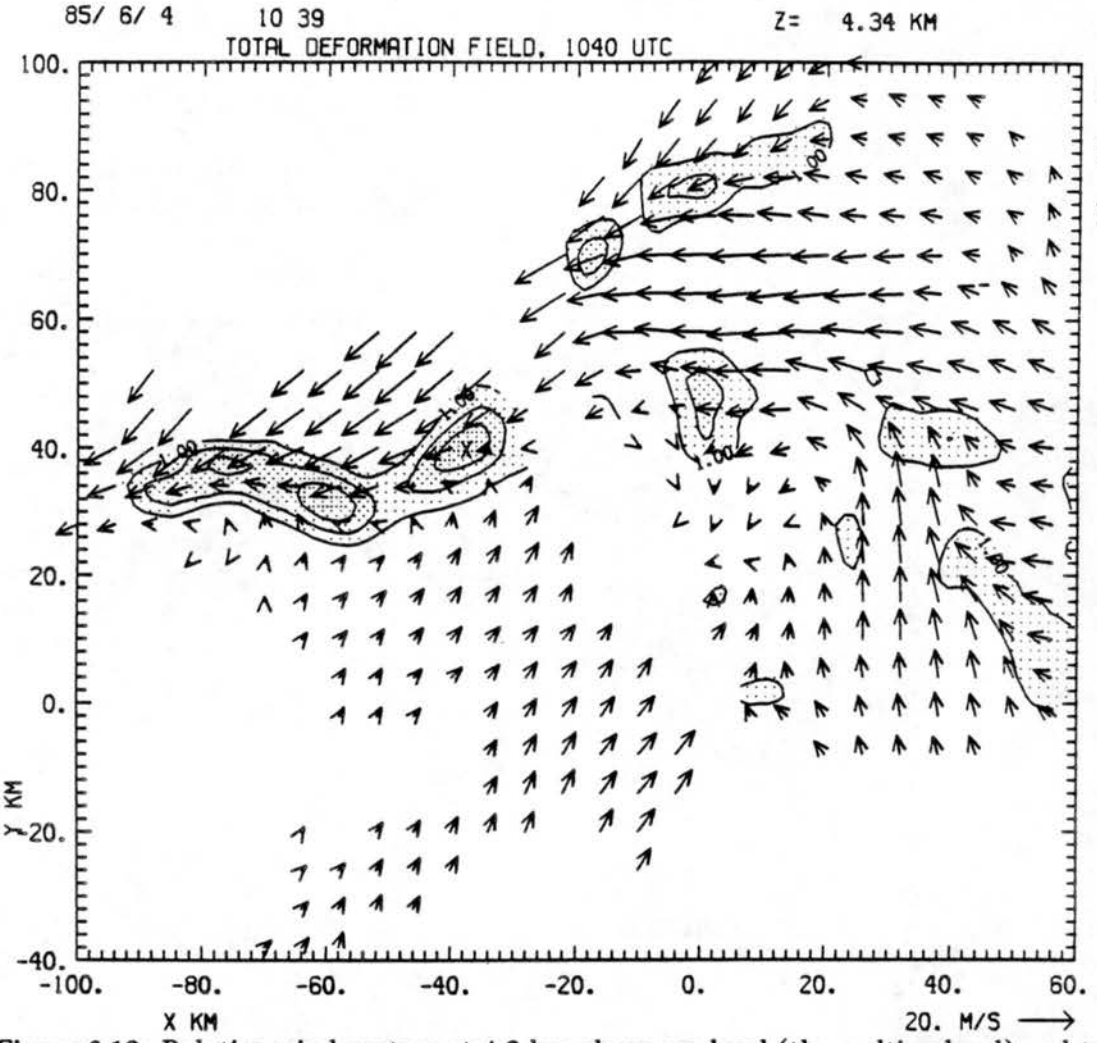

Figure 6.12: Relative wind vectors at 4.3 km above sea level (the melting level) and tota deformation field (contoured) in units of $1 \times 10^{-3} s^{-1}$.

east–west axis that separated rearward from forward flow, there were other zones tha exhibited strong deformation in Fig. 6.12. One region between P and R may be relate to the earlier presence of the "apex" of the frontal wave. The band near (0, +80) in th north seemed to demarcate northerly (cold) inflow from easterly flow; this feature wa present only in mid–levels. Finally, a deformation zone entered the eastern side of th figure. In middle and upper levels this zone appeared in lieu of the shear zone marked b the dashed line south of R on previous figures (both zones were equally strong at 3 km) Front–to–rear flow met southerly inflow in this zone.

Both this feature and the northern band coincided with newer alignments of meso–β- scale convective echo, in the emerging spiral pattern (see Fig. 6.17). Thus the mesoscal

convective bands, even the transient ones, are associated with several frontal–like zones on the scale of $\sim$ 100 km with different orientations within the same MCC.

At 7 km (not shown), the vorticity center at R was located even farther west, and the rear inflow did not enter more than 20 to 40 km into the echo. Consequently the axis of cyclonic shear lay further south and west, tending to parallel the rear margin of echo. The strong wind east of R was southeasterly rather than southerly at this level; at higher levels it tended to be easterly. Also at higher levels, the flow was increasingly divergent and anticyclonic, particularly in the northern half of the domain of these figures.

Some cross sections through this domain are located on Fig. 6.10. Along a vertical section through A–A′ (not shown), the rear inflow layer extended as far as the shear axis through R, but it did not manifest any slope. Along the section B–Q, through the notch N, however, the region of inflow did slope downward toward the front of the system (Fig. 6.13). The "nose" at the front of the inflow region lay near the anticyclonic gyre S, and was, at its lowest point, 1.5 km above the ground. In these sections, the wind

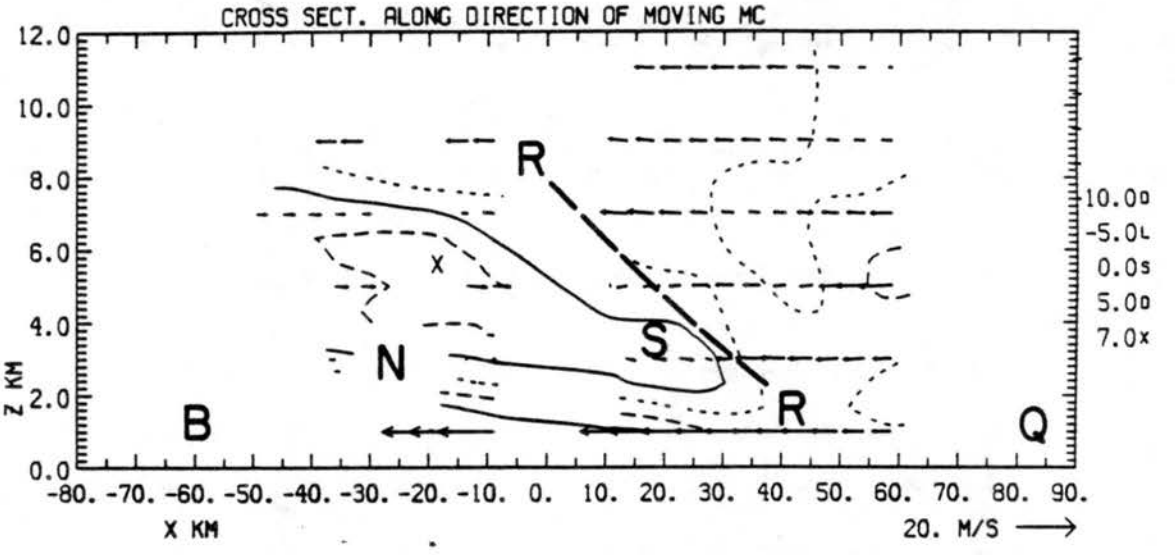

Figure 6.13: Vertical cross section of wind component u* along the rotated x axis, in the direction of line B–Q (on Fig. 6.10). The dashed line locates the north–south shear axis plotted on Figs. 6.9 to 6.11. Positive values are within the solid contour and indicate relative flow from rear to front.

components u* and v* represent (respectively), the components into and perpendicular to the direction of motion of the MCC, which is the orientation of line B–Q. Note that

the axis of cyclonic shear through R on the previous figures is plotted here as a sloping dashed line that tilted westward (rearward) with height.

Another cross section through DD′ depicted strong front–to–rear flow (Fig. 6.14). The relative velocities were unusually high in the middle of this section from 2 to 6 km in height; the maximum speeds exceeded 20 ms^{-1} just north of U, which implied flow from the northeast in a *ground–relative* sense. This stream converged into the enhanced stratiform reflectivity band parallel to the rear margin of the MCC; the band can be seen southeast of F′ on Fig. 6.10. Also, weak rear inflow can be seen in an elevated layer from 5 to 7.5 km in height on the left edge of the section.

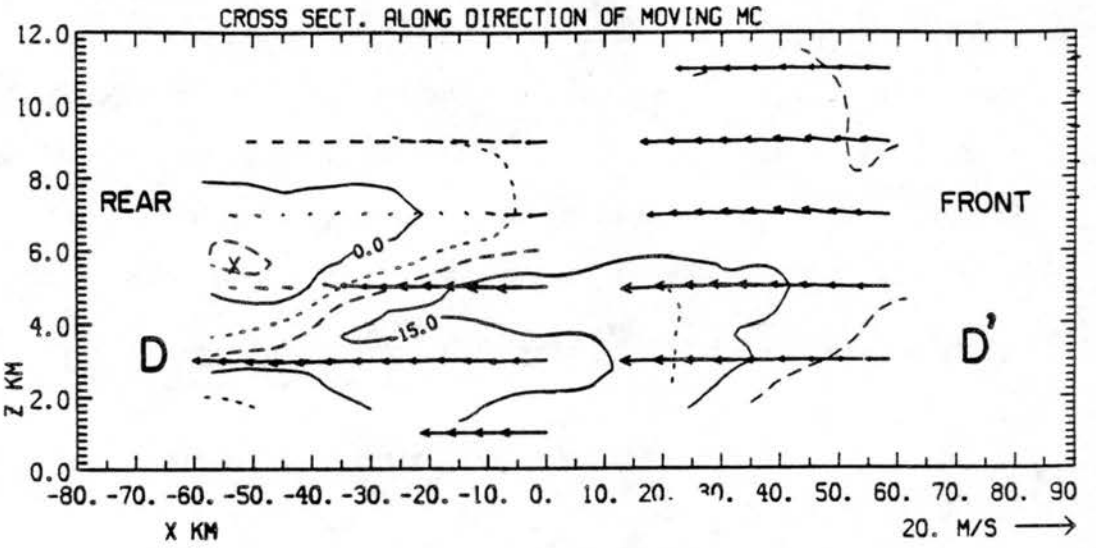

Figure 6.14: Cross section as in the previous figure, but along line D–D'.

Finally, a section along FF′ near the rear margin of the echo and perpendicular to the previous sections depicted the extent of the rear–to–front and front–to–rear flow (Fig. 6.15). A steeply sloping boundary (sloping northwest with height) separated the regimes. Along FF′ the rear inflow appeared to exhibit fairly uniform speeds from 3 km to 6 or 7 km in height. The front–to–rear flow, in contrast, maximized near 4 km in height. Section FF′ was not well positioned to depict the front–to–rear flow because the dual Doppler winds did not extend north of y=60 on Fig. 6.10.

Considerably more confidence can be placed in horizontal averages of second–order properties such as wind divergence than in point values, even when locally smoothed.

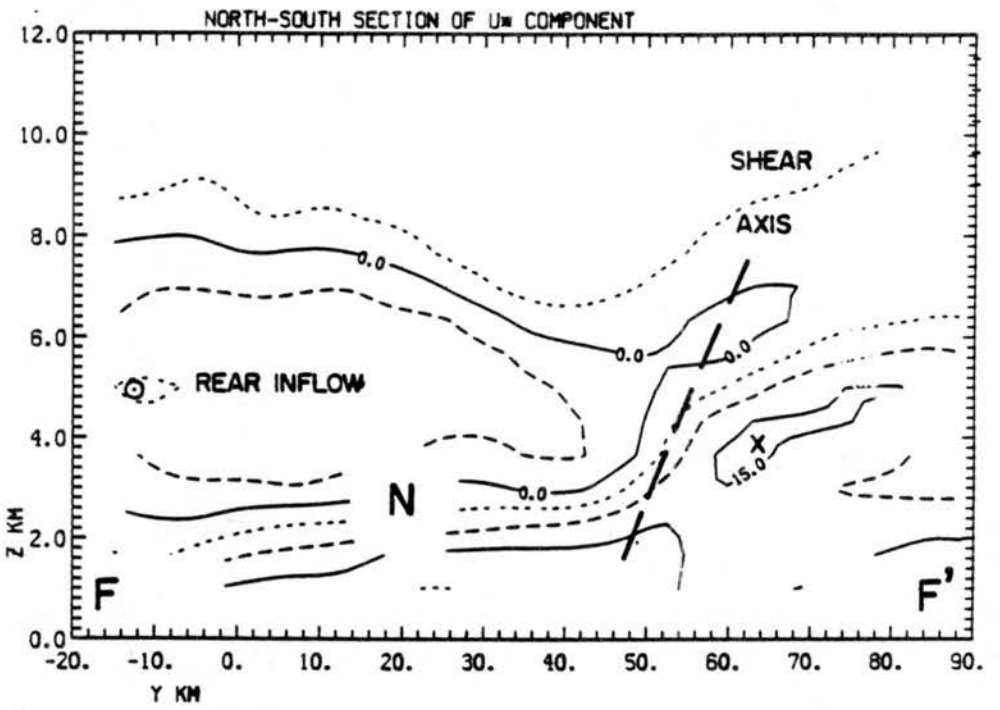

Figure 6.15: Cross section as in the previous figure, but along line F–F' from southeast to northwest. Positive values denote flow out of the page.

The vertical profile of the horizontally averaged convergence, plotted in Fig. 6.16a for the large domain at 1040, exhibited three parts: divergence below 2.5 km and above 8 km, and convergence in a deep middle layer. The peak value of $10^{-4}s^{-1}$ occurred near 5 km. Vertical integration of the divergence from top down yielded the profile of subsiding motion beneath 5.5 km and rising motion above that level in Fig. 6.16b, with the maximum horizontal average of w near 20 cm s^{-1} in both regimes. These results agree very well with kinematic profiles of other mesoscale convective complexes in the literature, both composited results and case studies. They also agree with the profiles of Srivastava et al. (1986) who employed the "extended VAD" method on a squall line. However, their peak vertical velocities were $\sim$ 50% greater in the squall line, and the shallow layer of rising motion they found beneath 1 km could not be observed with our data.

6.6 Discussion of 3–D wind fields

The wind analysis was extended outside the Doppler domain (boxed) on Fig. 6.17 by adding the aircraft data at a flight level of 465 mb, data from the McPherson profiler (MCP, located above P), and sounding data in Oklahoma, as shown on the same figure.

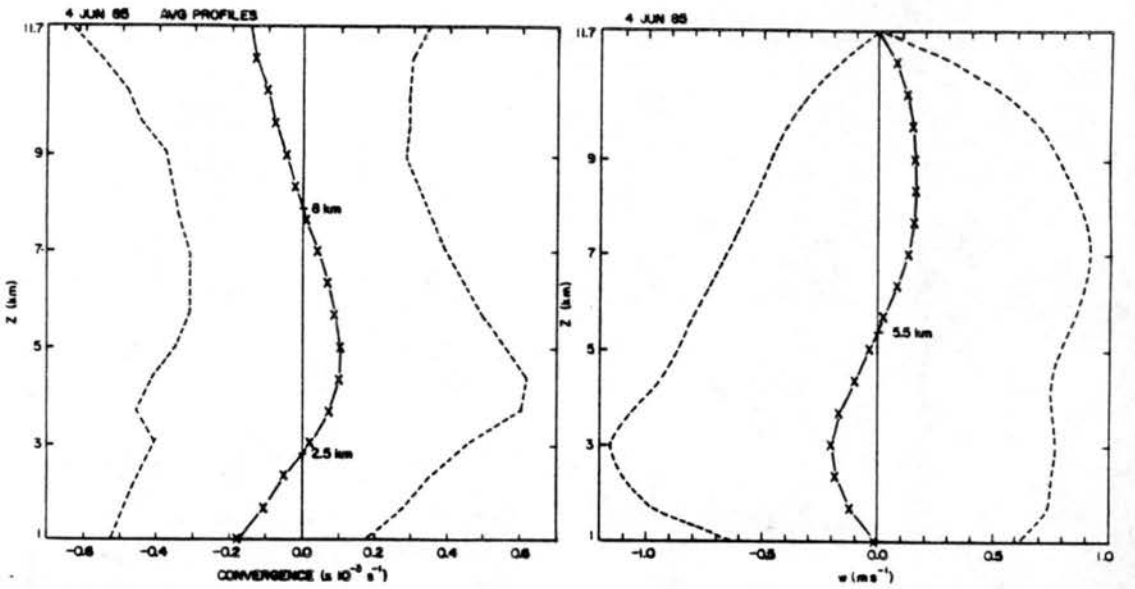

Figure 6.16: Vertical profiles of mass convergence (a) and vertical velocity (b) averaged horizontally over the domain of Doppler data at 1040 UTC.

The relative cyclonic circulation, elongated along the dashed line (T–P or T–R, on earlier figures) can be seen to have extended from the southwest, rear flank of the stratiform precipitation, where rear inflow was strongest, toward the region P–R where the spiral pattern of convective bands had been centered from 20 to 60 minutes earlier. The vorticity was concentrated along the shear axis that separated front–to–rear flow on its north side, from rear–to–front on its south. The profiler wind at MCP and aircraft data at 1035 agreed with the radar–derived front–to–rear flow. As discussed in Section 6.3, however, aircraft data west of the cloud edge indicated flow from the rear toward the cloud, which suggested that the aircraft flew through the sloping boundary between the two flow regimes somewhere near the rear margin of echo. In the Doppler data, the rear inflow layer may not have differed much in depth from place to place, but it did reside at higher levels (5–8 km) to the rear of the system. Also, the radial velocity data from CP–3 in this region did show convergence on the edge of the echo, and support the analysis of convergence of inflow with outflow there. Profiler data shown elsewhere suggested that the inflow layer was indistinguishable from the upper–tropospheric jet, far to the rear of the MCC.

At least one cross Section (Fig. 6.13) positioned the leading "nose" of the rear inflow about 1.5 km above ground level, under the anticyclonic gyre S seen at the 3 km level.

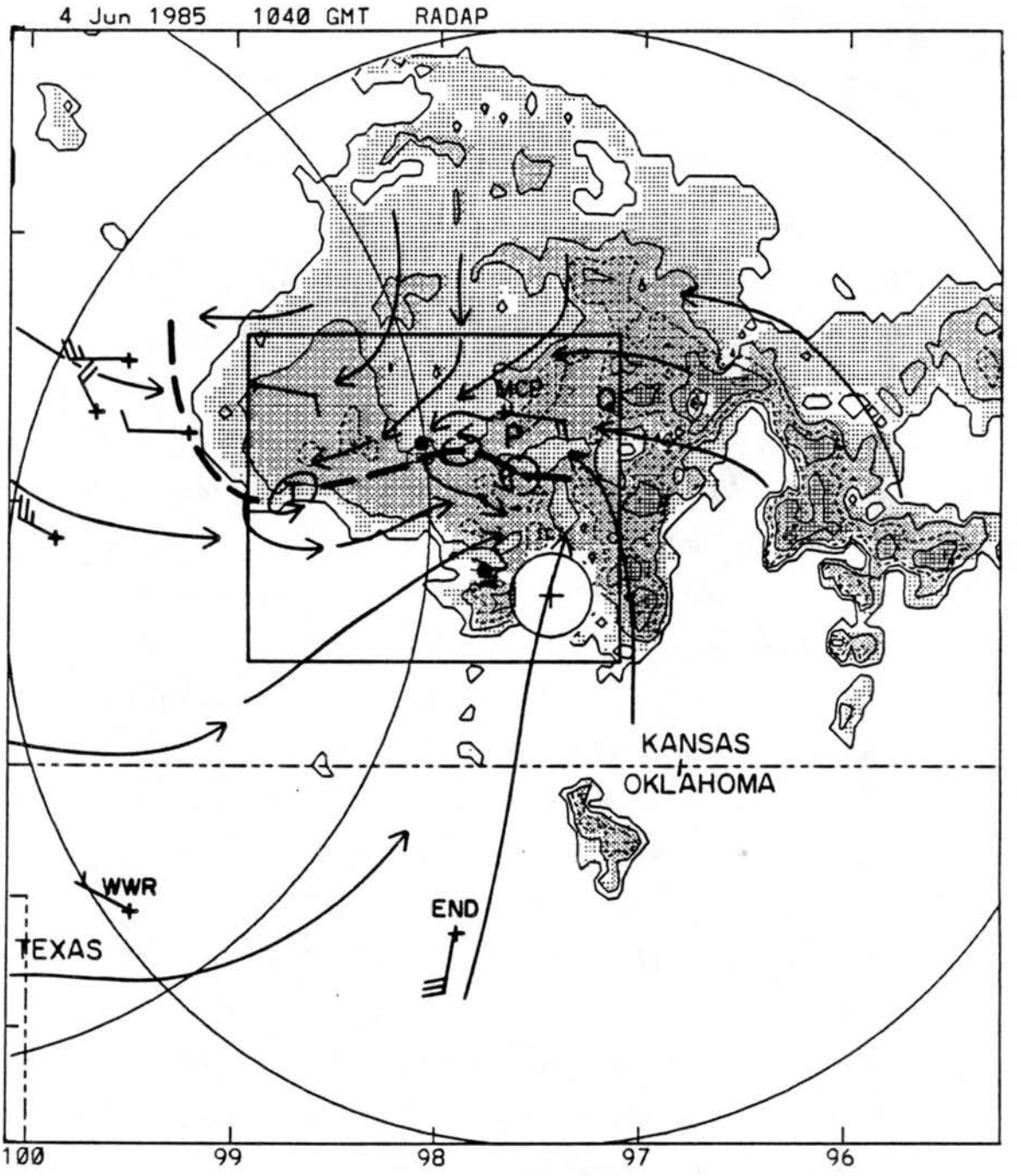

Figure 6.17: Relative streamlines in the 5 to 6 km layer in and around system C at its mature stage, over the reflectivity (shaded) from Wichita radar at 1040 UTC. Wind within the box was analyzed from dual Doppler data; aircraft data at 465 mb are plotted as wind barbs, and data from a profiler (MCP) and rawinsoundings are added.

and just behind the sloping interface R–R which separated the warm conveyer belt from rear inflow in mid–levels. It should be noted that relatively larger downward motions were observed at S in the Doppler data.

Two smaller centers of cyclonic vorticity were located at T, on the rear margin of echo, and 20 km south of the MCP profiler, where the "apex" of the vortical pattern was located 20 to 30 minutes earlier. This is further evidence that a cyclonic circulation some 4 km deep was associated with the vortical patterns in radar and surface data.

The "southerly jet" east of R covered more area and backed to a southeasterly regime from 2 to 7 km in height. It is located in the midst of recent convective activity that was being transformed to stratiform character. Convective updrafts probably transported southerly momentum from the top of the boundary layer to the middle levels, where it appears to have been accelerated, perhaps by a negative pressure perturbation in the evolving cyclone, as it curved around R and through P. It is reasonable to infer that the air detrained from convective and meso–β–scale updrafts in this region continued to ascend in a "warm conveyor belt". At levels at and above 7 km, the strongest winds were relative southeasterlies located north of P and U. They would have transported ice particles from the convective regions, far to the north and northwest, the directions into which the stratiform cloud grew the fastest.

These Doppler wind volumes were not well positioned to observe the "cool conveyor belt" which was positioned north of the P–Q axis. Modest easterly relative flow prevailed in the still–convective northeast corner of the domain; further west and closer to the evolving vortex, the relative velocity was greater near the cross section R–R′, and backed with height up to 5 km (cold advection) then veered with height above that. Descending motion was inferred in the middle levels in this same, small portion of the earlier velocity field. The cooler air north of the pre–existing frontal zone (which was observed only below 5 km in synoptic data) thus appeared to be drawn into the cyclone from the north in the lower troposphere. The convergence from both the south and the north, also observed in sounding data, would have intensified a frontal zone along the increasingly curved or S–shaped boundary between front–to–rear and rear–to–front flow.

The above synthesis of the 3–D wind field from Doppler radar, aircraft, and profiler data sets greatly aided the depiction of airflow through a prototypical MCC shown in Fig. 9.5 and Fig. 9.8.

6.7 Summary discussion of system C

This development of the third MCC in 24 hours demonstrated that these convective systems can recur repeatedly on the same path at intervals of about eight hours. This third system exhibited the most chaotic pattern of convective activity of all the MCCs studied, and even when some organization was present in the core region, other regions still manifested the chaotic patterns. It is felt that the chaotic distribution of new convective clusters resulted from attainment of conditional instability and elimination of a "capping" layer over a wide area at the same time, because moisture arrived in sufficient quantity fairly quickly in an accelerating low–level jet. All of the above were part of the recovery process after mesoscale downdrafts of a previous MCC deposited dry air with low values of θ_e into the previous sub–cloud layer. The recovery process was observed twice in the same region, after system A and after B, and required 6 to 8 hours. Furthermore, the existence of the shallow, very stable surface layer, only about one–half kilometer deep (itself a product of the previous MCC), may have aided the onset of chaotic convection because the layer of instability was decoupled from surface features and air–mass boundaries, and because the near absence of friction permitted the low–level jet to accelerate more quickly. In this view, the cumulonimbus cells appeared in locations unrelated to any terrain features or meteorological boundaries in the surface layer.

Halfway between the initiation and the mature stages of system C, a weak open–wave pattern of convective bands did emerge from the chaotic pattern of clusters in the core region for about 90 minutes. After that, instead of an occlusion, a spiral band of convection 250 km in diameter was manifested for about one hour, at the mature stage. The open–wave pattern could be traced back to the initiation stage even though it consisted of a much smaller cluster of echo at the earlier time. The intersection of the bands (the "apex" region) could be tracked smoothly and consistently over 5 hours. At the same

time, discrete new convective clusters were developing up to 300 km ahead of the core of the MCC; some, in fact, developed outside of the main cloud shield.

The frontal wave pattern also was analyzed in the surface wind and temperature fields in association with the convective bands. "Cusps" associated with weak low pressure regions propagated not only on the wind confluence line in Kansas, but also on the "real" front in Oklahoma. The "cusp" in Kansas developed in the core region of numerous, but still largely discrete, convective clusters. The one in Oklahoma harbored no convection nor even cloud.

The scant upper-air data in system C were consistent with the conception of the 3-D airflow inferred for system B. Velocity fields obtained for three times in the last hour before the mature stage, from Doppler radar observations of the spiral convective band and the stratiform cloud to its rear, greatly augmented the upper air data. Front-to-rear flow, convergent in the convective regions and divergent elsewhere, filled the lower layers up to 2.5 km.

From this level up to about 6 km, the "warm conveyor belt" accelerated and converged into the concave side of the convective spiral from the east. Flow also converged into the more intense segments of echo from the convex side. In one such segment, northeasterly inflow which perhaps was part of the cool conveyor belt was descending. Front-to-rear flow predominated in the stratiform region. A well defined boundary of shear vorticity and deformation separated this regime from rear-to-front flow, which intruded more and more with time into the southwest quadrant of the stratiform cloud. As the convectively active apex or spiral region propagated along the old stationary front aloft, it left behind this frontal-like boundary. Indeed the new boundary was located where the old baroclinic zone had been, but after the core of the disturbance passed, *dry* air with lower values of θ_e occupied the south side (right side) of the boundary at least in middle levels.

Profiler and aircraft data confirmed that, at a given level, the rear margin of the stratiform cloud was a sharp boundary between dry rear-to-front wind and saturated front-to-rear wind in cloud. The boundary at the rear margin sloped west with height, and the east-west boundary discussed above sloped slightly north with height. At high level

above 7.5 km, front–to–rear flow, increasingly from the south with height, and increasingly divergent and anticyclonic, swept ice in the stratiform cloud toward the northwest and north in the relative sense.

The evidence for an emerging cyclonic circulation which shaped the frontal–like boundaries between the "conveyor belts" in middle and lower levels is stronger in system C than in system B. More of the stratiform cloud lay west of (behind) the convectively active core region in C than in B. Perhaps as a consequence, the dry rear inflow was observed more to the *south* of the path of the core region than was the case in B in which the rear inflow was strongest in the north. Stronger rear inflow toward the south of the MCC core would favor spin–up of the cyclone rather than oppose it.

The convective activity on the "mesoscale cold front" was weaker and briefer in system C than the activity in B (which spawned a tornado). Consequently, the convective line did not generate a stratiform anvil that was advected towards the front of the MCC, as B did. The forward anvil may have hindered gradient–wind adjustment to the convergent core in B. A relative "stagnation zone" in middle and upper levels lay downwind (northeast) of both MCCs. Thus, the low–speed inflow might spin up more slowly on the downwind side, than the relatively faster ambient winds might do on the upwind side (the rear) of an MCC.

In the next chapter we will investigate the history of an MCC which generated a long–lived and extensive stratiform cloud immediately behind a squall line on the pseudo–cold front. We will see that the MCC evolved into a true occlusion.

Chapter 7

AN EXAMPLE OF AN OCCLUDING MESOSCALE VORTEX

One of the best examples of a convective system that developed a mesoscale comma cloud with features of an occlusion was observed earlier (May 7, 1985) in the PRE-STORM experiment. The system spun up a deep, long lasting cyclone which was favorably located in the network. Many features of the cyclone have been reported by Brandes (1989). We extend his analysis here, especially with more surface analysis and more discussion of the occlusion.

Before it reached MCC status, this system was preceded for seven hours by widely scattered clusters of storms, many of them severe, in the panhandles of Texas and Oklahoma and western Kansas. Woodward county, OK (at 'WWR' on Fig. 7.1a) accounted for more than half of all reports of severe weather from this system (Storm Data, 1985). Most of the reports were of hail, from $\frac{3}{4}$ to 1 inch in diameter, but one F0 tornado, and rainfall up to six inches, were reported. A glance at all the panels of Fig. 7.1 shows that high reflectivity echoes were present in the Woodward area for more than 8 hours. The long duration of locally intense convection may have contributed to the buildup of a stable vortex by continual release of latent heat until the wind field approached a gradient wind balance with the warm anomaly.

The system qualified as an MCC at 0430 UTC initiation, reached its maximum extent of cloud area three hours later (maturity), and disqualified at 1130 UTC (dissipation). It was relatively slow to organize a so–called mesoconvective stage, when the cloud shield is cold and compact and rainfall volume is large; this stage lasted from 0700 to 1100 UTC. The cloud tops were also relatively warm compared to most MCCs (R.L. McAnelly, personal communication). Collection of supplemental sounding and Doppler data was

good, but "the scheduling of research aircraft for this situation proved to be difficult" (Meitín and Cunning, 1985) so that an opportunity to observe the MCC from an aircraft was missed . Even as the precipitation structure became less organized after 1100 UTC the cloud shield continued to evolve a spiral shape with anticyclonically curving fingers of cirrus especially apparent on the north side (the strongly sheared side).

7.1 Evolution of convective and stratiform structure

The evolution of the radar reflectivity pattern on 7 May 1985 is depicted in Fig. 7.1 at intervals of one to two hours. For some 5 h previous to the time of the first panel,thunderstorms had been active in the Oklahoma panhandle and western Kansas. Two mesoscale clusters with some intense cells were present in this region at 0300 UTC (Fig. 7.1a). Both clusters (marked as *A* and *B*) generated stratiform echo that moved northward and filled the intervening area amidst new convective clusters in Kansas, by the time of panel b . The new clusters tended to form near a stationary front that lay close to the state line.

Within 90 minutes (Fig. 7.1c), two hail–producing clusters *b* and *d* dominated the system that resulted from the merger of the previous systems. A leading squall line at *A* generated a stratiform echo expanding north and west. Within an hour the convex, bow-shaped line from *A* to *D* harbored the strongest echoes of the MCS; the broken east–west band developed into a nearly continuous convective line from *D* to *E* (Fig. 7.1d). A transient convective band at *F* formed parallel to *D–E*, like the parallel bands in the episode of June 3, 4, and in accord with Maddox' (1981) observation on the frequency of bands parallel to a front.

The occlusion–like character of the convective echo became prominent over the next two hours. The strong meso-β echo at the intersection *D* of the convex squall line with the east–west line did not persist after 0900. But enhanced precipitation in the stratiform cloud and some embedded convective echo (*G*) developed west of the intersection where the mid–level circulation was observed to develop, on Fig. 7.2a,b,c. The enhanced upward motion and precipitation is analogous to what occurs in an extratropical cyclone at the same stage.

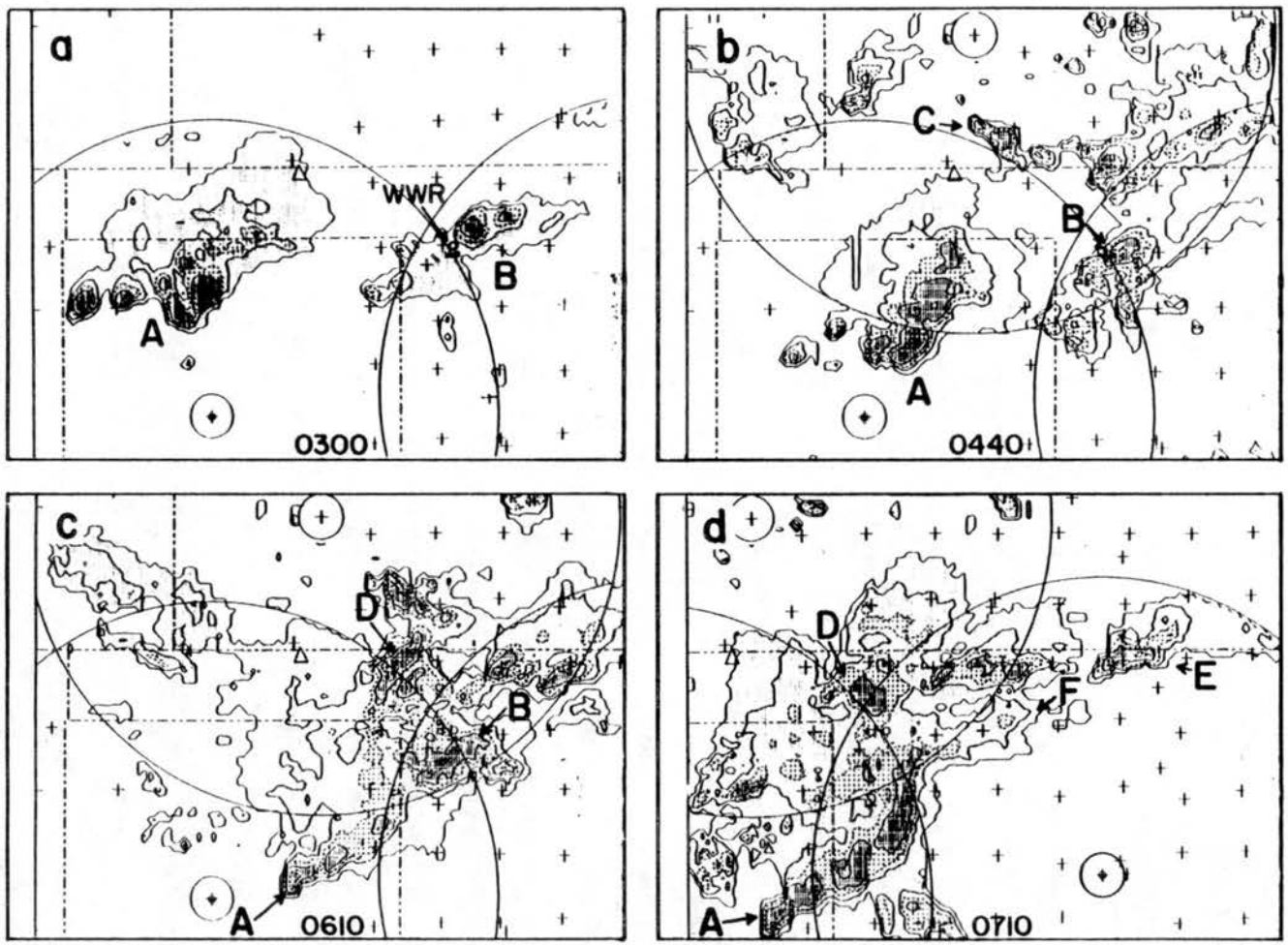

Figure 7.1: Radar reflectivity depictions of the early storms and early stages of the MCC on May 7, 1985, at roughly 90 minute intervals. The UTC hour is beneath the echo; gray shades are keyed to dBZ levels at lower right; letters point to features discussed in the text. The maps are composited from base scans at the OKC, GCK, and AMA radars.

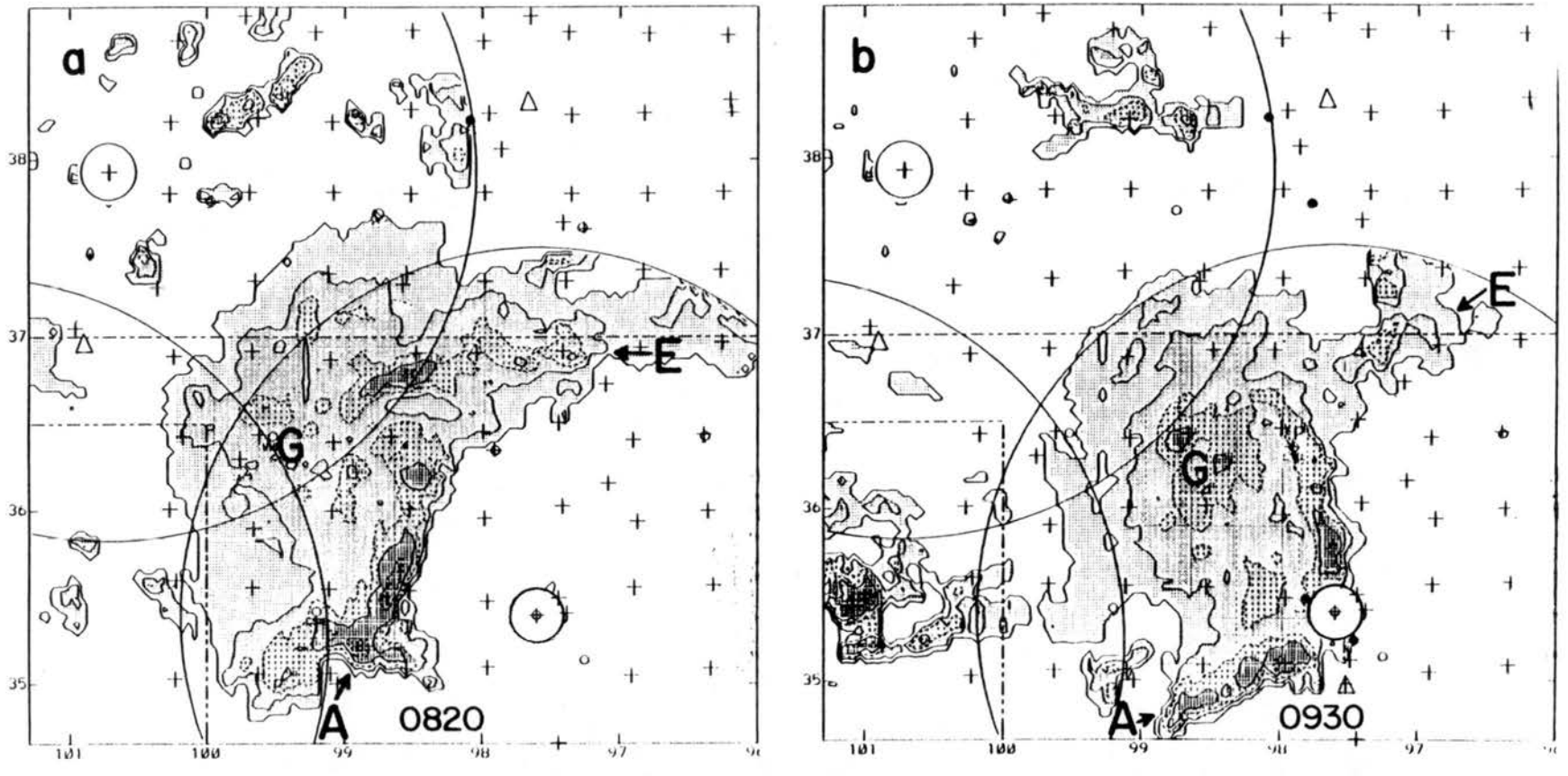

Figure 7.2: As in the previous figure but at the mature and late stages. Times are (a) 0820, (b) 0930, (c) 1025, and (d) 1200 UTC 7 May 1985.

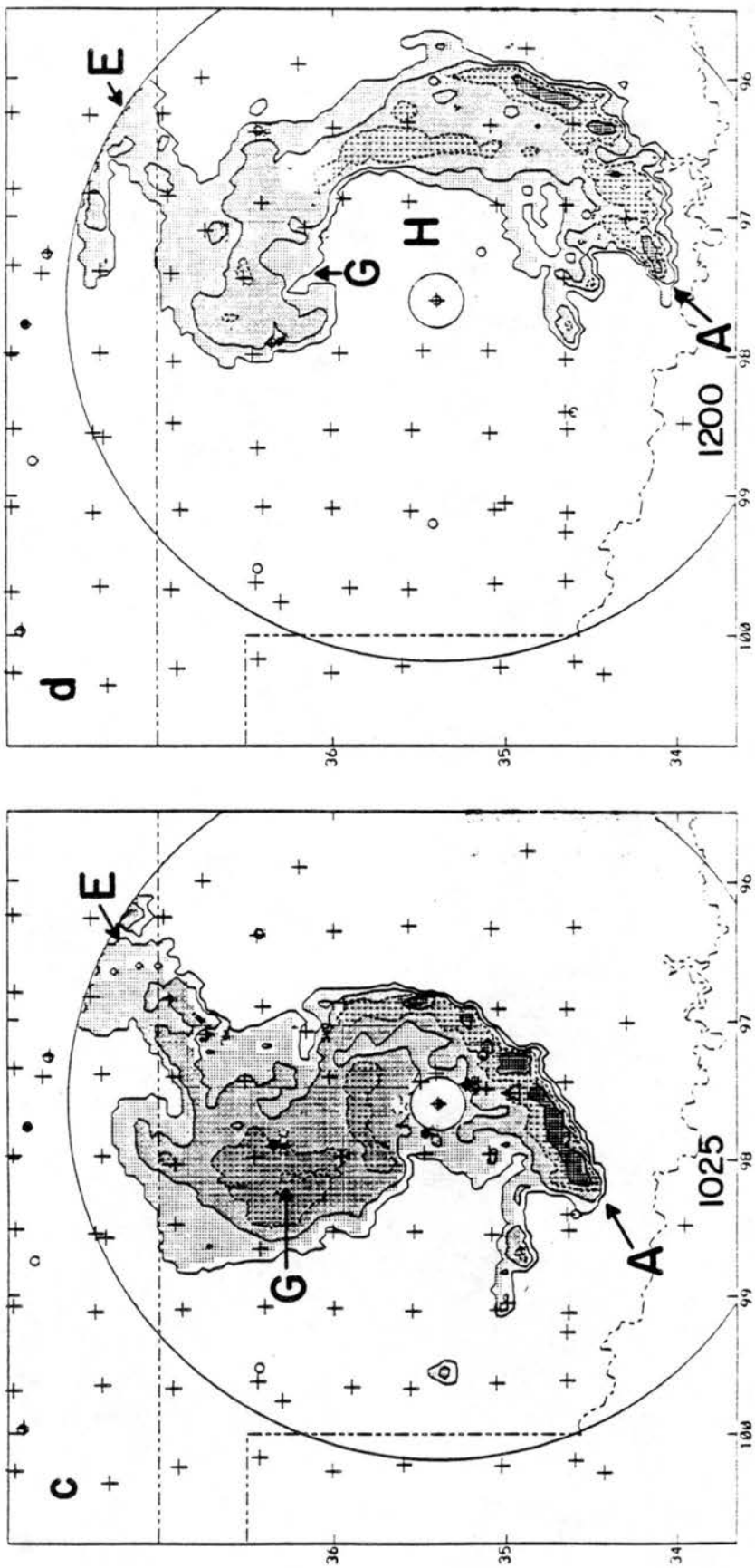

Figure 7.2: Continued.

From 0930 to 1030 UTC (panels b and c) a broad notch started to erode the rear edge of the stratiform echo west of the convex convective line A, which became more intense on the southwest flank at the same time that it lost its convective character on the north end near the region of intersection. Convergence continued to feed a rainband with some convective cells (E) along the stationary front at later stages.

The last map at 1200 UTC (Fig. 7.2d) displays to good advantage the comma shape of this MCC, after the broad notch had eroded the center out of the stratiform cloud, and a new "dry tongue" at G wrapped around the east side of the hook–shaped tip of the comma. The hooked tip is co–located with the deep mid-level vortex, by this hour well developed.

7.2 Synoptic environment

The National Weather Service analyzed a stationary front through Kansas and the Texas panhandle through the period. The mesonetwork data pinpointed the front on or just south of the Oklahoma / Kansas state line. Even before this MCC passed through, smaller meso-β clusters had spread some cool air that effectively positioned portions of the front further south; passage of the MCC dislocated the front to southern Oklahoma.

Relatively weak anticyclonic flow prevailed over the region above 850 mb. A fairly flat ridge extended northwest into the northern Rockies. The anticyclonic regime resembled that on 4 June but the flow magnitude and shear were much weaker.

A sharp trough in New Mexico and Colorado at 850 mb (and to a lesser extent at 700 mb) focused a low level jet over Oklahoma and west Texas into western Kansas. Velocity maxima of 12 to 17 m s^{-1} were found below 750 mb; the axis of peak moisture lay from Oklahoma City (OKC) to Dodge City (DDC); the top of the moist layer sloped from 850 mb in north Texas to 600 mb at the Kansas border, where convergent winds indicated the presence of the front. As the MCC swept east, the low level jet accelerated and maintained its axis just east of the convex convective line.

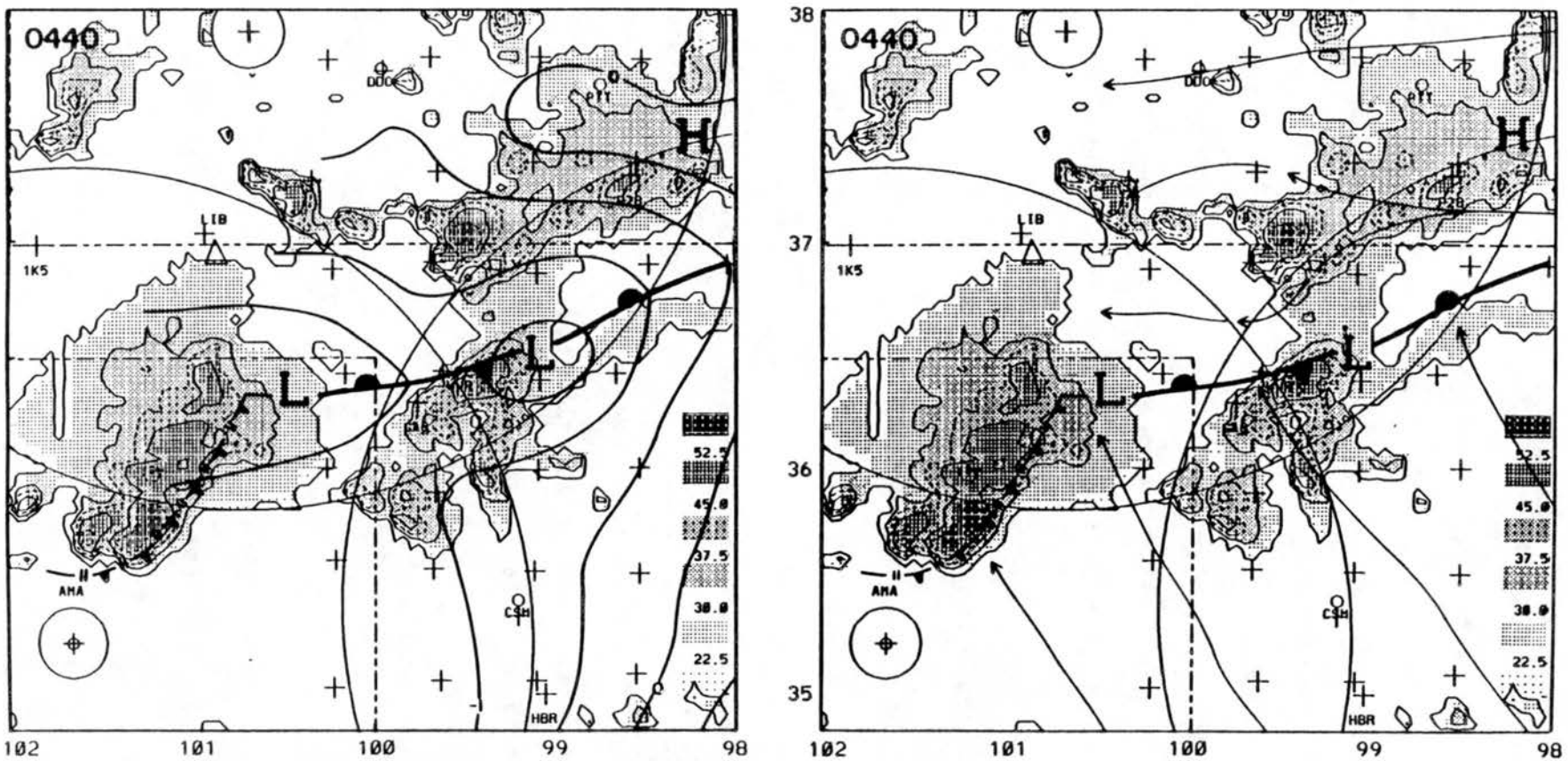

Figure 7.3: Mesoscale surface analysis of pressure perturbation (a) and streamlines (b) on the radar reflectivity (shaded) previously mapped in Fig. 7.2, at 0440 UTC. In (a) the perturbation from the 24–h mean pressure is contoured every 0.5 mb. Boundaries of rain–cooled outflow are depicted by frontal symbols with small, closely spaced barbs, according to the convention proposed by Young and Fritsch (1989). Synoptic scale fronts are depicted with large barbs.

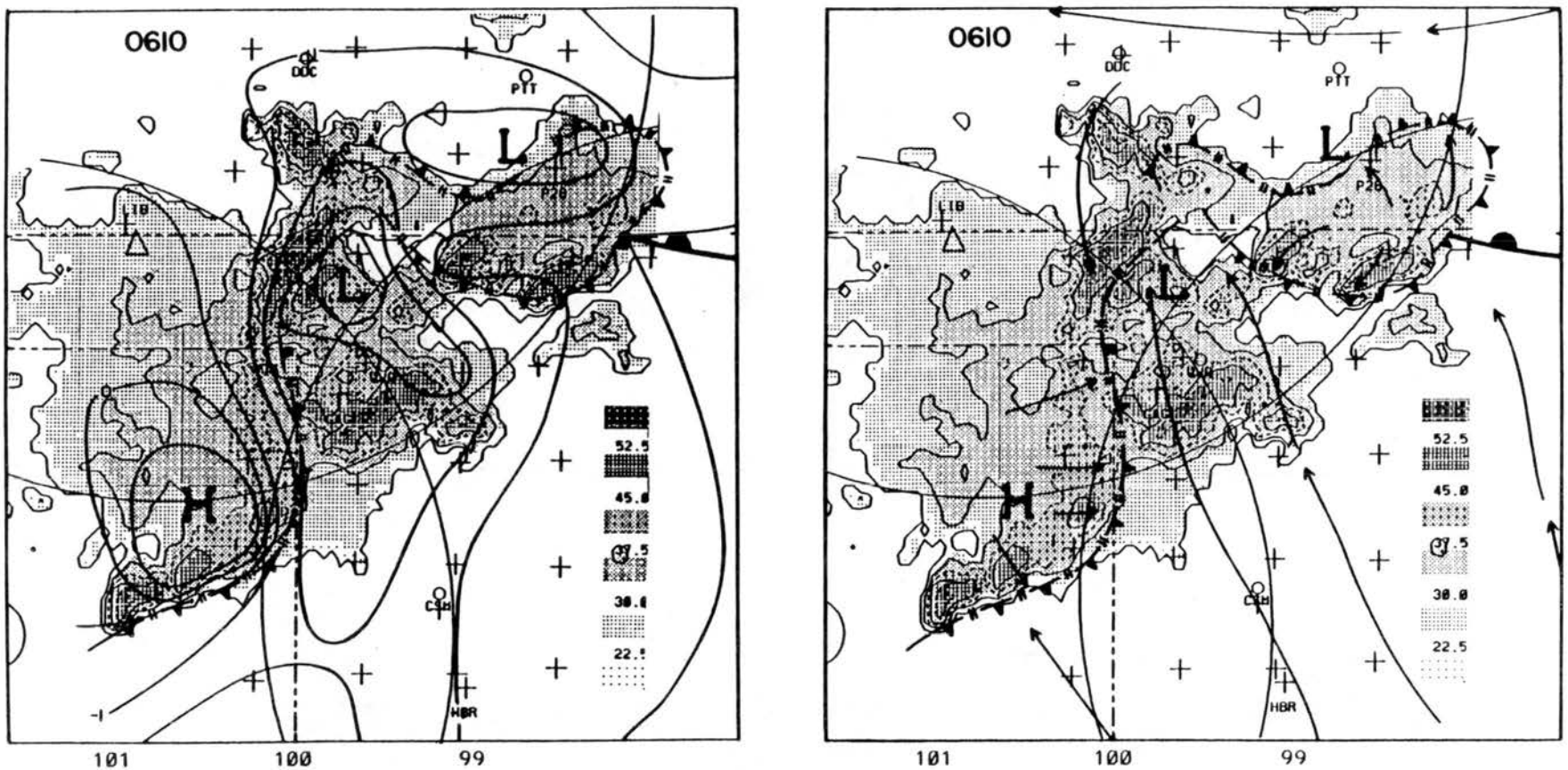

Figure 7.4: Surface analysis as in previous figure but at 0610 UTC.

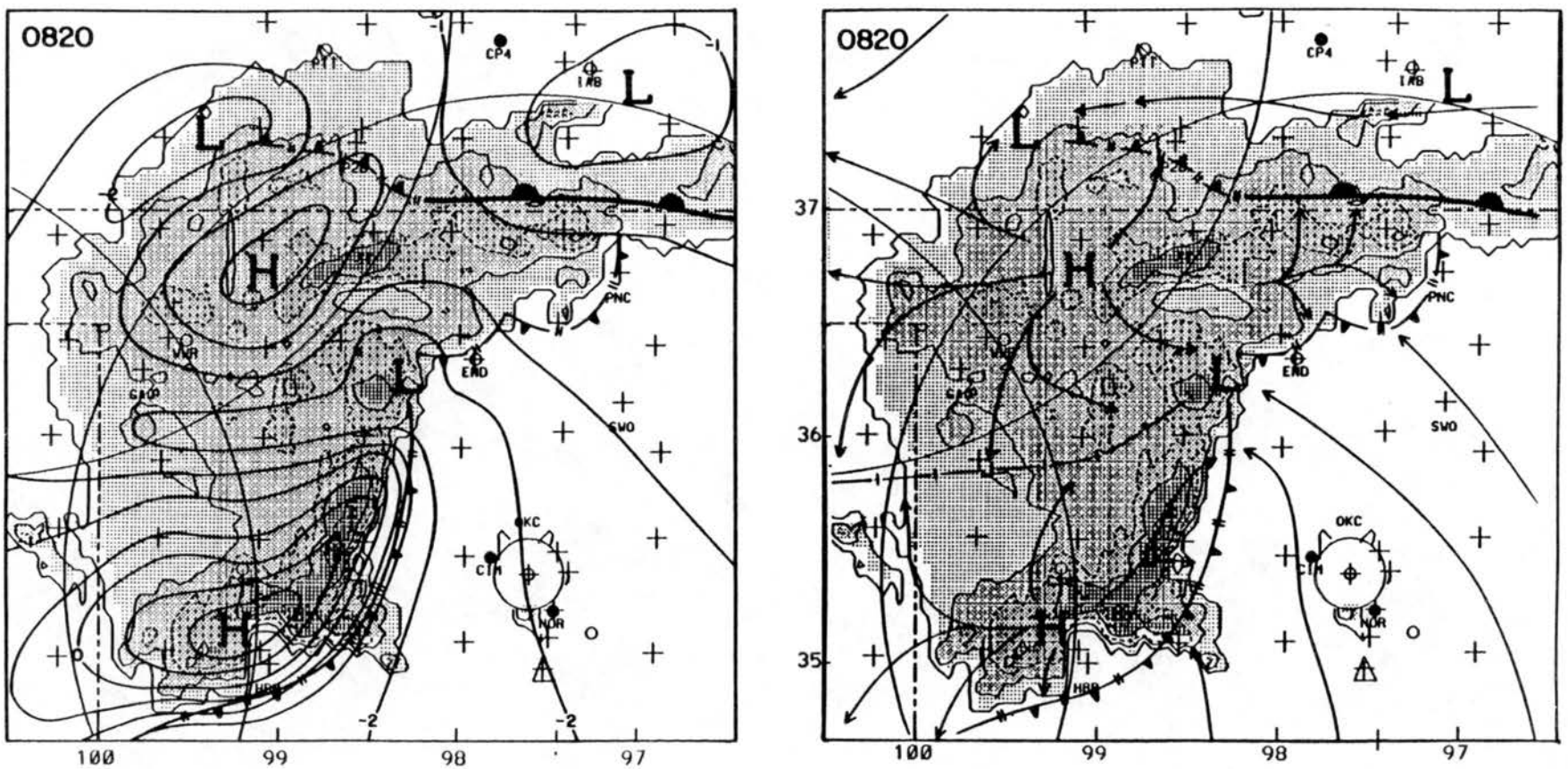

Figure 7.5: Surface analysis as in previous figure but at 0820 UTC.

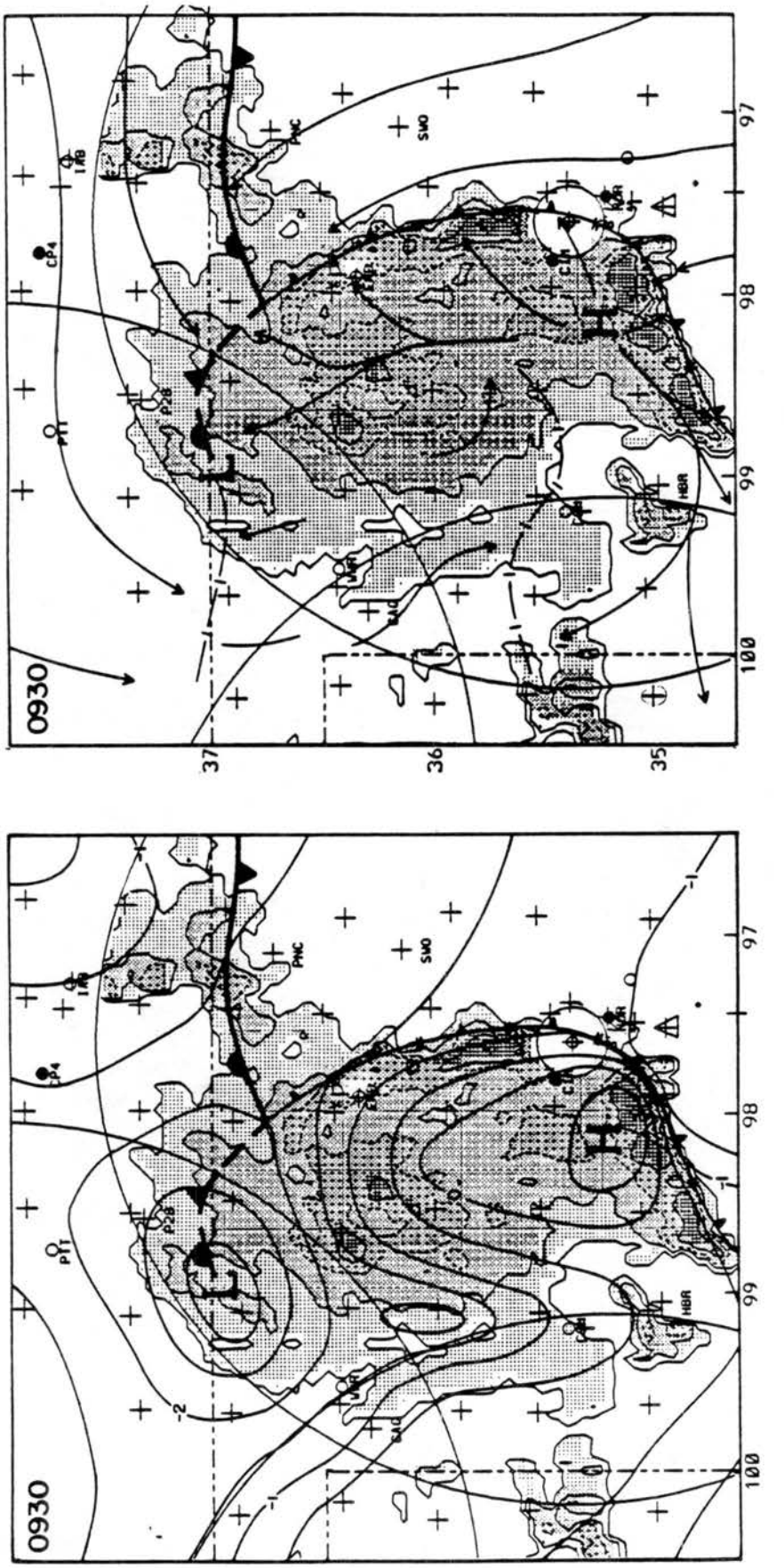

Figure 7.6: Surface analysis as in previous figure but at 0930 UTC.

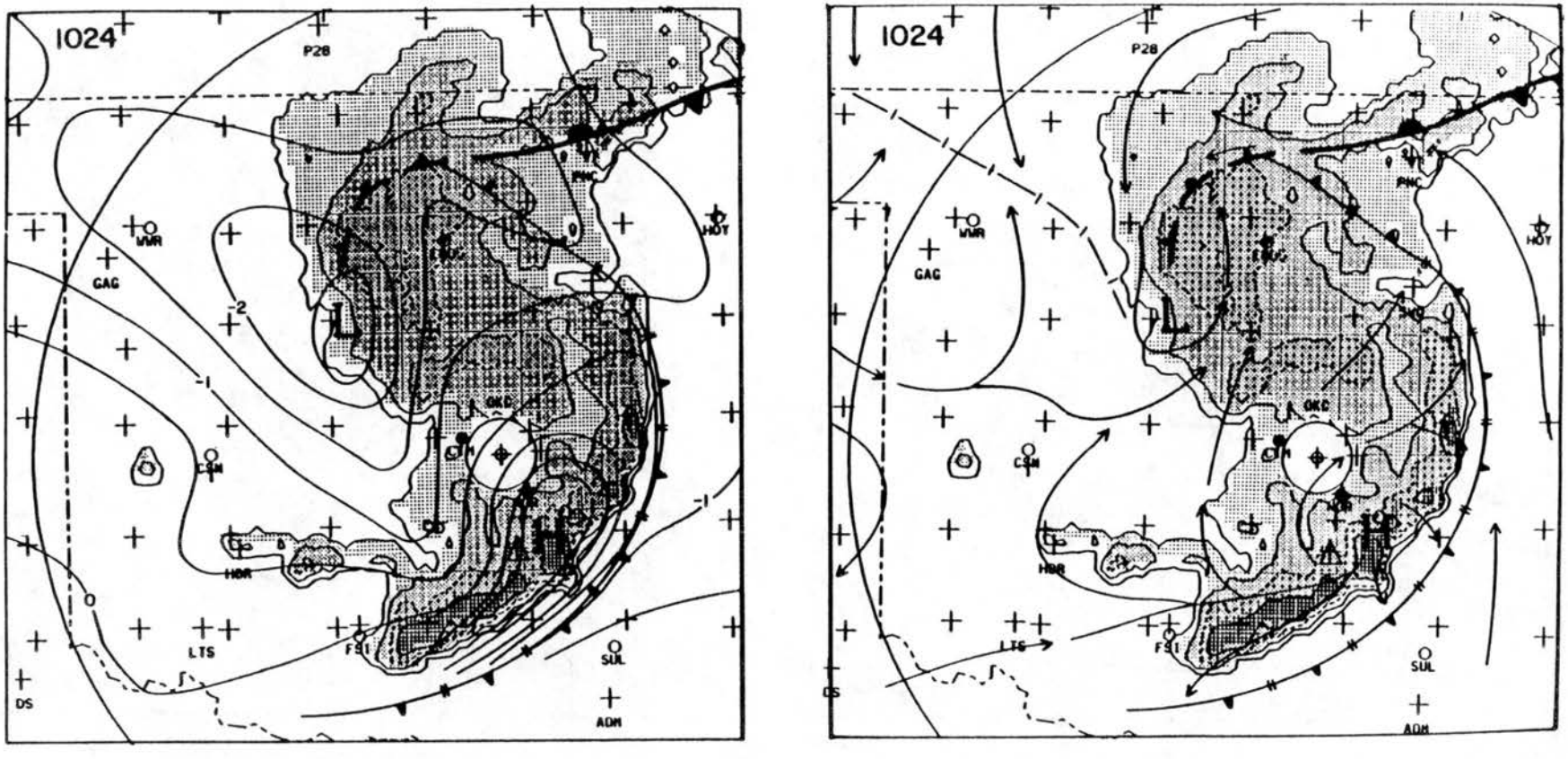

Figure 7.7: Surface analysis as in previous figure but at 1025 UTC.

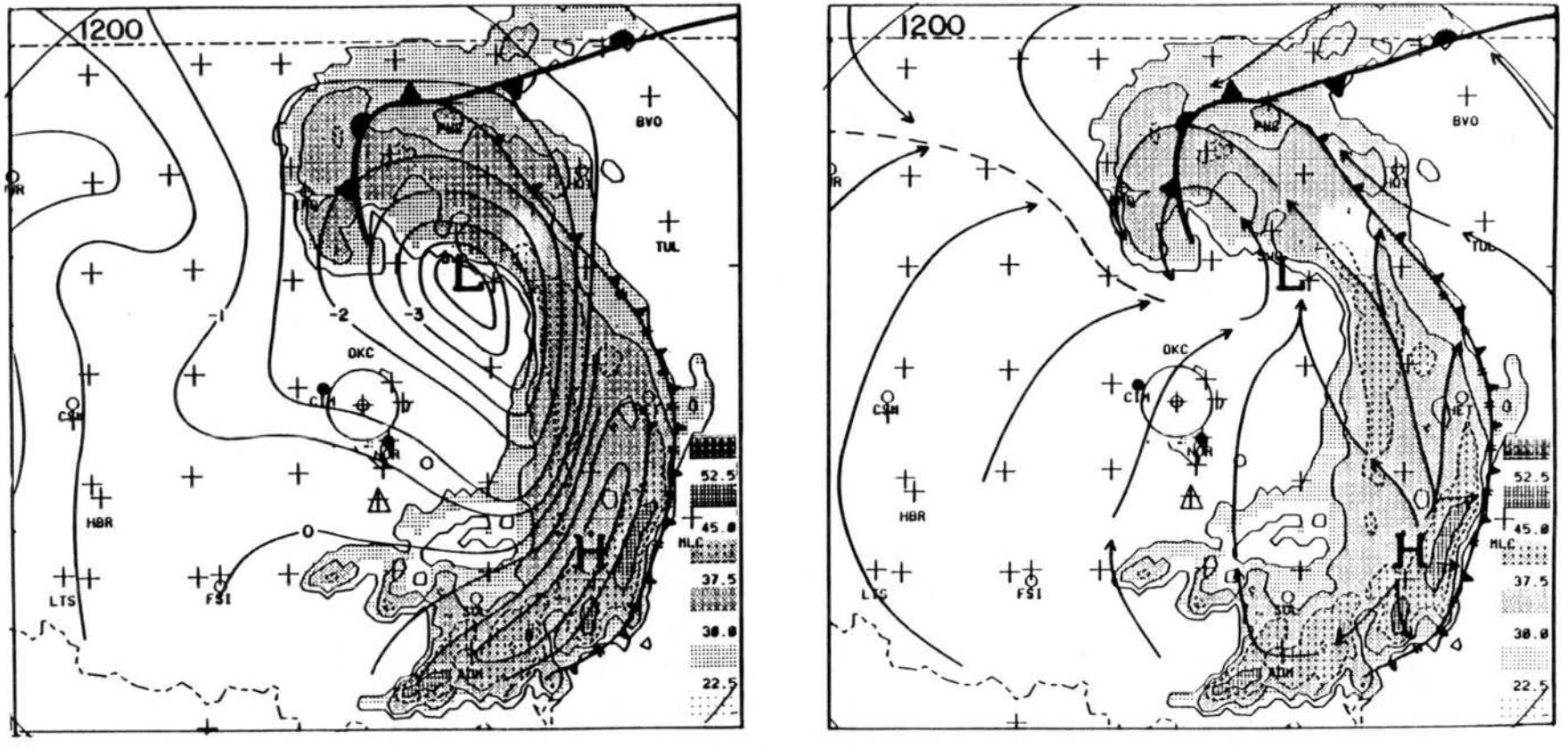

Figure 7.8: Surface analysis as in previous figure but at 1200 UTC.

7.3 The evolution of the meso-cyclone at the surface

Although convective systems have been observed to spin up mesoscale cyclones in the middle troposphere, the cyclones rarely are observed at the surface; it is more common to observe purely convergent inflow to convective regions and purely divergent outflow from cold pools. The passage of this MCC within the SAM network led to the recognition of a closed cyclone at the surface. Brandes (1989) briefly discussed the surface perturbation pressure field for 3 times in the late stages of the MCC. This section discusses our own wind, pressure, and temperature analyses for the complete life of the system. The analyses are displayed for the same times as shown in section 7.1.

At 0300 UTC south or southeast winds over Oklahoma converged with easterly winds over Kansas along the stationary front mentioned before. The temperature gradient across this front was 5 K at sunset but decreased considerably through the night. Outflow from the hailstorm near WWR (see Fig. 7.1a) affected only two SAM stations. The pressure field was not strong, with a gradient of 3 mb per 500 km across the PAM / SAM network from the northeast to the southwest corners.

At 0440 UTC, at least three separate meso-β scale systems were about to merge. The pressure field was beginning to respond to them: a weak meso-trough was underneath the hailstorm at WWR and along the stationary front (Fig. 7.3). One would expect a pressure dome under an MCS of the size of the western system, which had not yet entered the surface network. Except for nonpersistent thunderstorm outflows, the wind field had not responded to the convection.

As the systems merged (analysis not shown), a ridge of higher pressure was building between two meso-troughs located along the two most intense lines of hailstorms, which were 20 km south and 60 km north of the front. By 0610 UTC, a region of storm outflow on the old front could be outlined inside the broken barbed curve on Fig. 7.4, between two meso-low centers. One low coincided with a southerly "warm surge" which apparently re-configured the front into the wave pattern shown. The gust front and meso-high of the western system, which had an extensive stratiform echo, had entered the network.

Two hours later, at system maturity, the pressure field was complex (Fig. 7.5). Two meso-high centers, one probably due to cool outflow from the hailstorms near the apex of the frontal wave, the other associated with the squall line at the southern end of the system, were co-located with centers of strong divergence. Two of the three meso-lows deserve mention. A "wake low" was forming on the northwest margin of the MCC; and an "apex low" was found on the triple point intersection of the southern squall line, the convergence line between the two outflow regions, [1] and the outflow of storms along the stationary front.

After another hour these meso-lows merged into one as the precipitation in the northern part of the MCC apparently was not sufficient to maintain the northern dome of high pressure against the (probably multiple) processes deepening the meso-lows. At the same time the pseudo-cold front, having just surged northward and eastward, overtook the old stationary front and thereby caused a veritable occlusion (Fig. 7.6). The new "occluded front", which was analyzed from the triple point northwest into the one dominant meso-low, was seen in the surface data as a line of confluence between the rain-cooled southerly outflow and the ambient easterly flow in Kansas. The meso–low is continuous with a wake pressure trough, which had just formed in a north/south direction along the rear edge of the heavier precipitation, along the 30 dBZ contour (medium shading) in Fig. 7.6.

Two phenomena on our next analysis at 1025 UTC (Fig. 7.7) deserve mention. As the "notch" started to erode the southern part of the stratiform cloud from the west, and eventually produce the comma shape, surface air modified by the passage of the MCC began to flow toward the northeast into the wake trough behind the rain system. East of the trough, within the stratiform rain area, the wind there (also blowing toward the northeast) appeared to have largely adjusted to the pressure field between the meso-high and meso-low. Lastly, a new boundary extended northwest from the meso-low. It marked

---

[1] A line of thunderstorms apparently formed along this convergence line in the next hour. The echoes can be seen extending into the Texas panhandle from the middle rear portion of the stratiform region, and just north of the incipient "rear inflow" notch, on Fig. 7.6).

the confluence of system–modified air and the ambient flow in Kansas that was being accelerated from the north into the wake trough.

A closed cyclonic circulation was unambiguously present on the surface analysis at 1200 UTC (Fig. 7.8), directly under the tip or "hook" of the comma cloud pattern. It was not co-located with the meso-low pressure center, which was 40 km to the east, probably because the winds were slow to adjust to the rapidly moving center. The precipitation in this intervening region dissipated after this time, so that an enhanced area of precipitation remained with the vortex, which increasingly lagged behind the arc–shaped rain band along the pseudo-cold front. The two other confluence lines remained: one extended northwest from the vortex, the other was the stationary front, on which convective cells continued to form.

7.4 The evolution of the vortex above the surface

The supplemental rawinsonde and dual Doppler data analyzed by Brandes (1989) were sufficient to define a cyclonic vortex in the low and middle troposphere of the MCC. The winds in Fig. 7.9 and following figures are shown relative to a vortex motion of 8.3 m s^{-1} from 275° .

Brandes obtained this velocity from the motion of a shear anomaly observed by two Doppler radars. The vortex, if it is correctly described by this speed, is much slower than the gust front (18.7 m s^{-1}), the meso–high and wake low pressure centers (21 and 29 m s^{-1} , respectively), and the large scale reflectivity patterns. It also propagated more slowly than any features observed in the episode of 3 MCCs on 3, 4 June (Tables 5.1 and 6.1). Its speed is comparable to (but still slower than) the movement of the cloud shield measured on satellite images *up to* the hour of maturity, that is, from the time of Fig. 7.3 to the time of Fig. 7.5. During that interval the cloud shield moved at 11.2 ms^{-1} from 260° ; but after 0800 UTC it speeded up to 20 ms^{-1} from 310° , more than twice as fast as the vortex, as the southern portion of the squall line continued to generate a cloud shield as it separated from the vortex region.

Before passage of the MCC a temperature gradient exceeding 5 K was directed across the state line in the eastern part of the network, and directed towards the northeast

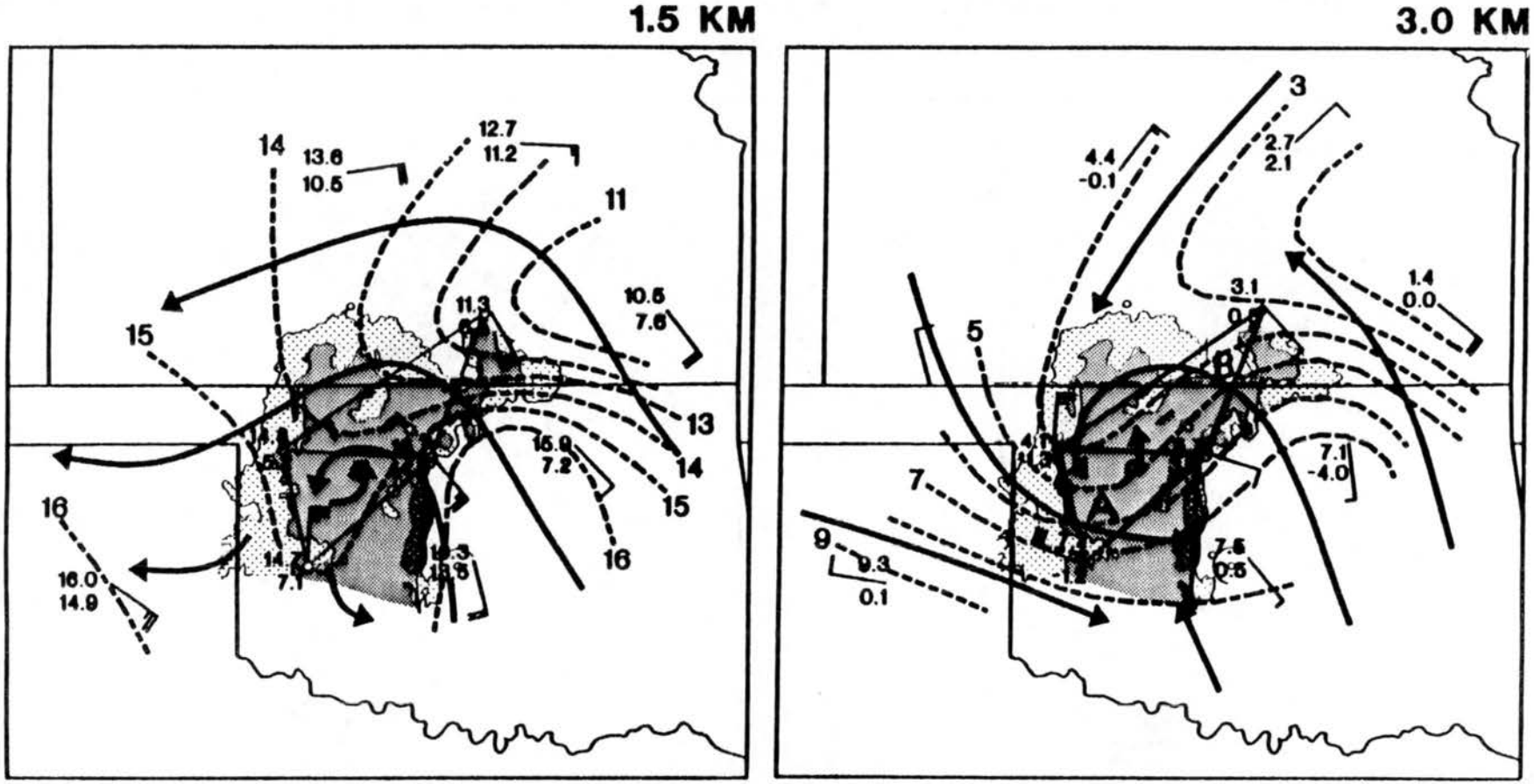

Figure 7.9: Observed winds and temperature at (a) the 1.5 km level and (b) the 3 km level with radar echo (shaded), at 0900 UTC 7 May 1985. Winds are relative to the moving vortex, and are plotted as flags. Temperature (top) and dew point (below) are plotted in ° C. Solid lines are streamlines, dashed lines are isotherms. Reprinted from Brandes (1989), but we added radar echo and triangles A and B.

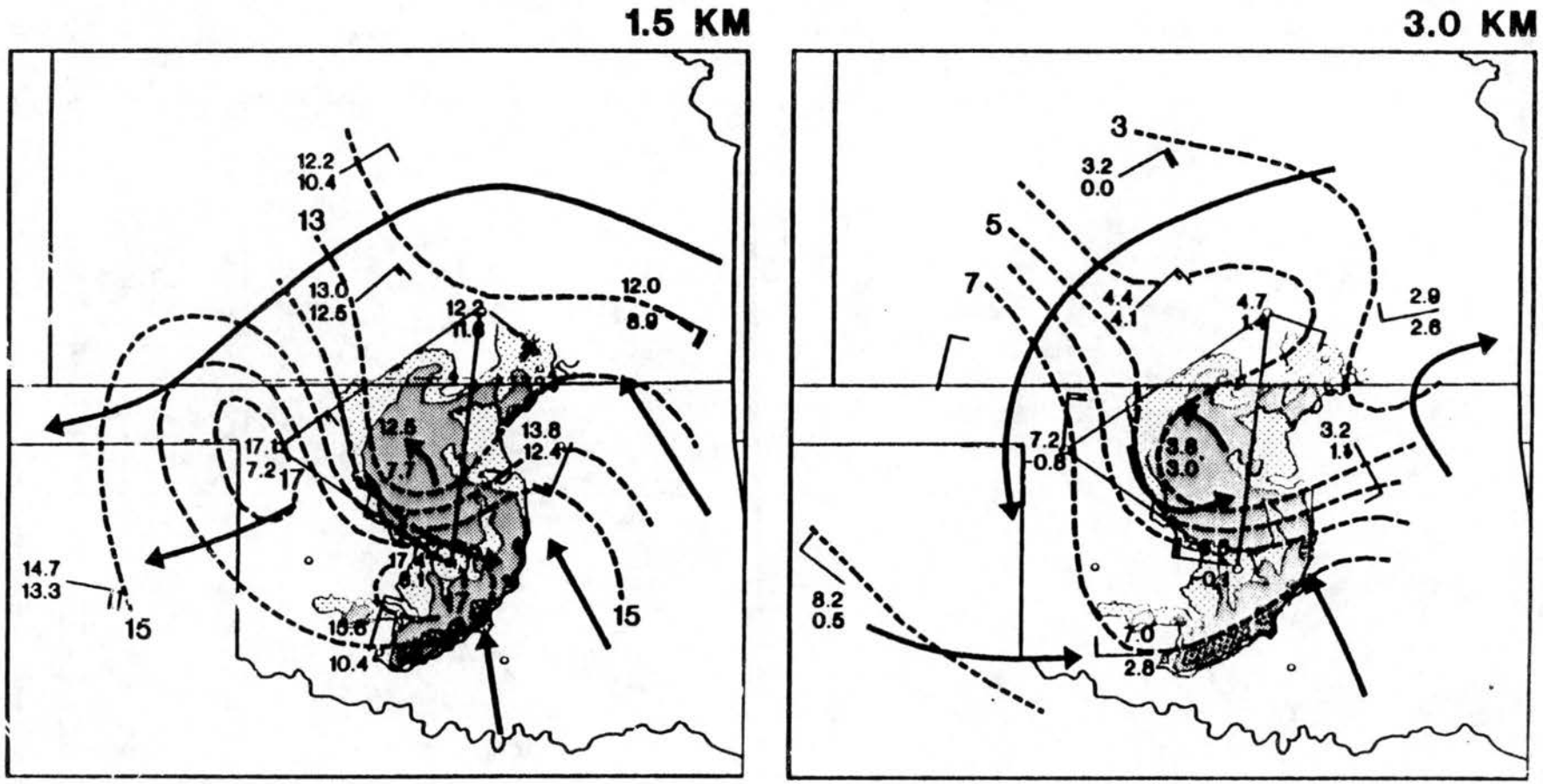

Figure 7.10: As in previous figure but for 1030 UTC. From Brandes (1989); Triangle C has been added.

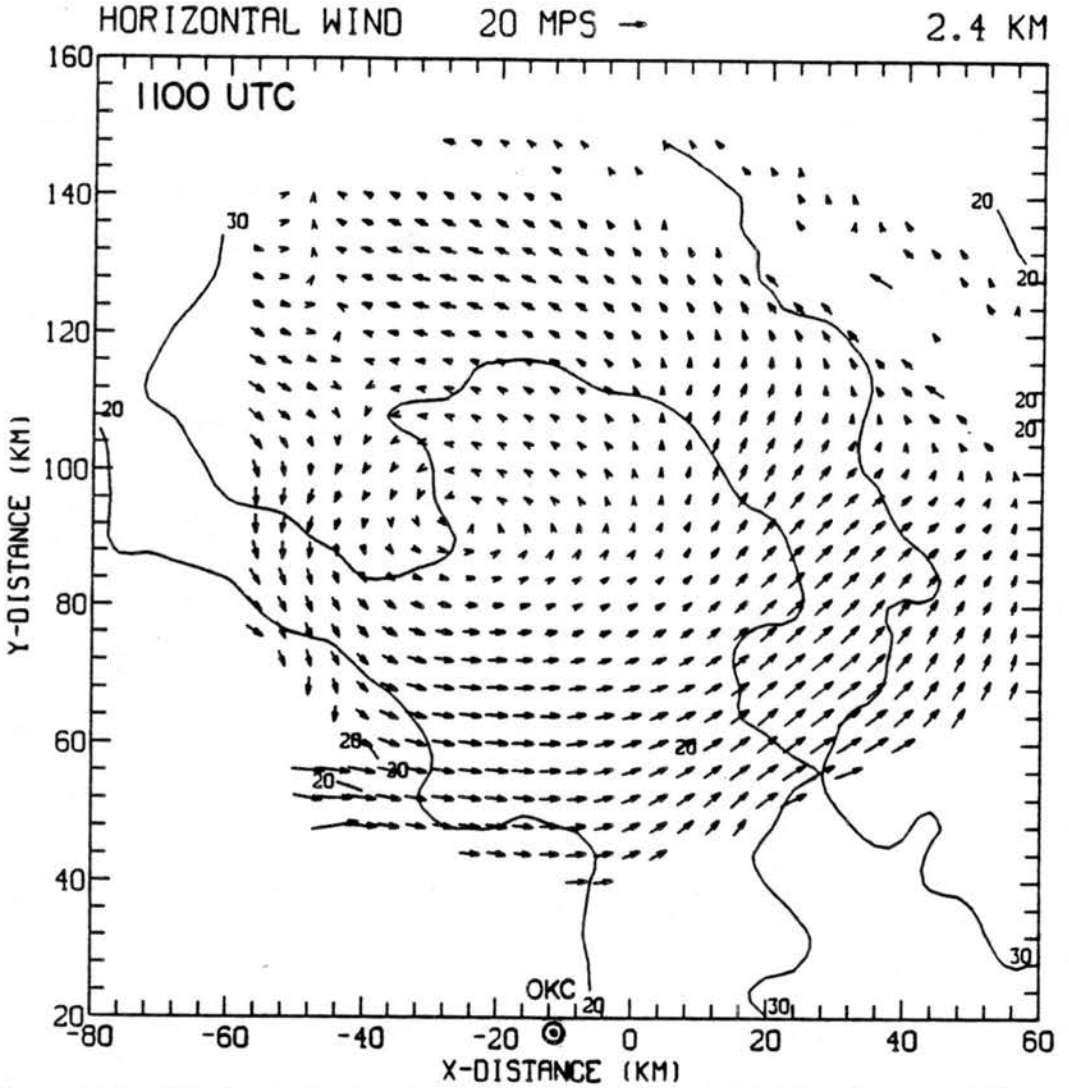

Figure 7.11: Wind relative to the moving vortex at the 2.4 km level, and 20 and 30 dBZ contours of reflectivity, from a dual Doppler synthesis based on NSSL radar data. Oklahoma City (OKC) is located on the lower axis. From Brandes (1989).

(toward colder temperatures) in the western part, at levels up to 3 km. Passage of the MCC distorted the temperature field into an S–shaped pattern, due to southerly flow in advance of the system and northerly flow in and behind the stratiform cloud (Fig. 7.9). At 1.5 km (left), temperatures in the stratiform cloud are only $\sim$ 1.5 K lower than those ahead of the system, which may reflect evaporative cooling rather than cold advection as the figure implies. The circulation is probably not yet closed at this level, as Brandes' streamlines imply; the evidence rather suggests a divergent outflow to the south and to the rear. But the circulation does appear closed at 3 km (Fig. 7.9b) where cool air entered

the cyclone from the north, and (further to the south, where the temperature was 7.2° C and the dew point -1.2° C) ambient warm, unusually dry air entered from the west. At this location a relative inflow jet of 28 m s^{-1} was reported at the 6 km level.

After the mature stage the notch began to be evident in the southern part of the stratiform cloud, and the circulation was evidently closed at the levels shown (Fig. 7.10). At the 1.5 km level a tongue of anomalously warm and dry air curved from behind the system into the notch (panel a). The tongue was oriented along the relative wind direction at 6 km. These properties resulted from dry adiabatic subsidence in the rear inflow. At 3 km (Fig. 7.10b), the warm anomaly was not as warm, but the vortex itself was cold core. At levels above 6 km, the vortex was warm core. Thus this part of the system had acquired a lens of high potential vorticity.

One half hour later the vortex passed 100 km north of Oklahoma City such that the NSSL radars at Norman and Cimarron could obtain dual Doppler data from it. The relative wind at the 2.4 km level from this one volume synthesis is shown in Fig. 7.11. A vortical circulation was centered on the tip of a hook shaped echo defined by the 30 dBZ reflectivity contour. The 30 dBZ contour here defined a large part of the comma shaped rain area. The strongest relative flow was westerly inflow south of the vortex. Horizontally averaged, vertical profiles of divergence were obtained from the Doppler data; the convergent inflow was strongest at the freezing level and set up a deep zone of subsidence from 1 to 6 km above ground.

Kinematic profiles were also obtained by Brandes over larger regions with use of Bellamy (1949) triangles on the sounding data. The divergence δ, vorticity ζ, and vertical motion ω in triangles A and B (located on Fig. 7.9) are profiled in Fig. 7.12. The vortex was in triangle A at 0900, and was evidently deep: the vorticity was positive and greater than 1.5×10^{-4} s^{-1} from 1 to 7 km in height The deep zone of ascent above 4.5 km and descent beneath that is in accord with the usual conception of the vertical structure of a mesoscale convective vortex. Profiles of the northern stratiform region (triangle B, where the stationary front had been, and where the occluding front was forming) in Fig. 7.12b showed weaker cyclonic vorticity up to 5 km, and no anticyclonic outflow zone like the

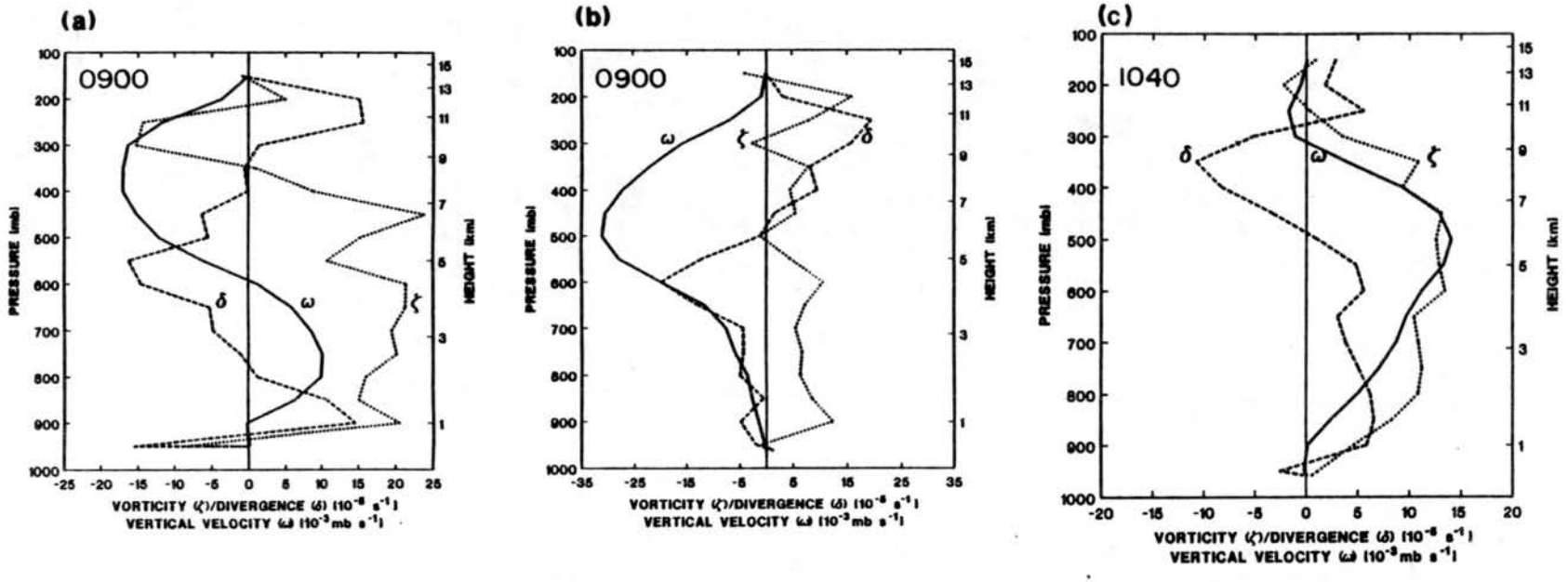

Figure 7.12: Vertical profiles of relative vorticity ζ, divergence δ, and vertical velocity ω in p–coordinates, averaged over the areas of the corresponding triangles *A*, *B*, and *C* located on Figs. 7.9 and 7.10. From Brandes (1989).

zone between 300 and 200 mb in triangle (a). The lower level mesoscale subsidence was also entirely lacking in triangle b. In both regions, convergence was maximized near 600 mb.

Triangle C encompassed the vortex region and most of the stratiform cloud on Fig. 7.10 at the post–mature stage. The extremely deep zone of divergence (from 6 km down to 1 km) and subsiding motion (from 9 km down) was said to be due to strong westerly flow at OKC, directed out of the triangle and into the notch region. Nonetheless, the subsidence is believed to have deepened with time in this system. The cyclonic vorticity was $10^{-4}\,s^{-1}$ through a deep layer from 1 to 9 km.

Brandes calculated that the main generator of vorticity was the amplification of existing vorticity in the convergent layer that underwent vertical stretching. Thus the ambient dry, low valued θ_e air fed the northern part of the vortex from the front, and the southern part from the rear. Convergence of air with planetary vorticity f at the observed rate of inflow could have spun up the vortex in a matter of 1.5 h.

At the levels beneath 4 km dominated by mesoscale subsidence, evaporatively cooled air some 2 to 5 K cooler than ambient air lay to the left of the velocity vector (from west to east) in the rear inflow. Thus, the temperature gradient ∇T vector pointed south, and horizontal vorticity would have been oriented along a vector nearly opposite to the wind vector. Brandes noted that a downwind gradient of vertical velocity of 0.5 ms^{-1} per 100 km would have tilted the vorticity into the vertical sufficiently, such that this mechanism could have contributed to cyclogenesis at the 3 km level as much as the middle–level stretching did.

7.5 The warm conveyor belt

The upper levels of the vortex warmed as much as 5 K in six hours at the 10 km level, according to Brandes, although an undiluted updraft would have been 5 K warmer still. The air was generally cloudy and saturated with respect to ice, and warm advection prevailed there. The kinematic analysis (above) showed ascent from 4.5 to 14 km in height. This properties are consistent with a warm conveyor belt in moist adiabatic ascent, like

an extratropical cyclone except that the evolution in section 7.1 indicated that a large part of the ascent occurred convectively. Brandes noted that the southerly low level jet accelerated twice as fast from 0100 to 0600 UCT as the nocturnal jet usually does, and that it was channeled in front of the active convective line. The veering typical of the nocturnal jet was not observed, probably because the MCC blocked a westerly flow. But an evolving vortex could also explain the observed southerly acceleration and the lack of veering.

7.6 The dry airstream

The rear inflow ("dry conveyor belt") markedly influenced the evolution of this MCC, as it is known to influence a squall line, but in this case it curved around the southern and eventually the eastern sides of the vortex. Brandes reported that the low levels up to 4 km were characterized by cool advection and an associated wind profile that backed with height, despite the subsidence warming. In fact, temperatures at the 3 km level were below environmental and pre-MCC values. The lowest values of θ_e, below 325 K, were found in the "onion" portion of the soundings, within this descending air stream. Dry adiabatic conditions from 750 to 600 mb and confluent flow above 3 km in the sounding gave evidence of subsidence in this airstream. Since these values of θ_e resembled the values in upwind environmental air at levels from 4 to 7 km, it was inferred that the dry inflow into the southern half of the system originated from behind the MCC. However, the presence of similar properties in system–relative easterly and northeasterly flow in the Woodward (WWR) sounding and other soundings, led him to postulate that mid-level air in *front* of the vortex was the source of the descending air on its northern side. We would interpret this stream as a cool conveyor belt.

In fact there was no clear distinction between the cool and dry conveyor belts in this case. The direction of the relative inflow varied smoothly from westerly to northerly as one proceeds from south to north behind the cloud shield. This can be seen at the 3 km level in Fig. 7.9 and Fig. 7.10. On the same figures, cool air flowed directly out of the incipient vortex at the 1.5 km level at 0900 UTC; but by 1030 UTC the air was distinctly

warmer. By this hour the dry airstream may have subsided to this level, and not only wrapped around the vortex, but also began to spread anticyclonically further south behind the squall line – exactly what happens at 850 mb in an extratropical cyclone.

After the mature stage of the MCC, the rear inflow deepened and eroded a growing echo–free notch in the precipitation in the center of the cloud shield. The inflow occurred in the layer from 1.5 to 7 km at Oklahoma City (OKC), 50 km west of the leading convective band and some 30 km east of the rear edge of the echo; OKC lay squarely in the path of the intruding "dry tongue".

This storm system served as a prototype for the *rotating* MCC evolving toward an occlusion, a conceptual model of which will be sketched in chapter 9.

7.7 Discussion of this case

This is perhaps the best example yet documented of an occlusion occurring in a mesoscale convective vortex, aspects of which have been documented by Brandes and this author. A convective complex slowly developed from several hailstorms, short squall lines, and meso-β scale storm clusters over a period of 6 to 8 h. The large scale forcing was weak in middle and upper levels; the low level jet was strong and directed into a stationary front on which many of the storm clusters, and the MCC itself, developed.

Our surface analysis revealed that the convectively generated mesoscale cyclone eventually developed down to the surface just before the dissipation of the MCC as such. Before it did so, there was a complex pattern of multiple meso-high pressure centers, induced by evaporation of rain, and meso-low centers. Early in the life cycle the meso-lows were found in the stronger low-level convergence zones where the meso-β storm clusters developed. Later, "wake" meso-lows or troughs were found on the trailing edge of the precipitation shield of the MCC, in accord with Johnson and Hamilton (1988). Just after the mature stage the multiple centers were replaced by one pair. The dominant meso-high propelled a squall line which constituted the southern portion of the leading arc–shaped convective region of the MCC. The dominant meso–low emerged as the wake low migrated southeast toward the advancing edge of the echo–free notch on the rear margin of the precipitation. The pressure continued to drop even as the precipitation diminished in extent and

intensity, and the surface winds began to adjust to the pressure field. Some 2 h after the dominant meso-low center emerged, a closed cyclonic circulation was seen at the surface, lagging behind the rear of the pressure center, but directly under the middle level vortex on the tip of the comma–shaped cloud. It is reasonable to assume that downward vorticity advection became increasingly important at this stage.

As the circulation closed off at the surface, the evaporatively cooled air in the stratiform region southeast of the vortex was accelerated northward by the increasing pressure gradient. This may have propelled the pseudo–cold front into occluding with the existing stationary front. The new boundary separated system–modified cool air from ambient easterly flow north of the old front.

It is noteworthy that surface meso–highs were not observed underneath the strong meso-β scale storms (of diameter 20 to 50 km) that repeatedly developed near Woodward and that led to numerous reports of hail. Hail may have contributed inefficiently to generating surface high pressure because it would have evaporated less rapidly than (usually smaller) rain drops of equivalent mixing ratios. The latent heating in the hail clouds must have been substantial. The hydrostatic pressure fall beneath them may explain the transient meso–lows sometimes observed under the hail cells. The cumulative latent heating released in the hailstorms over several hours, in the area where the apex of the occlusion was forming, may have strengthened the convergence into the warm core, and kept it warm long enough for the winds to adjust toward a gradient–wind balance.

Rawinsonde and dual Doppler data together depict the evolution of the vortex in the northern stratiform region as the MCC matured. The circulation distorted the temperature and θ_e fields, and later the clouds and precipitation, into S–shaped patterns, as in the episode of 3, 4 June but much more so. Cold advection from the north and evaporation beneath the stratiform cloud led to a vortex that was cold core beneath 6 km; it was warm core above 6 km. Its center was tracked on the radial velocity display of the Doppler radars at the very slow rate of 8.3 m s^{-1} , slower than all other wind, pressure, and radar echo features in this and other systems examined.

Brandes calculated that cyclogenesis took place in middle levels primarily by vertical stretching of the convergent inflow, which entered most vigorously from the rear but

also entered from the front (between discrete convective clusters). Lower level vorticity could have been generated by tilting of horizontal vorticity, baroclinically generated by the thermal gradient between the cold core vortex to the left of the wind, and the warmer inflow that was subsiding dry adiabatically to the right, in the notch region. The horizontal vorticity vector would have pointed opposite to the velocity vector. If the mesoscale subsidence increased in the downwind direction, it would have tilted the horizontal vorticity in the correct sense into the vertical. In lower levels the contribution of tilting was estimated to be as large as the role of stretching.

Properties of different regions of the MCC are here interpreted in terms of the conveyor belt model. The warm belt was drawn into the vortex from the southeast, extended from 4.5 km to the tropopause, was saturated with respect to ice, and was ascending. From examination of the cases in other chapters, a large portion probably ascended in meso-β scale updrafts in the east–west oriented rainbands. The dry belt originated in the 4 to 7 km layer, at the levels where θ_e was lowest, mainly from behind the MCC. Cool advection predominated below 4 km; the airstream was observed to be subsiding as its depth increased with time. The third airstream, the easterly "cool conveyor belt" is only hinted at by Brandes. The cool air drawn into the vortex from the north and west would constitute the cool belt, and from the soundings it appears to descend in the core. There was no clear–cut difference between the dry and cold airstreams in the clear air behind the MCC. By analogy with the episode of 3, 4 June, and from the analyses presented here at 1.5 and 3 km, there *was* a definite boundary on the south side of the vortex, that is, between the comma head and the growing notch. The cool airstream beneath the vortex was colder and more moist than the dry inflow, and this led to Brandes' postulate of baroclinic generation of vorticity.

The bow–shaped convective line propagated farther and farther from the enhanced precipitation in the vortex as the system lost MCC status. High clouds remained with the vortex for 12 more hours. Once developed, this cyclone resisted break-up for at least that long.

Chapter 8

SLANTWISE CONVECTION AND CONDITIONAL SYMMETRIC INSTABILITY IN TWO MESOSCALE FRONTAL WAVE BANDS

The possible combination of inertial instability, which generates horizontal forces perpendicular to the wind, and convective instability, which generates vertical forces, has been termed *symmetric instability* and causes overturning on slanted mesoscale surfaces (Bennetts and Hoskins, 1979; Emanuel, 1979). When the air is conditionally unstable to moist convection, but stable to dry overturning, the combination is termed *conditional symmetric instability* (CSI), which Bennetts and Hoskins (1979) proposed as responsible for the circulations that cause many precipitation bands to align with the thermal wind, and to be mesoscale in character.

Certain special conditions must be met if conditional symmetric instability is to be solely responsible for accelerating a parcel while ordinary inertial instability or convective instability are ruled out because they are not present. A saturated parcel is conditionally unstable if its wet bulb potential temperature θ_w or equivalent potential temperature θ_e decreases with height. Instead of evaluating the gradient of θ_e or θ_w in the vertical direction, as is usually done when evaluating convective instability, one evaluates the gradient on a sloping surface of constant geostrophic angular momentum M, on which parcels tend to move in a baroclinic environment. If one ignores the vorticity of the local flow curvature, as Emanuel (1983, 1988) did, then M is defined by $M \equiv v_g + f\chi$, where v_g is the geostrophic wind in the direction of the thermal wind, f is the Coriolis parameter and χ is a distance measured along the temperature gradient. In sloping frontal zones, it is possible to have regions where both the contours of θ_e and of M slope with height, such that M increases with height and θ_e also increases with height, but θ_e slopes *more steeply*,

such that θ_e decreases with height *on the surface of constant* M. Under theses conditions, a parcel is inertially stable, and it is conditionally stable to buoyant forces acting in the vertical direction, but as it travels up or down the M surface the parcel is conditionally *un*stable and will be accelerated. The momentum surfaces should be storm-relative, but as long as the MCC propagates in the same direction as the thermal wind vector, the horizontal and vertical gradients of M will not be affected by the choice of ground-relative or storm-relative winds.

Two practical techniques for assessing the presence of local CSI are the use of cross sections of radiosonde data (Emanuel, 1983) and the measurement of temperature and moisture in an aircraft flying on a surface of constant M (Emanuel, 1988). Here the technique of Emanuel (1983) is applied to supplemental rawinsonde data from system B on 3, 4 June and the occluding MCC of May 7. It is recognized that the definition of M ought to be generalized to include the local curvature of the flow, especially in the more rotational systems like that on 7 May, and that the assessment of the role of CSI is preliminary until this is done. It is also recognized that the technique applies to synoptic-scale CSI because the gradient wind (not the actual wind) is used. The emphasis here is to evaluate the possible presence of CSI in the synoptic environment just before the arrival of the MCCs.

8.1 The possible role of CSI in the pseudo–warm front of system B

Doppler radar analyses described in chapter 5 depicted mesoscale ascent taking place in a band 35 km wide in a zone of enhanced reflectivity that we have called the "pseudo–warm front" or the "stationary front". Since this was a baroclinic zone with a pronounced thermal wind even before the MCC passed through, it is a strong candidate for having mesoscale overturning organized by CSI. Furthermore, there were two parallel bands of heavier precipitation, one in the stratiform area, and the other on the front, with a trough of reflectivity between them (see Fig. 5.7d). To assess this possibility, three cross sections A, B, and C through the front were analyzed as shown in Fig. 8.1. The vertical sections are oriented perpendicular to the mean geostrophic wind in the layer depicted in

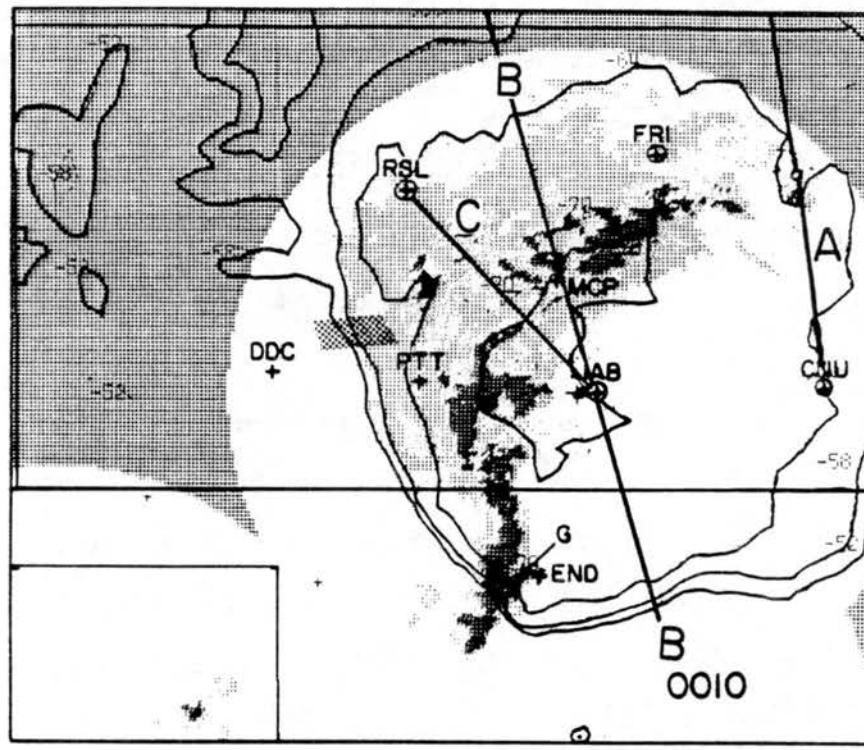

Figure 8.1: Locations of cross sections through system B for assessing conditional symmetric instability. Radar reflectivity (shaded) and 4 contours of cloud top temperature on the satellite image (solid lines) are taken from Fig. 5.7c, for 00:10 UTC 4 June. Cross section A used soundings at CNU, TOP and 3NO (off the map). Section B used HET, OKC, IAB, RSL, FRI, 3NO, and LBF. Section C used only IAB and RSL.

the sections. The mean geostrophic wind is also aligned in the direction that the MCC propagated. Section A cut through the existing stationary front at a point just in front of the precipitation of the MCC. The contours of momentum M (in units of ms^{-1}) and θ_e (deg K) are plotted in this section in Fig. 8.2. As expected, M increased with height in this baroclinic zone, but note the shallow layer where M decreased with height beneath 920 mb; this is the zone of easterly wind. Inspection of the dashed contours of θ_e show a relative minimum near 850 mb in the cool air on the left, and also near 550 mb in the middle troposphere. A relative maximum near 850 mb lay in the warm air overlying cooler air on the right side. The frontal zone from the surface to 800 mb above TOP exhibited a stronger vertical gradient of M (due to wind shear) and a horizontal gradient of θ_e. In the lightly shaded region, values of θ_e decreased upward along M surfaces; two layers

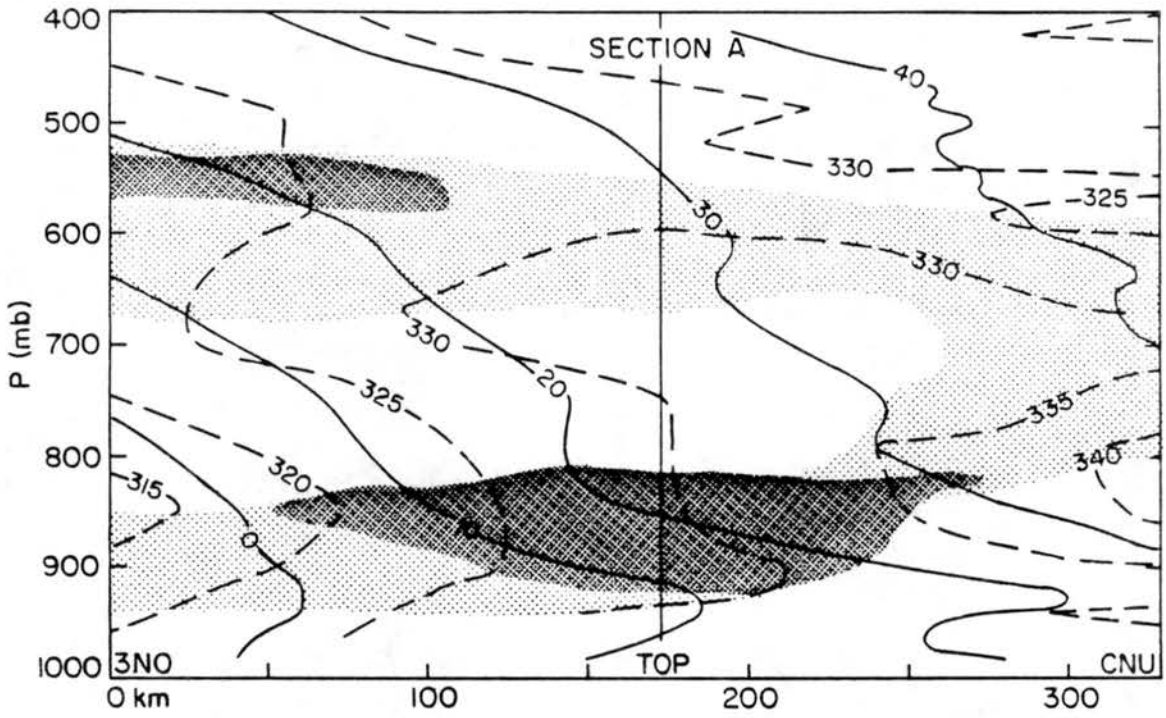

Figure 8.2: Cross section A from Omaha (3NO, at left) to Chanute (CNU, at right) of momentum M (solid, ms^{-1}) and θ_e (dashed, deg K). Regions of convective instability along M surfaces are lightly shaded. Regions where the above is true *and* are stable to vertical displacements are shaded dark. CSI may be responsible for mesoscale instability in the latter region.

(from 940 to 820 mb, and 650 to 550 mb) met this test over a broad region. Normally this would suggest CSI in the lightly shaded region, but to rule out ordinary convective instability as a factor, we applied the additional criteria that $\partial\theta_e/\partial z$ be positive in the vertical direction. The zone where both criteria were met is shaded dark. It included the layer from 920 to 820 mb in a zone about 180 km wide centered on Topeka (TOP).

This is precisely where the stratiform rainfall fell within an hour after this time, and is the layer where the warm conveyor belt began its ascent in the steeply sloped part of the front. The fact that $\partial\theta_e/\partial z$ was positive in the vertical sense but negative along the sloping M surface, meant that the air would have been negatively buoyant in convective updrafts and would have required external forcing to reach its level of free convection; however, it would have been positively "buoyant" if it glided up the M surface.

The evidence is good that conditional symmetric instability might have helped the ascent of the warm air before it reached a level of free convection.

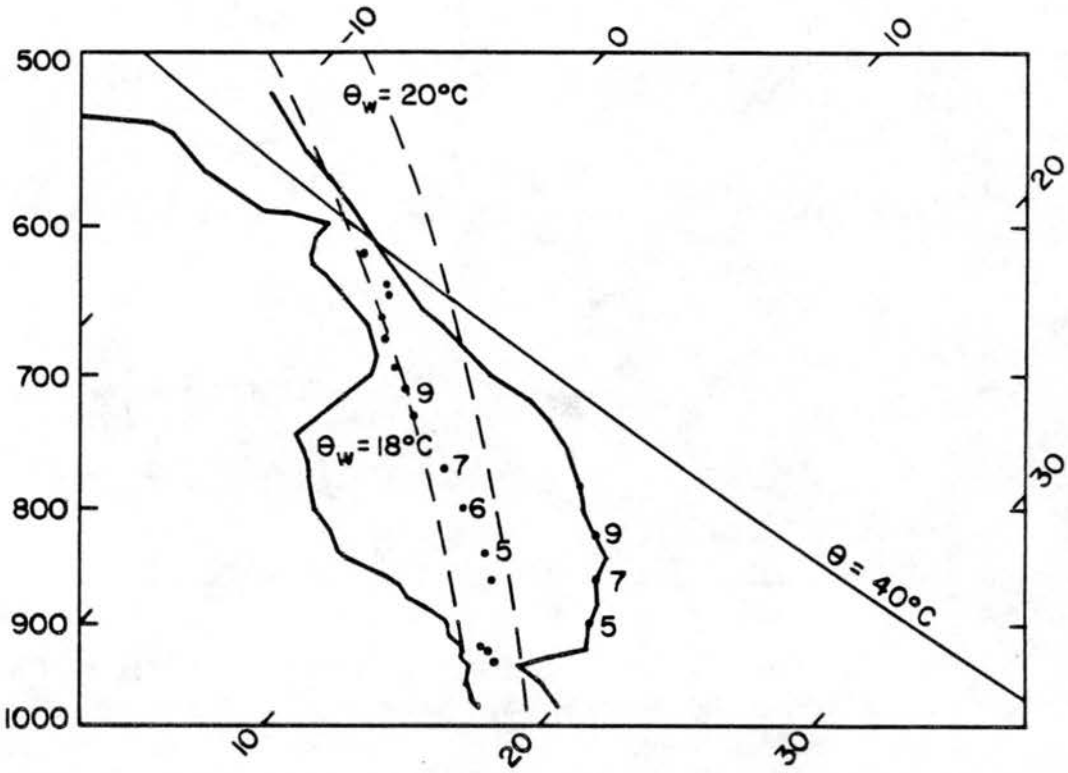

Figure 8.3: Thermodynamic sounding along the M=20 surface of the previous figure, on a skew T–log P diagram. Dashed lines are two contours of constant θ_w = 18° C and 20° C. The numbered dots between them are the saturation points of parcels originating at the numbered dots on the temperature profile curve.

An alternative graphical method for assessing CSI is to plot a conventional sounding of temperature and moisture along a constant M surface. This was done in Fig. 8.3 for the M=20 surface of the cross section in Fig. 8.2. Possible CSI is indicated in layers where the wet–bulb potential temperature θ_w decreases with height. The saturation points are indicated by dots between the two dashed lines of constant θ_w. The θ_w parameter did decrease with height from point 5 to point 9, for the layer between 900 and 820 mb, although the decrease was a modest 1.4 degrees K. Note that the layer of possible CSI was in unsaturated air just above the frontal temperature inversion.

Another section "B" in Fig. 8.1 cut through the precipitating pseudo–warm front and a large area of stratiform rain. The zone that met the two criteria for CSI extended from

Wichita (IAB) north to the northern edge of the stratiform rain, and from 910 to 850 mb. Surprisingly, *no layers above 850 mb* met the tests for CSI.

Finally, a section from IAB to RSL that cut through the apex region was evaluated. This region was not yet convectively active but became so within one half hour. The tests for CSI were met in the 930 to 860 mb layer along the whole length of the section. However, instead of θ_e decreasing with height, the values of θ_e were essentially constant on the M surfaces. This may signify that the layer was neutral to slantwise convective adjustment, that it was already in the process of slantwise overturning along this section.

Thus, in three regions of the baroclinic zone on which his MCC evolved and propagated, conditional symmetric instability may have been acting to initiate the slanting overturning motions on the meso–β–scale, in a layer about 100 mb deep on top of the pre–existing frontal inversion. Above 820 mb, further overturning would have had to be maintained by external forcing or some other instability which was not CSI. Convective instability, of course, is probably responsible, but only in the regions of higher reflectivity, which did not constitute the full length of the pseudo–warm frontal zone. It is significant that CSI could be responsible for initiating the vertical circulation in at least part of the steeply sloping warm conveyor belt. If it was, then the vertical circulation in this system may have changed from a largely convective character to a more mesoscale, stratiform character at an earlier stage.

8.2 The assessment of CSI in the strongly rotating system on May 7

A cross section through the stationary front from Pratt (PTT) through Enid (END) to Oklahoma City (OKC) in advance of the MCC at 0600 UTC 7 May, when it was in its growth stage, was analyzed. Refer to Fig. 7.4 for the precipitation echo mapped at that time, and to Fig. 7.5 for the locations of the stations. The intention was to check for the presence of CSI in the environment through which the MCC propagated, and just before it moved through. This analysis was at a time two hours before the mature stage and four hours before the system acquired a comma-shaped radar echo and exhibited a closed mid-level circulation.

There were two notable differences between the environments of June 3,4 and May 7. In the latter case, the horizontal gradients of θ_e were weaker while the vertical gradients were stronger than on June 3,4. The convective instability was greater on May 7, especially in the layer from 900 to 800 mb, but there was little slope to the θ_e contours. Also the wind and momentum profiles were quite different in the 820 to 620 mb layer: there was very little vertical shear in the component of wind perpendicular to the cross section, so that the isolines of momentum M were vertically oriented or even sloped "backwards" from north to south with height.

Consequently there were no regions where the θ_e contours sloped more steeply than the M contours. In the zones where the atmosphere was convectively *stable*, there were no zones of conditional symmetric instability. The mesoscale convection that began to occur shortly after this analysis time can safely be attributed to release of ordinary convective instability in two layers: the first from 900 to 850 mb (from 900 to 800 mb in the south of the domain), and the second from 750 to 620 mb. Convective instability was notably stronger in the south, that is, in central and southern Oklahoma where the squall line was most intense and a strong, long–lived surface meso–high developed.

Chapter 9

PROTOTYPES OF WEAKLY AND STRONGLY ROTATING MCCS

9.1 Plan views of idealized MCCs before and after rotation develops

The results from the previous cases can be summarized by depicting the relative flow in two contrasting, idealized MCCs at several levels, and then in three dimensions. One prototype will be an MCC with a well developed frontal wave pattern but weak evidence of meso–α–scale rotation. The rotation may develop at a later stage, or it may *never* develop, so we will call this prototype "weakly rotating". The analyses of systems A, B, and C on 3, 4 June 1985, have been combined in this prototype. The figures depict a convective and stratiform pattern that looks very much like system B, but they do not depict B specifically but rather a "generic" pre–cyclonic MCC with a wave–cyclone pattern of convection. The prototype will be contrasted with a generic MCC closer to rotational adjustment and with still–active convective and stratiform regions. This "strongly rotating" prototype combines the analyses of the May 7, 1985 MCC with descriptions in the literature on mesoscale convective vortices.

Conditions at the surface can be summarized by reviewing once again the previous analyses of system B on 3, 4 June as an example of a weakly rotational MCC, of system C as an example of a system with more rotation, and of the May 7 case as an example of a strongly rotating *and* occluding MCC. In the first 2 cases (refer back to Fig. 5.9 and Fig. 6.6), the MCCs develop entirely *north* of the surface front and propagate along the stationary frontal zone aloft, which may be associated with a wind confluence axis at the surface. The meso–high pressure dome propagates with the apex region or even north of it, and well within the zone of stratiform rainfall. Meso–lows are either not present in the apex region or they are very weak. No closed vortex develops at the surface.

In contrast, a substantial portion of the rotational MCC (Fig. 7.7) develops *south* of the surface front and can tap a deeper layer of unstable air. In addition to a cold pool generated by the convection in the apex region, a stronger cold pool and meso–high develop far south of the first one, in association with vigorous convection on the pseudo–cold front. The apex region is a junction of that front with the pre–existing front, and does harbor a pre–MCC low. That low center displaces the meso–high center, combines with the wake low during the process of occlusion, and eventually the occluded low may spin up cyclonic circulation at the surface.

The layer from 1 to 2 km above the surface lies above the cold pool from previous rainshower activity (if there was any) and accounts for much of the source volume of the warm conveyor belt. In Fig. 9.1, warm belt air with θ_e values from 340 to 350 K is accelerated through the convective regions in both panels **a** and **b**; acceleration is depicted by streamlines that thicken along their length. In both **a** and **b**, the warm air converges head–on with rain–cooled air along the pseudo–cold front (heavy line) but the convergence is oblique along the stationary front (dashed line). The warm air rises vertically in numerous convective cells along the cold front and in a few cells along the stationary front, but in the latter case it also passes between cells to glide up through the sloping frontal zone.

In the northern half of the stratiform region, much cooler air (with θ_e values from 320 to 330 K) enters the precipitation zone from the northeast in both panels. This air descends at first in gradual mesoscale unsaturated downdrafts. In the strongly rotating case (panel **b**), a part curls around the center of the vortex, in the region of the "comma head". In the weakly rotational case (panel **a**), the streamlines manifest a gentle wave motion in easterly flow, first cyclonic then anticyclonic as the cool air descends from mid–levels and diverges below 850 mb.

A major difference between the two cases is that the dry airstream descends to this level in case **b** but not case **a**. This air (with $\theta_e \sim 325$ K) descends in a very diffluent manner into the notch and behind the convective line. Part of it curves cyclonically and

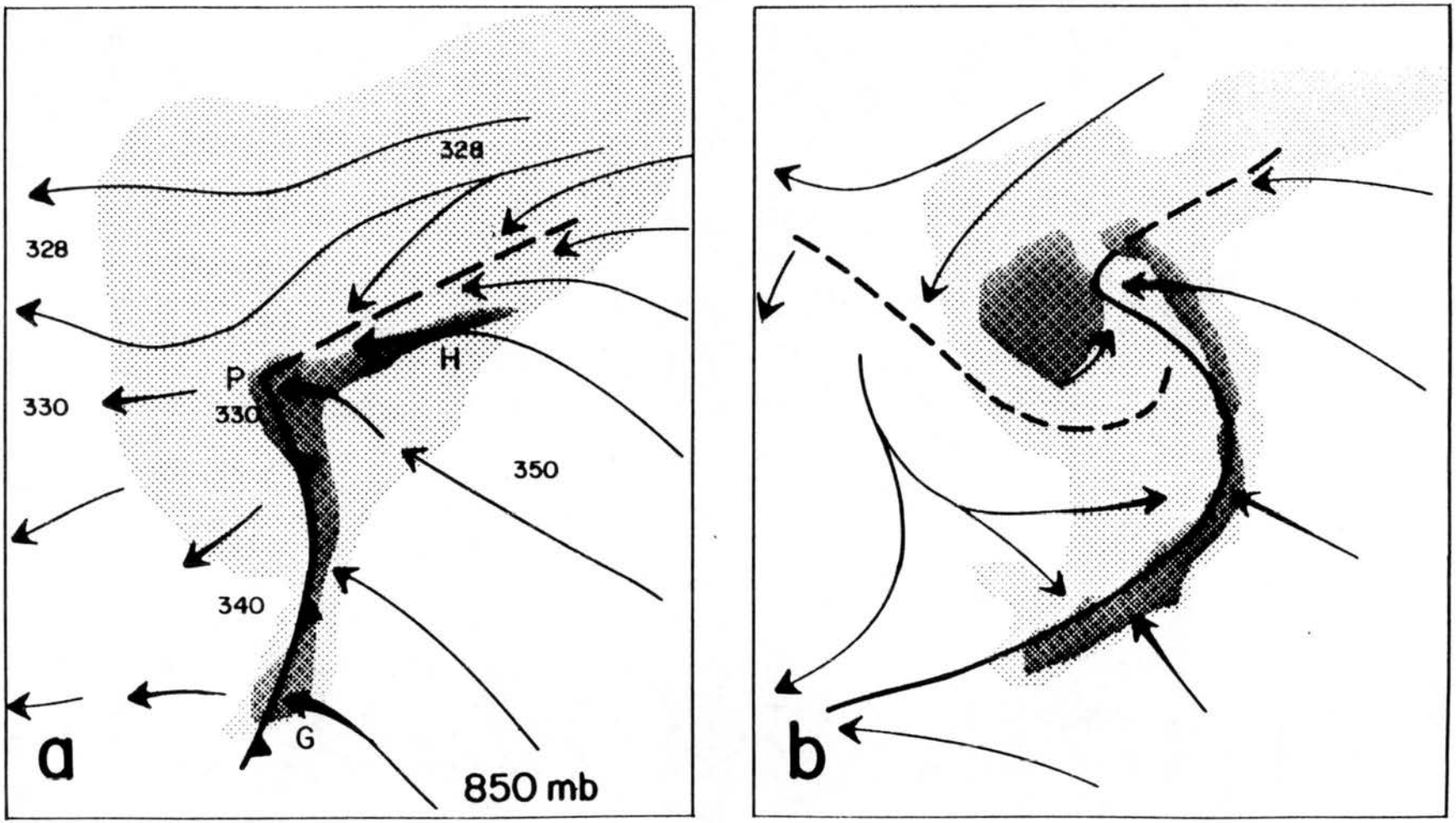

Figure 9.1: Idealized relative flow in the 1 to 2 km layer (nominally 850 mb) in (a) the prototype of the pre–rotational MCC with a wave–cyclone convective pattern, and (b) the rotational MCC developing an occlusion. Dark shading indicates convective precipitation and light shading, stratiform precipitation. Numbers indicate typical values of equivalent potential temperature θ_e.

eventually erodes a rain–free notch between the vortex and the cold front. In case **a**, rain–cooled saturated outflow from downdrafts is accelerated towards the rear at this level just as it is at the surface.

We postpone discussion of the flow at 700 mb because it resembles the flow at 500 mb and can be discussed with it. At 500 mb (Fig. 9.2) or 5 to 6 km AGL, an S–shaped convergent frontal zone (heavy dashed line) passes through the MCCs. This front is deformed into this shape by the strongly converging flow about the apex region, which sits on the inflection point of the S. Front–to–rear flow is accelerated through the convective regions (especially at the apex) where it ascends rapidly. The flow is accelerated by the addition of mass from lower levels, and by the pressure gradient into a convectively induced, warm core low. Initially the low pressure is a probable hydrostatic response to warming in convective updrafts (Lemone et al., 1984) but as the upward motion increasingly takes place in meso–β–scale clusters especially in the apex region and in the sloping east–west band, the low expands in scale. Ultimately it becomes a meso–α–scale response to vertical motion in and beneath the precipitating stratiform cloud. Air converges into the low pressure from all sides. It is accelerated through the convective region (between towers or entrained in updrafts or both) and continues to rise all the way to the rear of the stratiform region.

There it encounters a frontal–like boundary, that parallels the rear margin of the precipitation at this level. The dry airstream enters from the west and south and descends beneath 500 mb at the boundary. The presence of a boundary between the opposing airstreams might explain the turbulence that has been reported by aircraft scientists when the P–3 aircraft flew beneath the edges of cloud shields (Margaret LeMone, personal communication). The dry inflow is strongest into the northern half of the cloud shield in case **a**, because most of the stratiform precipitation is found there. Further south, the dry "rear" inflow is *southerly*, flows parallel to the convective line and behind it, and does not curve cyclonically. The flow into the strongly rotating MCC (case **b**) is quite different: the fastest part of the dry stream curves from the *west* into the southern half of the system, where it enhances the spin–up of the cyclone in cooperation with the warm and the cool

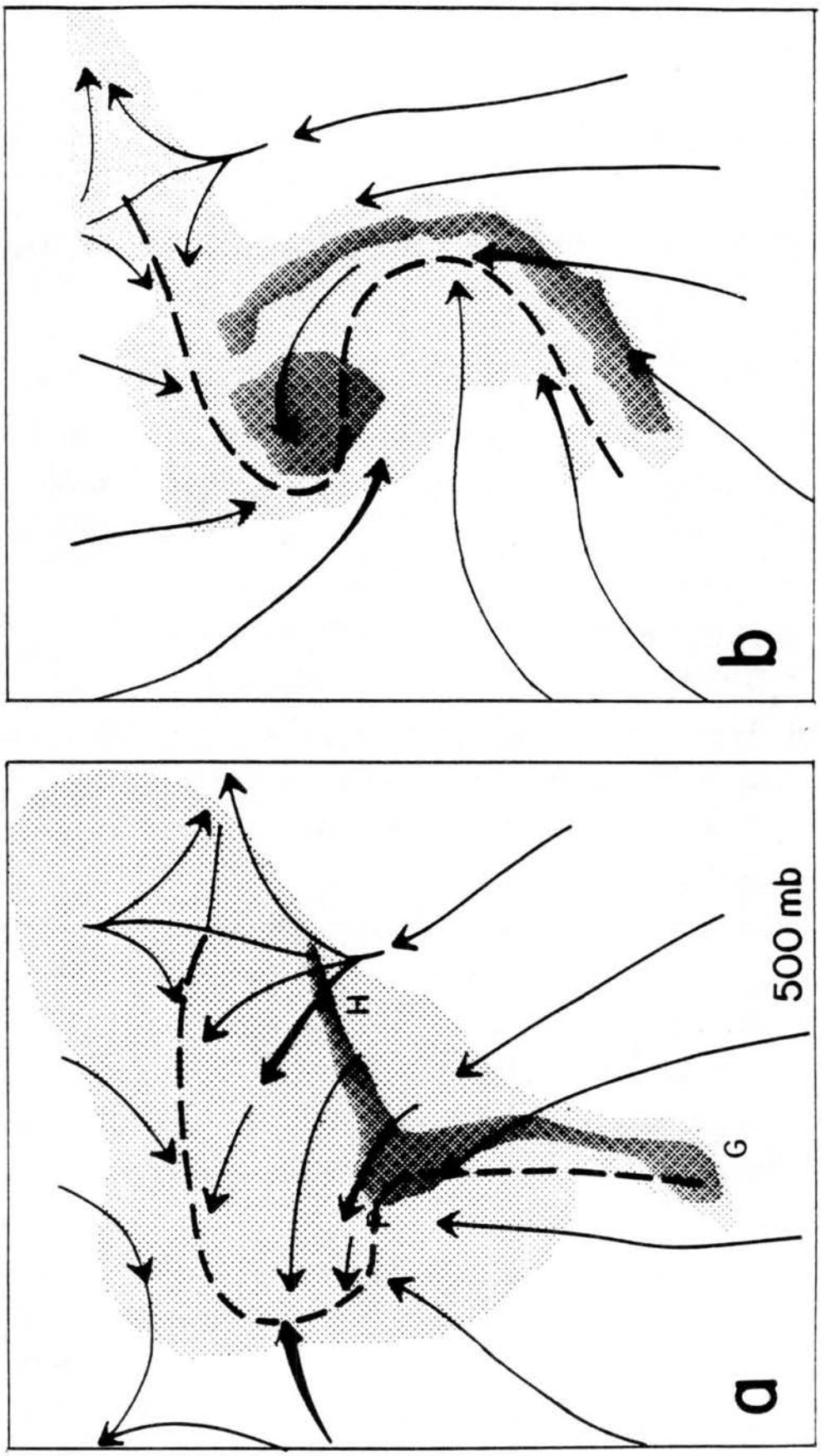

Figure 9.2: As in Fig. 9.1 for the 5 to 6 km layer, nominally 500 mb.

conveyor belts. It should be added that the vorticity center lies closer to the center of the stratiform precipitation in case **b** than in case **a**.

In both **a** and **b** an elevated "cool conveyor belt" flows some distance into the stratiform cloud from the north. As it approaches the warm conveyor belt, this airstream descends in mesoscale downdrafts to yield the upper portion of the "double onion" profiles of temperature and moisture.

The pattern at 700 mb, or 3 to 4 km (not shown), is quite similar to Fig. 9.2, with one major difference: the area of ascending motion and front–to–rear flow seems to be confined to the active convective regions. This area is much smaller at 700 mb that at 500 mb. Consequently, the northerly cool conveyor belt penetrates to the center of the MCC: in the weakly rotating system (case **a**), it flows as far as the confluent convective band on the stationary front, and as far as a westward extension of the same from the apex region to the rear of the system. In the strongly rotating system (case **b**), it penetrates to the center of the vortex, which is cold core at this level.

At the level of outflow from the system's updrafts, nominally 200 mb, a highly divergent and weakly anticyclonic pattern characterizes both cases (Fig. 9.3). Divergence is intense from the apex region, where the mesoscale updrafts are strongest, and from the stronger convective clusters on the pseudo–cold front. A heavy black line marks an upper–level front along the western and northern margins of the cloud shield, where ambient flow (15 to 30 ms^{-1} relative velocities from the rear) converges with ice–saturated, cloudy outflow from the system's updrafts. Thus, the MCC induces an anticyclonic jet streak to form along its northern margin.

Downstream of the southern convective line, the "obstacle" creates a stagnation zone where the winds have the same momentum as the middle levels. A stratiform cloud may be advected forward of the line in some cases, while in others it is blown almost parallel to the line, towards the center of the MCC. The enhanced vertical motion in the east–west pseudo–stationary front also creates a source of mass at high levels. Flow diverges northeast, east, and perhaps southeast, so that this band of enhanced rainfall is embedded within an expanding stratiform cloud. There may be a *secondary* band of enhanced vertical motion north of, and parallel to, the primary band.

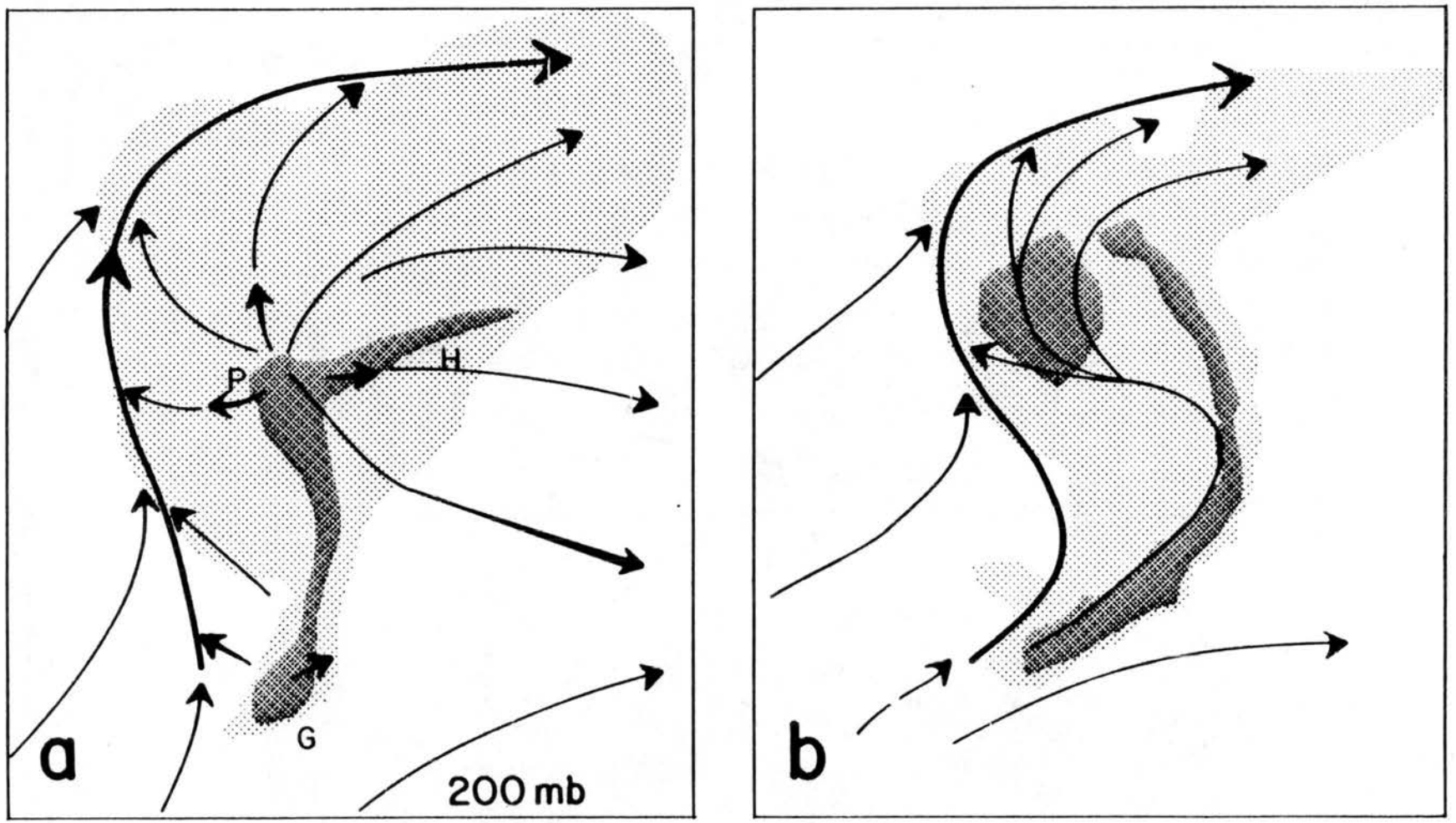

Figure 9.3: As in Fig. 9.1 for the 11 to 13 km layer, nominally 200 mb.

9.2 Cross sectional perspectives of the conveyor belts

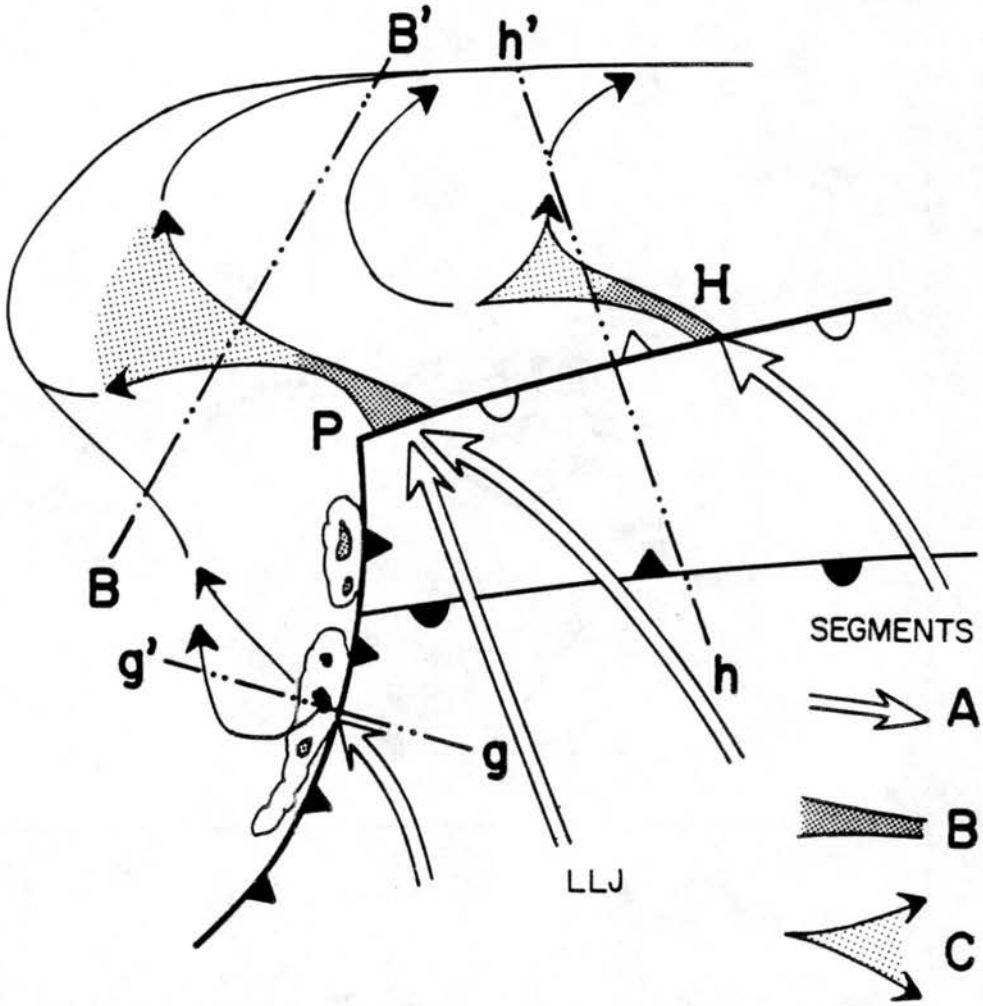

Figure 9.4: Plan view of the warm conveyor belts in the weakly rotational prototype MCC. The apex region is at P; a strong convective cell at G; a sloping upglide region in a frontal zone at H; low–level jet at LLJ; cross sections along g–g′, h–h′, and B–B′ are shown in subsequent figures. Three successive segments A, B, C of the warm conveyor belt are explained in the text.

To better convey the three–dimensional flow in the weakly rotating MCC, some vertical sections through key regions of it are presented. It will be helpful to refer to a three–dimensional perspective from the rear of the idealized weakly rotating MCC in Fig. 9.5. Before discussing it, a plan view (from above) of the warm conveyor belt is presented in Fig. 9.4. The low–level jet, the source of warm air, converges into both the pseudo cold front and the (elevated) stationary front in segment A; but before it reaches the latter, it must ride over a very shallow layer of stable air on the surface. Heavy black segments

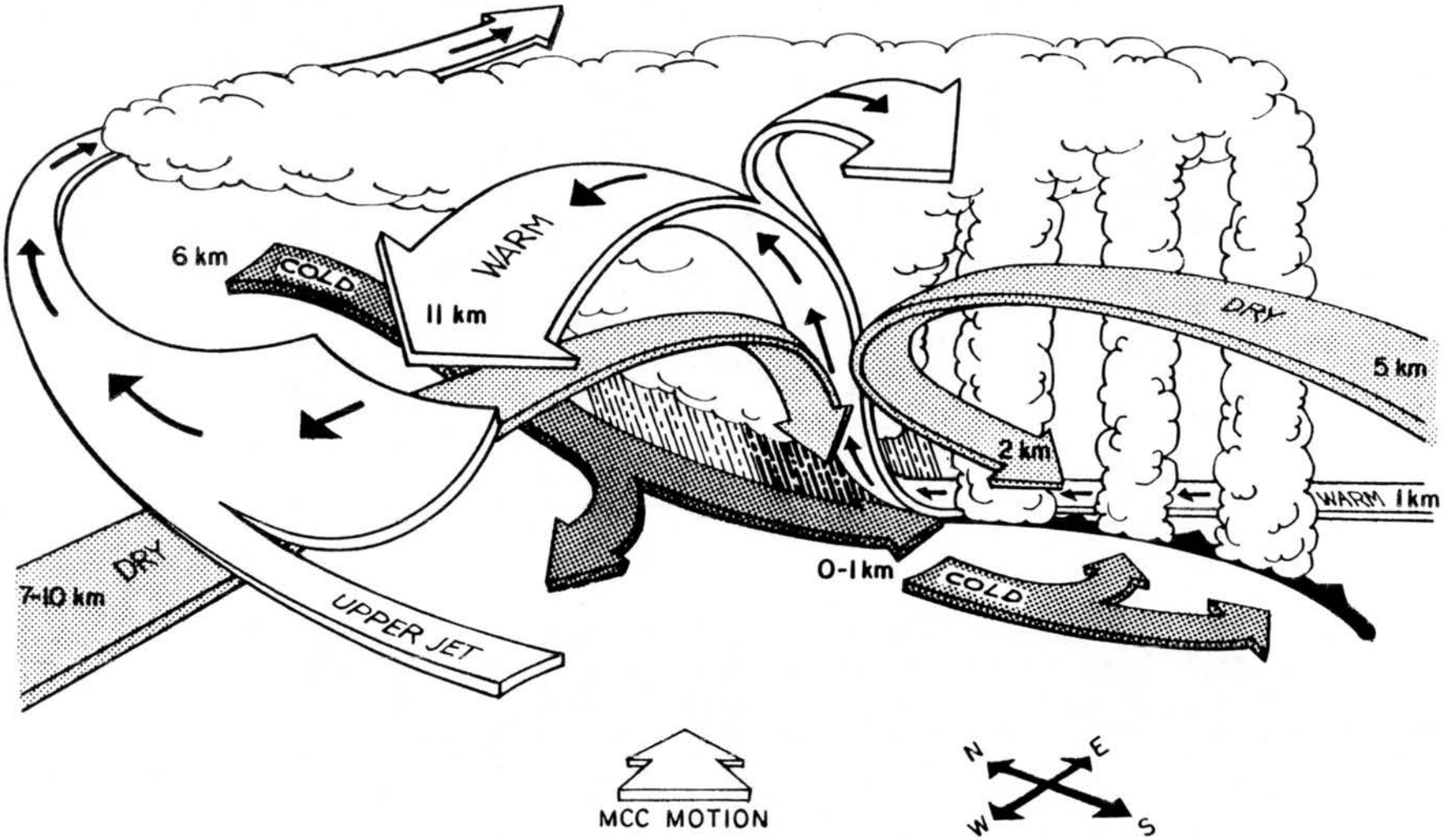

Figure 9.5: Perspective drawing of an idealized, weakly rotating mesoscale convective complex as viewed from the rear. The apex region is located where the heavier rain is drawn. The cumulonimbus towers at right form on the mesoscale cold front. The mesoscale warm front and the forward part of the stratiform region are not shown in this view.

depicts the next segment B, in which the warm air rises steeply in convective updrafts, which may be vertical (at G) or sloping (at H) or both (at P). Then segment C bounded by diverging streamlines depicts the mesoscale upglide motion from about 4 to 12 km in height. As the rate of ascent decreases, the saturated air spreads out to generate the massive precipitating stratiform cloud. The Doppler analyses indicate a jet, some 30 km wide, proceeds from the apex region to the rear of the cloud. This is, in fact, where the stationary front and its confluence zone had been a few tens of minutes earlier, before the center of the MCC passed through. The convergent motion from both north and south continues after the apex region passes onward. On its left, the warm "jet" is separated from the dry airstream flowing in the opposite direction, by the S–shaped frontal boundary or shear zone. On its right, the warm "jet" is "squeezed" by the cool conveyor belt which descends beneath it. The warm conveyor belt continues to rise, albeit with less vigor, in the upper half of the stratiform cloud, then diverges strongly in all directions and eventually joins the "outflow jet" that delimits the western and northern extent of the cloud shield, near the tropopause.

The vertical path through convective cell G on the pseudo–cold front is depicted in Fig. 9.6 and is exactly like the flow in a multicellular cluster. Convective downdrafts generate a cold–air dome and associated meso–high which impel the pseudo–cold front eastward; this lifts the moist low–level jet through a capping layer of negative buoyancy and into the convective towers. The cold dome also accelerates cool air far southward, which stabilizes a broad region for the next 6 to 10 hours. This flow is out of the page, depicted by $\odot$; the low–level jet and all the flow in the mid–troposphere flows into the page, depicted by $\otimes$. The positive feedback between the advancing cold dome and the new convection is believed to maintain the main convective band along the pseudo cold front; it maintains the band perpendicular to the existing stationary front, and thus is responsible for the wave–cyclone pattern that endures for a few hours.

A section along the line h–h′ in Fig. 9.4 cuts through the stationary front and depicts the relative interaction of the warm and cool conveyor belts (Fig. 9.7). The low–level jet first passes over the shallow, cool easterly–wind layer on the surface, between the surface

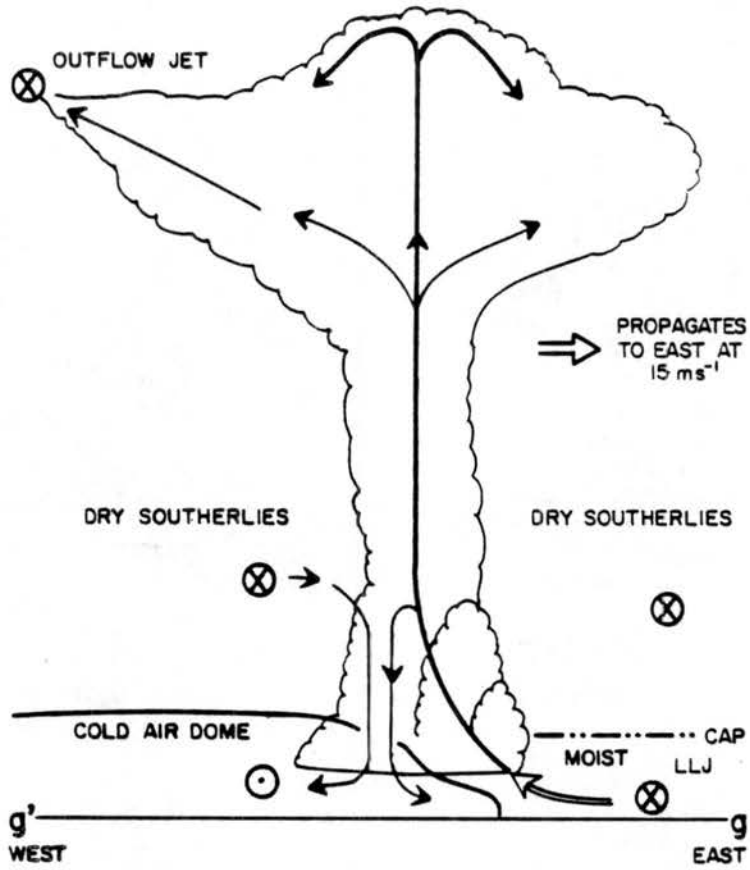

Figure 9.6: Cross section along g–g′ on Fig. 9.4 through the multicellular convective line on the pseudo–cold front.

front and the front aloft. The uplift here is so small that no clouds are formed. Then the jet ascends steeply through the frontal zone aloft from 1 to about 5 km. From about 5 to 12 km above ground the warm conveyor belt spreads north and curves increasingly to the west (cyclonically). The outflow from the mesoscale upglide is exhausted anticyclonically into the jet streak on the north margin of the cloud shield.

In and beneath the base of this cloud shield, the cool conveyor belt is accelerated from the northeast into the low pressure region in the base of the stratiform cloud. It descends in mesoscale unsaturated downdrafts, but the air at the surface is saturated and potentially much cooler, probably due to convective downdrafts. The cool conveyor belt may mix with convective downdrafts in the heavier rain behind the steeply sloping part of the warm conveyor belt (see Fig. 9.5).

Finally, we depict the region west of the apex where the warm conveyor belt has lifted itself well above the surface, along the cross section B–B′ in Fig. 9.8. This structure can

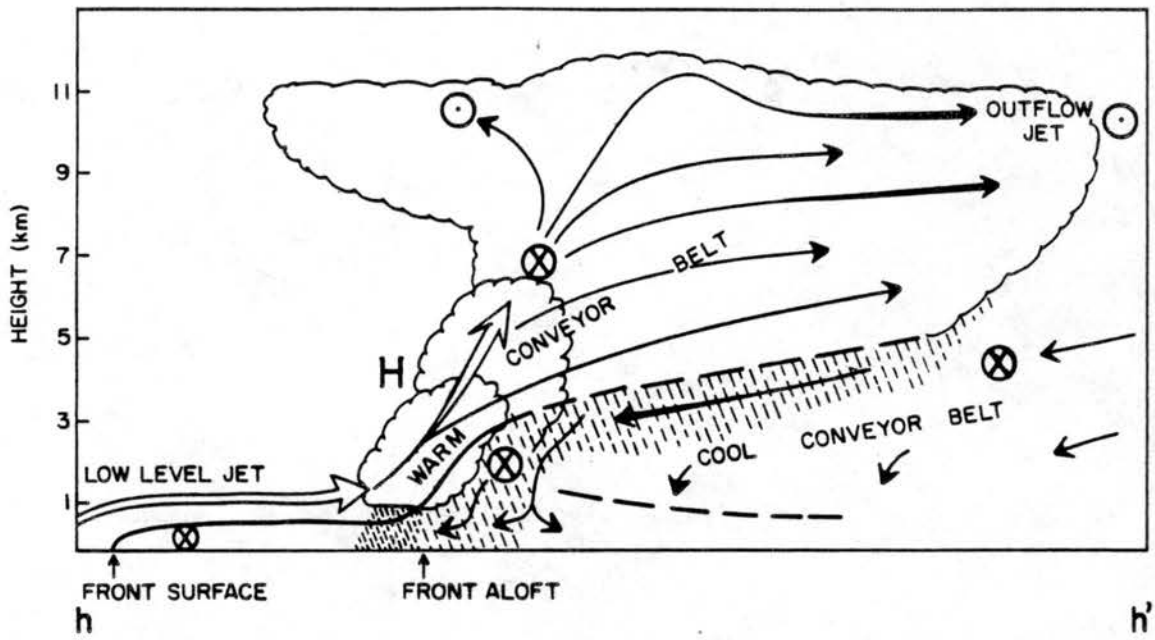

Figure 9.7: Vertical section along h–h′ in Fig. 9.4 through the stationary frontal band, showing the warm conveyor belt gliding over the cool conveyor belt. Flow into the page is depicted by ⊗, flow out of the page by ⊙.

be thought of as an incipient occluded front because the dry airstream "squeezes" the warm jet which is lifting with time. As in the other cross sections, the warm belt rises steeply to about 5 km then increasingly spreads out, but here the flow is concentrated in a jet (⊗) from front–to–rear (into the page), where the stationary front had been earlier. A band of enhanced reflectivity is associated with the enhanced upward motion above this convergent zone. This is a low pressure region because of the warm anomaly above it, so the dry airstream and the cool conveyor belt converge toward the region from the southwest (the left) and the northeast (the right), respectively. In the prototype of the MCC that never develops strong rotation, the dry inflow is primarily from the south, and abruptly descends soon after it encounters the heavier precipitation in the confluent shear zone. A part of this descending airstream may be turned around and flow southwest in the 2–3 km layer, the driest layer in the onion profile typically observed there (lightly shaded belt on the right side of Fig. 9.5).

The cool conveyor belt descends here, too, in unsaturated fashion, except that the portion diving beneath the front–to–rear, warm conveyor jet becomes saturated, descends more vigorously, and builds a meso–high cold dome there.

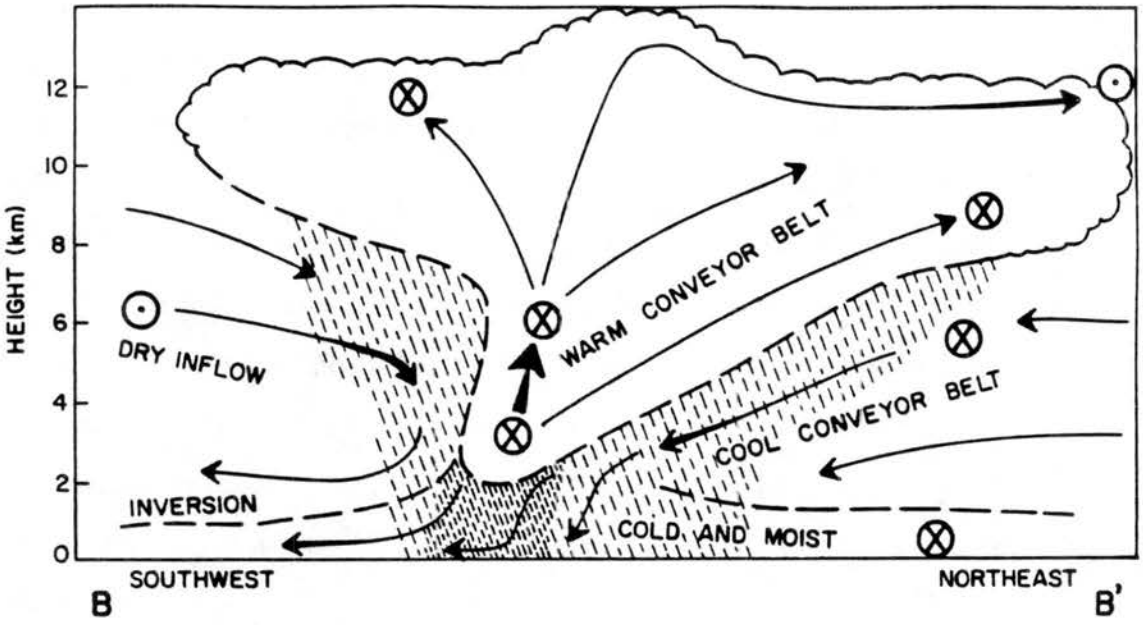

Figure 9.8: Cross section along B–B′ on Fig. 9.4, from southwest to northwest, through the front–to–rear ascending warm conveyor belt, and showing the convergence of the dry inflow (from left) and the cool conveyor belt (from right). Light and dark shading indicates light and heavy stratiform precipitation. The ⊗ marks flow into the page (towards northwest); ⊙ marks flow out of the page (towards southeast).

In the strongly rotating MCC, the dry inflow is more westerly than southerly, and converges more into the convective core region and southern region, above which there is a greater volume of stratiform cloud. For these reasons the generation of vorticity through vertical stretching may be more successful than in the frontal wave case.

The interplay of the various conveyor belts can perhaps be visualized with the help of the perspective drawing in Fig. 9.5. This view is from the the rear of a system propagating northeast, away from the observer.

9.3 Relationship of vortical patterns of convection to development of a vortex

The convective organization of the two dozen or so MCS observed in PRE–STORM ran the gamut from completely chaotic (June 17) to highly linear (June 11 and others). The three MCCs in the episode of June 3 and 4 exhibited a wave–cyclone pattern, with system B exhibiting it very clearly for 2 1/2 hours, and system C manifesting a weak pattern for one hour, then a spiral pattern for another hour. The May 7 system developed at first a comma–shaped cloud and precipitation shield, and later an occluded frontal

pattern. Other systems, such as on May 21, manifested one or another of the above patterns usually associated with rotation.

The evidence presented in the thesis suggests that the rainfall patterns that resemble a wave–cyclone are established in the first half of the life cycle of an MCC, specifically about midway between the initiation and the mature stages [the "growth" stage of Cotton et al. (1989)]. The rotation itself develops in the second half of the life cycle, soon *after* the mature stage, at least on the meso–β–scale and sometimes on the meso–α–scale. Cyclonic vorticity is observed first in the middle troposphere on the surface of shear that separates the warm conveyor belt from the dry inflow. It is manifested first on the meso–β–scale, possibly one or two hours before maturity. But the vorticity appears on the meso–α–scale of the stratiform rainfall or the cloud shield an hour or a few hours after that early manifestation, as the wave–like patterns of convection may actually be disappearing.

Thus, the meso–α–scale cyclonic circulation cannot be causing the wave–cyclone convective patterns because the circulation develops later. It is also unlikely that the convective band configuration is causing the vortex to develop, except that the intersection of two convective bands in a frontal wave pattern does enhance the convective activity and associated meso–β–scale convergence at the junction. Given enough time, this will enhance larger scale convergence and eventual cyclonic adjustment, so in this sense, the frontal wave pattern may be said to aid cyclogenesis.

What, then, causes the frontal wave organization? The convective complex tends to propagate along a pre–existing frontal zone where weak convergence from both sides is already established. The additional mesoscale convergence of the MCC generates rainbands along the existing front. The other convective band, orthogonal to the first, could be traced back to convective clusters that developed in the warm air near high terrain before the initiation of the MCC. Whatever the trigger of that cluster was (possibly a transient mid–level wave trough, orographic influences, or removal of a capping inversion in the diurnal cycle), once started, the low–level cold pool expanded to meso–α–scale size as it merged with the outflows of smaller clusters. A common outflow boundary developed on the east (downshear) side, extended southward, and advanced into the warm air. With

time a good fraction of the potentially buoyant inflow into the MCC was lifted along this north–south boundary, which acquired the characteristics of a squall line or mesoscale cold front. Greatest lifting and convective activity became focused on the intersection region of the old and the new fronts.

Although important in the early stages, the pseudo–cold front is not an enduring component of the MCC. In two cases (systems A and B) the front lagged behind the cloud shield and became a broken line; in one case (system C) it never was intense and soon vanished; in another (May 7) it propagated much faster than the bona fide vortex and dissipated. Once a core region of enhanced convective activity is established, as it was in the apex region in the first half of the life cycle, the core tends to endure for the life of the MCC, perhaps due to increasing inertial stability as the flow approaches a gradient wind balance.

9.4 Causes and effects of a chaotic development of convection

A common feature of nearly all the MCCs studied here was the development of convective storms in chaotic patterns in the early stages of the life cycle. One MCC (on June 17) never evolved any other pattern *but* chaotic, though Verlinde and Cotton (1988) documented several meso–β–scale pairs of vortices in the stratiform cloud. Why would discrete cumulonimbus clusters erupt in a scattered fashion almost simultaneously over an area some 300 km in diameter? On scrutinizing the evolution of the thermodynamic profiles between systems A and B, and between B and C, on 3 and 4 June 1985, the following hypothesis is offered.

The earlier MCC stabilized the lower troposphere to such an extent that its temperature profile exhibited an extreme example of the onion–shaped sounding. A saturated, foggy, cool (15° C) layer from 300 to 500 m deep was capped by an inversion some 15 degrees Kelvin strong. Not only was the air above the inversion potentially very warm (θ $\sim$ 36° C) but the relative humidity was as low as 25 percent. After a period of suppressed wind in the lower layers, the ambient wind profile returned some three hours after the MCC departed. The low level jet then steadily moistened the layer just above the inversion during the next three hours. The return of the moisture from the south could also be

tracked on horizontal analyses. At the same time, the ambient winds cooled the middle layer from 600 to 350 mb, which had been warmed by the previous MCC. At 5 to 6 hours after the departure of the MCC, the layer above the still–strong inversion quickly attained conditional instability over a wide area as the mixing ratio reached a critical value. The conditionally unstable layer continued to deepen as more moisture was advected in, and it was at this time that myriad convective cells began to develop. The fact that the unstable layer was decoupled from the surface is thought to be important in preventing the focusing of convective activity on any outflow boundary or terrain feature. The early storms in each MCC thus developed completely free of any influences from the surface and might be initiated by minor inhomogeneities in the wind or moisture fields in the elevated layer of instability. Thus the spatial pattern of the first storm cells would appear chaotic on the mesoscale.

In the episode of 3, 4 June, surface analysis did reveal weak but definite low pressure centers where the early convective clusters developed in chaotic patterns in advance of the MCCs. This suggests that low level convergence was enhanced in a mesoscale region even as the divergence field remained more noisy on smaller scales.

How would a chaotic distribution of convective cells affect an MCC that grows from the merger of their anvil clouds? By not allowing a focused meso–β–scale core of clusters, or a squall line to develop, it is felt that they projected latent heating on the meso–α–scale at an early stage, and maintained the heating long enough for the winds to partially adjust to the α–scale warm anomaly. The duration of predominantly chaotic organization was approximately 4 hours each in systems A, B, and C on 3 and 4 June, long enough for a healthy start of the adjustment process. Ultimately the chaotic pattern was replaced by the frontal wave cyclone pattern that emerged in the core region; but it may never have been completely replaced, as the forward sectors of the MCCs could have had a chaotic pattern of storms which would not have been observed because the MCC was exiting the radar station network. The evolution of the MCC on June 17 bears this out.

It was mentioned in chapter 7 that the repeated occurrence of discrete hail storms in the Woodward area, prior to the consolidation of the MCC on May 7, may have helped

to establish a partially adjusted mesoscale cyclone. The latent heating in the hail storms must have been significant over the 4 to 5 hour episode of hail, and may have persisted long enough for the observed degree of geostrophic adjustment. Additionally, it was noted that the hail storms did not generate surface meso–highs, which otherwise would focus the convective activity on expanding outflow boundaries. Perhaps the significant effect of a relative lack of cooling beneath the hailstorms is that mesoscale convergence could be maintained over a broad area without disruption by diverging cold pools.

9.5 Location of stratiform precipitation relative to convective activity

The different evolution of the two MCCs that served as prototypes may be attributed perhaps to the direction into which the precipitating stratiform clouds were blown. Prevailing winds at the 11 km level in the genesis region of our episode on 3, 4 June were typically 30 to 40 ms^{-1} from the southwest, about 50 percent greater than the prevailing winds in the same genesis region on 7 May. The difference in direction may be more significant than the speed difference, as the westerly wind in the deep layer from 7 to 12 km on 7 May swept the stratiform ice cloud directly east over the warm (inflow) air, and ensured that a large fraction of that cloud lay south of the stationary front and the most active convective region which propagated along the front. In contrast, not only were the upper cloud layer winds 50 percent stronger on 3 and 4 June, but the southwest winds carried most of the ice north of the apex region and the existing front. Most of the stratiform cloud, and all of its more intense bands of precipitation, lay northwest or north of the convective bands in all 3 MCCs of the episode. It was also noted that the dry inflow was most intense where it entered the stratiform cloud *north* of the embryonic circulation center.

The analysis of all these cases confirms the hypothesis of Stumpf (1988) that the stratiform precipitation is primarily responsible for commencing an inflow from the rear, and that heavier precipitation causes stronger inflow. In the three–dimensional cases in this thesis, it was seen that an inflow converges from *all* directions, including the north, east, and south. Inflow from the north is likely to be cooler and inflow from the south,

drier than the ambient air in the baroclinic zone in which the MCC propagates, especially in the lower troposphere where the temperature gradients are stronger. Thus, the so–called "cool" and "dry conveyor belts" are established. Inflow from the east, of course, draws in saturated, still buoyant air from the convectively active core, which ascends to maintain the stratiform cloud.

If that cloud is sheared north of the convective region as the buoyant air ascends, convergence will be induced beneath it in mid–levels, but the westerly inflow into the base of the northern stratiform cloud will oppose the emergence of a cyclonic circulation around the convective core region. On the other hand, if a weaker shear profile permits an upper–level ice cloud to accumulate all around the core region, the latent heating in the convective and stratiform regions act in concert to enhance convergence into the core, and the rotational adjustment of the wind will not be opposed in one sector of the system.

The unidirectional wind shear above 3 km during the episode on 3, 4 June positioned the stratiform cloud northeast of the core, a poor location for cooperative spin–up. The shear on 7 May, which was southerly in mid–levels but westerly from 7 to 12 km, positioned more of the cloud east of the core and also behind the rapidly advancing squall line. Thus, the dry airstream developed vigorously behind the squall line, south of the emerging circulation in the core, and wrapped around the core cyclonically.

9.6 Analogies with extratropical cyclones

As described in chapter 2, a mesoscale vortex can develop from convective cloud systems if the clouds can release latent heat over scales comparable to the Rossby radius of deformation λ_R during periods of time comparable to a half pendulum day. This radius identifies the scale at which the inertial stability of rotation in the horizontal plane becomes as important as the gravitational stability of buoyant motions in the vertical direction. The definition has been extended to include the effect of local curvature of the flow (Cotton et al., 1989):

$$\lambda_R^2 = \frac{C_N^2}{(\zeta + f)(f + 2V/R)}$$

where C_N is the phase speed of an inertial–gravity wave, ζ the relative vorticity, f the Coriolis parameter, V the tangential component of the wind speed, and R its radius of curvature. As discussed in that paper, the calculation of C_N is not straightforward because the Brunt–Väisälä frequency changes as the atmosphere becomes cloudy and saturated. The phase speed C_N was determined from an explicit simulation of a mesoscale convective system by Tripoli and Cotton (1989a). Some values estimated for the weakly rotating MCC (4 June) and the strongly rotating MCC (7 May) are:

	(weakly rotating)	(strongly rotating)
$C_N = 28\ ms^{-1}$		
$f = 0.84 \times 10^{-4}\ s^{-1}$		
	$V \sim 7\ ms^{-1}$	$V \sim 10\ ms^{-1}$
	$R \sim 290$ km	$R \sim 120$ km
	$\zeta \sim 0.4 \times 10^{-4} s^{-1}$	$\zeta \sim 1.5 \times 10^{-4} s^{-1}$
	$\lambda_R = 220$ km	$\lambda_R = 116$ km

The relative vorticity may even be overestimated for the weakly rotating system, as the above value was not observed through a deep layer. The radius of curvature R is also not easily estimated in a system that is more convergent than rotational in character; R was estimated from the curvature of the warm conveyor belt from the southeastern through the northeastern and northern sectors of system B.

The Rossby radius of about 120 km for the strongly rotating system is comparable to the actual radius of the MCC. The weakly rotating MCC, however, is somewhat smaller than a circle described by its Rossby radius of about 220 km, which is a low estimate. This is consistent with the view that the 4 June prototype is not close to geostrophic or gradient–wind balance. A system which develops relative vorticity greater than f, like the case on 7 May, becomes increasingly stable as the Rossby radius is more than halved from the effect of the inertial stability provided by local vorticity.

The divergent response to the latent heating is boosted if precipitation melts and evaporates as it falls into dry air, so that the lower portion of a column of air is chilled while the upper portion is warmed. Vertical stretching of the column, and convergent inflow into the middle of it, can concentrate the relatively modest amount of planetary vorticity f into a meso–α–scale cyclone in a matter of a few hours.

The above conception is for a symmetric vortex. One way that the mesoscale convective vortex can be asymmetric is when it develops near synoptic–scale frontal zones. As the cyclone spins up, the inflows from both the warm side and the cool side tend to wrap around the center. If the warm inflow ascends and the cool inflow descends in rain-chilled mesoscale downdrafts, then the MCC evolves like a three-dimensional spiral helix. In central North America another airstream of middle or upper tropospheric origin can enter the MCC. This can be boundary layer air from the elevated Mexican plateau, advected in the 700 to 800 mb layer, or upper tropospheric air which might descend in a synoptic scale trough to mid–levels, as Carlson (1980) discussed.

We have described at least three airstreams in terms of "conveyor belts" which interact with each other at frontal zones. A warm conveyor belt originates in the low-level jet, which is known to favor the development of MCCs; it ascends in buoyant convective clusters in the low troposphere and in slantwise updrafts in the upper troposphere. Part of the warm airstream may acquire some rotation; it may then wrap around the north side of the system from the east. The cool, unsaturated air (from 3 to 7 km in height) on the north side of the vortex may converge and descend in a core region. This can be imagined as a cool conveyor belt. However, the cold conveyor belt in Carlson's model is believed to ascend in the core.

Dry inflow may enter the core from the rear and the sides at levels above and below the cloud base. That which enters above cloud base tends to evaporate the cloud (which chills the air). That which is below cloud base would warm dry adiabatically as it subsides (which leads to a hydrostatic wake pressure low at the surface near the rear margin of the MCC), but then is cooled moist adiabatically as falling precipitation evaporates into it. This leads to spatially separated meso-highs and meso-lows at the surface, conducive to

sustained strong winds. This dry airstream is analogous to the dry tongue that erodes a spiral, cloud-free notch into the comma-shaped cloud system of an occluding cyclone.

The bow-shaped mesoscale outflow boundary at the leading edge of rain-chilled air plays the role of the cold front. The pseudo-cold front is propelled by pressure gradient forces on the front side of the meso-high pressure center. Another hypothesized forcing agent is the downward transport of mid–level momentum from the rear, but this does not explain the propagation of the mesoscale front in the several cases in which the mid level inflow came from the south or southwest. The warm front or stationary front is often already present in the environment favorable for MCCs. After further development of the mesoscale vortex, rain-cooled subsiding air originally from the dry rear inflow, may wrap around the front of the vortex from the south. This air may then encounter the cool conveyor belt coming from the north in lower levels; thus, the pseudo-cold front "occludes" with the stationary front. It is often observed that the vortex lags behind the pseudo-cold front, and this would aid the occlusion.

Few mesoscale convective systems attain such a clearly evident occlusion, because of the time required for the dry inflow to intrude to the core of the mesoscale ascent region, and wrap around its leading edge. As the dry intrusion deepens and wraps around the circulation center, it will eventually cut off the supply of buoyant air in the warm conveyor belt. In cases of mesoscale convective vortices reported elsewhere (e.g., Menard and Fritsch, 1989), the cloud system indeed ceased to be convectively active even as the cyclonic circulation persisted for periods as long as a few days. It has been observed that convective activity later can develop in the vortex for other reasons.

If the vortex lasts long enough (~8 hours) and grows large enough (~500 km) it may become inertially stable, capable of persisting for days. The low–level convergence induced by surface friction may, in some cases, lead to renewed convection in the center despite an unfavorable stratification in its warm core.

9.7 Analogies with supercell thunderstorms

In the late 1970's a critical mass of observations led to new hypotheses on the evolution of the supercell thunderstorm, especially two components of it, the mesocyclone and the

tornado. Analogies were drawn between their evolution and that of the extratropical cyclone.

Ludlam (1963) stated that "with only alterations in scale, especially the horizontal, ...thunderstorms resemble the dominant form of convection in the presence of shear, which is the large–scale baroclinic disturbance." Lemon and Doswell (1979) synthesized a conceptual model depicted (in plan view) in Fig. 2.4. A significant element was the "rear flank downdraft", colder, drier, and having lower θ_e values than the main or forward flank downdraft. Although Lemon and Doswell hypothesized that the downdraft was forced downward by dynamic high pressure as ambient air impinged on the obstacle of the main updraft, Rotunno and Klemp (1985) argued that cyclostrophic low pressure in the low–level vortex drew the mid–level, low–valued θ_e air downward. In their view, the rotation in low levels was more important than rotation in the mid–levels, at least for initiating the rear flank downdraft. On reaching the surface, the downdraft air can advance into the warm inflow much like a pseudo–cold front, but it can also advance into the rain-cooled forward downdraft much like an occluded front. In the view of Lemon and Doswell, the occlusion eventually chokes off the inflow of warm air to the mesocyclone, which then collapses.

The analogy between the supercell and the mesoscale convective vortex is partial. The rear flank downdraft is a response to the interaction between the slow moving updraft of a supercell and a layer of strong environmental winds; as such it develops later in the storm. Barnes (1978) believed that the downdraft was initiated by negative buoyancy after a certain amount of mixing with cloudy air. Lemon (1979) stressed the importance of the dynamic pressure rise from the obstacle effect, while Klemp and Rotunno (1983) emphasized the role of rotation in inducing vertical pressure gradients. This rear downdraft is analogous to the rear inflow of dry air into the MCC. Both acquire some negative buoyancy from evaporation and melting of precipitation, and both start to turn cyclonically on descending. The mesoscale cold front of the MCC may generate a line of cumulonimbi, some of them supercells in their own right, as it advances like a bow-shaped squall line. In other chapters we have documented detached clusters of storms propagating with the

mesoscale cold front as if they were on a southern extension of it. This may be analogous to the flanking line of cumulus congestus that accompanies a supercell.

The rear flank downdraft of the supercell seems to descend almost vertically. The rear inflow of the MCC has been thought to descend over distances of 100 km or more, but in the weakly rotating examples studied here, the inflows reached a point well within the MCC where the descent was sudden.

The geometry of the evolving mesocyclones may be different. The mesoscale convective vortex may fundamentally depend on the superposition of cloudy, still buoyant and still precipitating air in the warm conveyor belt *over* unsaturated air in the dry and cool airstreams. This geometry maintains the anomaly of potential vorticity. The supercell does not require this kind of special vertical arrangement to maintain its cyclone, although for longevity its updrafts ought to slope such that precipitation falls into the downdrafts and the mid level cyclone should be stacked above the low level occlusion.

The rear flank downdrafts on both scales may be accelerated forward and downward by low pressure zones. In the supercell, the low pressure is found at very low levels, and competes with a tendency toward high pressure caused by evaporative cooling of rain. In the mesoscale convective complex, the low pressure is found beneath the stratiform cloud in *mid*-levels, and is primarily a hydrostatic response to the buoyant warm air in the stratiform cloud. The low pressure may extend to the surface, in which case a "wake low" is observed, but only outside of the precipitating region, because of the above mentioned effect of evaporating rain on the pressure field.

There is not much analogy between the forward flank downdraft of the supercell and any component of the MCC. That deep downdraft is generated in the supercell after precipitation falls from the updraft. The analogous structure in the MCC would be the the cool conveyor belt, which existed as a cool air mass long before the MCC began. Inasmuch as the northern cool air is drawn into the mesoscale vortex and is chilled by stratiform rain, it does descend cyclonically beneath the warm conveyor belt over a mesoscale area.

Finally, the small scale and strong winds of supercells means that dynamic pressure forces are quite important. Such is not the case in MCCs; their large horizontal extent implies that hydrostatic and buoyant pressure forces dominate.

9.8 Locus of significant weather

Reports of severe weather were common from the storms on the pseudo–cold front that extended south from the main precipitation shield of these MCCs. In one MCC a damaging tornado was reported, and in all of them reports of large hail and strong winds were numerous. The tornado was produced by a long lived storm cluster on the extreme southern terminus of the mesoscale cold front, where it was advancing into the deeper unstable air that lay on the surface in this region, unlike further north where the unstable air was decoupled from the surface. The hail, some of which caused much damage to field crops and property, tended to fall from the discrete storms that later coalesced into the mesoscale convective complexes. In a minority of the MCCs, hail was also reported from the broken convective lines that extended south from the dissipating systems, and in one case, hail continued to fall from storms on the southern flank of the mesoscale cloud shield.

The other significant weather is flooding from excessive rainfall in a localized area. The three systems in the episode of 3, 4 June together dropped 8 to 15 cm of rain within 24 hours in an 80 km wide swath of east central Kansas. The radar images show that the rain fell from discrete convective clusters that formed in the stationary frontal zone aloft. Locations that received much rainfall from the passage of one MCC were likely to be in the path of the core regions of subsequent MCCs.

If conditions are ripe for development of an MCC along a stationary frontal zone aloft which might be identifiable in profiler data or model output, forecasts of the potential for floods might be achievable for a narrow, well–defined region. Similarly, if the origin and path of mesoscale convective complexes could be forecast with some skill in the future, then one could forecast higher probabilities of severe weather in the region of first storms, and along the expected path of the southern margin of the cloud shield.

Chapter 10

CONCLUSIONS

Mesoscale convective complexes (MCCs) that manifested some form of vortical pattern of convective activity comprised a significant fraction of the MCCs observed in the PRE–STORM field program. An analysis of four such MCCs has led to conceptual models of two prototypes for the vortical systems:

The **weakly rotating MCC** may manifest a rotational pattern such as a spiral or a frontal–wave cusp in the distribution of convective echo, and does exhibit a strong response of the *divergent* wind to the convectively–generated heat source and heat sink, but it does *not* exhibit a strong response of the rotational component of the wind. It may or may not develop a strong rotational response by the time it disqualifies as an MCC.

The **strongly rotating MCC** not only manifests vortical patterns of cloud and precipitation, but also generates a meso–α–scale cyclone that slowly approaches gradient-wind balance with time.

Actual MCCs can be readily diagnosed as weakly or strongly rotating if wind profiles or soundings through the system are available with a spatial resolution of about 100 km. A kinematic analysis like that in chapters 5 and 7 could be automated and quickly applied. Dual Doppler observations can also diagnose the degree of rotation, with less certainty than a network of soundings because of the limited range of current radars, usually less than the diameter of an MCC.

A perspective drawing in Fig. 9.5 depicts the structure of the weakly rotating MCC. The airflow in both prototypes can be discussed by analogy to the "conveyor belt" model advanced for the extratropical cyclone.

- The warm conveyor belt transports and releases the convectively available potential energy of the system. Its path consists of:

- a low level jet from 0.5 to 2 km above ground that is accelerated by the MCC into several convective regions;
- a portion that ascends vertically in multicellular storms, some of them severe, on a "pseudo–cold front" that often extends south from the core region (the **apex**);
- a portion that rises steeply in a sloping, elevated frontal zone that preceded the MCC, and on which the MCC propagates;
- a portion that ascends in one or more meso–β–scale clusters in the apex where the two fronts intersect. This portion turns cyclonically to flow towards the rear in a "jet" some 50 km wide that occupies the former frontal zone. As it rises it fills the middle and upper levels with nimbostratus cloud.
- The outflow from mesoscale ascent is exhausted in all directions. Upstream of the MCC, an upper level front is found along the upwind and northern edge of the cloud shield where ice–saturated outflow converges with ambient winds diverted around the north side of the MCC.

• The dry airstream is accelerated most vigorously into and beneath that portion of the stratiform cloud where the precipitation is most intense. An S–shaped boundary that slopes to the rear with height separates the dry inflow from the warm conveyor jet; this boundary exhibits strong horizontal shear vorticity and deformation. The dry inflow differs in the two prototypes:

- The inflow may converge from all directions not blocked by the warm conveyor belt in the weakly rotating MCC. If the main part of the stratiform precipitation is situated north of the pre–existing frontal zone, the dry inflow may be accelerated in a direction counter to the cyclonic circulation that would develop around the convective region.
- In the more strongly rotating MCC, the dry airstream descends to lower levels, approaches the core of the convective region more closely, and wraps around

the developing mid–level cyclonic vorticity center, to a greater extent, than in the pre–rotating MCC.

- The cool conveyor belt enters beneath the stratiform cloud from the north or northeast at heights from 4 to 7 km. On encountering light precipitation, it first descends in mesoscale unsaturated subsidence, but the portion that reaches the core of the MCC descends from the 2 or 3 km level to the surface in saturated downdrafts.

Some MCCs develop an effective mesoscale vortex, while others do not although they may manifest rotational organization of convective activity. Some of the factors that may aid effective genesis of a meso–α–scale circulation are:

- A profile of shear which is *not* unidirectional in the middle and upper troposphere. A shear profile that spreads the stratiform cloud in many directions, so that it partially surrounds the convective core region, enables the stratiform and the convective precipitation processes to cooperatively enhance convergence in the same region.

- Development of vigorous convective activity well away from the existing front on which the embryonic vortex will form. The surface cold pool associated with the activity will also be vigorous, and reinforces the multicellular convection on the mesoscale cold front. The resulting stratiform cloud enhances dry rear inflow south of the vortex.

Apparent rotational patterns of convection develop in the *first* half of the life cycle of some MCCs, midway between the initiation and mature stages. A vortical circulation itself, if it does develop, is observed in the second half of the life cycle, that is, after the mature stage. It is concluded, then, that the mesoscale convective vortex does not cause the wave cyclone patterns in the convection.

The *frontal wave* pattern consists of two convective bands: a sloping, typically east–west rain band of meso–β–scale width on the pseudo–warm front, and a narrow multicellular convective line on the pseudo–cold front, oriented north–south. There may be one or more bands of enhanced stratiform rainfall parallel to the east–west convective band. The

former develops from MCC–enhanced convergence in a pre–existing frontal zone, usually stationary. The mesoscale cold front may develop from the merger of cold air outflow boundaries from intense, early storm clusters or squall lines that precede the MCC south of the pre–existing front.

By focusing convergence and convective uplift near the intersection of the two pseudo–fronts, the frontal wave pattern may enhance the development of a meso–α–scale warm core and subsequent vortex.

A chaotic pattern of convective activity early in the life cycle of an MCC may also favor eventual spin–up by dispersing the release of latent heat over meso–α–scale spatial scales. A hypothesis for the cause of the chaotic development requires a previous mesoscale rain system to deposit a chilled stable layer that decouples the low level jet from the surface during the approach of a subsequent MCC. If horizontal variations of moisture content, vertical motion, or other factors that lead to the onset of free convection, are less pronounced in the decoupled layer than in a surface-based layer, then convection may be initiated in the decoupled layer nearly simultaneously over a large area. The actual sites of the first storms may be randomly distributed since they are less likely to be associated with surface features.

In one frontal–wave case, conditional symmetric instability was perhaps responsible for lifting stable, negatively buoyant air to its level of free convection, where a combination of conditional symmetric and convective instability enabled the warm conveyor belt to ascend through the stationary frontal zone.

Hail, damaging wind or other severe weather are more likely to occur in the southern portion of the pseudo–cold front or squall line especially where it extends south of the MCC cloud shield. The precursor storms that precede initiation of a mesoscale convective system also commonly generate severe weather. Excessive rainfall may accumulate in the swath under an elevated stationary front when a number of MCCs repeatedly propagate along the front.

Recommendations for future research.

The major unanswered questions that a national STORM program might address are:

- The factors that impede attainment of an inertially stable balanced vortex in some systems. The fixed network of observations in PRE–STORM did not observe an MCC through its entire life cycle. A larger fixed network or a mobile airborne system consisting of rapid–scan Doppler radar and dropsondes would be needed to "chase" an MCC through most of its life.

- The mutual interdependence, if there is any, between the mesoscale circulations around the core region of an MCC, and the intense cellular convection that often produces severe weather south of it.

- The importance of the cool conveyor belt in the dynamics of the system, and the details of its interaction with the more heavily precipitating region. Does the remarkably stable air left on the surface in the wake of an MCC originate wholly in the cool belt?

Mesoscale convective vortices may be able to develop in ways other than the two prototypes discussed here. Are the chaotic MCCs more or less likely to develop organized vortices? Do the tropical systems which develop mid–level cyclonic circulations in their anvil clouds differ from the mid–latitude systems studied in PRE–STORM? Do the large, severe squall lines of interior North America generate mesoscale vortices less frequently, and if so, is this of any consequence? The origin and evolution of different kinds of convectively generated vortices deserve further study.

To confirm our conclusions advanced for frontal–wave and other apparent vortical MCCs, it would be useful to composite the properties of hundreds of mesoscale convective systems, classified into several groups according to patterns observed by conventional National Weather Service radars, and according to the synoptic-scale environment. Digitized reflectivity data have been archived from as many as ten operational radars since 1985; those data should provide an adequate sample from the approximately 150 MCCs that have occurred since then.

A two–dimensional mesoscale model with explicit simulation of the larger convective entities could simulate the onset of conditional symmetric instability and its role relative to vertical convection, in existing frontal zones. It would be illuminating to determine whether the growth of slantwise circulations abets the cyclogenesis on the scale of the MCC, and how the nonlinear effect of local flow curvature on angular momentum affects the growth of such circulations.

A simulation of the fully three–dimensional frontal–wave prototype of the MCC would be desirable. Requiring a nested grid approach in three dimensions, such a simulation challenges current capabilities, but a series of numerical experiments could explore the combination of factors that favor the evolution of an inertially stable vortex, and other combinations that impede it. Isolating the important environmental factors would aid the forecasting of long-lived mesoscale rain systems before they develop.

REFERENCES

Atkinson, B.W., and P.A. Smithson, 1978: Mesoscale precipitation areas in a warm frontal wave. *Mon. Wea. Rev.*, **106**, 211–222.

Augustine, J.A., and K.W. Howard, 1988: Mesoscale Convective Complexes over the United States during 1985. *Mon. Wea. Rev.*, **116**, 685–701.

Bellamy, J.C., 1949: Objective calculations of divergence, vertical velocity and vorticity. *Bull. Amer. Meteorol. Soc.*, **30**, 45–49.

Bennetts, D.A., and B.J. Hoskins, 1979: Conditional symmetric instability—a possible explanation for frontal rainbands. *Quart. J. Roy. Meteor. Soc.*, **105**, 945–962.

Blanchard, D.O., and A.I. Watson , 1986: Modes of mesoscale convection observed during the pre–STORM program. *Preprints,* 23rd Conf. on Radar Meteorology, Snowmass, CO, Amer. Meteorol. Soc., Boston, MA, J155–J158 pp.

Bluestein, H.B., and M.H. Jain, 1985: Formation of mesoscale lines of precipitation: Severe squall lines in Oklahoma during the spring. *J. Atmos. Sci.*, **42**, 1711–1732.

Bluestein, H.B., G.T. Marx, and M.H. Jain, 1987: Formation of mesoscale lines of precipitation: nonsevere squall lines in Oklahoma during the spring. *Mon. Wea. Rev.*, **115**, 2719–2727.

Bosart, L.F., and F. Sanders, 1981: The Johnstown Flood of July 1977: A Long–lived Convective System. *J. of Atmos. Sci.*, **38**, 1616–1642.

Bosart, L.F., 1986: Kinematic vertical motion and relative vorticity profiles in long–lived mesoscale convective system. *J. of Atmos. Sci.*, **43**, 1297–1299.

Brandes, E.A., 1989: Evolution and structure of the 6–7 May 1985 mesoscale convective system and associated vortex. Submitted to *Mon. Wea. Rev.*,

Browning, K.A., and T.W. Harrold, 1970: Air motion and precipitation growth at a cold front. *Quart. J. Royal. Meteor. Soc.*, **96**, 369–389.

Browning, K.A. 1971: Radar measurements of air motion near fronts. *Weather,* **26**, 320–340.

Businger, S., and B. Walter, 1988: Comma cloud development and associated rapid cyclogenesis over the Gulf of Alaska: A case study using aircraft and operational data. *Mon. Wea. Rev.*, **116**, 1103–1123.

Caracena, F., and J.M. Fritsch, 1983: Focusing mechanisms in the Texas Hill country flash floods of 1978. *Mon. Wea. Rev.*, **111**, 2319–2332.

Carlson, T.N., 1980: Airflow through midlatitude cyclones and the comma cloud pattern. *Mon. Wea. Rev.*, **108**, 1498–1509.

Carr, F.H., and J.P. Millard, 1985: A composite study of comma clouds and their association with severe weather over the Great Plains. *Mon. Wea. Rev.*, **113**, 370–387.

Ceselski, B.F., and L.L. Sapp, 1975: Objective wind field analysis using line integrals. *Mon. Wea. Rev.*, **103**, 89–100.

Chen, S., and W.R. Cotton, 1988: The sensitivity of a simulated extratropical mesoscale convective system to longwave radiation and ice–phase microphysics. *J. Atmos. Sci.*, **45**, 3897–3910.

Clark, J. D., A.J. Lindner, R. Bornemen, and R.E. Bell, 1980: Satellite observed cloud patterns associated with excessive precipitation outbreaks. *Preprints*, Eighth Conf. on Weather Forecasting and Analysis, Denver, CO, Amer. Meteorol. Soc., Boston, MA, 463–473 pp.

Cotton, W.R., M.S. Lin, R.L. McAnelly, and C.J. Tremback, 1989: A Composite model of mesoscale convective complexes. *Mon. Wea. Rev.*, **117**, 765–783.

Cotton, W.R., 1989: **Storms.** To be published.

Cotton, W.R., and R.A. Anthes, 1989: **Storm and cloud dynamics.** Academic Press Inc., San Diego, CA, in press.

Cunning, J.B., 1986: The Oklahoma–Kansas Preliminary Regional Experiment for STORM-Central. *Bull. Amer. Meteorol. Soc.*, **67**, 1478–1486.

Emanuel, K.A., 1979: Inertial instability and mesoscale convective systems. Part I: Linear theory of inertial instability in rotating viscous fluid. *J. Atmos. Sci.*, **36**, 2425–2449.

Emanuel, K.A., 1983: On assessing local conditional symmetric instability from atmospheric soundings. *Mon. Wea. Rev.*, **111**, 2016–2033.

Emanuel, K.A., 1988: Observational evidence of slantwise convective adjustment. *Mon. Wea. Rev.*, **116**, 1805–1816.

Fortune, M., 1980: Properties of African squall lines inferred from time–lapse satellite imagery. *Mon. Wea. Rev.*, **108**, 153–168.

Fortune, M.A., and R.L. McAnelly, 1986: The evolution of two mesoscale convective complexes with different patterns of convective organization. *Preprints*, 23rd Conf. on Radar Meteorology, Snowmass, CO, Amer. Meteorol. Soc., Boston, MA, J175–J178 pp.

Gamache, J.F., and R.A. Houze, 1982: Mesoscale air motions associated witha tropical squall line. *Mon. Wea. Rev.*, **110**, 118–135.

Gamache, J.F., and R.A. Houze, 1983: Water Budget of a Mesoscale Convective System in the Tropics. *J. of Atmos. Science*, **40**, 1835–1871.

Harrold, T.W., 1973: Mechanisms influencing the distribution of precipitation within baroclinic disturbances. *Quart. J. Royal Meteor. Soc.*, **99**, 232–251.

Hobbs, P.V., T.J. Matejka, P.H. Herzegh, J.D. Locatelli, and R.H. Houze, 1980: The mesoscale and microscale structure and organization of clouds and precipitation in midlatitude cyclones. I: A case study of a cold front. *J. of Atmos. Science*, **37**, 568–596.

Hoskins, B.J., M.E. McIntyre, and A.W. Robertson, 1985: On the use and significance of isentropic potential vorticity maps. *Quart. J. Roy. Met. Soc.*, **111**, 877–946.

Houze, R.A., 1977: Structure and dynamics of a tropical squall–line system. *Mon. Wea. Rev.*, **105**, 1540–1567.

Houze, R.A., S.A. Rutledge, M.I. Biggerstaff, and B.F. Smull, 1989a: Interpretation of Doppler weather radar displays of midlatitude mesoscale convective systems. *Bull. Amer. Meteor. Soc.*, **70**, 608–619.

Houze, R.H., B.F. Smull, and P. Dodge, 1989b. Mesoscale organization of springtime rainstorms in Oklahoma. Submitted to *Mon. Wea. Rev.*

Huschke, R.E., 1959: **Glossary of Meteorology.** Amer. Meteorological Soc., Boston, MA, 638 pp.

Johnson, R.H., S. Chen, and J.J. Toth, 1989: Circulations associated with a mature-to-decaying midlatitude mesoscale convective system. Part I: Surface features—heat bursts and mesolow development. *Mon. Wea. Rev.*, **117**, 942-959.

Johnson, R.H., and P.J. Hamilton, 1988: The relationship of surface pressure features to the precipitation and airflow structure of an intense midlatitude squall line. *Mon. Wea. Rev.*, **116**, 1444–1472.

Johnston, E.C., 1982. Mesoscale vorticity centers induced by mesoscale convective vomplexes. *Preprints,* Ninth Conf. on Weather Forecasting and Analysis, Seattle, WA, Amer. Meteorol. Soc., Boston, MA, 196–200 pp.

Klemp, J.B., and R. Rotunno, 1983: A study of the tornadic region within a supercell thunderstorm. *J. Atmo. Sci.*, **26**, 390–398.

Klemp, J.B., 1987: Dynamics of tornadic thunderstorms. *Annu. Rev. Fluid Mechanics,* **19**, 369–402.

Leary, C.A., and E.N. Rappaport, 1987: The life cycle and internal structure of a mesoscale convective complex. *Mon. Wea. Rev.*, **115**, 1503–1527.

Leary, C.A., and T.M. Bals, 1989: Evolution of the 3–4 June Pre–STORM mesoscale convective system. *Preprints,* 24th Conf. on Radar Meteorology, Tallhassee, FL, Amer. Meteorol. Soc., Boston, MA, 471–474 pp.

Lemone, M.A., G.M. Barnes, and E.J. Zipser, 1984: Momentum flux by lines of cumulonimbus over the tropical oceans. *J. of Atmos. Science,* **41**, 1914–1932.

Ludlam, F.H., 1980: **Clouds and storms.** The behavior and effect of water in the atmosphere. Pennsylvania State University Press, 342–346 pp.

Maddox, R.A., 1980: Mesoscale convective complexes. *Bull. Amer. Meteorol. Soc.*, **61**, 1374–1387.

Maddox, R.A., 1981: The structure and life–cycle of midlatitude mesoscale convective complexes. Atmos. Science Paper No. 336, Dept. of Atmospheric Science, Colorado State University, Fort Collins, CO, 311 pp.

Maddox, R.A., 1983: Large scale meteorological conditions associated with midlatitude, mesoscale convective complexes. *Mon. Wea. Rev.*, **111**, 1475-1493.

McAnelly, R.H., and W.R.Cotton, 1986: Meso–β–scale characteristics of an episode of meso–α–scale convective complexes. *Mon. Wea. Rev.*, **114**, 1740–1770.

McAnelly, R.L., and W.R. Cotton, 1989a: A meso–β–scale pulse of convective precipitation during the early growth of mesoscale convective complexes. *Preprints*, 24th Conf. on Radar Meteorology, Tallhassee, FL, Amer. Meteorol. Soc., Boston, MA, 482–485 pp.

McAnelly, R.L., and W.R. Cotton, 1989b: The precipitation life cycle of mesoscale convective complexes over the central United States. *Mon. Wea. Rev.*, **117**, 784–808.

Meitín, J.G., and J.B. Cunning ,1985. The Oklahoma–Kansas preliminary regional experiment for STORM–Central. Vol. I: Daily Operations Summary. NOAA Tech. Memo. ERL ESG–20, Weather Research Program, NOAA, Boulder, CO, 313 pp.

Meitín, J.G., 1987 . The Oklahoma–Kansas preliminary regional experiment for STORM–Central. Vol. II: Radar Data Summary. NOAA Tech. Memo. ERL ESG–26, Weather Research Program, NOAA, Boulder, CO, 84 pp.

Meitín, J.G., and A.I. Watson, 1987. The Mesoscale Convective Complex of 3–4 June 1985, Part I: Kinematic Structure and Precipitation Characteristics. Poster presented at Third Conf. on Mesoscale Processes, Aug. 21–26, 1987, Vancouver, B.C., Canada. Extended Abstracts, Amer. Meteorol. Soc., Boston, MA.

Meitín, J.G., 1988 . The Oklahoma–Kansas preliminary regional experiment for STORM–Central. Vol. III: Aircraft Mission Summary. NOAA Tech. Memo. ERL ESG–30, Weather Research Program, NOAA, Boulder, CO, 109 pp.

Meitín, J.G., and A.I. Watson, 1989: Comparison of the kinematic structure and precipitation characteristics of squall and non–squall mesoscale convective systems. *Preprints*, 24th Conf. on Radar Meteorology, Tallhassee, FL, Amer. Meteorol. Soc., Boston, MA, 486–489 pp.

Menard, R.D., and J.M. Fritsch, 1989. A mesoscale convective complex–generated inertially stable warm core vortex. *Mon. Wea. Rev.*, **117**, 1237–1261.

Merceret, F.J., and H.W. Davis, 1981: The determination of navigational and meteorological variables measured by NOAA/RFC WP3D aircraft. NOAA Tech. Memo. ERL RFC-7, Environmental Research Lab, NOAA, Miami, Florida.

Miller, L.J., C.G. Mohr, and A.J. Weinheimer, 1986: The simple rectification to Cartesian space of folded radial velocities from Doppler sampling. *J. Atmos. Oceanic Tech.*, **3,** 162–174.

Mohr, C.G., L.J. Miller, R.L. Vaughan, and H.W. Frank, 1986: The merger of mesoscale datasets into a common format for efficient and systematic analyses. *J. Atmos. Oceanic Tech.*, **3,** 143–161.

Newton, C.W., and J.C. Fankhauser, 1975. Movement and Propagation of Multicellular Convective Storms. *Pure and Applied Geophysics,* **113,** 747–764.

Petterssen, S., and S.J. Smebye, 1971: On the development of extrtratropical storms. *Quart. J. Roy. Met. Soc.*, **97,** 457–482.

Purdom, J.F.W., and P.C. Sinclair, 1988: Using satellite data to aid in diagnosing and forecasting convective development and intensity along arc cloud lines. *Preprints,* 3rd Conference Satellite Meteorology and Oceanographic, Anaheim, CA. American Meteor. Society, Boston, 166–171 pp.

Raymond, D.J., 1989: A theory for long–lived mesoscale convective systems. Submitted to *Quart. J. R. Meteor. Soc.*

Rockwood, A.A., D.L. Bartels, and R.A. Maddox, 1984: Precipitation characteristics of a dual mesoscale convective complex. NOAA Tech. Memo. ERL ESG–6, Environmental Sciences Group, ERL, NOAA, Boulder, CO.

Rotunno, R., and J. Klemp, 1985: On the rotation and propagation of simulated supercell thunderstorms. *J. Atmos. Sci.*, **42,** 271–292.

Rutledge, S.A., and R.A. Houze, 1989: Single and dual–Doppler radar observations of a mesovortex in the 28 May 1985 mesoscale convective system observed during Pre–STORM. *Preprints,* 24th Conf. on Radar Meteorology, Tallhassee, FL, Amer. Meteorol. Soc., Boston, MA, 498–501 pp.

Sladewski, R., 1986: RADAP II Archived Data Description. Oklahoma Climatological Survey, Norman, OK, 57 pp.

Smull, B.F., and R.A.Houze, 1985: A midlatitude squall line with a trailing region of stratiform rain: radar and satellite observations. *Mon. Wea. Rev.*, **113,** 117–133.

Smull, B.F., and R.A. Houze, 1987: Rear inflow in squall lines with trailing stratiform precipitation. *Mon. Wea. Rev.*, **115,** 2869–2889.

Smull, B.F., and J.A. Augustine ,1989 : Structure and environment of a non–squall mesoscale convective complex observed during Pre–STORM. *Preprints,* 24th Conf. on Radar Meteorology, Tallhassee, FL, Amer. Meteorol. Soc., Boston, MA, 502–505 pp.

Srivastava, R.C., T.J. Matejka, and T.J. Lorello, 1986: Doppler radar study of the trailing anvil region associated with a squall line. *J. Atmos. Sci.*, **43,** 356–377.

Stirling, J., and R.M. Wakimoto, 1989: Mesoscale vortices in the stratiform region of a decaying midlatitude squall line. *Mon. Wea. Rev.*, **117,** 452–458.

Stumpf, G.J., 1988. Surface pressure features associated with a midlatitude mesoscale convective system in O.K. Pre–STORM. Atmospheric Science paper no. 435, Dept. of Atmospheric Science, Colorado State University, Fort Collins, CO.

Stumpf, G.J., and R.H. Johnson , 1988: Lower tropospheric profiling needs in relation to the initiation of mesoscale convective systems. *Extended Abstracts,* Lower Tropospheric Profiling: Needs and Technologies, a symposium, Boulder, CO, Amer. Meteorol. Soc, Boston, MA.

Tripoli, G.J., and W.R. Cotton, 1989, a and b: Numerical study of an observed orogenic mesoscale convective system. Part 1: Simulated genesis and comparison with observations. Part 2: Analysis of governing dynamics. *Mon. Wea. Rev.,* **117,** 273–304 and 305–328.

Uccellini, L.W., P.J. Kocin, R.A. Petersen, C.H. Wash, and K.F. Brill, 1984: The Presidents' Day cyclone of 18–19 February 1979: Synoptic overview and Analysis of the subtropical Jet Streak influencing the pre–cyclogenetic period. *Mon. Wea. Rev.,* **112,** 31–55.

U.S. Dept. of Commerce, 1987. National weather radar network observing and reporting procedures. Federal Meteorological Handbook, no. 7, Weather Radar Observations, Part A.

Verlinde, J., and W.R. Cotton , 1988: Observed structure and evolution of a mesovortex in the trailing stratiform region of a MCC. *Preprints,* 10th Intern. Cloud Physics Conf., Bad Homburg, Germany. Amer. Meteorol. Soc., Boston, MA, 196–200 pp.

Weather Research Program , 1987: Annual Report. Environmental Research Laboratory, NOAA, Boulder, CO.

Weisman, M.L., and J.B. Klemp, 1986: Characteristics of isolated convective storms. Chap. 15, **Mesoscale Meteorology and Forecasting,** P.S. Ray, ed. Amer. Meteorol. Soc., Boston, 793 pp.

Wetzel, P.J., W.R. Cotton, and R.L. McAnelly, 1983: A long–lived mesoscale convective complex. Part II: Evolution and structure of the mature complex. *Mon. Wea. Rev.,* **111,** 1919–1937.

Whitaker, J.S., L.W.Uccellini, and K.F. Brill, 1988: A model–based diagnostic study of the rapid development phase of the Presidents' Day cyclone. *Mon. Wea. Rev.,* **116,** 2337–2365.

Young, G.S., and J.M. Fritsch, 1989: A proposal for general conventions in analysis of mesoscale boundaries. Unpublished manuscript.

Zhang, D.L., and J.M.Fritsch, 1986: Numerical simulation of the meso–β–scale structure and evolution of the 1977 Johnstown flood . Part I: Model description and verification. *J. Atmos. Sci.,* **43,** 1913–1943.

Zhang, D.L., and J.M.Fritsch, 1987: Numerical simulation of the meso–β–scale structure and evolution of the 1977 Johnstown flood . Part II: Inertially stable warm core vortex and the mesoscale convective complex. *J. Atmos. Sci.,* **44,** 2593–2612.

Zhang, D.L., and J.M.Fritsch, 1988a: Numerical sensitivity experiments of varying model physics on the sructure, evolution and dynamics of two mesoscale convective systems. *J. Atmos. Sci.*, **45**, 261–293.

Zhang, D.L., and J.M.Fritsch, 1988b: A numerical investigation of a convectively generated, inertially stable, extratropical warm core mesovortex over land. Part I: Structure and evolution. *Mon. Wea. Rev.*, **116**, 2660–2687.

Zipser, E.J., 1977: Mesoscale and convective–scale downdrafts as distinct components of squall–line structure. *Mon. Wea. Rev.*, **105**, 1568–1589.